EFFECT OF DENSITY AND MOISTURE CONTENT ON THE RESILIENT RESPONSE OF UNBOUND GRANULAR MATERIAL

ELSABé VAN ASWEGEN

EFFECT OF DENSITY AND MOISTURE CONTENT ON THE RESILIENT RESPONSE OF
UNBOUND GRANULAR MATERIAL

ELSABé VAN ASWEGEN

A thesis submitted in partial fulfilment of the requirements for the degree of

PHILOSOPHIAE DOCTOR (ENGINEERING)

In the

FACULTY OF ENGINEERING

UNIVERSITY OF PRETORIA

June 2013

EFFEK VAN DIGTHEID EN VERSADIGINGSGRAAD OP DIE VEERKRAG REAKSIE VAN ONGEBONDE KORRELMATERIAAL

ELSABé VAN ASWEGEN

'n Proefskrif voorgelê ter gedeeltelike vervulling van die vereistes vir die graad

PHILOSOPHIAE DOCTOR (INGENIEURSWESE)

In die

FAKULTEIT INGENIEURSWESE

UNIVERSITEIT VAN PRETORIA

June 2013

THESIS SUMMARY

EFFECT OF DENSITY AND MOISTURE CONTENT ON THE RESILIENT RESPONSE OF
UNBOUND GRANULAR MATERIAL

ELSABé VAN ASWEGEN

Supervisor: Professor Doctor Wynand J vdM Steyn

Co-Supervisor: Doctor Hechter L Theyse

Department: Civil Engineering

University: University of Pretoria

Degree: Philosophiae Doctor (Engineering)

Unbound granular material is used in the pavement structure and usually comprises the bulk of the structural and foundation layers of a typical South African pavement. The term '*unbound granular material*' refers to the classification of natural material, which has not been modified in any way.

Various mechanistic-empirical models for the resilient response of unbound granular material have been developed over the years. However, few have incorporated important influencing parameters such as moisture or density on the basic stress-strain relationship or linked variables of the models to basic engineering properties of unbound granular material.

Theyse (2008a) has considered unbound granular material and developed a resilient response model taking moisture and density into account. However, the model was only successfully calibrated for crushed material and it was recommended that future research should focus on G4 to G10 material to calibrate a single model for these materials and that a wider range of moisture conditions should be evaluated. Based on Theyse's (2008a) recommendations and recent work in this area, this study was undertaken to select and calibrate a general resilient modulus model for unbound granular material applicable for all moisture and density conditions and to correlate applicable basic engineering properties determined through basic laboratory testing to the aforementioned model to facilitate quick and easy estimation of the resilient behaviour of natural unbound material by engineers.

The cord modulus model developed by Theyse (2012) was selected from recent work, since it modelled the trends observed in the data. These trends depict the stress dependent behaviour of unbound

granular material, where an increase in initial modulus is observed for increasing confinement pressure, as well as initial stress-softening with increasing stress ratio followed by stress stiffening. The model was calibrated for all bulk material samples under consideration. The calibration process included linking variables of the model to mathematical functions that approximate the trends observed when variables were considered against level of saturation. A parametric analysis indicated that the saturation and stress-dependent cord modulus model realistically predict material behaviour. The saturation and stress-dependent cord modulus model was refined further and calibrated for crushed and natural unbound granular material. This refinement did not negatively influence the accuracy or ability to realistically predict the material behaviour.

Basic material properties could be linked to predictive statistical distributions that could estimate the range of modulus values that can be expected for the material under consideration. However, the variables of the saturation and stress-dependent cord modulus model could not be linked to basic material properties due to the limit set of results available.

SAMEVATTING VAN PROEFSKRIF

EFFEK VAN DIGTHEID EN VERSADIGINGSGRAAD OP DIE VEERKRAG REAKSIE VAN
ONGEBONDE KORRELMATERIAAL

ELSABé VAN ASWEGEN

Promotor:	Professor Doktor Wynand J vdM Steyn
Mede-Promotor:	Doktor Hecther L Theyse
Departement:	Siviele Ingenieurswese
Universiteit:	Universiteit van Pretoria
Graad:	Philosophiae Doktor (Ingenieurswese)

Ongebonde korrelmateriaal word in plaveisel strukture gebruik en in 'n tipese Suid-Afrikaanse plaveisel struktuur bestaan die struktuur- en fundament lae gewoonlik oorwegend daaruit. Die term '*ongebonde korrelmateriaal*' verwys na die klassifikasie van natuurlike korrelmateriaal wat nog nie op enige manier verander is nie.

Verskeie meganistiese-empiriese modelle om veerkrag reaksie van ongebonde korrelmateriaal te simuleer is deur die jare is ontwikkel. Daar is egter wynig van die modelle wat belangrike parameters wat die veerkrag reaksie beinvloed, soos vog of digtheid op die basiese spannings-vervormings gedrag insluit of veranderlikes van die modelle met basiese ingenieurs eienskappe van ongebonde korrelmateriaal verbind.

Theyse (2008) het ongebonde korrelmateriaal ondersoek en 'n veerkrag reaksie model ontwikkel wat die invloed van vog en digtheid in ag neem. Die model was egter net suksesvol gekalibreer vir gebreekte klip en daar is voorgestel dat toekomstige navorsing moet fokus op G4 tot G10 materiaal om sodoende 'n enkele model vir alle ongebonde korrelmateriaal te kalibreer en dat 'n wyer reeks van vogtoestande ondersoek moet word. Gebaseer op Theyse (2008) se aanbevelings en onlangse navorsingswerk, is hierdie studie onderneem om 'n veerkrag reaksie model te kies en te kalibreer wat van toepassing is vir enige vog en digtheidstoestand, asook om basiese ingenieurs eienskappe wat van toepassing is en deur basiese laboratorium toetse bepaal kan word, aan die voormelde te koppel en sodoende vinnige en maklike beraming van die veerkrag reaksie van natuurlike ongebonde korrelmateriaal te fasiliteer.

Die koord modulus model wat deur Theyse (2012) ontwikkel is, is vanuit onlangse navorsingswerk gekies, aangesien dit die tendense waargeneem vanuit die resultate moduleer. Hierdie tendense wys die spanningsafhanklike gedrag van ongebonde korrelmateriaal, waar 'n toename in die aanvanklike modulus met 'n toename in omhullingsdruk waargeneem word, asook 'n aanvanklike spannings-versagting met toename in spanningsverhouding gevolg deur spanningsverharding. Die model is gekalibreer vir alle materiaal monsters wat deel van die studie was. Die kalibrasie proses het onder meer ingesluit die koppel van veranderlikes aan wiskundige funksies wat die waargeneemde tendense benader wanneer die veranderlikes teenoor vlak van versadiging oorweeg word. 'n Parametriese analise het aangedui dat die versadiging en spanningsafhanklike koord modulus model die materiaal gedrag realisties benader. Die versadiging en spanningsafhanklike koord modulus model is verder verfyn en gekalibreer vir gebreekte en natuurlike ongebonde korrelmateriaal. Hierdie verfyning van die model het nie 'n negatiewe invloed op die akkuraatheid van die model of vermoe van die model om die materiaal gedrag realisties te benader gehad nie.

Basiese materiaal eienskappe kon gebruik word in benaderende statistiese verspreidings om die reeks van modulus waardes wat verwag kan word vir 'n sekere materiaal te benader. Die veranderlikes van die versadiging en spanningsafhanklike koord modulus model kon egter nie aan basiese materiaal eienskappe verbind word nie weens die beperkte data stel beskikbaar.

ABSTRACT

Title:	Effect of density and moisture content on the resilient response of unbound granular material
Author:	Elsabé van Aswegen
Supervisor:	Professor Doctor Wynand J vdM Steyn
Co-Supervisor:	Doctor Hechter L Theyse
Department:	Civil Engineering
University:	University of Pretoria
Degree:	Philosophiae Doctor (Engineering)

Unbound granular material is used in the pavement structure and usually comprises the bulk of the structural and foundation layers of a typical South African pavement. The term '*unbound granular material*' refers to the classification of natural material, which has not been modified in any way.

Various mechanistic-empirical models for the resilient response of unbound granular material have been developed over the years. However, few have incorporated important influencing parameters such as moisture or density on the basic stress-strain relationship or linked variables of the models to basic engineering properties of unbound granular material.

This study builds on previous work by Theyse (2008a) and the cord modulus model developed by Theyse (2012). The Theyse (2012) model was selected to be further investigated, since it modelled the trends observed in the data realistically. The model depicts the stress dependent behaviour of unbound granular material, where an increase initial modulus is observed for increasing confinement pressure, as well as initial stress-softening with increasing stress ratio followed by stress stiffening.

The model was calibrated for all bulk material samples under consideration in this thesis. The calibration process included linking variables of the model to mathematical functions that approximate the trends observed when variables were considered against level of saturation. A parametric analysis indicated that the saturation and stress-dependent cord modulus model realistically predict material behaviour. The saturation and stress-dependent cord modulus model was refined further and calibrated for crushed and natural unbound granular material. This refinement did not negatively influence the accuracy or ability to realistically predict the material behaviour.

Basic material properties could be linked to predictive statistical distributions that could estimate the range of modulus values that can be expected for the material under consideration. However, the variables of the saturation and stress-dependent cord modulus model could not be linked to basic material properties due to the limit set of results available.

Vir Hardus

'*Hoeveel beter is dit om wysheid te verkry as goud, en verkiesliker om verstand te verwerf as silwer*'
Spreuke 16:16

ACKNOWLEDGEMENTS

TABLE OF CONTENTS

APPENDICES

LIST OF TABLES

LIST OF FIGURES

1   INTRODUCTION & BACKGROUND

1.1   INTRODUCTION

Unbound granular material is used in the pavement structure and usually comprises the bulk of the structural and foundation layers of a typical South African pavement. The term '*unbound granular material*' refers to the classification of natural material, which has not been modified in any way, as defined in Technical Recommendations for Highways 4 and Technical Recommendations for Highways 14. Unbound granular material is classified from a G1 to G10 quality according to its fundamental behaviour and strength characteristics (TRH4, 1996; TRH14, 1985).

A G1 quality material is defined as a '*graded crushed stone*', usually obtained from crushing solid un-weathered quarried or mined rock or boulders. G2 and G3 quality material are obtained by the same process as a G1 quality material, but may contain natural fines not derived from crushing the parent rock. Medium quality materials (G4, G5 and G6) are defined by the TRH14 (1985) as '*natural gravel or a mixture of natural gravel and boulders which may require crushing*'. Any of these materials may be modified using cement, lime, bitumen or polymers to enhance certain strength characteristics of the material. Lower quality materials (G7, G8, G9 and G10) are defined as gravel-soil (TRH14, 1985).

In this document the term '*crushed stone*' or '*crushed aggregate*' will be used to refer to G1 to G3 quality material and '*natural material*' will refer to G4 to G10 quality material. '*Unbound granular material*' will refer to both crushed stone and natural material (i.e. G1 to G10).

A typical South African pavement structure constructed from granular material, whether modified or not, is depicted in Figure 1.1. It indicates that the pavement structural layers are generally subjected to higher shear stresses than the pavement foundation layers and also larger plastic strains. When the wearing course is compromised, it leads to strength and bearing capacity deterioration of the structural pavement layers as moisture ingress takes place (Theyse, 2008a).

The type and volume of traffic the pavement structure must carry during its design life, dictates which material behaviour and strengths are required. Based on that, a pavement structure is designed accordingly to utilise the strengths of unbound or bound (modified) granular material.
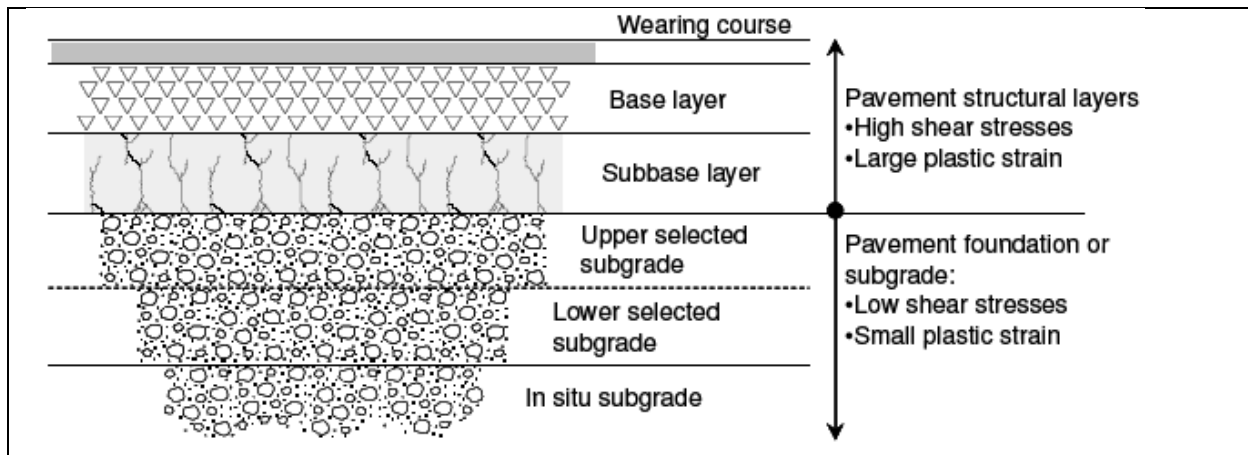
Figure 1.1:   Typical South African pavement structure (Theyse, 2008a).

The accurate modelling of the response of pavement layers, whether modified or not, is therefore of utmost importance when engineers design a pavement structure.

There is currently a comprehensive project underway which is jointly sponsored by the South African National Roads Agency Ltd (SANRAL) and the Council for Scientific and Industrial Research (CSIR). The project entails the revision of the South African Mechanistic-Empirical Design Method (SAMEDM) which has been one of the primary pavement design tools in South Africa since the early 1970s (Theyse, 2006). Some improvements were made to the original SAMEDM through the years, but the main components of the SAMEDM were still based on research conducted during the 1970s and 1980s. In May 2005 a workgroup was appointed to initiate the revision of the SAMEDM as it stood at that time (Theyse, 2006).

The South African Pavement Design Method (designated SAPDM as opposed to the SAMEDM) project was divided into various research areas which require revision. These include amongst others traffic demand analysis, material resilient response models and damage models calibrated for the effects of field variables and traffic loads. The entire SAPDM project is described in more detail in Appendix A.

The SAPDM research area focussing on material resilient response models is particularly relevant to this thesis. Data collected in the Project SAPDM/B1-a are utilised in this study.

1.2   BACKGROUND

Various mechanistic-empirical pavement design models for structural unbound granular pavement layers have been developed (Uzan, 1985; Lekarp *et al.*, 2000). Such models aim to approximate the stress and strain due to repeatedly applied wheel loading. The stress and strain applied by repeated wheel loads are usually small in comparison to the strength of the pavement structural layers. Most of

© University of Pretoria

the deformations in these layers are recoverable and proportional to the load magnitude and thus considered elastic (Kancherla, 2004; Kwon, Tutumluer and Al-Qadi, 2007; Kim, 2007). This characteristic behaviour is known as the resilient behaviour of the material (Kim, 2007). An appropriate resilient response model is therefore required for modelling the behaviour of unbound granular material in pavement layers.

However, parameters such as stress level, density, grain size, aggregate type, particle shape, moisture content and number of load repetitions all influence the resilient behaviour of unbound granular material. To model this complicated stress-strain relationship as accurately as possible, constitutive laws, as well as correlations with other properties should be utilised (George, 2004; Kim, 2007).

Numerous models to approximate the behaviour of unbound granular material based on resilient response exists, of which those listed in Table 1.2 are most widely recognised internationally. The models listed in Table 1.2 are based on tri-axial test data obtained from samples which were moulded from selected materials in the laboratory to obtain a desired density and moisture content representative of the field. The only variable during testing was confining pressure. From these results, the models were derived through curve-fitting procedures and focused on the stress-strain behaviour of the material. In Section 2.2.5.4 these models have been utilised as a basis from which further modifications have been done to take variable parameters such as moisture content and density into account.

Table 1.1: **Summary of resilient response models.**

Name of model	Model formulation	Model definition
Theory of elasticity (Lekarp et al, 2000)	$M_R = \frac{\Delta(\sigma_1 - \sigma_3)}{\varepsilon_{1,r}}$	M_R = resilient modulus; Δ = 'change in'; $\sigma_1; \sigma_3$ = major & minor principal stress; $\varepsilon_{1,r}; \varepsilon_{3,r}$ = recoverable axial & horizontal strain
K-θ model (Lekarp et al, 2000)	$M_R = K_1 \theta^{K_2}$ or $M_R = K_1 \left(\frac{\theta}{p_0}\right)^{K_2}$	θ = bulk stress = $(\sigma_1 + \sigma_2 + \sigma_3)$ or $(\sigma_1 + 2\sigma_3)$ or $(\sigma_d + 3\sigma_3)$ where $\sigma_d = (\sigma_1 - \sigma_3)$ (Kim, 2007 & Theyse, 2008a) p_0 = reference pressure (101,3 kPa) K_1, K_2 = regression coefficients
Uzan Model (Lekarp et al, 2000)	$M_R = k_1 \theta^{k_2} \sigma_d^{k_3}$	θ = bulk stress σ_d = deviator stress, k_1, k_2, k_3 = regression coefficients
Universal model (Lekarp et al, 2000)	$M_R = k_1 \cdot P_a \cdot \left(\frac{\theta}{P_a}\right)^{k_2} \cdot \left(\frac{\tau_{oct}}{P_a}\right)^{k_3}$	θ = bulk stress τ_{oct} = octahedral shear stress, P_a = reference pressure k_1, k_2, k_3 = regression coefficients
Boyce's model (Lekarp et al, 2000)	$K = \frac{K_i p^{(1-n)}}{1 - \beta\left(\frac{q}{p}\right)^2}$ and $G = G_i p^{(1-n)}$ Volumetric strains & deviatoric strains of the model are related to the mean normal stress & deviatoric stress as follows: $\varepsilon_v = \left(\frac{1}{K_i}\right) p^n \left[1 - \beta\left(\frac{q}{p}\right)^2\right]$ and $\varepsilon_q = \left(\frac{1}{3}G_i\right) p^n \left(\frac{p}{q}\right)$	β = $(1-n)\frac{K_i}{6G_i}$ p = mean normal stress q = deviator stress ε_v = volumetric strain ε_q = shear strain

1-4

George (2004) reported that basic soil index properties such as liquid limit, plasticity index and material passing 0.075 mm sieve can be correlated to resilient response and are influencing parameters on the resilient response of lower strength materials. For higher strength materials, moisture content and density was found to be the most influential parameters (George, 2004).

A historical literature study, contained in Section 2.2 of this study, showed that international models incorporating moisture, in various forms, and density are mainly based on the universal model. These models were also derived from curve-fitting procedures after laboratory tests conducted on selected materials and are therefore only valid for specific materials.

South African models (Section 2.2.7), tend to attempt to incorporate fundamental properties of the material into the resilient response models with variable degrees of success. By incorporating fundamental properties, the models may be more applicable to a wider range of materials. The most recent South African model discussed in the literature was developed by Theyse (2008a). Theyse was able to successfully calibrate a resilient response model, which incorporated moisture content and density, for crushed aggregate (G1 to G3). However, Theyse was unable to calibrate a single model for natural material, due to insufficient data (G4 to G10).

Research discussed in Section 2.3 focus on work done in South Africa as part of the SAPDM project, in which the focus is to develop or calibrate a model suitable for unbound granular material. The aim of this study is to build on the work discussed in Section 2.3 and to calibrate an accurate resilient response model for unbound granular material which is generally applicable and can be correlated to basic engineering properties.

1.3   PROBLEM DEFINITION

Various mechanistic-empirical models for the resilient response of unbound granular material have been developed over the years. However, few have incorporated important influencing parameters such as moisture content or dry density on the basic stress-strain relationship or linked variables of the models to basic engineering properties of unbound granular material.

Theyse (2008a) has considered unbound granular material and developed a resilient response model taking moisture and density into account. Theyse (2008a) incorporated materials ranging from G1 to G10, but could only calibrate a single resilient modulus successfully for crushed aggregate (G1 to G3). It was recommended that future research should focus on G4 to G10 material to calibrate a single model for these materials and that a wider range of moisture conditions should be evaluated.

This thesis focuses on the resilient behaviour of unbound granular material (G1 to G10) under a wider range of moisture conditions. The calibration of a more generally applicable resilient modulus model

based on the results obtained from investigating resilient behaviour over a wider range of moisture conditions will be addressed. Furthermore, statistical methods will be utilised to link basic engineering properties, obtained through basic laboratory tests, to a calibrated model which reflect the behaviour observed due to the influence of moisture condition, but not relying on detailed input.

1.4   OBJECTIVES

The objectives of this study are:
a) Selecting and calibrating a general resilient modulus model for unbound granular material applicable for all moisture content and dry density conditions for level 2 analysis, since no such model currently exists; and
b) To develop a method through which resilient behaviour of unbound natural materials can be predicted for level 3 analysis in the absence of detailed material properties, to facilitate quick and easy estimation of the resilient behaviour of unbound granular material by engineers.

1.5   SCOPE

The following tasks fall within the scope of this thesis:
- Defining and classifying unbound granular material as used in the pavement structure through a literature survey. The definitions and classifications as applicable in this study will be stated;
- Describing resilient response and aspects thereof which influence accurate modelling of resilient response as indicated by a literature survey;
- Identifying and critically discussing resilient response models in literature which incorporate influencing parameters, such as moisture content and dry density; and resilient response models linked to basic engineering properties, such as Grading Modulus (GM) for example;
- Identifying a resilient response model which will be suitable for further investigation to evaluate its applicability to all unbound granular material, since no single model valid for all unbound granular material is available;
- Investigate the effect of a wide range of moisture content and matric suction pressure on resilient response of unbound granular material by conducting tri-axial tests;
- Calibrate the identified resilient response model with the tri-axial test results to more accurately and confidently model resilient response of unbound granular material, and
- Linking the refined unbound granular material model to basic engineering properties obtained from basic laboratory test results which are generally conducted in South Africa;

It falls outside the scope of work to analyse:
- The resilient response of modified granular material, since the combinations of modifiers and application rates are too large to fully investigate under this study;

- The cross-anisotropic response of unbound granular material because it is a research area on its own, involving time-consuming and expensive testing, not lending itself to routine testing. One of the aims of this study is to develop a model dependent on basic engineering properties, and

- Basic engineering properties which will be investigated will only include grading, Atterberg limits, Apparent Relative Density (ARD), Bulk Relative Density (BRD), Maximum Dry Density (MDD) and Optimum Moisture Content (OMC). These are obtained through basic laboratory testing which does not require specialised equipment or training and are generally available to the engineer.

1.6   CONTRIBUTION TO STATE OF KNOWLEDGE

This thesis presents a general resilient modulus model for unbound granular material applicable to any moisture and density condition. A statistical method is presented, to correlate resilient behaviour and basic engineering properties obtained through basic laboratory testing, as a tool for engineers to estimate the resilient modulus of a material without detailed material property input.

1.7   RESEARCH PROGRAM

Research was conducted in the following sequence:
1. Sample sites for bulk sampling of material was identified and sampled;
2. Routine testing was carried out on the bulk samples collected. Routine testing included grading analysis, determination of Atterberg indicators, determination of compaction characteristics, determination of volumetric and gravimetric properties, determination of California Bearing Ratio (CBR) and determination of durability through the Durability Mill Index (DMI);
3. Experimental design of static and resilient modulus tri-axial tests was determined;
4. Static tri-axial tests were conducted and the results analysed to determine the loading requirements for the resilient modulus tri-axial tests;
5. Resilient modulus tri-axial tests were conducted according to the test protocol (Appendix C);
6. Resilient modulus tri-axial test results were processed and analysed by means of templates in MS Excel;
7. Analysed resilient modulus data were used to calibrate the selected model, and
8. Routine test results were used to link to calibrated model variables.

1.8   STRUCTURE OF REPORT

The structure of the report is depicted schematically in Figure 1.2 and indicates the main purpose of each Chapter.
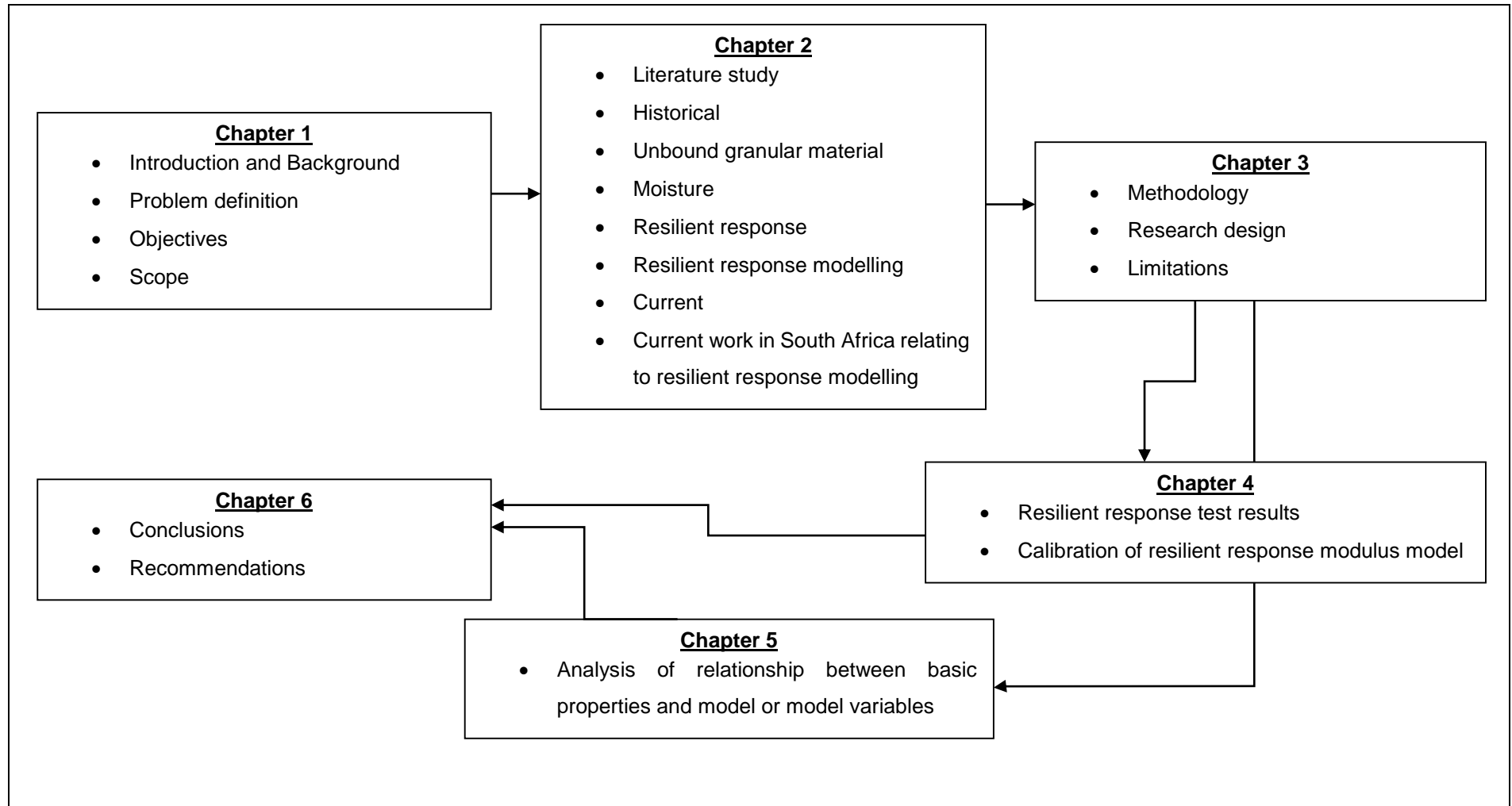
Figure 1.2: **Schematic layout of thesis structure.**

1.9 REFERENCES

George, K.P. (2004). '*Prediction of resilient modulus form soil index properties*', Final Report, Mississippi Department of Transportation, Research Division, Jackson, Mississippi, USA.

Kancherla, A. (2004). '*Resilient modulus and permanent deformation testing of unbound granular materials*', Masters Dissertation, Texas A&M University, Austin, Texas, USA.

Kim, M. (2007). '*Three-dimensional finite element analysis of flexible pavements considering nonlinear pavement foundation behaviour*', PhD Thesis, University of Illinois, Urbana, Illinois, USA.

Kwon, J.; Tutumluer, E.; Al-Qadi, I.L. & Anochie-Boateng, J. (2007). '*Geomaterial characterizations of full scale pavement test sections for mechanistic analysis and design*', proceedings of the Geo-Denver 2007: New Peaks in Geotechnics; Congress, Denver, USA, 18-21 February 2007, pp. 10.

Lekarp, F., Isacsson, U. & Dawson, A. (2000). '*State of the art. I: Resilient response of unbound aggregates*', Journal of Transportation Engineering, Volume 126, No. 1, January/February, 2000, pp. 66 - 75.

National Cooperative Highway Research Program (NCHRP) (2004). '*Project 1-37A: Guide for Mechanistic-Empirical Design of New and Rehabilitated Pavement Structures*', National Cooperative Highway Research Program, Transportation Research Board, of the National Research Council, USA

Theyse, H.L (2006). '*An improved pavement design method for Southern Africa: Research and development framework*', Report No. CSIR/BE/IE/IR/2006/0042/B, Pretoria, CSIR Built Environment Unit, RSA.

Theyse, H.L. (2008a). '*A mechanistic-empirical design model for unbound granular pavement layers*', PhD Thesis, University of Johannesburg, Johannesburg, South Africa.

TRH 4 (1996). '*Draft TRH 4 : Structural design of flexible pavements for interurban and rural roads*', Department of Transport, Pretoria, South Africa.

TRH 14 (1985). '*TRH 14 : Guidelines for road construction materials*', Department of Transport, Pretoria, South Africa.

Uzan, J. (1985). '*Characterisation of granular material*', Transportation Research Record 1022, Transportation Research Board, Washington D.C., USA.

2 LITERATURE STUDY

2.1 INTRODUCTION

The literature study is divided into two sections, the first focussing on historical literature and the second focussing on current literature. Historical literature includes work that has been published and has been tested by other researchers over the years. Historical literature related to fundamental knowledge regarding materials, resilient behaviour and resilient response modelling is overviewed. Current literature includes work that has been completed since January 2011 under the SAPDM Project, but that is not publicly available at this stage. The work that is included is mainly project literature. The intention of the SAPDM sponsors is to publish work upon the completion of the project. The current literature related to resilient behaviour and resilient response modelling is overviewed.

It is important to unpack and understand the keywords in the title of this thesis. Therefore, this historical literature review focuses on keywords in the thesis title as depicted by Figure 2.1.

Effect of **DENSITY** and **MOISTURE CONTENT** on the **RESILIENT RESPONSE** of **UNBOUND GRANULAR MATERIAL**

Granular material
Why is material important?
Why unbound granular material?
What is natural or unbound granular material?

Density
Relationship with moisture condition?
Why important?

Moisture Content
How can moisture content be expressed?
Are there different types of moisture?

Resilient Response
Basic definitions?
Influencing factors on resilient behaviour?
Modelling of the behaviour?

Figure 2.1:   Schematic layout of Chapter 2

2.2 HISTORICAL LITERATURE

2.2.1 Natural Material

2.2.1.1 *Introduction*

Unbound granular material is of particular importance world-wide and especially in South Africa, since granular material is used in the pavement structure and usually comprises the bulk of the pavement's structural and foundation layers. This is evident in the quantities of granular material produced and used world-wide. Constantino (2012) summarised information reported to the United States (US) Geological Survey that aggregate production increased overall in the US in the first quarter of 2012. An estimated 216 million metric tons (Mt) of crushed stone were produced and shipped for consumption (increase of 9.4 percent), construction sand and gravel produced and shipped for consumption was 136 Mt (increase of 10 percent) and construction aggregates produced and shipped for consumption was 352 Mt (increase of 9.7 percent) compared with that of the same period in 2011. In South Africa the production of sand and aggregate historically also increased, in 2005 by 5.5 per cent (49 970 kt), in relation to 47 382 kt produced in 2004 (Baloyi, 2006). The annual per capita consumption of construction aggregate (G1 to G10) is about 2 000 kg per capita in South Africa and 10 000 kg per capita in the United States (ASPASA, 2006).

2.2.1.2 *Definition*

Natural material is obtained from various geological formations. Each formation has a characteristic upper portion depending on the climate and topography, consisting of various thicknesses of residual weathering products or transported materials. These weathering products or transported materials are defined as stone, gravel or sand. Not all natural materials are suitable for road construction and more often than not, surface materials are considered unsuitable (Steyn and Paige-Green, 2009).

2.2.1.3 *Material properties*

Material properties are those characteristics of a material that distinguishes it from other materials. In pavement engineering there are a number of properties that are regarded as essential fundamental characteristics. These characteristics are obtained through routine tests such as:

- Sieve analysis (grading) to determine the particle size distribution of the material;
- Atterberg indicator tests to characterise the fine fraction of the material, such as plastic limit, liquid limit, plasticity index and linear shrinkage;
- Volumetric properties characterised through for example Apparent Relative Density (ARD) and Bulk Relative Density (BRD) and water absorption;
- Gravimetric properties characterised through Maximum Dry Density (MDD) and Optimum Moisture Content (OMC) using a recognised compaction method; and
- California Bearing Ratio (CBR) of the material to indicate the materials bearing capacity;

These fundamental characteristics or properties are used to classify a material into a specific group of which the behaviour and limitations when used in pavement structure can be deduced. Section 2.2.1.4 discusses material classification and which properties are used in the classification system mainly referred to in this thesis.

2.2.1.4   Classification

The term '*unbound granular material*' refers to the classification of natural material, which has not been modified in any way, as defined in TRH4 (1996) and TRH14 (1985). Unbound granular material is classified from a G1 to G10 according to its fundamental behaviour and strength characteristics (TRH4, 1996, TRH14, 1985).

A G1 quality material is defined as a '*graded crushed stone*', usually obtained from crushing solid un-weathered quarried - or mined rock or boulders. G2 and G3 quality material are obtained by the same process as a G1 quality material, but may contain natural fines not derived from crushing the parent rock. G4, G5 and G6 quality material are defined as '*natural gravel or a mixture of natural gravel and boulders which may require crushing*'. Any of these materials may be modified using for example cement, lime, bitumen or polymers to enhance certain strength characteristics of the material. G7, G8, G9 and G10 quality material are defined as gravel-soil (TRH14, 1985).

In this thesis the term '*crushed stone*' or '*crushed aggregate*' is used to refer to G1 to G3 quality material and '*natural material*' will refer to G4 to G10 quality material. '*Unbound granular material*' refers to both crushed stone and natural material (i.e. G1 to G10).

Table 2.1 gives an abbreviated summary of the criteria used to classify unbound granular materials in terms of TRH 4 and TRH 14, as well as indicating the approximate similar AASHTO classification for the same material.

Table 2.1:   **Abbreviated summary of unbound granular material as per TRH 4 (1996), TRH 14 (1985) and AASHTO (1928) classification system.**

General definition	Classification (TRH 4 and TRH14)	Abbreviated specifications	Approximate AASHTO classification
Crushed material	G1	Maximum size 37,5 mm 86 – 88% apparent relative density Soil fines PI < 4	A-1-a A-1-b A-3
	G2	Maximum size 37,5 mm 100 – 102% Mod AASHTO or 85% bulk relative density Soil fines PI < 6	
	G3	Maximum size 37,5 mm 98 – 100% Mod AASHTO Soil fines PI < 6	

General definition	Classification (TRH 4 and TRH14)	Abbreviated specifications	Approximate AASHTO classification
Natural material	G4	Minimum CBR = 80% @ 98% Mod AASHTO Maximum size 37,5 mm 98 – 100% Mod AASHTO Soil fines PI < 6 (PI ≤ 8 for calcrete) Maximum swell 0,2% @ 100% Mod AASHTO	A-2-4 A-2-5 A-2-6 A-4 A-5
	G5	Minimum CBR = 45% @ 95% Mod AASHTO Maximum size 63 mm or 2/3 of layer thickness Density as prescribed Soil fines PI < 10 Maximum swell 0,5% @ 100% Mod AASHTO	
	G6	Minimum CBR = 25% @ 95% Mod AASHTO Maximum size 63 mm or 2/3 of layer thickness Density as prescribed Soil fines PI < 12 Maximum swell 1,0% @ 100% Mod AASHTO	
	G7	Minimum CBR = 15% @ 93% Mod AASHTO Maximum size 2/3 of layer thickness Density as prescribed Soil fines PI < 12 or 3GM+10 Maximum swell 1,5% @ 100% Mod AASHTO	A-2-6 A-2-7 A-6 A-7-5 A-7-6
	G8	Minimum CBR = 10% @ 93% Mod AASHTO Maximum size 2/3 of layer thickness Density as prescribed Soil fines PI < 12 or 3GM+10 Maximum swell 1,5% @ 100% Mod AASHTO	
	G9	Minimum CBR = 7% @ 93% Mod AASHTO Maximum size 2/3 of layer thickness Density as prescribed Soil fines PI < 12 or 3GM+10 Maximum swell 1,5% @ 100% Mod AASHTO	
	G10	Minimum CBR = 3% @ 93% Mod AASHTO Maximum size 2/3 of layer thickness Density as prescribed or 90% Mod AASHTO	

Classifying a material that has been in use for some time may be more complex. Jooste *et al.* (2007) developed a material classification approach for consistent classification of pavement materials based on the TRH 4 (1996) and TRH14 (1985) classification system. In this approach, all available information is used to give a consistent, rational and objective assessment of a material class. Utilising all the information, the certainty that a material belongs to a particular material class is determined using Fuzzy Logic and Certainty Theory. Certainty theory in essence provides the framework from which hypotheses can be tested using vague and uncertain evidence (Jooste *et al.*, 2007).

In the application of this approach, a Certainty Factor (CF) associated with a specific test is assigned. This is done by defining a simple distribution of the data set for that specific test/parameter using the 10th, median and 90th percentile statistics. Most pavement materials tests provide only a partial indication of material behaviour, and therefore a certainty factor is assigned to each test. This certainty factor represents the confidence in the ability of a test to serve as an accurate indicator of material performance in the pavement layer (0 represents poor and 1 absolute confidence) (TG 2 Appendix A, 2009). Table

2.2 gives an example of the confidence rating which is associated with plasticity index values and Table 2.3 an example of the recommended adjustment of CF based on sample size.

Table 2.2: Confidence rating for Plasticity index (Jooste *et al.*, 2007).

Material type	Plasticity Index measured on Fraction Passing 0.425 mm sieve									
Crushed stone	< 4	4 - 5	6 - 7	8 - 10	> 10					
Natural gravel			< 5	5 - 6	6 - 10	10 - 12	> 12			
Gravel-soil						< 11	11 / 12	13 - 15	> 15	
Sand, silty sand, silt, clay							< 12	12 - 14	14 - 20	> 20
PI rating	1	2	3	4	5	6	7	8	9	10

Table 2.3: Recommended adjustment of CF based on sample size (Jooste *et al.*, 2007).

Sample size (number of observations)	Adjustment factor
1	0.2
2	0.3
3	0.6
4 to 6	0.7
6 or greater	1.0

The result of this approach is a Design Equivalent Materials Class (DEMAC). '*The DEMAC denotes a material that exhibits shear strength, stiffness, durability and flexibility properties similar to a newly constructed material of the same class. The DEMAC implies that the material may not meet the exact specifications for a particular material class, but in terms of behaviour the material is similar*' (TG2, 2009).

In this thesis material are classified using the TRH 4 (1996) and TRH14 (1985), DEMAC (Jooste TG2, 2009) and AASHTO (1928) systems.

2.2.1.5 *Levels of material property evaluation*

The criteria used in Table 2.1 to classify natural material are based on inherent material properties. Material properties can be evaluated on three levels, namely performance properties, engineering properties and fundamental properties (Steyn, 2007).

The most basic level of evaluation is by performance properties. A performance property does not indicate why this specific behaviour occurs, or which properties of the material influence the performance. It does indicate what can be expected from this specific material in this specific state and under the specific conditions. For example, performance properties such as permanent deformation of

a G5 material at a certain moisture content, PI and swell are only indicative of that specific scenario and cannot indicate behaviour when a different G5 material is subjected to the specific conditions or the conditions change, higher moisture content, lower PI and lower swell (Steyn, 2007).

Engineering properties of a specific material provide a more detailed understanding of the material and its potential responses to loading conditions or changes, while remaining constant for a wider range of parameters. For example, an engineering property such as the stiffness of a material will remain constant at particular moisture content and density, but change under different loading conditions (Steyn, 2007).

Properties which are not determined by external conditions (such as temperature or load) but always remain the same and directly influence the engineering and performance properties of the material are called fundamental properties. For example, from the grading of a granular material the expected performance as well as engineering properties can be derived (Steyn, 2007). Atterberg Indicator tests include Plasticity Index (PI), Liquid Limit (LL), Grading Modulus (GM), etc. and are often referred to as the fundamental properties of the material.

Classifying material according to engineering or fundamental properties and using that in modelling the behaviour of material is the aim of any good model. Figure 2.2 illustrates schematically the levels of evaluation that can be applied to material properties. In Chapter 4 and 5, linking a material model to fundamental properties will be explored.
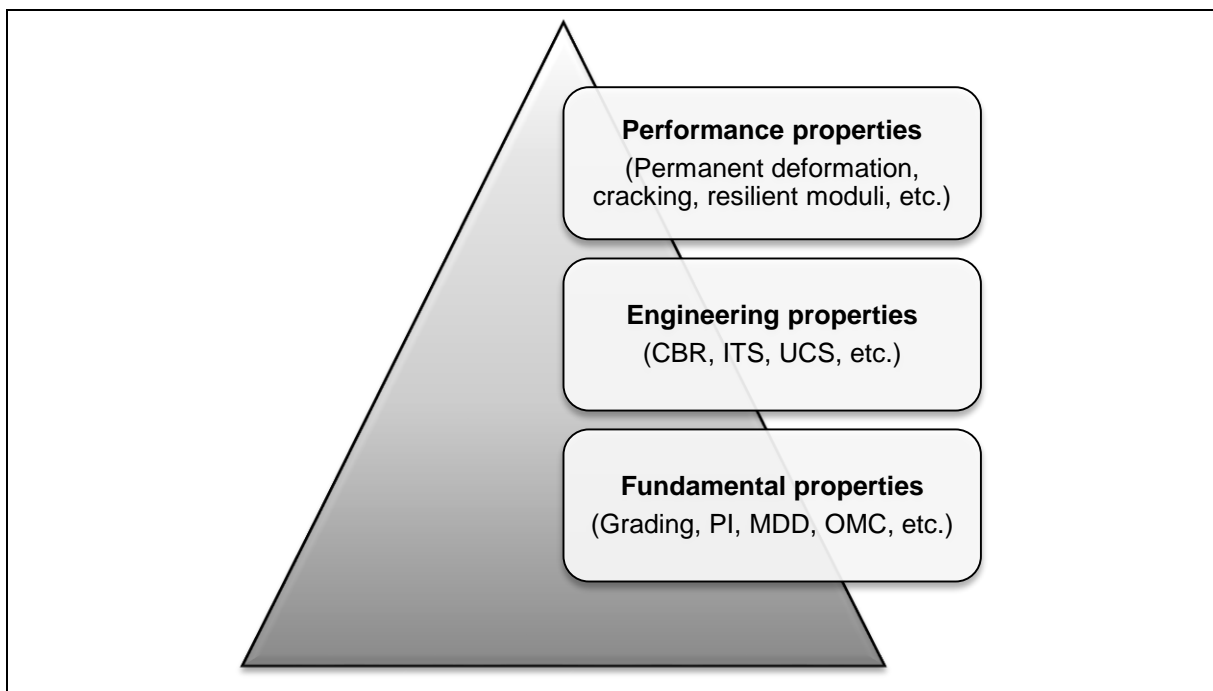
Figure 2.2: **Evaluation levels for material properties.**

2.2.2 Resilient response

2.2.2.1 Basic definitions

There are basic mechanics of material definitions which must be defined to avoid misunderstanding of terms in the following sections. These are as follows:

Elasticity, stress and strain

Elasticity is the physical property of a material by which it returns to its original dimensions during unloading (i.e. the removal of stress) (Gere, 2001). Stress is defined by the force exerted on a specific area, while strain is the ratio of elongation to length at infinitely small scale (Gere, 2001; Dawson, 2009).

Stiffness

Stiffness is the resistance of a body to deformation by an applied force. Elastic modulus is sometimes used as an indication of the stiffness of a material (Gere, 2001).

Resilience

Resilience represents the ability of a material to absorb and release energy within the elastic range of that material (Gere, 2001).

Elastic modulus / Hooke's Law

Elastic modulus or modulus of elasticity is described by Hooke's Law, after Robert Hooke. It describes elastic modulus through the equation $\sigma = E(\epsilon)$ in which σ is stress, ϵ is strain and E a constant of proportionality known as modulus of elasticity. It defines the linear relationship between applied loads (stress) and resulting elongation (strain) (Gere, 2001). It states that strain is directly proportional to stress throughout a materials elastic range, i.e. for stresses below the yield strength. The ideal elastic behaviour of an ideal material is illustrated in Figure 2.3 and denoted by numbers 1 to 4. Number 3 on the curve indicate the elastic limit after which permanent deformation takes place until the material yields at number 4 on the curve. The position of numbers 1 to 4 on the stress strain curve is determined by the stress as the curve dimensions increase with increasing stress (Gere, 2001).

	Where
	σ = Stress
	ε = Strain
	1 = True elastic limit
	2 = Proportionality limit
	3 = Elastic limit
	4 = Offset yield strength
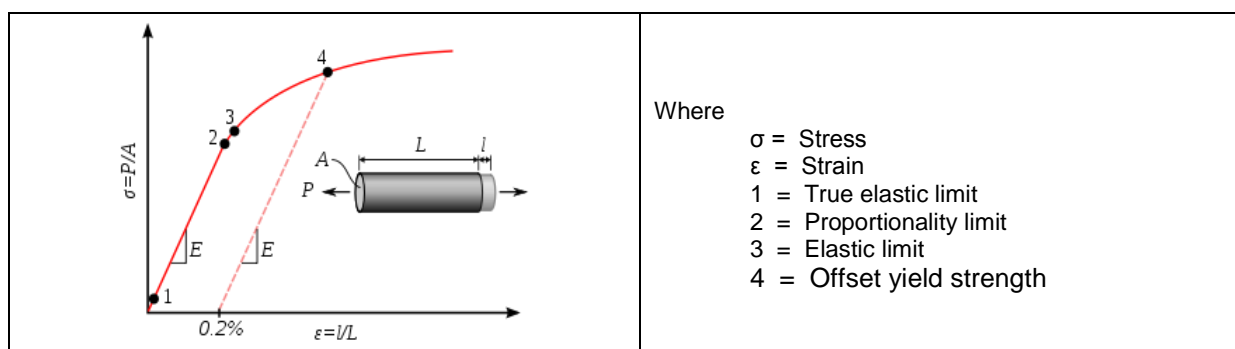
Figure 2.3: **Stress strain curve for nonferrous alloys (Gere, 2001).**

Young's modulus

Several parameters measuring the strength of materials arise from the generalised Hooke's Law such as Young's Modulus, Bulk Modulus (K) and Shear Modulus (G) (De Beer and Maina, 2008).

Young's modulus is often incorrectly also called the elastic modulus or modulus of elasticity. Thomas Young investigated the tension and compression properties of prismatic bars, where he introduced the idea of 'modulus of elasticity', but this 'modulus of elasticity' included properties of the bar, as well as the material (Gere, 2001). Young's modulus describes the response of a material to linear strain (De Beer and Maina, 2008).

Bulk modulus measures the resistance of a substance to uniform compression, i.e. describes the response of a material to uniform pressure. It is defined as the increase in pressure required resulting in a given relative decrease in volume (De Beer and Maina, 2008).

Shear modulus is sometimes referred to as the modulus of rigidity and is defined as the ratio of shear stress to shear strain. In the case of road building materials, shear modulus is concerned with the deformation of a solid when it experiences a force parallel to one of its surfaces while its opposite face experiences an opposing force, such as friction (De Beer and Maina, 2008).

Poisson's ratio

Poisson's ratio, named after Simeon Poisson, is the ratio of lateral strain to axial strain, caused by a load parallel to the axis in which axial strain is measured (Yoder and Witczak, 1975; De Beer and Maina, 2008). For a perfectly incompressible material such as rubber, which deforms elastically at small strains, Poisson's ratio is exactly 0.5. When Poisson's ratio is greater than 0.5, dilation occurred in the material. Figure 2.4 illustrates the concept of Poisson's ratio (De Beer and Maina, 2008). In flexible pavement design, Poisson's ratio is usually assumed or obtained through the use of correlations (Anochie-Boateng *et al.*, 2009)

Assuming the material is compressed along the axial direction then:

$$v = \frac{d\varepsilon_{trans}}{d\varepsilon_{axial}} = -\frac{d\varepsilon_y}{d\varepsilon_x} = -\frac{d\varepsilon_z}{d\varepsilon_x}$$

Where:

v = resulting Poisson's ratio
$d\varepsilon_{trans}$ = transverse strain
$d\varepsilon_{axial}$ = axial strain
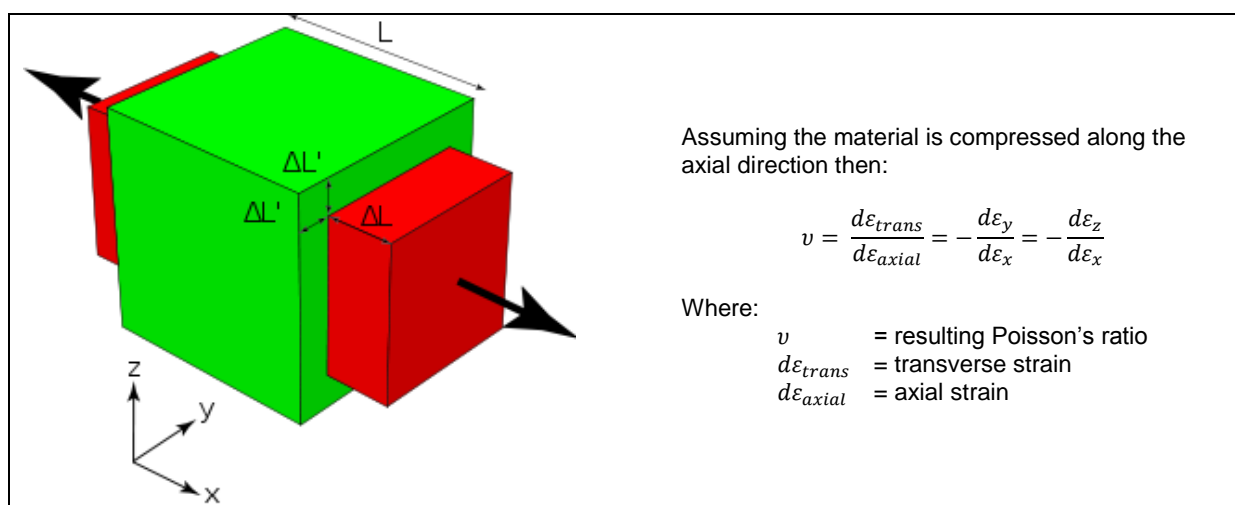
Figure 2.4: **Rectangular incompressible specimen subject to compression, with Poisson's ratio of approximately 0.5 (De Beer & Maina, 2008).**

2.2.2.2 *Definition of resilient response for granular material*

The theory of elasticity is usually used for flexible pavement design. The theory assumes that all materials in the pavement structure are homogeneous, isotropic and linear elastic. Based on this theory, Poisson's ratio and modulus of elasticity would be required to calculate the stresses, strains and deflections in the pavement layers.

Seed *et al.* (1962) introduced the concept of resilient modulus (M_R) for the characterisation of elastic response of subgrade soils in flexible pavements. Later the resilient response of unbound granular materials was used in the American Association of State Highway and Transportation Officials (AASHTO) design guide for pavement structures (Anochie-Boateng, 2009). Traditionally, the term resilient modulus (M_R) is used to define the elastic stiffness of pavement materials and is defined as the repeatedly applied wheel load stress divided by the recoverable strain determined after shakedown of the material (Anochie-Boateng, 2007). The shakedown theory describes the observed permanent deformation behaviour of unbound material and is not specific in terms of the critical parameter that controls the permanent deformation of the material (Theyse, 2006).

In mechanistic-empirical flexible pavement design a resilient modulus value determined in the laboratory is preferred, although field measurement through back-calculation procedures from Falling Weight Deflectometer (FWD) data is acceptable (Anochie-Boateng, 2009). During a resilient modulus tri-axial test, both elastic and plastic deformations occur at the initial stage of load application. As the number of load applications increases, the amount of plastic deformation decreases until a stage where the deformation is practically all recoverable. At that stage the resilient modulus is obtained based on the recoverable axial strain under the applied dynamic load (Figure 2.5). Resilient modulus is defined by:

$$M_R = \frac{\sigma_d}{\varepsilon_r}$$

Where

σ_d =   dynamic deviator stress

ε_r =   resilient (recoverable) strain
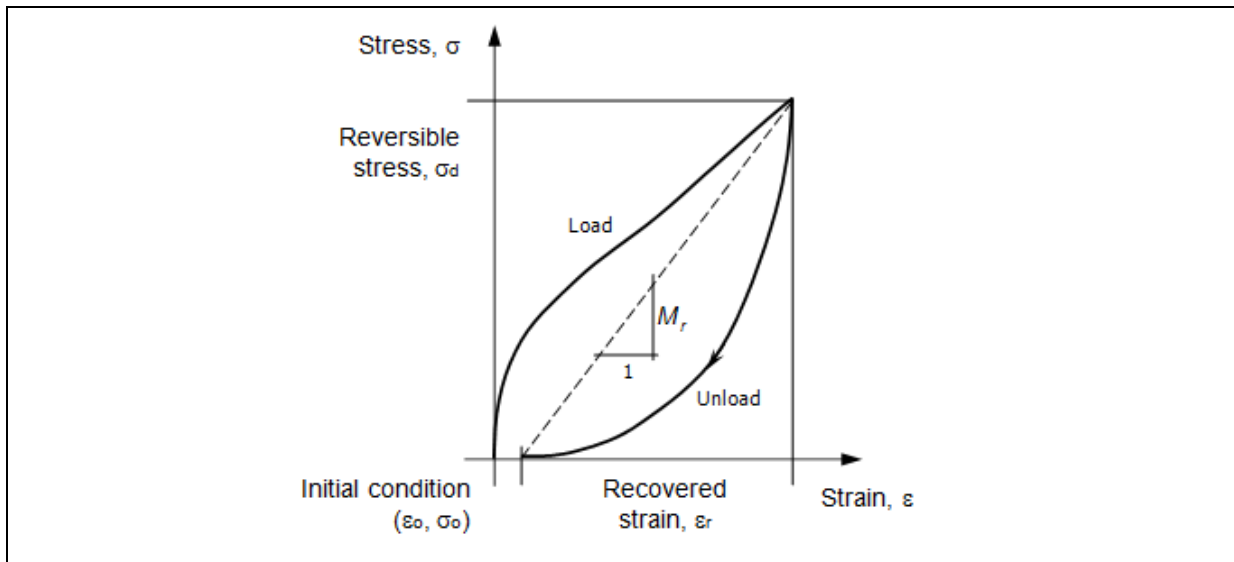
Figure 2.5:   Strains of unbound granular material under repeated load testing (Anochie-Boateng, 2009).

The secant modulus can also be used to express the resilient behaviour of a material and is defined as the slope of the hysteresis loop from the initial stress-strain condition to the fully loaded stress-strain condition. The tangent modulus, less frequently used to express the resilient behaviour of a material, is defined as the instantaneous slope of the hysteresis loop at any point during the loading cycle (Theyse, 2008a). The cord modulus represents the instantaneous stiffness of the material at any point on the stress-strain hysteresis loop (Theyse, 2012). Figure 2.6 depicts the secant, tangent and cord modulus.

Secant Modulus: $M_S = \dfrac{\Delta\sigma}{\Delta\varepsilon}$

$$\text{Tangent modulus: } M_t = \lim_{\Delta\varepsilon\to 0}\frac{\Delta\sigma}{\Delta\varepsilon}$$
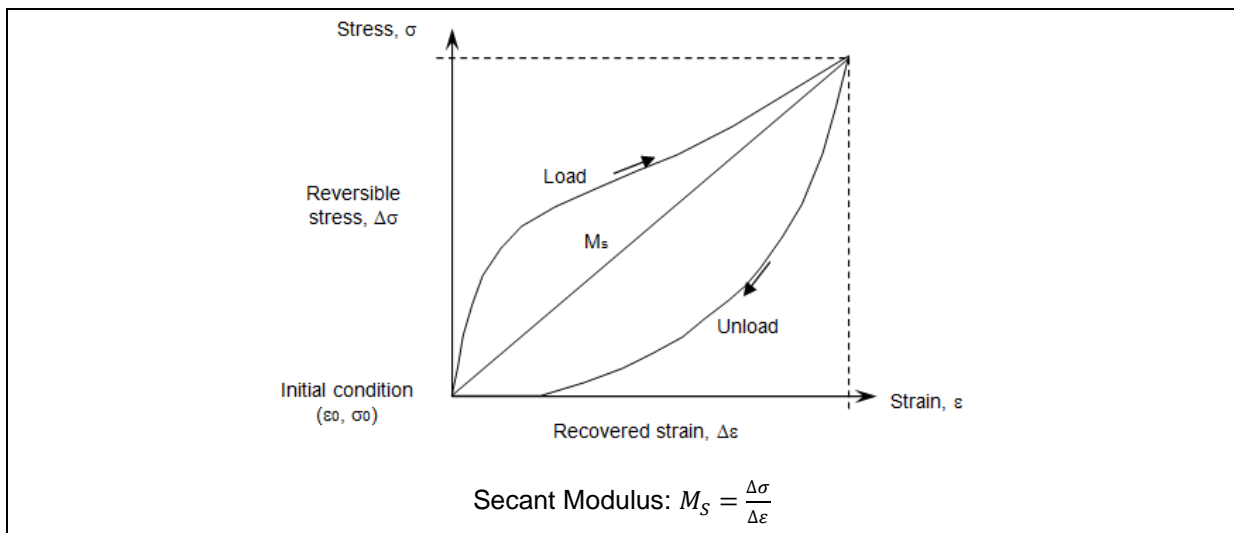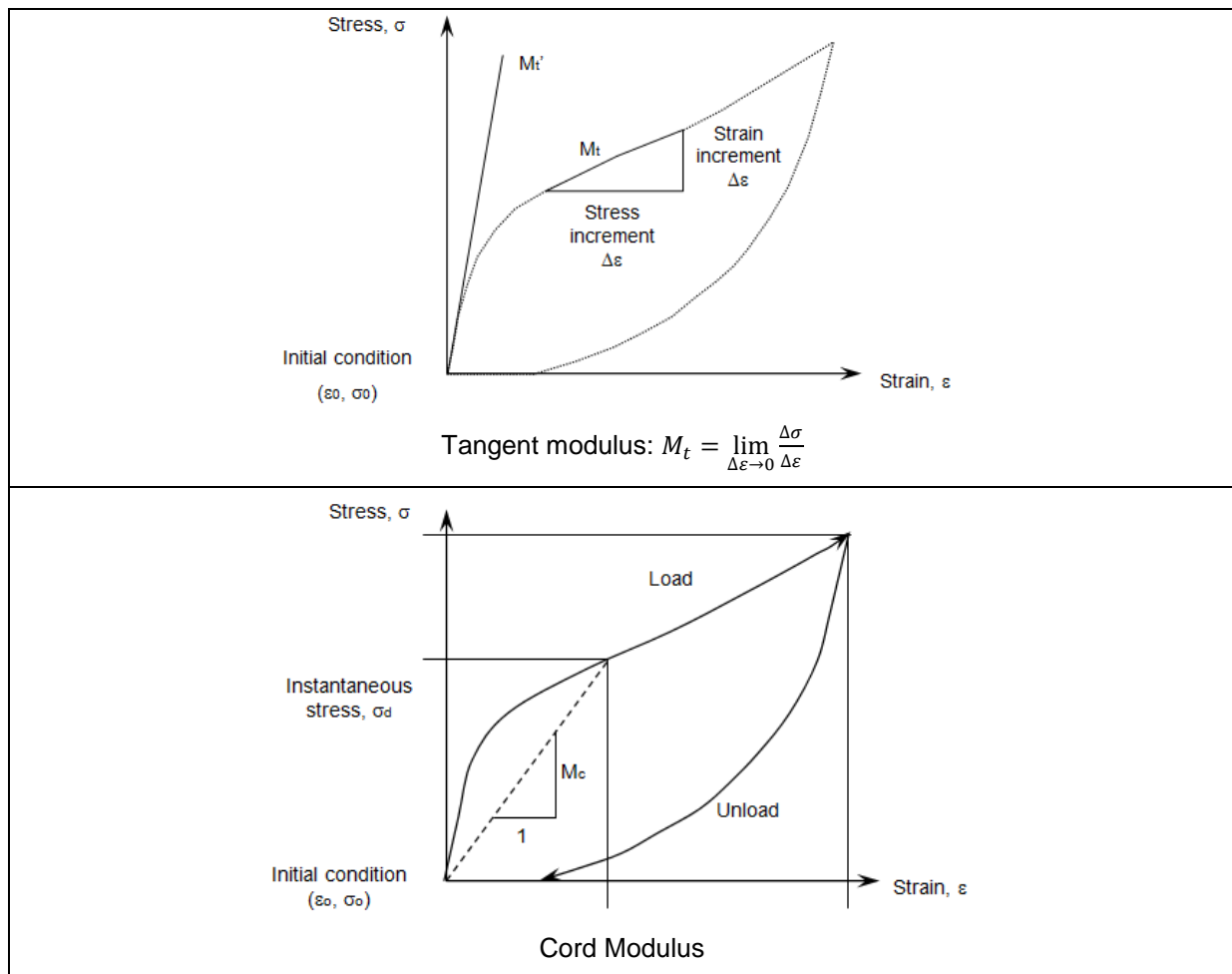
Cord Modulus

Figure 2.6: **Secant, tangent and cord modulus.**

Whenever reference is made to elasticity, stiffness, resilience, resilient modulus, etc. in this thesis, the definitions as given in this section apply.

2.2.2.3 *Factors influencing resilient response*

Apart from inherent material properties, such as the strength of aggregate of unbound material, which is specific to each material, other factors appears to affect the resilient behaviour of unbound material. Factors which seem to affect the resilient behaviour of unbound material in varying degrees are the following.

Effect of stress

Various studies conducted from the 1960's to late 1990's indicate that the level of stress is the most significant factor that affects resilient modulus of granular materials. The resilient modulus of untreated granular material was found to increase considerably with increase in confining pressure and sum of principal stresses. An increase in resilient modulus of 500 per cent was reported for a change in confining pressure from 20 kPa to 200 kPa by researchers for untreated granular material as described

by Lekarp *et al.* (2000). Conflicting results are reported regarding the influence of deviator stress or shear stress on unbound granular material, but it appears little to none (Lekarp *et al.*, 2000).

Effect of density

In general granular material responds stiffer and stronger with an increase in density. However, this statement seems true for uncrushed or partially crushed material, but not necessarily for crushed material. The resilient modulus was reported to increase with relative density for partially crushed aggregate, but remained almost unchanged when the aggregate was fully crushed (Maree, 1978; Lekarp *et al.*, 2000). It was also found that with an increase in fines content, density decreased for well graded aggregate (Hicks and Monismith, 1971). The effect of density seems to be less profound at high stress levels than at lower stress levels (Barksdale and Itani, 1989 as quoted by Lekarp *et al.*, 2000).

Effect of grading, fines content and maximum grain size

Previous research has shown that the stiffness of the material is dependent, to some degree, on the particle size and its distribution. Hicks and Monismith (1971) reported some reduction in resilient modulus with increasing fines content for well-graded partially or uncrushed material, with little to no effect on well-graded crushed material. Jorenby and Hicks (1989) (as quoted by Lekarp *et al.*, 2000) reported initial increase in stiffness followed by a reduction in stiffness when clayey fines were added to well-graded crushed aggregate due to the increased contacts as pore space is filled, followed by the excess fines displacing the coarse particles, ultimately being the particles on which stiffness relies (Lekarp *et al.*, 2000).

So far researchers could not conclusively prove the influence of grading and maximum grain size of material when these values are within acceptable specification ranges and it is deemed to have a minor influence on the stiffness. Various researchers have found that uniformly graded material yielded only slightly stiffer results than well-graded material (Lekarp *et al.*, 2000).

Effect of moisture content

Moisture content has been found to significantly influence unbound granular material both in in-situ conditions and laboratory conditions. Numerous researchers have reported that the resilient response of dry and most partially saturated material is similar, and that as saturation increased, especially past the optimum value, resilient response decreased (Lekarp *et al.*, 2000). Haynes and Yoder (1963) reported a 50 per cent decrease in resilient modulus in gravel as the degree of saturation increased from 70 to 97 per cent (as reported by Lekarp *et al.*, 2000).

De Beer and Maina (2008) noted that the inverse of bulk modulus indicates the compressibility of a substance, which in essence is what resilient modulus measures (compressibility or resistance to compressibility). The bulk modulus of water is 2 200 MPa, which would have great implications for saturated material when impulse loading is applied to determine the resilient modulus. The fact that a

decrease in resilient modulus is measured when a material is saturated or close to saturation may be because the resilient modulus of water is measured, instead of the granular material.

Excess pore-water pressure develops in saturated granular material under repeated loading. As pore-water pressure develop the effective stress in the material decreases with a subsequent decrease in both strength and stiffness of the material. It can be argued that it is the pore-water pressure which influences the resilient response rather than the level of saturation (Lekarp *et al.*, 2000). Another interpretation is that the moisture content determines the level of lubrication of particles which determines how easily deformation can take place, decreasing the resilient modulus (Lekarp *et al.*, 2000). It was also presented that localised pore suction pressure decrease with increased saturation, leading to lower inter particle contact forces (Lekarp *et al.*, 2000).

The effect of moisture on resilient behaviour is discussed in more detail in Section 2.2.3.2.

Effect of stress history and number of load cycles

Various researchers investigated the effect of stress history on resilient modulus through tri-axial testing (Dehlen, 1969; Boyce *et al.*, 1976; Hicks, 1970; Allen, 1973; Brown and Hyde, 1975 and Mayhew, 1983 as quoted by Lekarp *et al.*, 2000). Most reported that stress history manifests as some densification and particle re-arrangement, but that this can be reduced by some preloading of a few cycles of the current loading regime. Hicks (1970) reported that 100 loading cycles and Allen (1973) 1000 loading cycles would be sufficient as preloading (as quoted by Lekarp *et al.*, 2000). Brown and Hyde (1975) and Mayhew (1983) reported that stress history had limited effect if the stresses applied were kept low enough to prevent substantial permanent deformation in the material (as quoted by Lekarp *et al.*, 2000). Studies to investigate the effect of the number of load cycles applied on resilient modulus yielded that the resilient modulus would increase with increase in number of load cycles if some moisture were lost during the test. Otherwise, with no moisture loss, it was found that the resilient properties of the material would remain unchanged irrespective of the number of load cycles (Lekarp *et al.*, 2000).

Effect of particle shape

Numerous previous research studies have indicated that crushed aggregate provides better load spreading properties and have a higher resilient modulus than uncrushed or natural gravel (Hicks, 1970; Hicks & Monismith, 1971; Allen, 1973; Allen & Thompson, 1974; Thom, 1988; Barksdale and Itani, 1989; Thom & Brown, 1989 as quoted by Lekarp *et al.*, 2000). This is due to the angular shape of the particles versus the rounder particles of uncrushed or natural gravel. Studies also indicated that particles with a rough surface have a higher resilient modulus than smooth particles. Angular, rough particles versus round, smooth particles of various types of material were investigated by Barksdale & Itani (1989) who observed that the resilient modulus of the rough, angular crushed material was higher by a factor of 50 per cent at a low mean normal stress and 25 per cent at a high mean normal stress (as quoted by Lekarp *et al.*, 2000).

Effect of load duration, frequency and load sequence

Researchers agree that the effect of load duration, frequency and load sequence has little to no effect on the resilient behaviour of granular material when these values are within acceptable specification ranges (e.g. Seed *et al.*, 1965; Morgan, 1966; Hicks, 1970; Boyce *et al.*, 1976; Thom and Brown, 1987 and Allen, 1973 as quoted by Lekarp *et al.*, 2000).

The resilient behaviour of unbound granular material is also influenced by properties such as LL, PI, specific gravity and organic carbon contents (Bejarano and Thompson, 1999).

2.2.3   Moisture

The effect of moisture on resilient response was discussed briefly in Section 2.2.2.3 and is elaborated on in this section.

2.2.3.1   *Expressing moisture content*

There can be two or three phases of composition of a material, depending on the level of saturation. An unsaturated and fully saturated material consists of two phases, namely solid soil particles and pore-air, or in the latter instance, pore-water. Partially saturated material is composed of three phases, namely solid soil particles, pore-air and pore-water. Figure 2.7 depicts these various phases of composition (Craig, 1997).
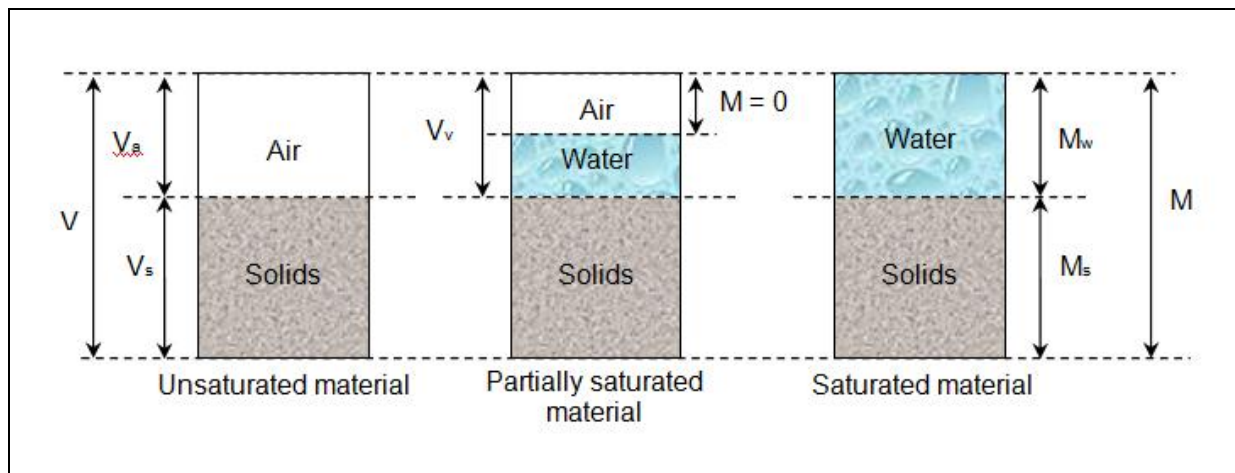
Figure 2.7:   Phase diagrams for unsaturated, partially saturated and saturated material.

Water content (w) or moisture content (m) is expressed by the ratio of the mass of water to the mass of solid particles in the material (Craig, 1997).

$$w \ (or \ m) = \frac{M_w}{M_s}$$ (2.1)

The degree of saturation (S_r) is the ratio of the volume of water to the total volume of void space (i.e. volume of air and volume of water) and can range between 0 and 1 (or 100 per cent) (Craig, 1997).

$$S_r = \frac{V_w}{V_v} \hspace{6cm} (2.2)$$

The degree of saturation generally reflects the combined effect of moisture content and density (Yeh and Su, 1989). Optimum Moisture Content (OMC) is the water content at which a Maximum Dry Density (MDD) is obtained for a particular compaction effort. Figure 2.8 illustrates density-water content curves for different compaction efforts (Craig, 1997). It is important to notice that the zero per cent air void line is also called the saturation line. Savage (2006) indicated that the OMC for compacted material occurs when the degree of saturation is approximately 80 per cent.
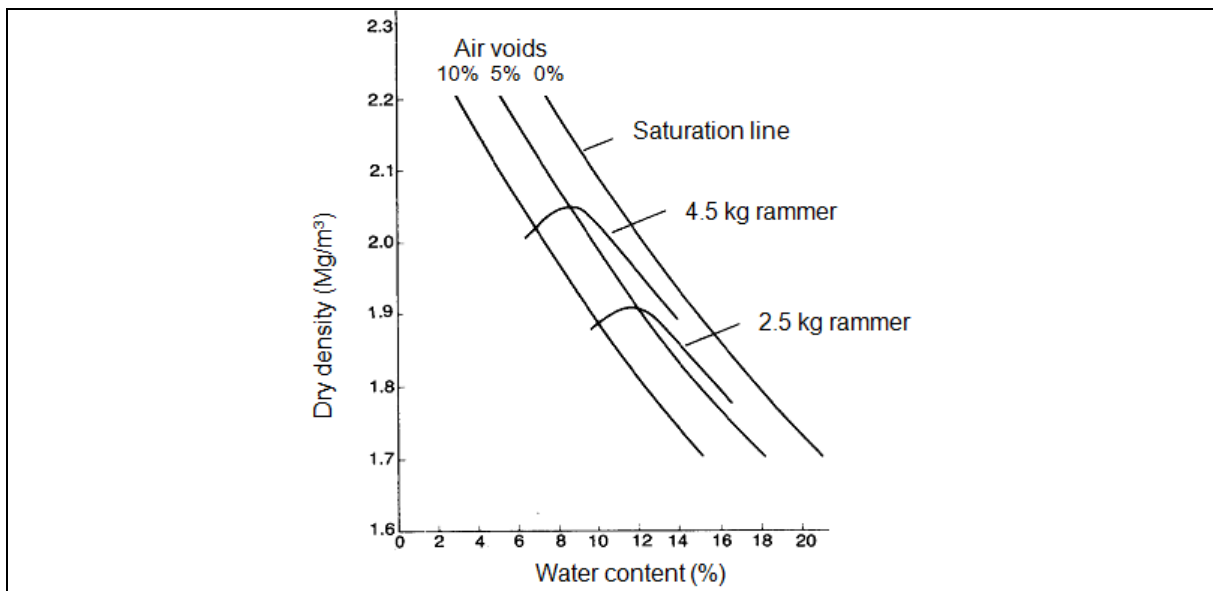
Figure 2.8: **Dry density-water content curves for different compactive efforts (Craig, 1997).**

When a material is compacted below OMC, the material tends to be stiff and difficult to compact (Craig, 1997). Density decreases with compaction above OMC, as increased water pushes soil particles apart by occupying more of the soil volume (Savage, 2006; Craig, 1997). This is illustrated in Figure 2.9 where the dry density curve starts to fall off after the maximum water content is added. The soil depicted in this figure is a silty clay, LL = 37, PI = 14, standard Proctor compaction.
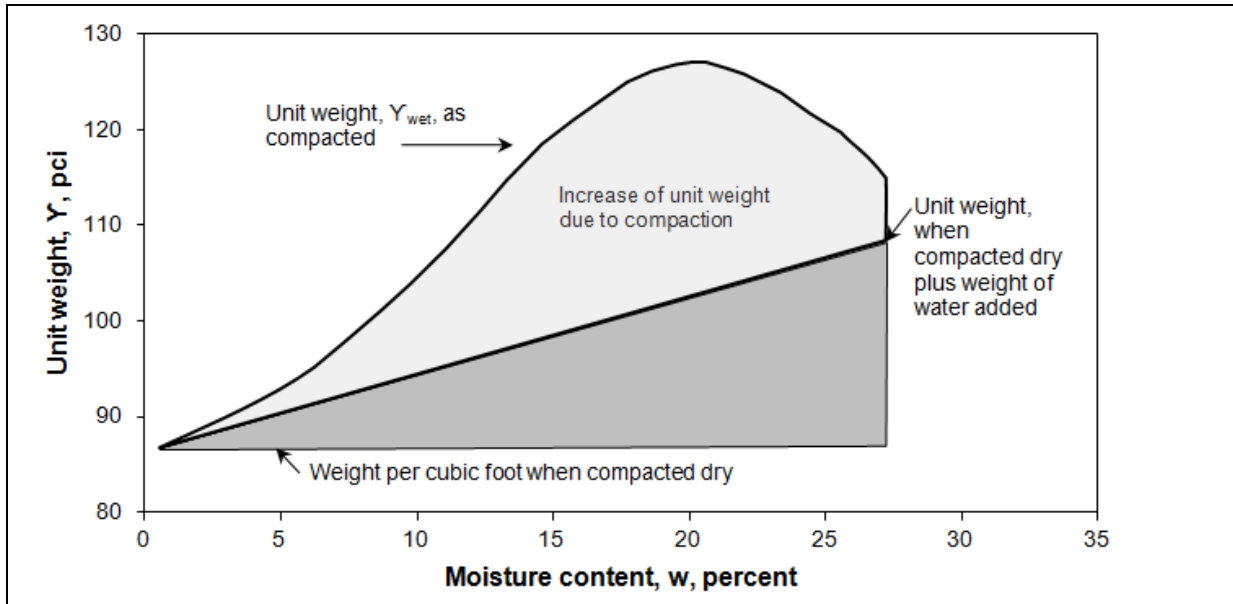
Figure 2.9: **Water content-density relationship indicating the increased density resulting from the addition of water and the applied compaction effort (TRB, 1990).**

2.2.3.2 Influence of moisture on resilient response

Research has proven that any increase in moisture content above OMC reduces the resilient modulus of a material (Cary and Zapata, 2010a). In studying the influence of moisture content on 11 subgrade soils from Tennessee, Drumm *et al.* (1997) tested resilient modulus at both OMC and higher than OMC. Apart from the expected decrease in resilient modulus with increase in moisture content, Drumm *et al.* (1997) also concluded that even relatively small changes in moisture content resulted in high impacts on the stress-strain behaviour (Craciun, 2009).

However, the extent of the influence of moisture content can be material dependent. For crushed stone, a slight decrease in resilient modulus with increasing moisture content was reported by Rada and Witczak (1981), but a higher decrease for a gravel aggregate (as quoted by Craciun, 2009). This was confirmed by Barksdale and Itani (1989) who investigate different aggregate types at varying moisture contents (as reported by Craciun, 2009).

The larger reduction in resilient modulus with increase in degree of saturation for fine-grained soil as opposed to that of coarse-grained soil, lead numerous researchers (Thom and Brown, 1987; Pappin *et al.*, 1992; Thadkamalla and George, 1995; Tian *et al.* 1998; Zapata *et al.*, 2007) to conclude that beside the moisture content, a loss of soil suction lead to a loss of strength (Craciun, 2009).

2.2.4 Suction pressure

In Section 2.2.2.3 the effect of moisture on resilient response was discussed and pore-water pressure was briefly mentioned. Pore-water pressure is defined as the pressure of water that is acting in a soil or

2-16

aggregate pore when it is saturated (Dawson, 2009). Pore-suction or suction pressure is defined as a pressure less than atmospheric in a soil or aggregate pore when it is partially saturated (Dawson, 2009). This negative pore-water pressure exerts an equal all-round internal suction which increases the effective stress, stiffness and shear strength of the material (Theyse and Kannemeyer, 2010). In this section suction pressure is defined and discussed in more detail.

2.2.4.1 *Definition of suction*

Soil suction, also referred to as total suction (Ψ), consist of two components namely matric suction ($u_a - u_w$) and osmotic suction (π) and can be defined as follows (Van Heerden, 2002; Craciun, 2009):

$$\Psi = (u_a - u_w) + \pi \tag{2.3}$$

Where

u_a = pore-air pressure;

u_w = pore-water pressure.

2.2.4.2 *Matric suction*

Matric suction is a function of the surface tension generated by the air-water interface within the soil structure (Craciun, 2009). Kelvin's equation expresses this definition as follow:

$$(u_a - u_w) = \frac{2T_s}{R_s} \tag{2.4}$$

Where

$(u_a - u_w)$ = matric suction;

T_s = surface tension of water;

R_s = radius of curvature of the meniscus.

Matric suction is inversely proportional to radius of curvature of the meniscus, i.e. as the matric suction of a soil increases, the radius of curvature of the meniscus decreases. In a soil structure the size of the meniscus is equivalent to the pore size of the soil matrix (Craciun, 2009). It can be assumed that for natural material the average or effective pore diameter is approximately 20 per cent of the effective grain size, D_{10} (Holtz and Kovacs, 1981 as quoted by Van Heerden, 2002). From this assumption the theoretical matric suction for a soil can be estimated.

Soil-Water Characteristic Curve

A Soil-Water Characteristic Curve (SWCC) illustrates the relationship between matric suction and degree of saturation over the possible range of saturation values from 0 to 100 per cent. Figure 2.11 illustrates such a curve schematically. The air-entry value is the point at which water starts to be expelled from the soil and air voids start to form in the inter-particle voids. This is followed by a primary transition

zone where more water is expelled and the degree of saturation reduces rapidly. During the secondary transition zone, water is still expelled, but the rate of change in the degree of saturation reduces. When little water is being expelled from the soil, resulting in a small reduction in the degree of saturation, the SWCC region is called the residual or de-saturation zone (Vanapalli *et al.*, 1996b as quoted by Theyse, 2009).

Figure 2.11 depicts such a curve for different sands (as quoted by Craciun, 2009) indicating the matric suction versus volumetric water content. Figure 2.12 depicts another form of the SWCC where the degree of saturation versus matric suction is depicted (Ekblad, 2006).
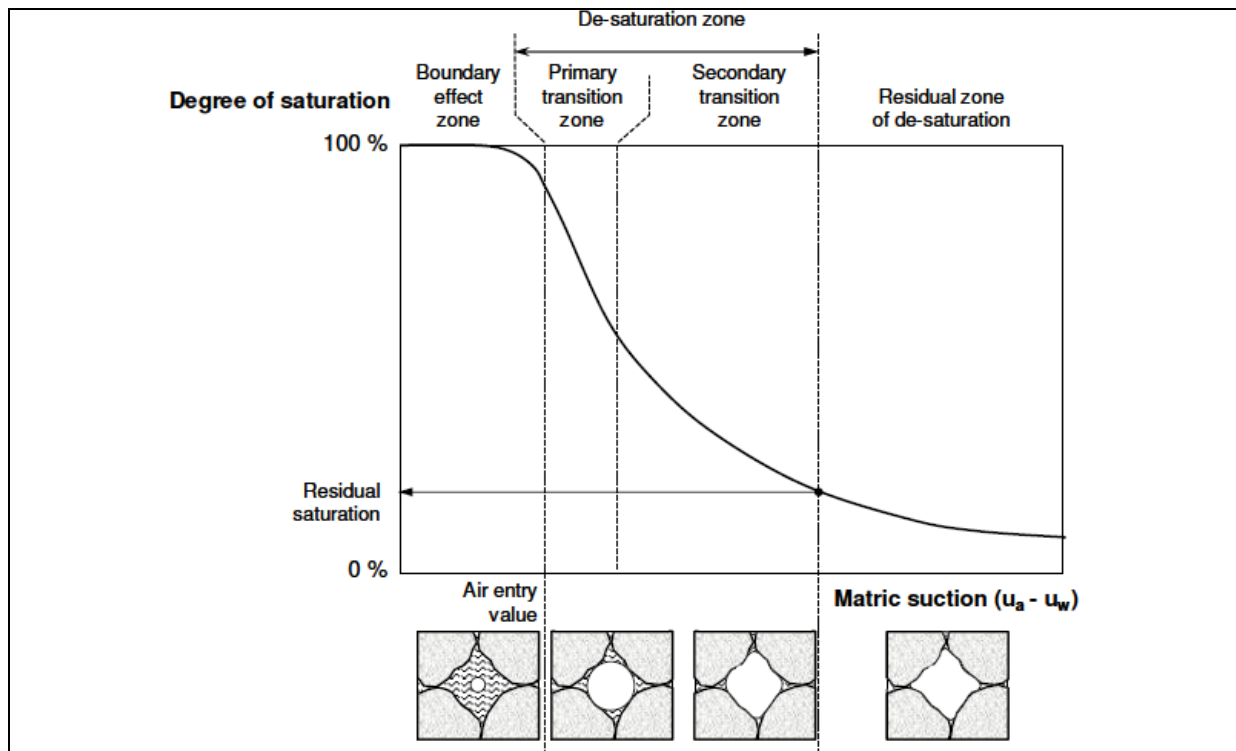
Figure 2.10:   Schematic illustration of the soil-water characteristic curve (Theyse, 2009).
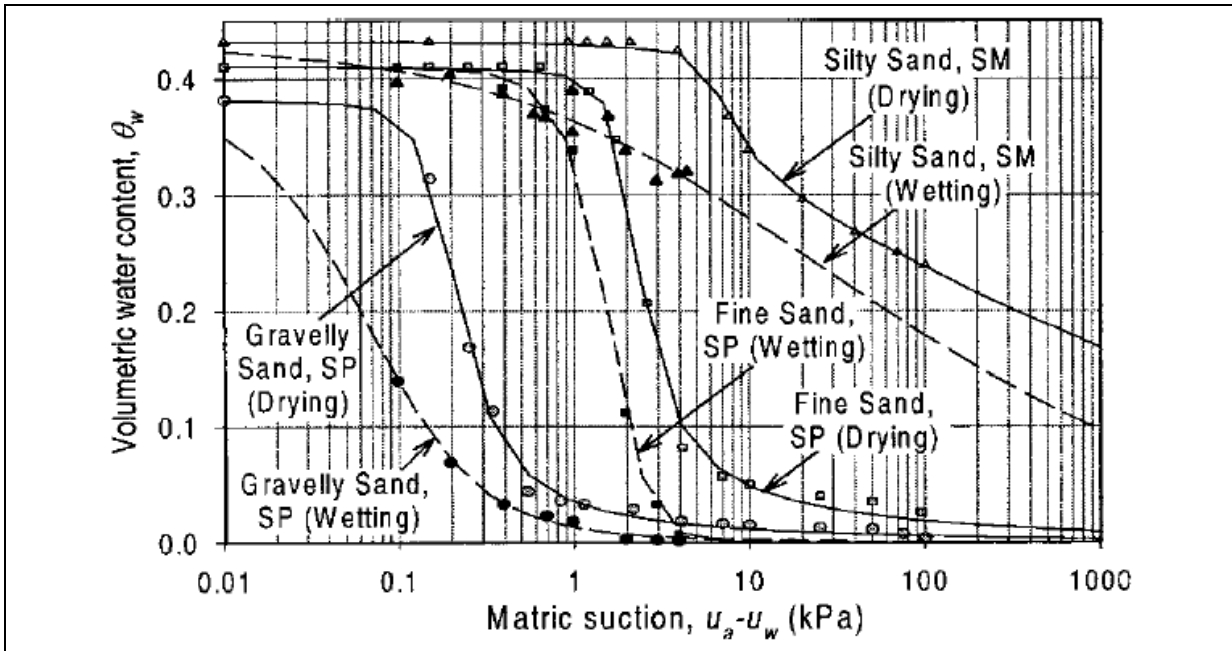
Figure 2.11:   SWCCs for different sands (Yang et al., 2004b as quoted by Craciun, 2009).
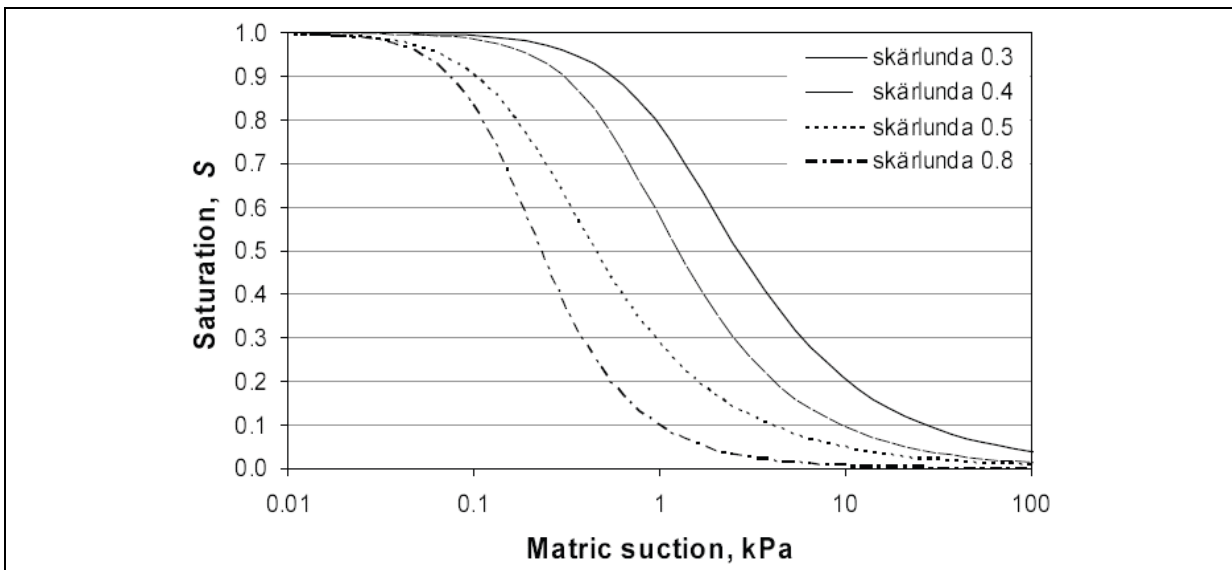
Figure 2.12:   SWCCs for crushed aggregate from Skärlunda, Sweden (Ekblad, 2006).

Various factors influence the matric suction profile of a soil, since matric suction is closely related to the surrounding environment. Blight (1980) as quoted by Van Heerden (2002) listed several factors, namely:

- Ground surface condition – The matric suction profile below an uncovered ground surface is affected significantly by environmental changes, while a covered ground surface is not;
- Environmental conditions – The matric suction in the soil increases during dry seasons and decreases during wet seasons;

2-19

- Vegetation – Vegetation on the ground surface has the ability to apply a tension to the pore-water of up to 2 MPa through the evapotranspiration process. This process removes water from the soil thus increasing the matric suction;

- Water table – The depth of the water table influences the matric suction. The deeper the water table, the higher the possible matric suction; and

- Permeability of the soil – The permeability of a soil indicates its ability to drain water, which dictates the degree to which environmental changes will affect matric suction.

2.2.4.3   Osmotic suction

Osmotic or solute suction represents a function of another solute (normally salt) in the pore water of saturated and partially saturated soils. It was defined by Aitchison (1965) as "*the equivalent suction derived from the measurement of the partial pressure of the water vapour in equilibrium with a solution identical in composition with the soil water, relative to the partial pressure of water vapour in equilibrium with free pure water*". Osmotic suction is generally negligible and a change in matric suction is seen as a change in total suction (Craciun, 2009).

2.2.4.4   Suction measurement

Various techniques and methods of measuring total suction, matric suction and osmotic suction separately exists. Essentially these techniques measure the partial vapour pressure of soil water (Van Heerden, 2002). Table 2.4 lists the more common methods of suction measurement together with their measurement ranges and response times.

Table 2.4:   Common suction measurement devices (from Van Heerden, 2002).

Instrument	Suction component	Suction range (kPa)	Response time
Filter paper (Ho, 1979; McKeen, 1981; Chandler and Gutierrez, 1986)	Total and matric	10 to 30 000	7 days
Psychrometer (Richards, 1965; Rawlins and Dalton, 1967)	Total	100 to 8 000	Minutes
Suction plate (Ridley, 1993)	Matric	0 to 90	Several hours
Pressure plate (Schofield, 1935)	Matric	1 to 1 500	Several hours
Thermal blocks (Sattler and Fredlund, 1989)	Matric	0 to 400	24 hours to 3 weeks
Gypsum blocks (Aitchison *et al.*, 1950)	Matric	100 to 1 000	2 to 3 weeks
Tensiometer (Ridley *et al.*, 1998)	Matric	0 to 90	Up to 2 hours
Imperial College Suction Probe (Ridley and Burland, 1993)	Matric	0 to 1 800	1 to 3 hours

However, suction measurement is notoriously difficult, particularly for granular materials, due to the low suction values occurring (Thom and Brown, 1987). Suction values can be deduced using the effective stress principle which is discussed in Section 2.2.4.5.

2.2.4.5 *Importance of estimation of resilient response*

Bishop formulated an effective stress equation for unsaturated material in 1959 (Bishop, 1959 as quoted by Theyse, 2009). The equation states that effective normal stress is increased by the product of the Bishop's parameter and matric suction (Equation 2.5). Bishop's parameter is related to degree of saturation and has the same limits as degree of saturation ($0 \leq \chi \leq 1$) (Theyse, 2009).

$$\sigma_n' = (\sigma_n - u_a) + \chi(u_a - u_w)$$
(2.5)

Where

σ_n' = effective normal stress (kPa);

σ_n = total normal stress (kPa);

u_a = air-pressure (kPa);

u_w = water pressure (kPa);

χ = Bishop's parameter related to the degree of saturation (Theyse, 2009).

The effect of suction on effective stress can be illustrated by the following scenario: When a sample is prepared for yield strength tri-axial testing and allowed to dry back from the target test moisture content, suction pressure develop in the sample. Suction pressure is therefore present in the sample before external confinement pressure is applied during the tri-axial test. The effect of this additional confinement is reflected in test results at zero confinement pressure (Theyse, 2009).

When considering Bishop's formulation for unsaturated material and the effect of suction reflected in yield strength tri-axial results, it can be concluded that suction pressure will increase the effective stress in a partially saturated material when an external load is applied (Figure 2.13).
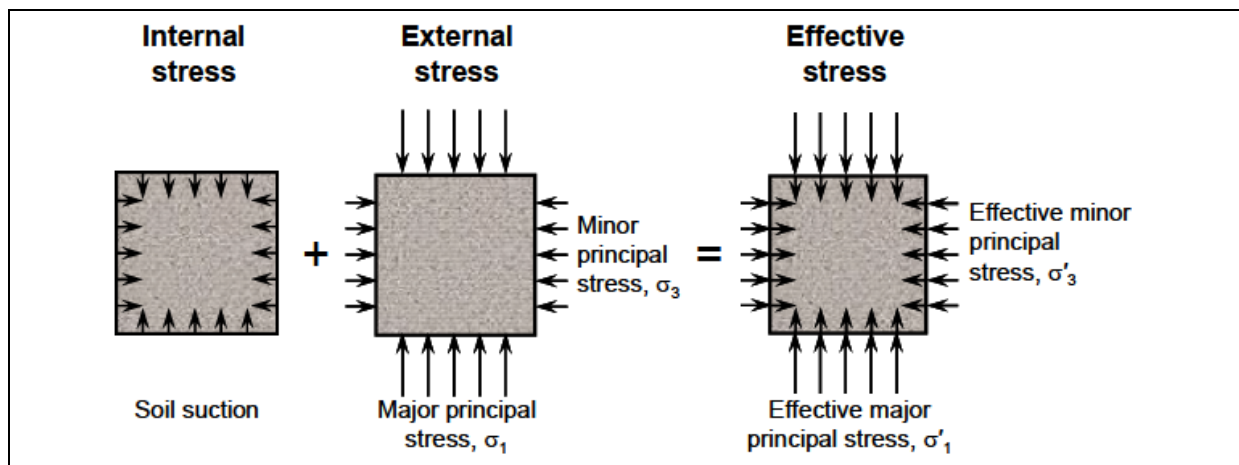
Figure 2.13:   **Effective stress in partially saturated granular material (Theyse, 2006).**

Resilient response is stress dependent and therefore suction pressure's impact on the effective stress impacts on the resilient response of a material (Theyse, 2008b).

2.2.5 Modelling

2.2.5.1 Levels of technology for evaluation

Three levels of technology for evaluation can be defined when the complexity of input data, behavioural models and decision criteria applicable to a specific problem are considered. The technology level of the problem may be basic, intermediate or advanced (Steyn, 2001).

Basic technology levels define those technologies where the input data, behavioural models and outputs are simple and from which general trends can be observed after analysis. These technologies supply sufficiently acceptable answers to specific problems. A specific technology may be at basic level due to lack of specialised input data, lack of adequately applicable behavioural model or lack of computational capacity (Steyn, 2001).

Intermediate technologies are defined as those where the input data, behavioural models and outputs are more detailed and interaction between various parameters may be observed. At this level, some aspects may be advance (e.g. input data), while other parameters may still be limited (e.g. behavioural models) which limits the overall process, therefore no benefit is gained from the advanced parameters (Steyn, 2001).

Advanced technology levels are those where the input data, behavioural models and outputs are as detailed as physically and practically possible. At this level, basic research can be performed and the confidence in the output is high. Increasing a technology level to advance level, will generally require an increase in capacity and resources (Steyn, 2001).

The Mechanistic-Empirical Pavement Design Guide (MEPDG) (NCHRP (2004)), based on the same principles as discussed above, adopted a hierarchical approach to design inputs, which aims to give the designer more flexibility in obtaining design inputs for a project based on the criticality of the project and available resources. The hierarchical approach is applied to traffic, materials and environmental inputs. In general, Level 1 inputs provide for the highest level of accuracy and thus would have the lowest level of uncertainty or error. Level 2 inputs provide an intermediate level of accuracy and would be closest to the typical procedures used with earlier editions of the AASHTO Guide. This level could be used when resources or testing equipment are not available for tests required for Level 1. Level 2 inputs typically would be user-selected, possibly from a database, could be derived from a limited testing program, or could be estimated through correlations. Level 3 inputs provide the lowest level of accuracy. This level might be used for designs where there are minimal consequences of early failure (e.g. lower volume roads). Inputs typically would be user-selected values or typical averages for the region (NCHRP, 2004).

For resilient modulus calculations at Level 1, MEPDG refers the designer to a constitutive equation that relates resilient behaviour to bulk stress, octahedral shear stress, and atmospheric pressure at any given location within the pavement. Input Levels 2 and 3 do not consider stress sensitivity. At Level 2, the designer estimate resilient behaviour at a reference moisture condition which is determined near at or near the optimum moisture content and maximum dry density. For input Level 3, an estimate of the resilient behaviour is sufficient (NCHRP, 2004).

Table 2.5 indicates the technology levels pertinent to the evaluation of resilient response as influenced by moisture. From Table 2.5 it is clear that to have an advance resilient response model, but the input parameters still depend on basic moisture content measurements is not ideal. The detail input data required is not obtainable from a basic moisture content determination. The aim is to have input parameters of the same level of technology as the model or one level lower. This thesis will consider a resilient response model of which the technology level is applicable, the model as generally valid as possible, and the input as easily accessible as possible to the practitioner.

Table 2.5:   Levels of technology to consider when modelling.

Technology Level	Resilient Response Model	Moisture	Material Properties
Advanced technology	Model based on advance tri-axial testing to determine the resilient response, incorporating moisture and suction measured.	Moisture content and suction measured.	Properties known at microscopic level, e.g. mineral composition
Intermediate technology	Model based on advance tri-axial testing to estimate resilient response	Moisture content of in-situ material measured and suction estimated.	Properties known at macroscopic level, e.g. plasticity index
Basic technology	CBR-M_R relationship used estimate resilient response	Moisture content of in-situ material measured.	None

2.2.5.2   Modelling of resilient response

Granular material is one of the main material components in any pavement structure and it is therefore vital to model its behaviour accurately. The three common modelling approaches utilised to model the behaviour of granular material is through empirical –, mechanistic – and mechanistic-empirical models.

Empirical models usually contain a dependent variable which is some indicator of the performance it models. Subjective indicators (riding quality, serviceability, etc.) and objective indicators (roughness, rutting, etc.) are used as dependent variables. These indicators are related to one or more explanatory variables, such as pavement structural strength, traffic loading and environmental conditions (Prozzi and Madanat, 2002).

Empirical models are often developed based on statistical considerations and not on actual behaviour. Models may include or exclude variables based on the statistical significance, while others, include

parameters regardless of their statistical significance, because it relates to the actual physical process it tries to simulate (Prozzi and Madanat, 2002).

Mechanistic models are based on the use of material behaviour and pavement response functions, which are believed to represent the actual behaviour of the pavement structure under the combined actions of traffic and the environment. Such models are simplifications and are applicable only under specified conditions (Prozzi and Madanat, 2002).

Mechanistic-empirical models make use of material characterisation (laboratory or insitu testing) and pavement response models (usually multi-layer linear elastic or finite element type models) to determine pavement response. Pavement response is correlated to pavement performance and finally calibrated to an actual pavement structure. The calibration consists of applying a bias correction factor (shift factor), which is usually based on engineering judgement and not on any statistical procedure (Prozzi and Madanat, 2002). Figure 2.14 illustrates the various options when using mechanistic-empirical modelling to model resilient response and on which basis material modelling will be discussed further (Theyse, 2008b). This thesis focuses on separate response modelling, in particular that of material models for unbound granular material.

Figure 2.14 continue…
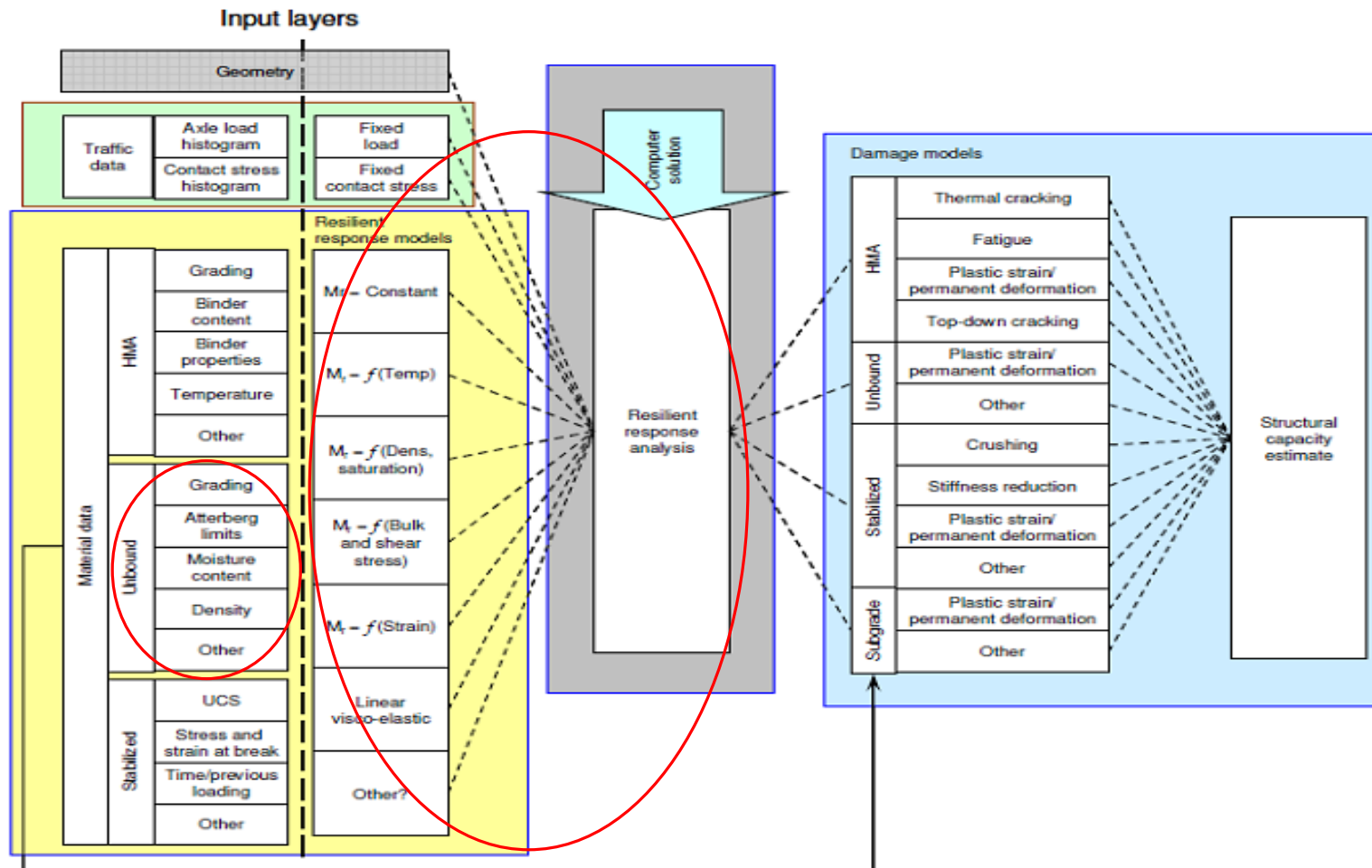
Figure 2.14: Modelling options for resilient response in mechanistic-empirical design (Theyse, 2008b).

From Figure 2.15 it can be seen that resilient modulus is not a linear function. Theyse (2008a) explained that often the terms 'non-linear behaviour' and 'stress-dependent behaviour' is referred to without consideration for the distinct difference between the two. This difference is depicted in Figure 2.15, which shows non-linear behaviour, stress-dependent behaviour and non-linear, stress-dependent behaviour. The majority of research has been focused on calibrating stress-dependent resilient modulus models (Theyse, 2008a).
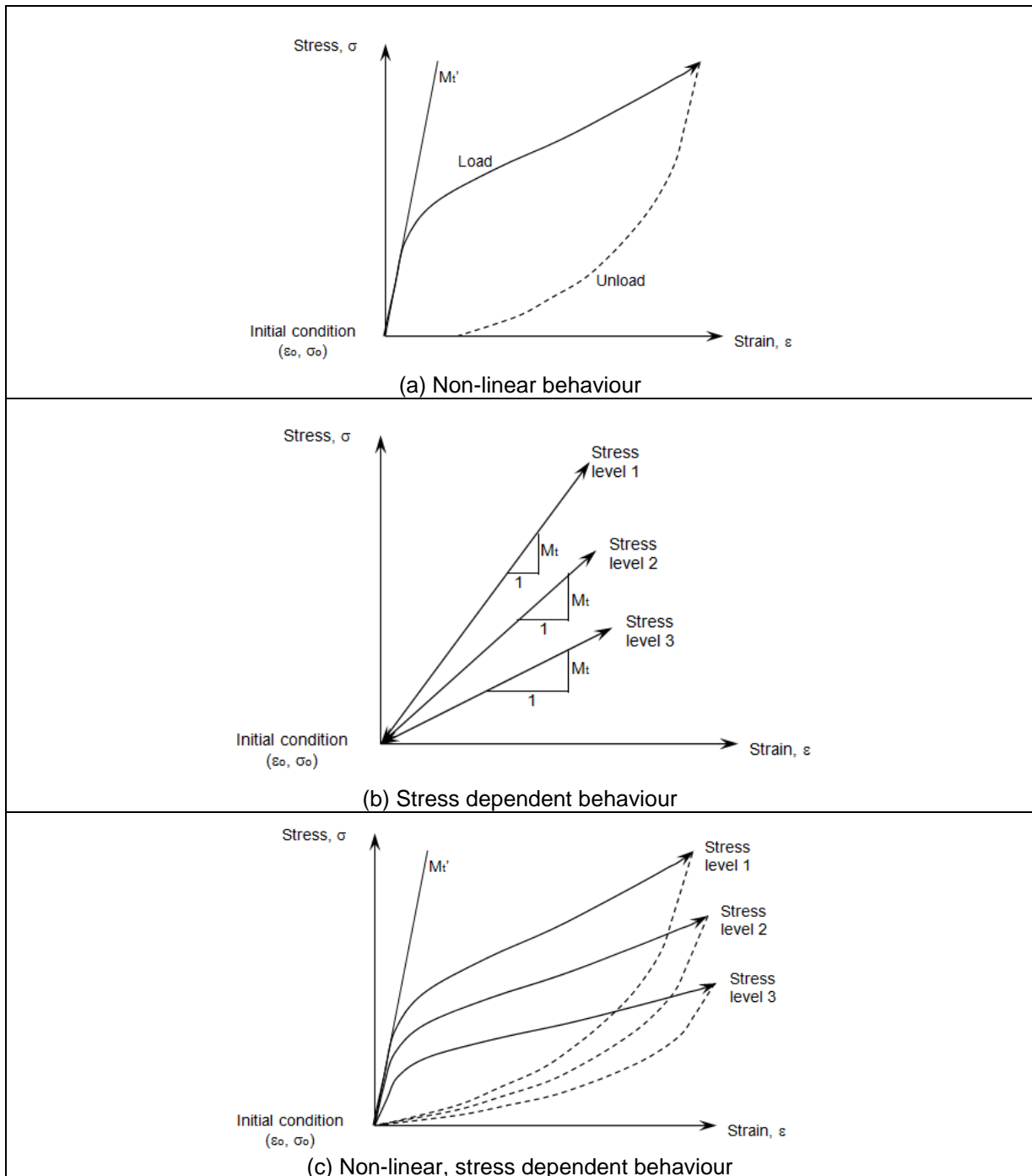
Figure 2.15: **Non-linear and stress-dependent resilient behaviour (Theyse, 2008b).**

2-27

A few models based on bulk (K) and shear (G) modulus constants of elasticity have also been developed, but is not as widely used as those based on elastic modulus (Theyse, 2008a). Most of these models are based on curve fitting procedures utilising laboratory tri-axial testing results (Lekarp *et al.*, 2000).

2.2.5.3 *Resilient response models*

From Section 2.2.5.2 it is clear that natural unbound granular material exhibit complex nonlinear, stress-dependent behaviour (Theyse, 2008a). Lekarp *et al.* (2000) concluded that researchers seems to agree that resilient response is influenced most by the level of applied stresses and the amount of moisture present in the material. Several authors have shown that the resilient response of unbound granular material can be reasonably characterised by using stress dependent models which express the modulus solely as nonlinear power functions of the applied stress states (Hicks and Monismith (1971) and Uzan (1985)).

The most widely used approach to model the resilient behaviour of natural granular material, is to utilise the stress-strain relationship of the material, which is characterised by a stress dependent resilient modulus and constant or stress dependent Poisson's ratio (Lekarp *et al.*, 2000). Literature suggests the following:

- Resilient modulus increases greatly with increase in confining pressure;
- Resilient modulus increases greatly with increase in sum of principal stresses, and slightly with deviator stress;
- Resilient Poisson's ratio increases directly with deviator stress;
- Resilient Poisson's ratio increases inversely with confining pressure; and
- At high saturation levels, resilient modulus and Poisson's ratio reduces drastically (Lekarp *et al.*, 2000).

Another approach is to decompose the stresses and strains comprising the stress-strain relationship into volumetric and shear components. In this approach the resilient response of the material is defined by bulk and shear moduli. From a theoretical point of view, the nonlinear response of natural material is addressed, and a more realistic physical meaning in a 3-dimensional stress regime is obtained. However, such models are complex and parameter values are difficult to obtain from collected data (Lekarp *et al.*, 2000).

Figure 2.16 shows schematically how some of the well-known stress dependent resilient response models take various parameters into account. For example, the k-θ model incorporates bulk stress, which may also be expressed in terms of deviator stress, but do not have a 3-dimensional component such as the Universal model. Table 2.6 summarise these resilient response models. More background about each of the listed models is given in Appendix B.
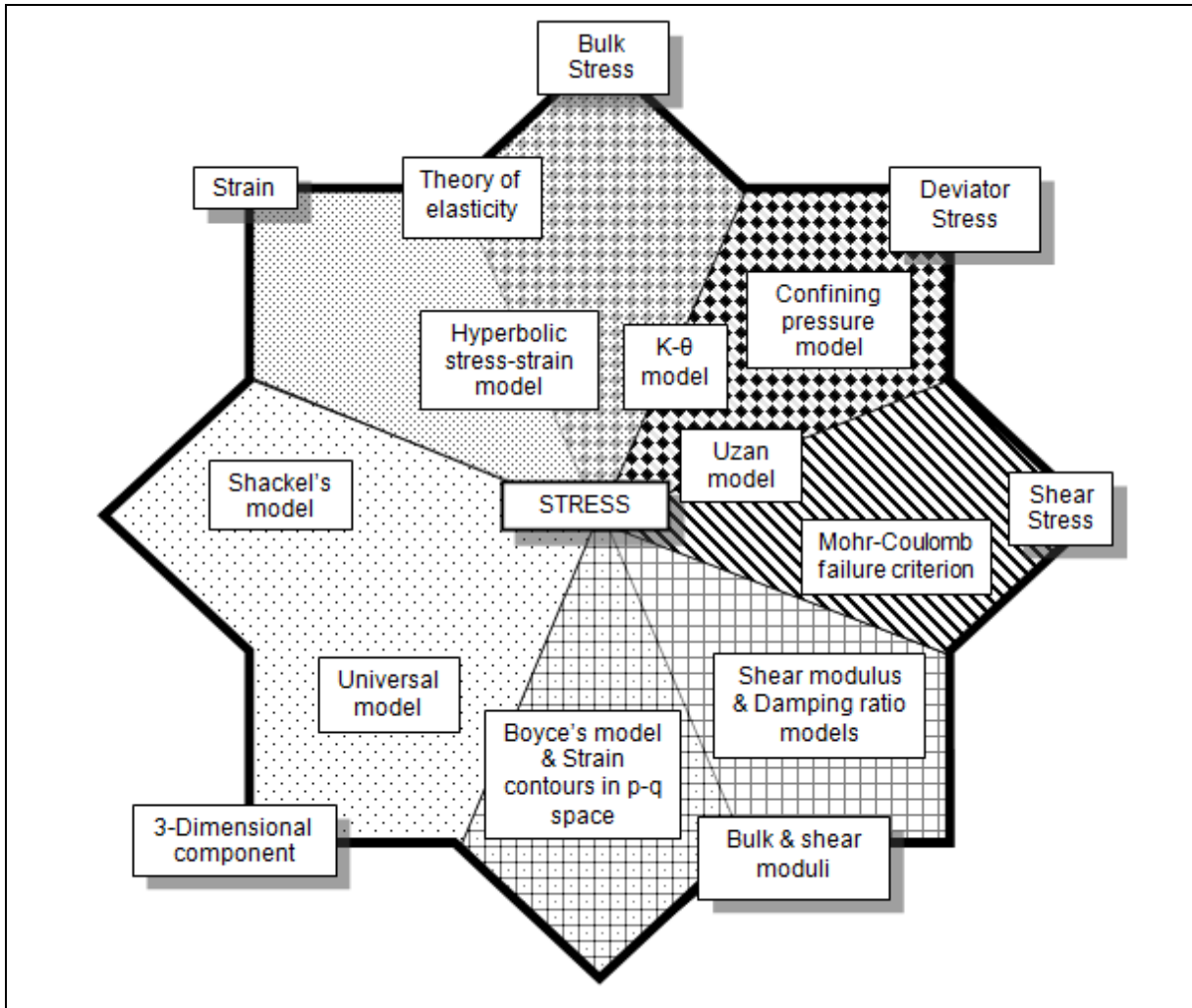
Figure 2.16: Schematic diagram of stress-dependent resilient response models.

Table 2.6: **Summary of stress-dependent resilient response models.**

Name of model	Model formulation	Model definition	Basic concept of model
Theory of elasticity	$M_R = \frac{\Delta(\sigma_1 - \sigma_3)}{\varepsilon_{1,r}}$	M_R = resilient modulus; Δ = 'change in'; $\sigma_1; \sigma_3$ = major & minor principal stress; $\varepsilon_{1,r}; \varepsilon_{3,r}$ = recoverable axial & horizontal strain	$M_R = \frac{stress}{strain}$
Mohr-Coulomb failure criterion	$\tau_{max} = c + \sigma_n tan\phi$	τ_{max} = shear strength; σ_n = normal stress at failure; c = cohesion intercept; $tan\phi$ = slope of the failure envelope; ϕ = friction angle.	$shear\ stress = c + normal\ stress$ Assume linear elastic, perfectly plastic behaviour.
Confining pressure model	$M_R = K_1(\sigma_3)^{K_2}$ or $M_R = K_1\left(\frac{\sigma_3^{K_2}}{p_0}\right)$	σ_3 = confining pressure; p_0 = reference pressure, often equal to atmospheric pressure (101,3 kPa) K_1, K_2 = regression coefficients.	$M_R = K_1(stress)^{K_2}$ Model yielded low correlation coefficients. Various modifications made to basic form of model.
K-θ model	$M_R = K_1\theta^{K_2}$ or $M_R = K_1\left(\frac{\theta}{p_0}\right)^{K_2}$	θ = bulk stress = $(\sigma_1 + \sigma_2 + \sigma_3)$ or $(\sigma_1 + 2\sigma_3)$ or $(\sigma_d + 3\sigma_3)$ where $\sigma_d = (\sigma_1 - \sigma_3)$ (Kim, 2007 & Theyse, 2008a) p_0 = reference pressure (101,3 kPa) K_1, K_2 = regression coefficients	$M_R = K_1(stress)^{K_2}$ Assume Poisson's ratio constant. Take confinement into account. Neglects shear stress.

2-30

Name of model	Model formulation	Model definition	Basic concept of model
Uzan model	$M_R = k_1 \theta^{k_2} \sigma_d^{k_3}$	θ = bulk stress σ_d = deviator stress, k_1, k_2, k_3 = regression coefficients	$M_R = k_1 stress^{k_2} shear\ stress^{k_3}$ Assume Poisson's ratio constant. Take confinement into account.
Universal model	$M_R = k_1 \cdot P_a \cdot \left(\frac{\theta}{P_a}\right)^{k_2} \cdot \left(\frac{\tau_{oct}}{P_a}\right)^{k_3}$	θ = bulk stress τ_{oct} = octahedral shear stress, P_a = reference pressure k_1, k_2, k_3 = regression coefficients	$M_R = k_1 \cdot stress^{k_2} \cdot (3D\ shear\ stress)^{k_3}$ Assume Poisson's ratio constant. Take confinement into account.
Hyperbolic stress-strain model	$\frac{\varepsilon}{\sigma_1 - \sigma_3} = \left[\frac{1}{E_i} + \frac{\varepsilon}{(\sigma_1 - \sigma_3)_u}\right]$	E_i = initial tangent modulus $(\sigma_1 - \sigma_3)_u$ = maximum or ultimate stress difference ε = axial strain	$\frac{strain}{stress} = \left[\frac{1}{E\ modulus} + \frac{strain}{(stress)_{ultimate}}\right]$ Neglects shear stress. Empirically derived parameters and limited to static loading.
Shackel's model	$M_R = K_1 \left[\frac{(\tau_{oct})^{K_2}}{(\sigma_{oct})^{K_3}}\right]$ $\sigma_{oct} = \frac{1}{3}(\sigma_1 + \sigma_2 + \sigma_3) = \frac{1}{3}I_1$ $\tau_{oct} = \frac{1}{3}[(\sigma_1 - \sigma_2)^2$ $\qquad\qquad + (\sigma_2 - \sigma_3)^2]$ $\qquad = \frac{\sqrt{2}}{3}(I_1^2 - 3I_2)^{\frac{1}{2}}$	K_1 = material regression constants obtained from tri-axial test data; I_1 = first stress invariant; I_2 = second stress invariant.	$M_R = K_1 \left[\frac{(3D\ shear\ stress)^{K_2}}{(3D\ normal\ stress)^{K_3}}\right]$ Early advance non-linear model, since it is defined by stress invariants.

2-31

Name of model	Model formulation	Model definition	Basic concept of model
Shear modulus & Damping ratio models	$E = \frac{\sigma_d}{\varepsilon_1}$ $\gamma = (1+\nu)\varepsilon$ $G = \frac{E}{2(1+\nu)}$ $D = \frac{A_L}{4\pi A_T} \times 100$	σ_d = deviator stress; γ = shear strain; ε_1 = axial strain; ν = Poisson's ratio; A_L = area of hysteresis loop which is equivalent to total energy dissipated in one cycle; A_T = total area representing the maximum strain energy	$E = \frac{shear\ stress}{strain}$ Based on cyclic triaxial test & resonant column test. Assumes Poisson's value in calculations.
Bulk-Shear modulus models (Boyce's model & Strain contours in p-q space)	$K = \frac{K_i p^{(1-n)}}{1 - \beta\left(\frac{q}{p}\right)^2}$ and $G = G_i p^{(1-n)}$ Volumetric strains & deviatoric strains of the model are related to the mean normal stress & deviatoric stress as follows: $\varepsilon_v = \left(\frac{1}{K_i}\right) p^n \left[1 - \beta\left(\frac{q}{p}\right)^2\right]$ and $\varepsilon_q = \left(\frac{1}{3}G_i\right) p^n \left(\frac{p}{q}\right)$	β = $(1-n)\frac{K_i}{6G_i}$ p = mean normal stress q = deviator stress ε_v = volumetric strain ε_q = shear strain	$strain = (bulk\ modulus) \cdot stress \cdot [1 - (bulk\ \&\ shear\ modulus)(stress)^2]$ $shear\ strain = (shear\ modulus) \cdot stress$

2-32

2.2.5.4 Resilient response models incorporating moisture and density

In Section 2.2.5.3 it was stated that along with the level of stresses applied, the moisture present in the material influence the resilient behaviour of the material (Lekarp *et al.*, 2000). The models reviewed in the preceding section focussed only on the stresses applied to describe the behaviour of material and no material parameters were taken into account. Emery (1985) concluded that material type, along with the moisture state of the material influences resilient behaviour. Closely linked to material type and moisture state is density, to which was referred to Section 2.2.3.1 (Yeh and Su, 1989). This section reviews some resilient response models which take moisture, in its various forms, as well as density into account.

2.2.6 International researchers

Table 2.7 summarises the international researcher's equations broken down into the basic concepts that are applied. A short discussion on each model in Table 2.7 follows.

2.2.6.1 Crockford et al. model

Essentially, this model simplifies to the universal model of Witczak and Uzan (1988) when the moisture term and normalised unit weight term is removed (Kim, 2007).

2.2.6.2 Lytton model

Lytton (1995) also utilised the universal model of Witczak and Uzan (1988) to incorporate the principles of unsaturated soil mechanics. Lytton was of the opinion that unbound materials in pavements are normally unsaturated and incorporated a suction term to evaluate the properties of unsaturated granular materials (Kim, 2007).

2.2.6.3 NCHRP Mechanistic Empirical Pavement Design Guide (MEPDG) model

The MEPDG (NCHRP, 2004) included a generalised constitutive model to characterise the resilient modulus of unbound aggregates in Chapter 2 of the guide. The equation is as follows and is a modification of the universal model:

$$M_R = k_1 \cdot P_a \cdot \left(\frac{\theta}{P_a}\right)^{k_2} \cdot \left(\frac{\tau_{oct}}{P_a} + 1\right)^{k_3} \tag{2.6}$$

Where

θ	= bulk stress
τ_{oct}	= octahedral shear stress,
P_a	= reference pressure
k_1, k_2, k_3	= regression coefficients

Table 2.7: Summary of international resilient response models incorporating moisture and density.

Name of model	Model formulation	Basic concept of model
Crockford *et al.* model	$M_R = \beta_0 \left(\theta + 3\Psi \frac{V_w}{V_t}\right)^{\beta 1} (\tau_{oct})^{\beta 2} \left(\frac{\gamma}{\gamma_w}\right)^{\beta 3}$	M_R $= \beta_0(stress + suction$ $\cdot water\ content)^{\beta 1}(3D\ shear\ stress)^{\beta 2}(density)^{\beta 3}$
Lytton model	$M_R = K_1 p_a \left(\frac{I_1 - 3\theta f h_m}{p_a}\right)^{K_2} \left(\frac{\tau_{oct}}{p_a}\right)^{K_3}$	$M_R = K_1(stress - suction \cdot$ $water\ content)^{K_2}(3D\ shear\ stress)^{K_3}$
NCHRP Mechanistic Empirical Pavement Design Guide (MEPDG) model	$\log \frac{M_R}{M_{Ropt}} = a + \frac{b-a}{1+\text{EXP}\left(\ln\frac{-b}{a}+k_m \cdot (S-S_{opt})\right)}$	$M_{R\,ratio} = M_{R\,ratio\,min} + \frac{M_{R_{ratio}}}{1+EXP\left(M_{R_{ratio}}+k_m \cdot (saturation)\right)}$
George's Mississippi sub-grade model	$M_R = k_1 \cdot P_a \cdot \left(\frac{\theta}{P_a}\right)^{k_2} \cdot \left(\frac{\tau_{oct}}{P_a}+1\right)^{k_3}$ Defined $k_{1\,to\,3}$ in terms of $P_{sieve\ size}$, w_c, w_{opt}, γ_s, γ_{opt} for specific material	
Long *et al.* model	$M_r = \frac{(p-\theta \cdot s)\left(1+\frac{0.4343}{S_\theta \cdot w}\right)}{\gamma_h(0.435)}\frac{(1+v)(1-2v)}{(1-v)}$	$M_r = (stress \cdot suction \cdot water\ content) \cdot Poisson$
Liang *et al.* model	$M_R = k_1 \cdot P_a \cdot \left[\frac{(\theta+\chi_m \psi_m)}{P_a}\right]^{k_2} \cdot \left(\frac{\tau_{oct}}{P_a}+1\right)^{k_3}$	$M_R = k_1 \cdot suction^{k_2} \cdot (3D\ shear\ stress)^{k_3}$
Cary and Zapata model	If saturation < 100%: $M_R = k_1' \cdot P_a \cdot \left(\frac{\theta_{net}}{P_a}\right)^{k_2'} \cdot \left(\frac{\tau_{oct}}{P_a}+1\right)^{k_3'} \cdot \left(\frac{(\psi_{m_0}-\Delta\psi_m)}{P_a}+1\right)^{k_4'}$ If saturation = 100% $M_R = k_1' \cdot P_a \cdot \left(\frac{\theta_{net}-3\cdot\Delta u_{w-sat}}{P_a}\right)^{k_2'} \cdot \left(\frac{\tau_{oct}}{P_a}+1\right)^{k_3'} \cdot (1)^{k_4'}$	$M_R = k_1' \cdot (stress)^{k_2'} \cdot (3D\ shear\ stress)^{k_3'} \cdot (suction)^{k_4'}$ $M_R = k_1' \cdot (stress - porewater\ pressure)^{k_2'} \cdot$ $(3D\ shear\ stress)^{k_3'} \cdot (1)^{k_4'}$

The model incorporates the stiffening effect of bulk stress and the softening effect of shear stress. Granular materials under repeated load generally display stress-hardening, while fine-grained cohesive soils show stress softening under repeated loads (Bejarano and Thompson (1999)). Thus, the resilient modulus of granular materials generally increases with increase in stress, whereas the resilient modulus of fine-grained cohesive soils decreases with increasing stress (Anochie-Boateng, 2009). Therefore, values for k_2 should be positive, since increasing bulk stress produces a stiffening of the material and values of k_3 should be negative to illustrate a softening effect. The model coefficients determined for each test specimen should be such that the multiple correlation coefficient R^2, exceeds 0.9. If this is not obtained through the test results and no errors are found, a different model should be considered. This model is proposed for use with both unbound aggregates and fine-grained subgrade soils (NCHRP, 2004; Kim, 2007).

In Chapter 3 of the MEPDG (NCHRP, 2004), a resilient response model to predict the changes in modulus due to moisture is included. This model is as follows (NCHRP, 2004):

$$\log \frac{M_R}{M_{R_{opt}}} = a + \frac{b-2}{1 + \exp\left(\ln \frac{-b}{a} + k_m \left(S - S_{opt} \right) \right)} \tag{2.7}$$

Where

$\dfrac{M_R}{M_{Ropt}}$ = resilient modulus ratio; M_R is the resilient modulus at a given time and M_{Ropt} is the resilient modulus at a reference condition;

a = minimum of $\log(M_R/M_{Ropt})$;

b = maximum of $\log(M_R/M_{Ropt})$;

k_m = regression parameter

$S - S_{opt}$ = Variation in degree of saturation expressed in decimal.

The model can also be incorporated into the generalised model to be defined as follows (Cary and Zapata, 2010b):

$$M_R = 10^{a + \frac{b-a}{1 + \text{EXP}\left(\ln \frac{-b}{a} + k_m \cdot \left(S - S_{opt} \right) \right)}} \cdot k_1 \cdot P_a \cdot \left(\frac{\theta}{P_a} \right)^{k_2} \cdot \left(\frac{\tau_{oct}}{P_a} + 1 \right)^{k_3} \tag{2.8}$$

In this modified universal model, the role of moisture changes is separate from the stress state variables (Cary and Zapata, 2010b).

Equation 2.8 approaches a linear form for degrees of saturation within $\pm$ 30 percent of degree of saturation at optimum conditions, S_{opt}, but flattens out for degrees of saturation lower than 30 percent below optimum. This is in agreement with known behaviour (NCHRP, 2004).

2.2.6.4 George's Mississippi sub-grade model

George (2004) reported on a LTPP-FHWA study program where the relationship between the resilient modulus and physical properties of unbound sub-grade materials were investigated. As part of this study equations were developed to calculate resilient modulus for selected material at a specific stress state from physical properties of the selected material. For example, one of the constitutive equations reported on were:

$$M_R = k_1 \cdot P_a \cdot \left(\frac{\theta}{P_a}\right)^{k_2} \cdot \left(\frac{\tau_{oct}}{P_a} + 1\right)^{k_3}$$

For coarse-grained sand soils the material specific constants were:

$$k_1 = 3.2868 - 0.0412P_{3/8} + 0.0267P_4 + 0.0137(\% \, Clay) + 0.0083LL - 0.0379w_{opt} - 0.0004\gamma_s k_2$$

$$= 0.5670 + 0.0045P_{3/8} - 2.98 \times 10^{-5}P_4 - 0.0043(\% \, Silt) - 0.0102(\% \, Clay)$$

$$+ 0.0041LL - 0.0014w_{opt} - 3.14 \times 10^{-5}\gamma_s - 0.4582(\frac{\gamma_s}{\gamma_{opt}}) + 0.1779(\frac{w_c}{w_{opt}})k_3$$

$$= -3.5677 + 0.1142P_{3/8} - 0.0839P_4 - 0.1249P_{200} - 0.1030(\% \, Silt) + 0.1191(\% \, Clay)$$

$$+ 0.0069LL - 0.0103w_{opt} - 0.0017\gamma_s + 4.3177(\frac{\gamma_s}{\gamma_{opt}}) - 1.1095(\frac{w_c}{w_{opt}})$$

Where

$P_{sieve \, size}$	= percentage passing size sieve;
w_c	= moisture content of the specimen (%);
w_{opt}	= optimum moisture content of the soil (%);
γ_s	= dry density of the sample (kg/m³);
γ_{opt}	= optimum dry density of the soil (kg/m³).

In his literature review, George (2004) evaluated various models which were made material specific and seems to be more generally applicable since it is linked to basic engineering properties, but concluded that these models were state specific and George was not able to apply it without modification to his study of Mississippi sub-grade material.

Incorporating fundamental engineering properties into a model should be done in such a way that it is generally applicable and not bound to specific materials or areas.

2.2.6.5 Long et al. model

Dawson (2009) reported on a model developed by Long *et al.* (2006) in which another approach was taken, relating the resilient modulus to suction and water content, rather than to saturation ratio, but still including some stress influence.

2.2.6.6 Liang et al. model

Yang *et al.* and Liang *et al.* presented in 2005 and 2008 respectively, models which incorporates the Bishop's parameter. Liang's model incorporates the effect of externally applied stress and matric suction on resilient modulus by including the Bishop's effective stress for unsaturated soils (Cary and Zapata, 2010b). This model is also a variation of the universal model and is defined as follows:

$$M_R = k_1 \cdot P_a \cdot \left[\frac{(\theta + \chi_m \psi_m)}{P_a}\right]^{k_2} \cdot \left(\frac{\tau_{oct}}{P_a} + 1\right)^{k_3} \tag{2.9}$$

Where

χ_m = Bishop's parameter;

ψ_m = matric suction

The general use of this model is hampered by the estimation of Bishop's parameter. Various methods to estimate the parameter has been presented in the past, but none of them widely adopted by the research community. This is due to difficulties in evaluation of the parameter and its dependence on saturation and on soil type. Since saturation is related to matric suction, it is thus possible that the parameter depends on suction as well. Furthermore, most methods used to estimate the parameter utilises inputs obtained from the SWCC geometric properties. Accuracy in SWCC testing practices therefore influences the accuracy of the parameter estimation (Cary and Zapata, 2010b).

2.2.6.7 Cary and Zapata

Another modified universal model was proposed by Cary in 2010 which incorporate matric suction as a fundamental state stress variable (Cary and Zapata, 2010a; Cary and Zapata, 2010b). It considers a smooth transition from unsaturated to saturated conditions in soils. The model is defined as follows:

If saturation < 100%:

$$M_R = k_1' \cdot P_a \cdot \left(\frac{\theta_{net}}{P_a}\right)^{k_2'} \cdot \left(\frac{\tau_{oct}}{P_a} + 1\right)^{k_3'} \cdot \left(\frac{(\psi_{m_0} - \Delta\psi_m)}{P_a} + 1\right)^{k_4'} \tag{2.10}$$

If saturation = 100%

$$M_R = k_1' \cdot P_a \cdot \left(\frac{\theta_{net} - 3 \cdot \Delta u_{w-sat}}{P_a}\right)^{k_2'} \cdot \left(\frac{\tau_{oct}}{P_a} + 1\right)^{k_3'} \cdot (1)^{k_4'} \tag{2.11}$$

Where

P_a = atmospheric pressure;

$\theta_{net} = \theta - 3u_a$ = net bulk stress;

τ_{oct} = octahedral shear stress;

$k_1' \geq 0 \,, k_2' \geq 0 \,, k_3' \leq 0 \,, k_4' \geq 0$ = regression constants;

Δu_{w-sat}	= build-up of pore water pressure under saturated conditions;
u_a	= pore air pressure;
ψ_{m_0}	= initial matric soil suction;
$\Delta\psi_m$	= relative change of matric soil suction with respect to ψ_{m_0}.

Net bulk stress is used in the model instead of the total bulk stress due to the use of the axis translation technique that should be applied for resilient modulus testing of unsaturated soils. As the soil goes from an unsaturated state to a saturated state, pore air pressure will approach zero and the net bulk stress will be equal to the total bulk stress. The model thus defaults to the universal model at 100 per cent saturation (Cary and Zapata, 2010b).

$\Delta\psi_m$ capture the variations of matric suction under undrained conditions and when it approaches zero, it reflects the drained condition.

It is interesting to note that except for Crockford *et al.* and Long *et al.*, all the models discussed are based on the universal model. Theyse (2008a) commented that the variables of the Uzan and universal models, namely θ and τ_{oct} or σ_d are not independent since these are derived from σ_1, σ_2 & σ_3.

Only George investigated the link with fundamental engineering properties, but could not formulate a general equation applicable to all material types.

2.2.7   South African researchers

2.2.7.1   *Visser's model*

Visser (1981) developed models for predicting the resilient modulus using data based on material from Brazil. The study concluded that the Brazil data was inadequate for evaluating moisture content influences on resilient modulus, possibly due to laterisation. Although moisture content could not be incorporated successfully, the models did utilise other fundamental engineering parameters to estimate the resilient modulus which is not bound by specific material or area. The 'short' model is defined by Model A1 (Visser, 1981, Visser *et al.*, 1983):

$$LMR = 3.041 + 0.0328LL + 0.749DV - 0.0060LL \cdot DV - 0.0573PL - 0.0159PL \cdot SD \qquad \text{Model A1}$$

Where

LMR	= log to the base 10 of resilient modulus in kgf/cm^2
LL	= liquid limit (%)
DV	= material type dummy variable:
	For clay materials DV =0
	For sandy materials DV =1

PL = plastic limit (%)

SD = deviator stress in kgf/cm^2

Visser (1981) recommended that further research to investigate moisture content influences, both below and above optimum moisture content, be carried out on both in-situ and laboratory compacted samples (Visser, 1981).

2.2.7.2   Emery's model

Emery (1985) investigated moisture content and its variations, seasonal and diurnal, under existing pavement structures. The aim of the study was to apply the findings regarding moisture content to pavement design procedures. Emery (1985) found that an equilibrium zone in the central part of the pavement exists, but, that extending in from the edge of the surfacing, 600 to 1 000 mm, seasonal variation in moisture content existed.

Emery (1985) developed general Equilibrium Moisture Content (EMC) prediction equations, as well as equilibrium to OMC-ratio prediction equations for specific materials and climatic regions. This EMC/OMC ratio was incorporated into a resilient modulus/soaked CBR relationship. The resilient modulus/soaked CBR relationship utilised a varying constant of proportionality, making it generally applicable. Emery (1985) also defined an unsoaked/soaked CBR relationship and combined it into an integrated resilient modulus equation. The equation is defined as follows and predicts resilient modulus at field moisture content and density from laboratory soaked CBR and moisture:

$$E = 187 \left(e^{-0.59 EMC/OMC} \right) \left(CBR_s^{0.20} \right) \tag{2.12}$$

Where

EMC/OMC = equilibrium moisture content to optimum moisture content ratio;

CBR_s = soaked CBR

Emery (1985) reported good agreement between the variation of the predicted resilient modulus and the generally accepted wet/dry modulus values as defined by Freeme (1983). The equation was used to compile a graph (Figure 2.17) indicating for each material class, the range of resilient modulus values which can be expected for certain EMC/OMC ratios. The upper limit to EMC/OMC ratio is the soaked condition.
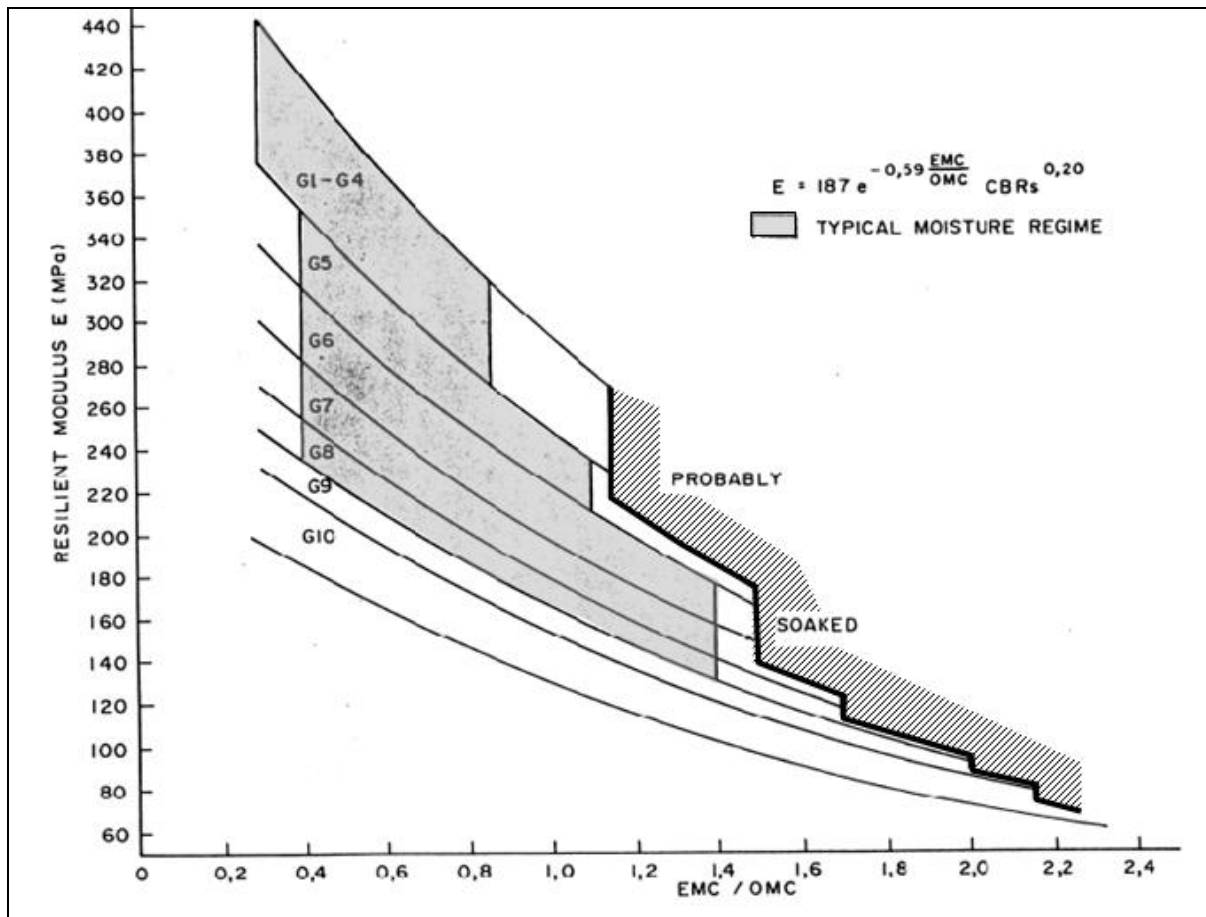
Figure 2.17: **Variation of resilient modulus with moisture for material classes G1 to G10 (Emery, 1985).**

2.2.7.3   Theyse's 2009 model

Theyse (2006, 2008, 2009) investigated resilient modulus and moisture. A wide range of materials, from fine-grained sand to crushed stone products, were part of the study.

Theyse (2008a) started by developing a yield strength or failure strength model which incorporates degree of saturation and solidity (density). The purpose of a yield strength model is to understand the yield strength behaviour of the material, before doing any actual testing. Yield or failure strength refers to the stress at which a material start to deform plastically, i.e. deformation is permanent and non-reversible (Gere, 2001). In his study, Theyse (2008a) used the yield strength model to do experimental design for further plastic strain testing. Plastic strain test results were used to calibrate a plastic strain damage model for crushed stone.

Theyse continued from the 2008 study to develop models to estimate the SWCCs and Suction Pressure Curves (SPCs) for partially saturated materials. The calibrated yield strength model was used as stepping stone for the SWCC and SPC models. The yield strength model is defined as follows:

$$\sigma_1^y = \frac{e^{aVD}}{e^{bS}}(\sigma_3 + \rho_{suc})^c - \rho_{suc} \qquad\qquad if \quad \sigma_3 \geq -\rho_{suc}$$

$$\sigma_1^y = Undefined \qquad\qquad if \quad \sigma_3 < -\rho_{suc} \qquad\qquad (2.13)$$

Where

σ_1^y	= yield strength (kPa) (compression positive);
S	= degree of saturation (ratio of voids filled with water to total voids);
VD	= volumetric density (ratio or the volume filled with solids to the total volume);
σ_3	= minor principal stress or confining pressure for the triaxial test (kPa);
ρ_{suc}	= suction pressure derived from the SWCC;
a, b, c	= effective stress yield strength model parameters.

The SPC was defined as follow (Theyse, 2009):

$$\rho_{suc} = \frac{\rho S}{e^{\omega S/VD}} \qquad\qquad (2.14)$$

Where

ω	$= 13.018GM^{-1.366}$ (GM = grading modulus)
ρ	$= 5.5605\omega^{3.2287}$

(variables as defined before)

The SWCC was defined as follow for material with PI < 15 (Theyse, 2009):

$$(u_a - u_w) = \frac{\rho}{e^{\omega S/VD}} \qquad\qquad (2.15)$$

(variables as defined before)

Also included in Theyse's (2008a) comprehensive study was a modified universal model, to include solidity (density) and saturation of the material. The resilient modulus values used as input data to develop the model was derived from the plastic strain tri-axial tests conducted and no resilient modulus tri-axial tests were conducted as part of the study. A resilient modulus model was defined as follows:

$$M_R = p_{atm}10^{K_0} \frac{SD^{K_{SD}}S^{K_S}\left(\frac{\theta'}{p_{atm}}\right)^{K_1}}{10^{K\left(\frac{S}{SD}\right)}\left(\frac{\sigma_d}{p_{atm}}\right)^{K_2}} \qquad\qquad (2.16)$$

Where

p_{atm}	= reference pressure (101.3 kPa)
SD	= solidity (%)
S	= degree of saturation (%)
θ'	= effective bulk stress (kPa)

σ_d	= deviator stress (kPa)
	$= \sigma_1 - \sigma_3$
$K_{SD}, K_S, K, K_0, K_1, K_2$	= regression model parameters

Theyse reported that the model gave accurate and more confident calibration results for crushed stone products than it did for natural gravels. This was due to the wider range of saturation levels and density tested for crushed stone than for natural gravels. The saturation levels for natural gravels tested as part of the study were mostly grouped to test either below 40 per cent or above 40 per cent saturation, not testing the entire spectrum of saturation between zero and 100 per cent. Theyse recommended that further studies in this field should focus on natural gravels and that a wide range of solidity and saturation levels should be investigated (Theyse, 2008a).

2.2.8 Conclusions

This historical literature section defined natural granular material, explored the various parameters which affect the resilient behaviour of natural granular material and concluded that moisture is one of the most important influencing factors. Moisture within a natural granular material was briefly discussed in terms of the various definitions of the moisture state, as well as the role that suction plays in resilient behaviour.

The modelling of resilient behaviour was investigated in terms of stress dependent models and models incorporating moisture and density. From this investigation it was evident that the aim of developing an accurate resilient response model, which is generally applicable and can be correlated to fundamental engineering properties, has not yet been achieved.

2.3 CURRENT LITERATURE

2.3.1 Introduction

The South African Pavement Design Method (SAPDM) project currently underway aims to re-evaluate the previous design method used in South Africa and to incorporate new knowledge gathered. One of the focus areas of the SAPDM project is resilient response models for unbound material. Project SAPDM/B-1a of the SAPDM project is dedicated to this and research work done since 2011 has been reported on. The work is not publicly available, but has been presented to a panel of researchers on a three monthly basis and internal reports have been distributed to all researchers involved in the overall project for review.

This section of the literature study evaluates work done since January 2011 as part of SAPDM/B1-a which focuses on the formulation of a stress-dependent resilient response model for unbound granular material.

2.3.2 Background

In Section 2.2.7.3 reference was made to work by Theyse (2008, 2009) which explored a stress-dependent resilient response model formulation for unbound granular material. Theyse reported that the model gave accurate and more confident calibration results for crushed stone material than it did for natural gravels. This was due to the wider range of saturation levels and density tested for crushed stone than for natural gravels. Theyse recommended that further studies in this field should focus on natural gravels and that a wide range of solidity and saturation levels should be investigated (Theyse, 2008a).

The experimental design of SAPDM/B1-a allowed for the preparation of 18 samples for resilient modulus tri-axial testing. These samples were tested at three different levels of saturation and two different density levels (Theyse, 2008b). A selection of materials was included in the study and consisted of a range of unmodified granular material. More detail of the experimental design is given in Chapter 3 of the thesis.

2.3.3 SAPDM/B1-A

2.3.3.1 Introduction

Often pavement response models are based on the integral transformation solution of a Multi-Layer, Linear Elastic (MLLE) system. However, with increasing computing capacity, Finite-Element (FE) analysis may become a viable analysis tool for routine pavement design in the near future. Even though FE analysis allows for the introduction of material non-linearity in terms of plasticity, some information on the resilient response characteristics of pavement materials are still required (Theyse, 2012). Given that both the MLLE and FE solutions are based on continuum mechanics, Hooke's law in terms of either an isotropic or anisotropic formulation governs the elastic material response with the elastic properties of the material expressed by a pair of constants such as Young's modulus and Poisson's ratio, bulk and shear moduli or Lame's constants (Theyse, 2012a). Theyse focussed on Young's modulus and Poisson's ratio, since these elastic constants are more familiar to most pavement engineers.

Young's modulus and Poisson's ratio are theoretical concepts of linear-elasticity that can at best approximate experimental results of actual material elastic response. In their basic linear elastic form, Young's modulus and Poisson's ratio are rather poor approximations of actual material behaviour as the behaviour of unbound granular material is:

- Stress-dependent i.e. the stiffness of the material depends on the level of confinement of the material and the shear stress imposed on the material;

- Non-linear i.e. there is not a linear relationship between the imposed stress and strain response of the material; and

- Inelastic (plastic) i.e. the material does not completely return to its original un-deformed shape when the imposed stress is removed (Theyse, 2012a).

The non-linear, stress-dependent behaviour of unbound granular material can, however, be simulated using the linear elastic model as a basis but with a proper constitutive material model that adheres to the observed material behaviour (Theyse, 2012a).
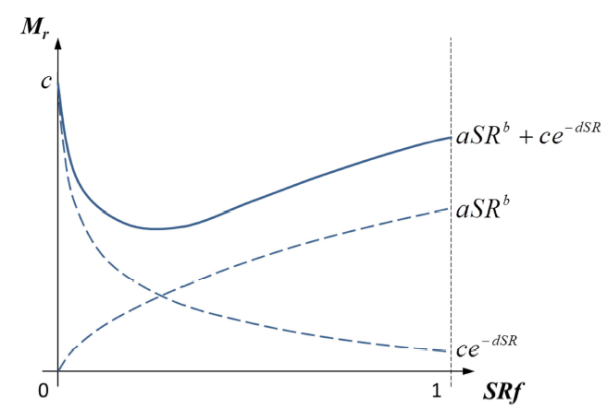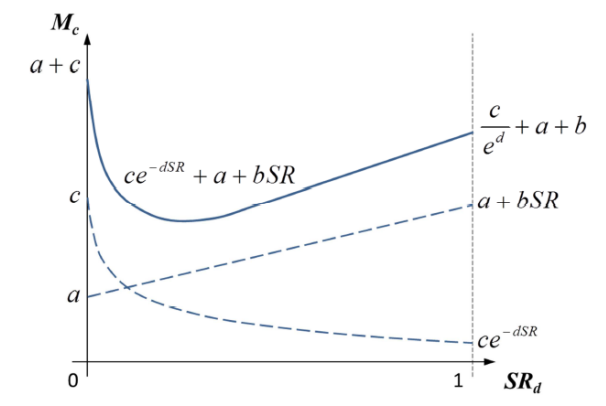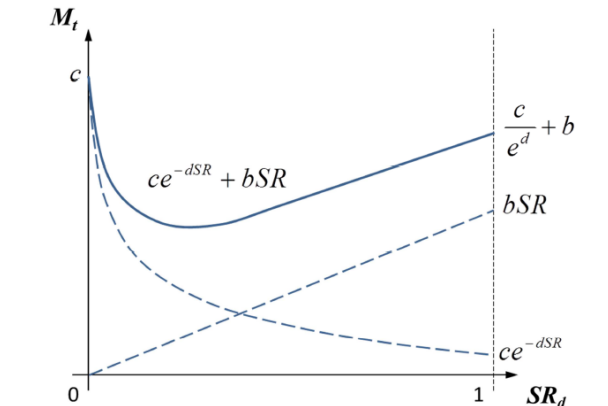
2.3.3.2 *Model development*

Theyse (2012) reiterates that the departure point for any model formulation should be a detailed study of the data and specifically patterns in the data. The resilient modulus models reported on are based on the trends observed in repeated load tri-axial test data. For the development of resilient models, results obtained from tri-axial tests on the base layer material from road N2-33 near Piet Retief and the crushed stone base layer of road N4 west of Pretoria were used (Theyse, 2012a).

Details of the test protocol and data processing are given in Chapter 3, since the same protocol and data processing were used in the evaluation of results on materials which formed part of this thesis.

Based on the characteristics observed when resilient data were evaluated, Theyse (2012a) formulated a resilient modulus-, a cord modulus- and a tangent modulus model. These models are each formulated as a function of stress ratio, and confinement pressure or minor principal stress is considered in the model coefficients. The models are illustrated in Table 2.8.

Table 2.8: Resilient-, cord- and tangent modulus models (Theyse, 2012a).

Resilient Modulus Model	Cord Modulus Model	Tangent Modulus Model
$M_r = aSR_f^b + ce^{-dSR_f}$	$M_c = a + bSR_d + ce^{-dSR_d}$	$M_t = bSR_d + ce^{-dSR_d}$
Where M_r = resilient modulus (MPa) SR_f = failure stress ratio $= \frac{\sigma_1}{\sigma_1^f}$ a,b,c,d = regression coefficients found from regression analysis	Where M_c = cord modulus (MPa) SR_d = deviator Stress Ratio (SR) $= \frac{(\sigma_d + \sigma_3)}{\sigma_d^f}$ a,b,c,d = regression coefficients found from regression analysis	Where M_t = tangent modulus (MPa) SR_d = deviator Stress Ratio (SR) $= \frac{(\sigma_d + \sigma_3)}{\sigma_d^f}$ a,b,c,d = regression coefficients found from regression analysis

2.3.3.3 Discussion of models

Resilient modulus model

Figure 2.18 shows the prediction accuracy of the model for two specimens of the N2-33 material at similar densities and different moisture conditions. The characteristics of the calibrated model for the same two specimens are shown in Figure 2.19. Theyse (2012a) reported that depending on the level of confinement pressure, there is an initial reduction in the resilient modulus of the material with increasing shear stress, which is represented by an increase in the stress ratio. Initial decrease in resilient modulus is followed by an increase with increasing stress ratio beyond about 10 to 20 percent. An ultimate stiffness appears to be reached when a stress ratio of 100 per cent is approached (Theyse, 2012a).

Volumetric density (VD) = 82.6% Degree of saturation (S) = 27% R^2 = 0.983 Standard error of estimate = 65.2 MPa Average error = 5.3%	Volumetric density (VD) = 83.0% Degree of saturation (S) = 46% R^2 = 0.980 Standard error of estimate = 40.9 MPa Average error = 4.3%

(a) Prediction accuracy

(b) Prediction accuracy

(c) Model plot

(d) Model plot
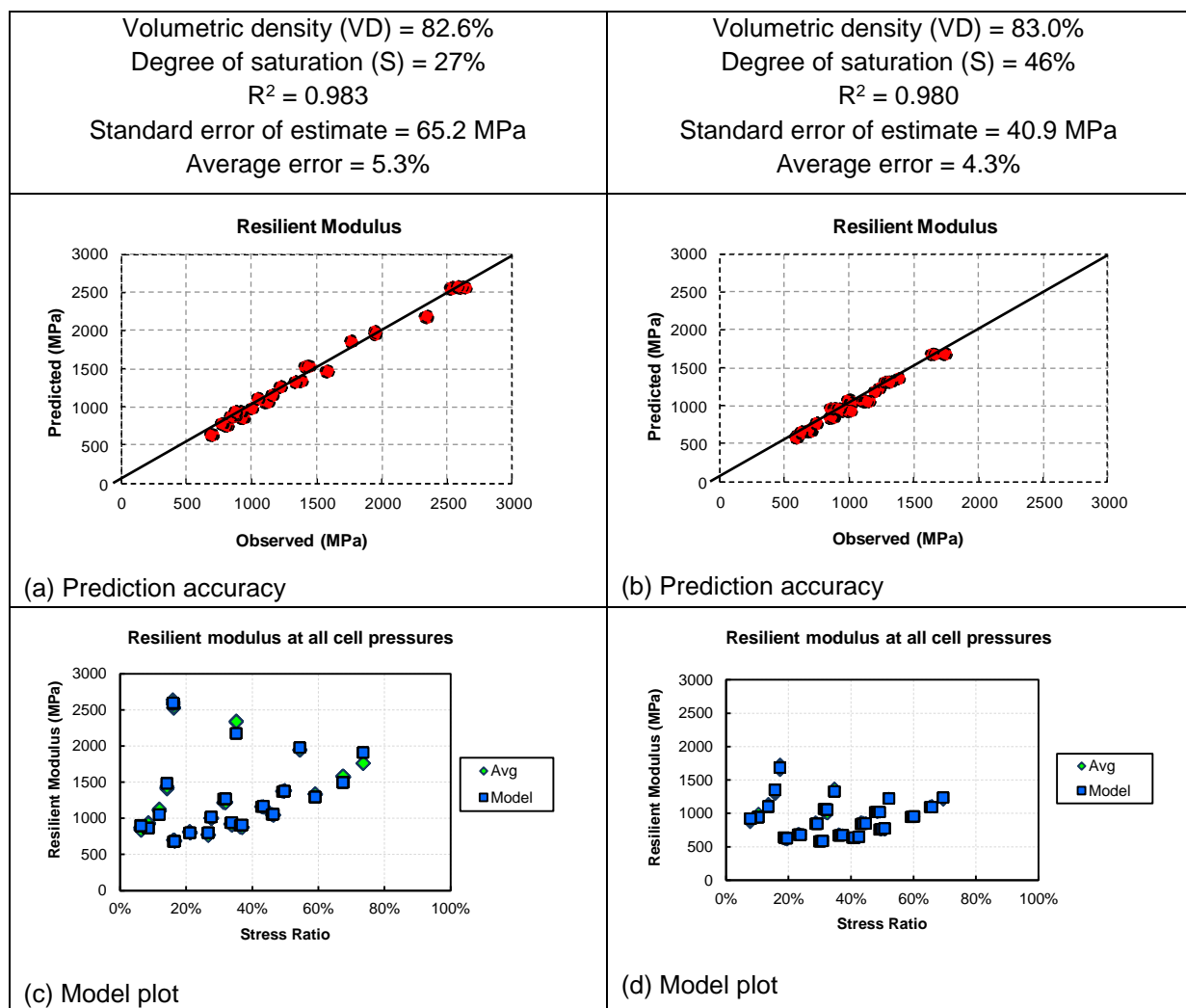
Figure 2.18:   Examples of resilient modulus model calibration for two specimens from N2-33 (Theyse, 2012a).
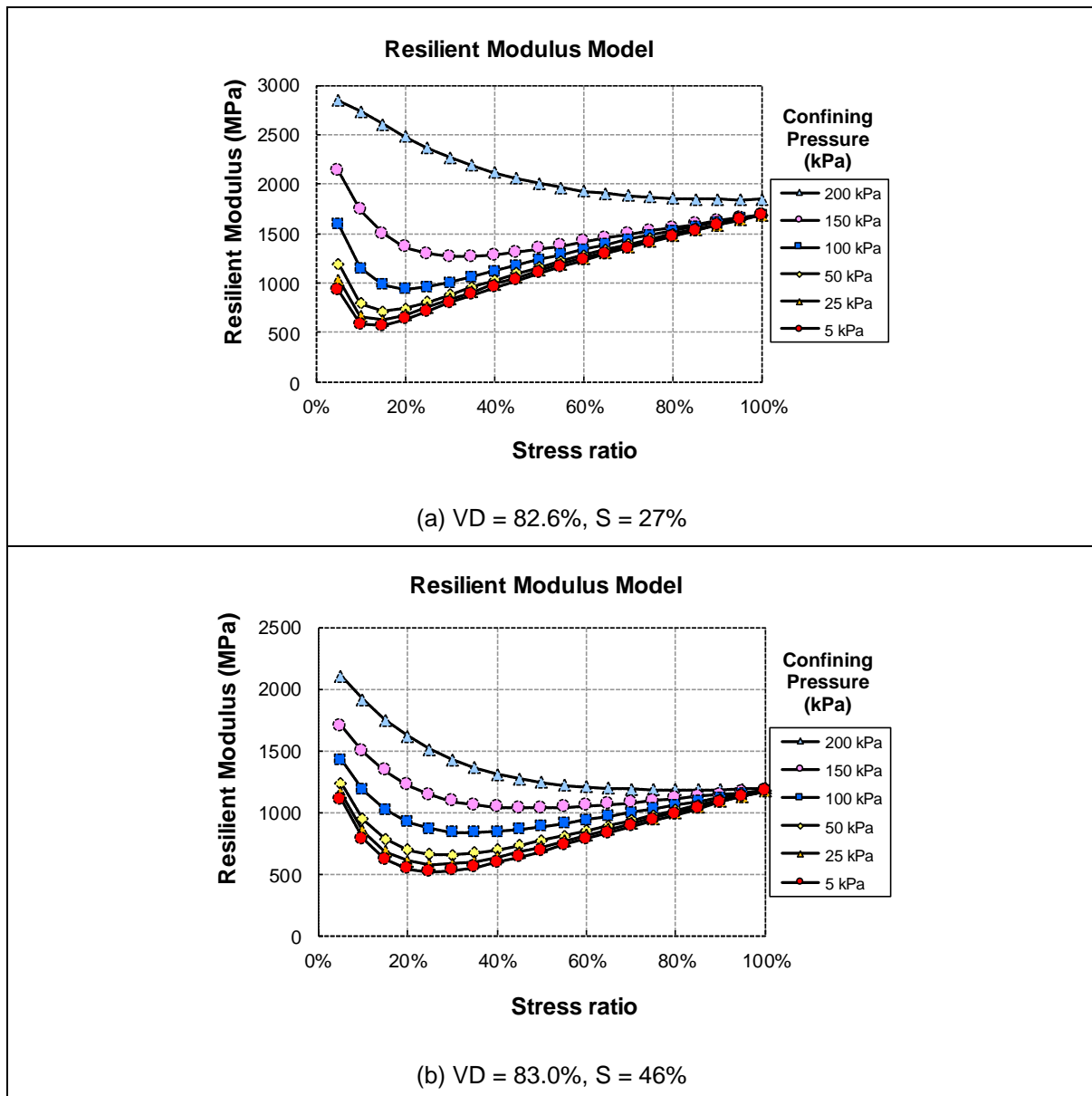
Figure 2.19: Characteristics of the resilient modulus model for two example cases from N2-33 (Theyse, 2012a).

Table 2.9 provides a summary of the resilient modulus model calibration results for the N2-33 material (Theyse, 2012a). Theyse noted that except for three specimens for whom the data quality prevented the model from being calibrated, the model calibrated with exceptional accuracy for all the specimens tested. The beta-parameters of the '*a*' and '*c*' model coefficients could also be set to zero without negatively impacting on the calibration accuracy of the model. The '*a*' and '*c*' model coefficients are therefore independent of the confinement pressure and only a function of volumetric density and degree of saturation (Theyse, 2012a).

Table 2.9: Summary of the resilient modulus model calibration results for N2-33 material (Theyse, 2012a).

Specimen	VD	S	a		b		c		d		R²	SEE
			α_1	β_1	α_2	β_2	α_3	β_3	α_4	β_4		
11357-01	0.827	0.297	1807	0	1.98	0.345	1666	0	14.897	0.060	0.977	58.3
11357-02	0.827	0.275	1702	0	1.32	0.235	2659	0	28.137	0.127	0.983	65.2
11357-03	0.824	0.286										
11357-04	0.83	0.463	1255	0	1.96	0.277	1817	0	3.039	0.028	0.982	34.3
11357-05	0.829	0.461	1178	0	2.23	0.348	1875	0	12.868	0.047	0.983	38.4
11357-06	0.824	0.519	943	0	3.18	0.452	1603	0	8.437	0.025	0.978	31.7
11357-07	0.819	0.694	524	0	5.03	0.406	954	0	16.166	0.067	0.971	27.7
11357-08	0.821	0.721	407	0	2.68	0.302	1156	0	16.877	0.069	0.930	37.1
11357-09	0.822	0.705										
11357-10	0.786	0.179	1635	0	2.35	0.350	2218	0	24.176	0.106	0.966	81.1
11357-11	0.785	0.163	1098	0	1.95	0.292	2661	0	38.195	0.179	0.984	60.2
11357-12	0.786	0.178	890	0	2.43	0.358	1727	0	34.730	0.163	0.983	46.5
11357-13	0.784	0.438	695	0	2.56	0.300	1188	0	12.797	0.050	0.590	35.3
11357-14	0.785	0.446	677	0	2.90	0.359	941	0	13.009	0.052	0.959	33.3
11357-15	0.786	0.436	622	0	1.85	0.274	1421	0	17.109	0.071	0.956	40.8
11357-16	0.785	0.69										
11357-17	0.782	0.665	424	0	3.42	0.428	868	0	13.801	0.053	0.873	39.6
11357-18	0.781	0.664	392	0	15.92	0.741	391	0	7.400	0.031	0.975	19.7

Tangent modulus model

The tangent modulus approach is better suited for FE solutions, since FE solutions can accommodate non-zero initial stress and strain conditions. Materials that behave non-linearly can therefore be loaded incrementally in a FE solution to follow the non-linear response of the system and was therefore considered by Theyse (2012). Only the loading portion stress-strain cycle was evaluated, although the tangent modulus was determined for the full cycle, because during the unload phase, the tangent modulus becomes negative (Theyse, 2012).

The calibration results for the N2-33 material are listed in Table 2.10. Theyse (2012) reported that the accurate results were obtained for linear relationships between the confinement pressure and the '*c*' and '*d*' model coefficient combined with a cubic relationship for the '*b*' model coefficient.

Table 2.10: Summary of the tangent modulus model calibration results for the N2-33 material (Theyse, 2012a).

Specimen	VD	S	b			c			d		R²	SEE
			α_2	β_2	γ_2	α_3	β_3	γ_3	α_4	β_4		
11357-01	0.83	0.30	3803	5.6	-0.047	728	16.7	-0.0589	14.4	-0.051	0.99	42.4
11357-02	0.83	0.28	3606	3.3	-0.021	652	16.9	-0.0435	17.4	-0.055	1.00	16.4
11357-03	0.82	0.29	3245	5.6	-0.028	1092	12.8	-0.0276	13.5	-0.040	1.00	30.9
11357-04	0.83	0.46	1965	9.6	-0.037	1245	11.9	-0.0306	10.9	-0.028	0.99	22.6

Specimen	VD	S	b			c			d		R^2	SEE
			α_2	β_2	γ_2	α_3	β_3	γ_3	α_4	β_4		
11357-05	0.83	0.46	1650	8.5	-0.033	950	10.6	-0.0271	10.9	-0.028	1.00	10
11357-06	0.82	0.52	1244	9.4	-0.034	1711	4.7	-0.005	7.9	-0.016	0.99	20.3
11357-07	0.82	0.69	485	5.2	-0.014	58	5.7	-0.0151	13.9	-0.034	1.00	7.6
11357-08	0.82	0.72	453	4.1	-0.014	-17	4.2	-0.0111	7.9	-0.023	1.00	2.6
11357-09	0.82	0.71	484	6.6	-0.020	-32	12.0	-0.0341	17.7	-0.034	0.99	10.5
11357-10	0.79	0.18	2825	6.9	-0.039	99	24.3	-0.0558	12.4	-0.022	1.00	30.7
11357-11	0.79	0.16	2184	4.3	-0.019	112	22.6	-0.0234	26.7	-0.075	1.00	23.9
11357-12	0.79	0.18	2271	4.7	-0.021	387	20.9	0.0302	23.6	-0.043	0.98	61.5
11357-13	0.78	0.44	1057	-0.7	0.003	81	10.7	-0.0333	9.0	-0.025	1.00	7.7
11357-14	0.79	0.45	1004	-1.8	0.009	87	23.2	-0.0847	13.3	-0.035	0.99	18.8
11357-15	0.79	0.44	1147	-3.9	0.017	157	12.5	-0.0413	9.1	-0.024	0.97	24.9
11357-16	0.79	0.69	431	1.6	0.020	251	0.8	0.0351	3.2	0.011	0.98	34.4
11357-17	0.78	0.67	554	7.7	-0.028	181	8.1	-0.0308	14.9	-0.052	1.00	8.5
11357-18	0.78	0.66	459	1.7	0.001	653	4.5	-0.0134	14.8	-0.038	1.00	7.8

Cord modulus model

Theyse (2012) explained why the cord modulus was considered after the formulation of the resilient modulus model, the latter being the most commonly theory used to model resilient behaviour. Firstly, when the resilient modulus is calculated, only the end-point of the stress-strain hysteresis loop is considered, discarding the majority of the information contained in the rest of the loop. Secondly, evaluation of the resilient data indicated that the behaviour of the 200 kPa confinement pressure was considerably different than that at lower confinement pressures. It was not clear whether this behaviour was real or apparent due to the processing of the data (Theyse, 2012a).

Figure 2.20 shows a comparison between the cord and resilient modulus for a single specimen. Theyse (2012a) observed that there is agreement between the cord and resilient modulus results and that the underlying stiffness behaviour of the material is the same regardless of the confinement pressure. More importantly, Theyse concluded that the resilient modulus results at 200 kPa confinement pressure calculated only from the end-points of the hysteresis loops creates a misconception that the stiffness reduces with increasing shear stress (stress ratio). The chord modulus from the full hysteresis loop indicates that there is a consistent and dramatic reduction in stiffness from very high initial stiffness values to a minimum stiffness in the region of 20 per cent stress ratio after which the stiffness increase with increasing stress ratio. The 200 kPa confinement pressure results were contributed to insufficient conditioning of the specimen (Theyse, 2012a).
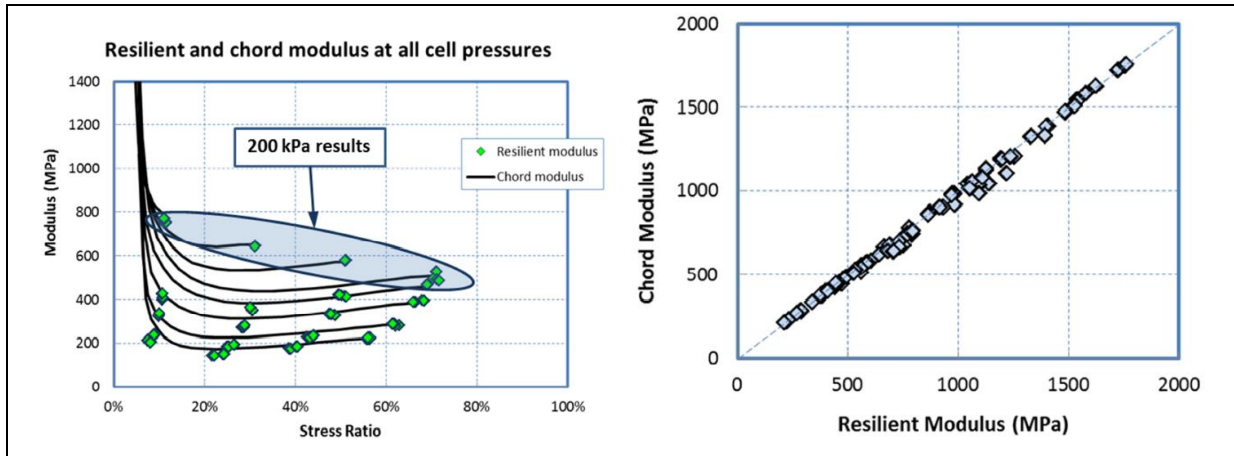
Figure 2.20: Comparison between cord and resilient modulus results for a single specimen (Theyse, 2012a).

Theyse (2012) listed the following benefits when using the cord modulus approach compared to the resilient modulus approach:

- The full hysteresis loop provide a comprehensive trace of the material stiffness over a wide stress ratio range facilitating model formulation and calibration;
- The chord modulus shows consistent material behaviour at all levels of confinement pressure;
- The number of stress levels at which the tri-axial test is done can be reduced by 75 per cent in terms of the current test protocol; and
- In terms of application of the chord modulus in modelling the response of a pavement layer or tri-axial specimen, the chord modulus describes the evolution of the stiffness of the material from an initial condition at rest through the full stress-strain cycle including the load and unload phases.

When further investigated by Theyse, it was found that mathematically the cord modulus is obtained by integration of the tangent modulus from a condition of zero strain to the value of the axial strain. This format of the modulus thus enables the utilisation of more data in analysis, bridging the gap between the resilient and tangent modulus format. Figure 2.21 depicts the cord modulus formulation when derived from integration of the tangent modulus. This format reduces the number of variables from four to three (Theyse, 2012b).

$$M_c = a + bSR_d + \frac{c}{SR_d}$$

Where

M_c = cord modulus (MPa)

SR_d = deviator stress ratio

a, b, c = regression coefficients found from regression analysis
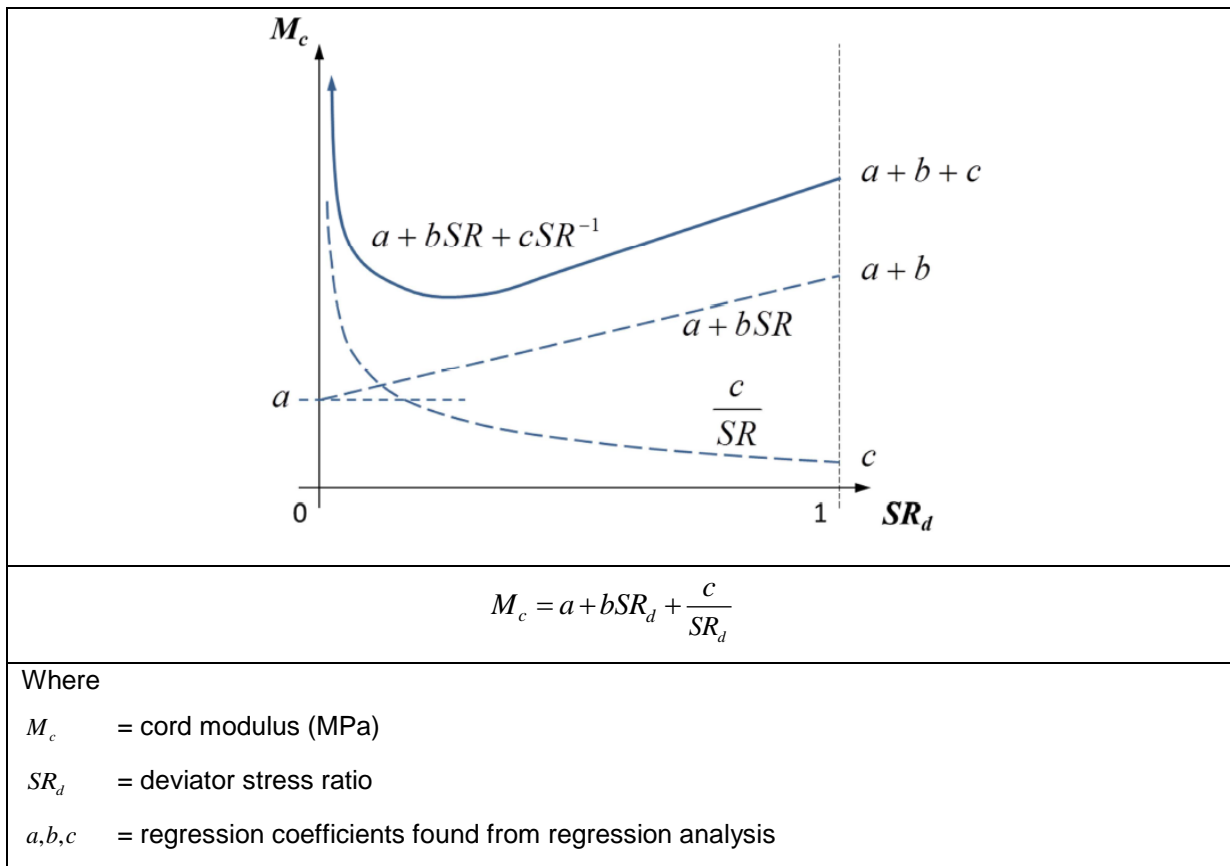
Figure 2.21: **Cord modulus derived from mathematical integration of the tangent modulus (Theyse, 2012b).**

Figure 2.22 depicts the cord modulus model derived through integration of the tangent modulus for two specimens from N2-33 Base layer.

Sample no. 11357-02	Sample no. 11357-07
Volumetric density = 82.7%	Volumetric density = 81.9%
Degree of saturation = 27.5%	Degree of saturation = 69.4%
R^2 = 0.996	R^2 = 0.989
Standard error of estimate = 25.4 MPa	Standard error of estimate = 13.0 MPa
Average error = 2.5%	Average error = 4.5%

(a) Prediction accuracy

(b) Prediction accuracy
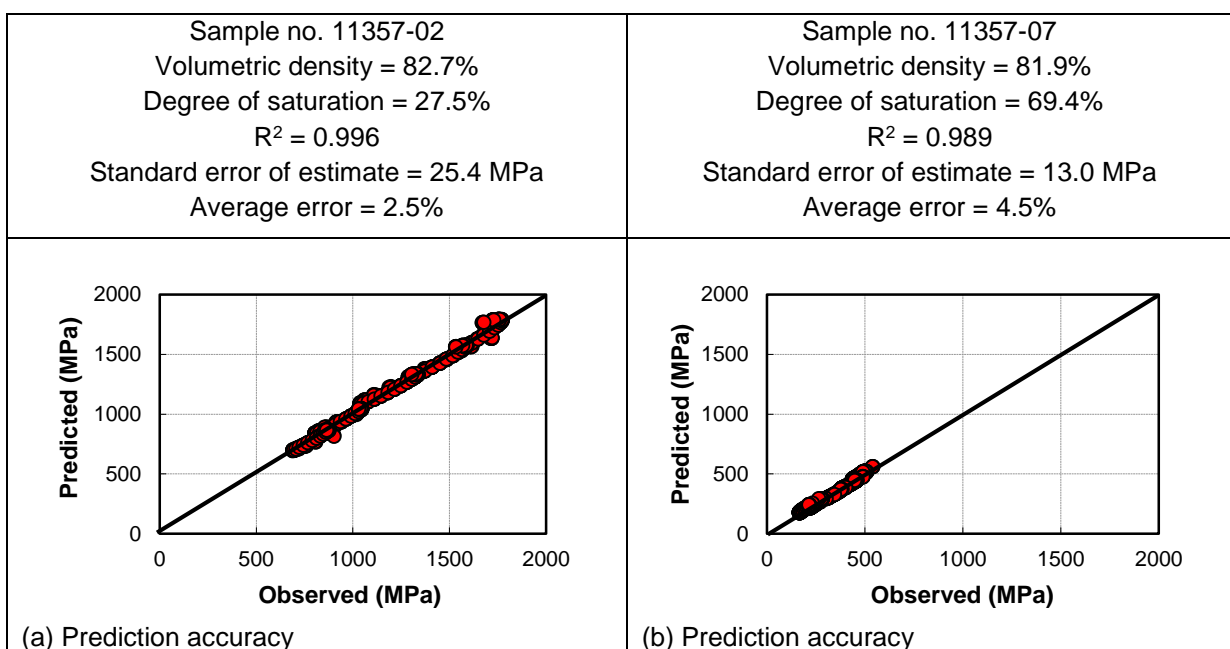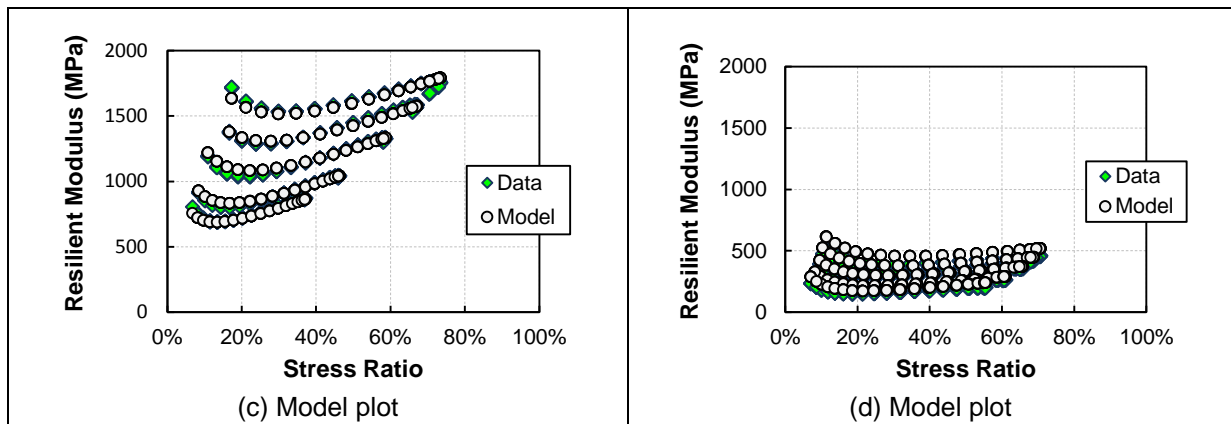
Figure 2.22: **Examples of revised cord modulus model calibration for two specimens from N2-33.**

The calibration results for the N2-33 material are listed in Table 2.11. Variables '*b*' was estimated by a constant value and variable '*a*' and '*c*' through a linear equation. The cord modulus model derived through integration of the tangent modulus could be calibrated with SEE below 51 MPa for all specimens tested.

Table 2.11: **Summary of the cord modulus model calibration results for N2-33 material.**

Specimen	VD	S	a		b	c		R²	SEE
			α_1	β_1	α_2	α_3	β_3		
11357-1	0.83	0.297	475	0.98	1247	4.9	0.724	0.97	50.5
11357-2	0.83	0.275	335	2.45	1119	6.6	0.498	1.00	25.4
11357-3	0.82	0.286	353	2.47	1122	34.0	0.692	0.99	33.5
11357-4	0.83	0.463	370	2.18	654	33.2	0.544	0.99	27.6
11357-5	0.83	0.461	228	1.63	699	42.7	0.503	0.99	23.5
11357-6	0.82	0.519	251	1.65	584	97.6	0.564	0.99	33.2
11357-7	0.82	0.694	-10	1.15	344	14.2	0.132	0.99	13.0
11357-8	0.82	0.721	25	0.70	288	19.5	0.221	0.99	16.0
11357-9	0.82	0.705	27	0.89	307	4.1	0.124	0.96	21.0
11357-10	0.79	0.179	27	0.89	307	4.1	0.124	0.96	21.0
11357-11	0.79	0.163	80	1.31	901	8.7	0.459	0.99	24.3
11357-12	0.79	0.178	69	1.35	1039	10.1	0.544	1.00	19.4
11357-13	0.78	0.438	168	0.88	312	-6.2	0.502	1.00	12.0
11357-14	0.79	0.446	148	0.76	293	14.0	0.285	0.99	16.7
11357-15	0.79	0.436	0	0.75	461	33.1	0.366	0.96	30.3
11357-16	0.79	0.690							
11357-17	0.78	0.665							
11357-18	0.78	0.664	7	1.34	210	21.2	0.081	0.99	13.7

2.3.3.4 *Conclusions*

Theyse (2012) concluded that the models formulated had potential for general application, but that more refinement of model formulation and calibration was required using data for a range of unbound granular materials. In this thesis Theyse's cord modulus model (Figure 2.21) will be used as a starting point for

further exploration into the effect of moisture on resilient behaviour of unbound natural granular material. As noted in the Section 2.2.7.3, a single resilient modulus model valid for crushed stone material could be successfully calibrated by Theyse (2009), but that the same was not possible for natural gravels. One of the objectives of this thesis is to calibrate a single resilient modulus model for unbound granular material.

2.4   REFERENCES

American Association for Highway Transportation Officials (AASHTO) (1928), M 145 or ASTM D3282, U.S.A.

Aggregate and Sand Producers Association of Southern Africa (ASPASA) (2006). http://www.aspasa.co.za web home page assessed on 23 April 2010.

Anochie-Boateng, J.K. (2007). '*Advance testing and characterisation of transportation soils and bituminous sands*', PhD dissertation, University of Illinois, Urbana, Illinois, USA.

Anochie-Boateng, J., Paige-Green, P. and Mgangira, M.B. (2009). '*Evaluation of test methods for estimating resilient modulus of modules of pavement geomaterials*', Paper presented at the 28th Annual Southern African Transport Conference 6 - 9 July 2009, CSIR International Convention Centre, Pretoria, RSA.

Austin, A. (2009). '*Fundamental characterisation of unbound base course materials under cyclic loading*', Masters dissertation, Louisiana State University & Agricultural and Mechanical College, Louisiana, USA.

Baloyi, R. (2006).'*Producers of sand and aggregate in the Republic of South Africa*', Directorate: Mineral Economics, Directory D14/2006, Department Minerals and Energy, Pretoria, RSA.

Bejarano, M.O. and Thompson, M.R. (1999). '*Subgrade soil evaluation for the design of airport flexible pavements'*. Technical Report, DOT 95-C-001, Federal Aviation Administration, U.S.A.

Brown, S.F. and Pappin, J.W. (1981). '*Analysis of pavements with granular bases*', Transportation Research Record 810, Transportation Research Board, Washington, D.C., USA.

Cary, C.E. and Zapata, C.E. (2010a). '*Resilient modulus testing for unsaturated unbound materials*', Proceedings of the 89th Annual Meeting of the Transportation Research Board, January 2010, Washington, D.C., USA.

Cary, C.E. and Zapata, C.E. (2010b). '*Comparative study of a mechanistic resilient modulus predictive equation for unbound materials*', Proceedings of the 2nd International Conference on Transport Infrastructure, 4-6 August 2010, Sao Paulo, Brazil.

Constantino, D. (2012). '*Statistics: First-quarter aggregate production up 9.7 percent*', Article published by North Coast Media electronically, 19 June 2012, on web page

http://www.pitandquarry.com/economics/statistics/news/first-quarter-aggregate-production-97-percent-3598

Correia, A.G. and De Almeida, J.R. (1998). '*Mechanical behaviour of unbound granular materials for modelling of flexible pavements*', p 1211-1220, Proceedings of the Fifth International Conference on the Bearing Capacity of Roads and Airfields, The Norwegian University of Science and Technology, Trondheim, Norway.

Craciun, O. (2009). '*Matric suction response of unbound granular base material subjected to cyclic loading*', PhD thesis, University of New South Wales, Australia.

Craig, R.F. (1997). '*Soil mechanics*', Sixth Edition, E & FN Spon, London & New York.

Dawson, A. (2009). '*Water in road structures – Movement, drainage and effects*', Geotechnical, Geological and Earthquake Engineering, Volume 5, Springer Science & Business Media B.V. (Based on WATMOVE study reported as COST Action No. 351).

De Beer, M and Maina, J.W. (2008). '*Some fundamental definitions of the elastic parameters for homogeneous isotropic linear elastic materials in pavement design and analysis*', Proceedings of the 27th Southern African Transport Conference (SATC), July 2008, Pretoria, RSA.

Ekblad, J. (2006). '*Influence of water on coarse granular road material properties*', KTH, Stockholm, ISSN 1650-867x.

Emery, S.J. (1985). '*Prediction of moisture content for use in pavement design*', PhD Thesis, University of Witwatersrand, Johannesburg, RSA.

Fredlund, D.G. and Rahardjo, H. (1993). '*Soil mechanics for unsaturated soils*', John Wiley & Sons, Inc.

George, K.P. (2004). '*Prediction of resilient modulus form soil index properties*', Final Report, Mississippi Department of Transportation, Research Division, Jackson, Mississippi, USA.

Gere, J.M. (2001). '*Mechanics of materials*', Fifth Edition, Brooks/Cole, USA

Gudishala, R. (2004). '*Development of resilient modulus prediction models for base and subgrade pavement layers from in situ devices test results*', Masters dissertation, Louisiana State University & Agricultural and Mechanical College, Louisiana, USA.

Hicks, R.G. and Monismith, C.L., (1971). '*Factors influencing the resilient properties of granular materials*', Transportation Research Record 345, Transportation Research Board, Washington, D.C., USA.

Jooste, F.J., Long, F.M. and Hefer, A.O. (2007). '*A Method for Consistent Classification of Materials for Pavement Rehabilitation and Design*', Technical Memorandum. Modelling and Analysis Systems, Cullinan, South Africa. SABITA/Gauteng Department of Public Transport, Roads and Works, Pretoria, 2007. (GDPTRW report number: CSIR/BE/IE/ER/2007/0005/B).

Kancherla, A. (2004). '*Resilient modulus and permanent deformation testing of unbound granular materials*', Masters Dissertation, Texas A&M University, Austin, Texas, USA.

Kim, M. (2007). '*Three-dimensional finite element analysis of flexible pavements considering nonlinear pavement foundation behaviour*', PhD thesis, University of Illinois, Urbana, Illinois, USA.

Kwon, J.; Tutumluer, E.; Al-Qadi, I.L. and Anochie-Boateng, J. (2007). '*Geomaterial characterizations of full scale pavement test sections for mechanistic analysis and design*', Proceedings of Geo-Denver 2007: New Peaks in Geotechnics; Denver, 18-21 February 2007, pp 10, USA.

Lekarp, F., Isacsson, U. and Dawson, A. (2000). '*State of the art. I: Resilient response of unbound aggregates*', Journal of Transportation Engineering, Volume 126, No. 1, January/February, 2000.

National Cooperative Highway Research Program (NCHRP) (2004). '*Project 1-37A: Guide for Mechanistic-Empirical Design of New and Rehabilitated Pavement Structures*', National Cooperative Highway Research Program, Transportation Research Board, of the National Research Council, USA

Prozzi J.A. and Madanat S.M (2002). '*A non-linear model for predicting pavement serviceability*', Proceedings of the ASCE Conference on Application of Advanced Technology in Transportation, Boston, Massachusetts, USA.

Savage, P.F. (2006). '*Insights into pavement material density and strength*', Proceedings of the 25th Southern African Transport Conference (SATC), July 2006, Pretoria, RSA.

Seed, H.C., Chan, C.K. and Lee, C.E (1962). '*Resilient characteristics of subgrade soils and their relation to fatigue failures in asphalt pavements*', Proceedings of International Conference on the Structural Design of Asphalt Pavements, University of Michigan, U.S.A.

Steyn, W.J. vdM. and Paige-Green, P. (2009). '*Evaluation of issues around road materials for sustainable transport*', Proceedings of 28th Southern Africa Transportation Conference (SATC), 6 – 9 July 2009, Pretoria, RSA.

Steyn, W.J. vdM. (2001). '*Vehicle-Pavement interaction for pavement design*', PhD thesis, University of Pretoria, Pretoria, RSA.

Steyn, W.J. vdM. (2007). '*Applications of observational techniques in pavement engineering*', Proceedings of Southern Africa Transportation Conference (SATC), July 2007, Pretoria, RSA.

TG 2, Appendix A (2009). '*Technical Guideline: Bitumen Stabilised Materials*', Second Edition, May 2009, Asphalt Academy, Pretoria, RSA.

Theyse, H.L. (2006). '*The suction pressure, yield strength and effective stress of partially saturated unbound granular pavement layers*', CSIR Built Environment, Pretoria, RSA.

Theyse, H.L. (2008a). '*A mechanistic-empirical design model for unbound granular pavement layers*', PhD dissertation, University of Johannesburg, Johannesburg, RSA.

Theyse, H.L. (2008b). '*The revision of the South African pavement design method (SAPDM): Detail planning for project SAPDM/B1-a*', Technical note PMC/TN/2008-007, 6 November 2008, RSA.

Theyse, H L (2009). '*Soil-water characteristic curves and suction pressure models for partially saturated unbound material*', Report No SANRAL/SAPDM/D2/2008-01, Pretoria: Pavement Modelling Corporation, RSA.

Theyse, H.L. and Kannemeyer, L. (2010). '*New directions in the design of unbound granular layers in road pavements*', SAICE Civil Engineering, Volume 18, No. 8, September 2010, RSA.

Theyse, H.L. (2012a). '*Stress-dependent Resilient Response Model Formulation for Unbound Granular Material based on Repeated Load Tri-axial Test Results*', Pavement Modelling Corporation, Pretoria, RSA. (Report Number: SANRAL/SAPDM/B1A-2012-01).

Theyse, H.L. (2012b). Personal communication on 22 August 2012.

Thom, N.H. and Brown, S.F. (1987). '*Effect of moisture on the structural performance of a crushed-limestone road base*', Transportation Research Record, 1121, Transportation Research Board, Washington, D.C., USA.

Transportation Research Board (TRB), 1990. '*State of the art report 8: Guide to earthwork construction*', Appendix E, p 14, National Research Council, Washington, D.C., USA.

TRH 14 (1985). '*TRH 14 : Guidelines for road construction materials*', Department of Transport, Pretoria, RSA.

TRH 4 (1996). '*Draft TRH 4 : Structural design of flexible pavements for interurban and rural roads*', Department of Transport, Pretoria, RSA.

Uzan, J. (1985). '*Characterisation of granular material*', Transportation Research Record 1022, Transportation Research Board, Washington, D.C., USA.

Van Heerden, J.H.F. (2002). '*Direct measurement of pore fluid suction in gold mine tailings*', Masters dissertation, University of Pretoria, Pretoria, RSA.

Visser, A.T. (1981). '*An evaluation of unpaved road performance and maintenance*', PhD Thesis, University of Texas at Austin, May 1981.

Visser, A.T., Queiroz, C and Hudson, W.R. (1983). '*Study of resilient characteristics of tropical soils for use in low-volume pavement design*', TRB 898, p 133-140, Washington, D.C, 1983.

Yeh, S.T. and Su, C.H. (1989). '*Resilient properties of Colorado soils*', Final report, report no CDOH-DH-SM-89-9, Colorado Dept. of Highways in corporation with FWHA, December 1989, USA.

Yoder, E.J. and Witczak, M.K., (1975). '*Principles of pavement design*', 2nd Edition, John Wiley and Sons.

3 METHODOLOGY

3.1 INTRODUCTION

In Chapter 2 the definition of unbound granular material, the definitions and effect of moisture on resilient behaviour of unbound granular material, as well as modelling of resilient response of unbound granular material was investigated. In terms of the problem statement, study objectives and scope of the study, a model to accurately model the resilient behaviour of unbound granular material under different moisture conditions must be selected and calibrated. This chapter presents the methodology followed for further development and refinement of such a model.

3.2 RESEARCH DESIGN

3.2.1 Problem statement and study objectives

The problem statement of this study is as follows: The influence of moisture and density, as main parameters influencing the resilient response of unbound granular materials, can be defined through basic engineering principles.

This study has two main objectives. Firstly, to select and calibrate a general resilient modulus model for unbound granular material applicable for all moisture and density conditions. Secondly, to correlate basic engineering properties determined through basic laboratory testing to the aforementioned model.

3.2.2 Techniques applied to problem statement

Laboratory tests were conducted on a selection of natural unbound material. These tests included routine laboratory tests (according to TMH 1 (1985)), as well as more specialised testing such as resilient modulus tri-axial tests. The resilient modulus tri-axial tests were conducted over a wide spectrum of moisture and density conditions, as well as material quality range.

These results were used in statistical modelling to calibrate the resilient modulus model, which was discussed in Chapter 2. Statistical modelling includes analysis with the correlation coefficient (R^2) and Standard Error of Estimation (SEE) to indicate accuracy of modelling. Thereafter, correlation between the model's variables, sub-variables and routine laboratory tests results were investigated.

3.3 METHODOLOGY

3.3.1 Research instruments

Routine laboratory tests were conducted on the various material samples to characterise the material before tri-axial testing commenced. Such routine tests included sieve analysis, Atterberg indicators, and compaction characteristics, to name a few, which are discussed in Section 3.3.2.2.

The main source of data for this study was resilient modulus tri-axial tests. Section 3.3.1.1 provides background regarding the tri-axial test, protocol followed (Appendix C) and sample preparation.

3.3.1.1 Resilient modulus testing

Resilient modulus testing is performed at various confining pressures and deviatoric stress states in an attempt to simulate typical wheel loadings of different vehicles at different depths in the pavement structure. During testing, cylindrical specimens are subjected to different repeated/pulsed stress states under various constant all-round confining pressures to simulate the lateral stress caused by the overburden pressure and dynamically applied wheel loadings. In the AASHTO T307 procedure, a haversine load pulse with 0.1 second loading and 0.9 second rest period is generally applied on the specimen for 100 load cycles with a minimum of 500 load cycles during the conditioning stage. The total duration of one load cycle is therefore 1 second (60 load applications per minute). NCHRP Project 1-28A specifies for subgrade materials a 0.2 second haversine load pulse and 0.8 second rest period (NCHRP 1-28A, 2004). The total resilient axial deformation response of the specimen and the applied deviator stress are measured and used to calculate the resilient modulus (Anochie-Boateng *et al.*, 2009). Figure 3.1 illustrate the tri-axial cell set-up theory.
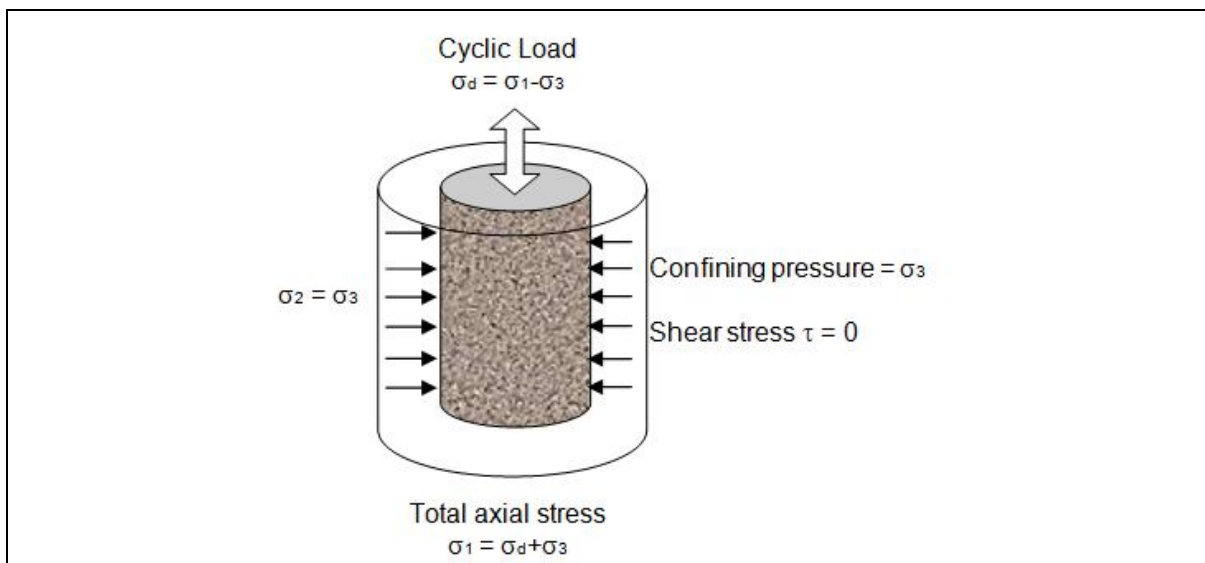
Figure 3.1:   Resilient modulus tri-axial test parameters.

Some agencies and researchers recommend that the load applications should start at the highest confining pressure with corresponding axial stress at the lowest level to avoid failure of the test samples at the beginning of the test program. This approach is usually adopted for fine-grained soils. An alternative approach is to determine the shear strength (Mohr circles) of the material using static tests at a range of confining pressures prior to repeated load testing and use this as a basis for defining the stress states to be used for dynamic testing (Anochie-Boateng *et al.*, 2009). In this thesis the latter method was used and the results of the static tests and stress state determination are summarised in Appendix D.

The theory of elasticity is usually used for flexible pavement design. The theory assumes that all materials in the pavement structure are homogeneous, isotropic and linear elastic. Based on this theory, Poisson's ratio and modulus of elasticity would be required to calculate the stresses, strains and deflections in the pavement layers. The Poisson's ratio is usually assumed or obtained through the use of correlations and the resilient modulus is used as the modulus of elasticity based on the recoverable strain under repeated loads. In mechanistic-empirical flexible pavement design, a resilient modulus value determined in the laboratory is preferred, although field measurement through back-calculation procedures from Falling Weight Deflectometer (FWD) data is acceptable (Anochie-Boateng *et al.*, 2009).

AASHTO has incorporated the resilient modulus of pavement layer materials since 1986 into the design and analysis process. Both the NCHRP and SAPDM design guides and other mechanistic based flexible pavement analysis and design approaches use the resilient modulus to characterise the unbound layers in the pavement system (NCHRP, 2004; SANRAL 2008). Laboratory determined resilient modulus values are used for new, reconstruction and rehabilitation pavement analysis in these guides and values obtained by FWD back-calculation for the analysis of reconstruction and rehabilitated pavements (Anochie-Boateng *et al.*, 2009).

3.3.1.2   *Development of resilient modulus testing procedures*

During the last few decades, research groups and agencies in different countries have proposed test methods and procedures for repeated load testing to help in establishing appropriate resilient modulus test procedures for pavement design. This development contributed considerably to the use of resilient modulus in some pavement design guides (Anochie-Boateng *et al.*, 2009).

The AASHTO pavement design guide (1986) used resilient modulus to characterise subgrade soils and to assign layer coefficients to granular base and subbase layers. In 1982, AASHTO adopted a resilient modulus testing procedure AASHTO T274-82 '*Resilient modulus of subgrade soils*', but in 1989 the AASHTO materials committee withdrew AASHTO T274-82 from their standard tests. In 1991 AASHTO approved an interim method of resilient modulus testing (AASHTO T292-1991, '*Resilient modulus testing of subgrade soils and untreated/subbase materials*'). This test method was included in the 1991 AASHTO interim testing methods Part II and was modified to AASHTO T294-1992 (Puppala, 2008).

Following this, the SHRP testing protocol (P46, '*Resilient modulus of unbound granular base/subbase materials and subgrade soil*') based on AASHTO T294-1992 was developed (Anochie-Boateng *et al*., 2009).

The SHRP protocol P46 was later also modified and developed into AASHTO standard, which was adopted as AASHTO T307-99. AASHTO T307-99 is currently the standard test adopted by AASHTO for determining the resilient modulus of pavement granular material in the laboratory. Several other test methods and procedures were or are being developed throughout the world. The University of Stellenbosch (South Africa) has proposed a test procedure for testing granular materials (Ebels and Jenkins, 2007 as quoted by Anochie-Boateng *et al*., 2009). Also the NCHRP has proposed new procedures for testing unbound materials (NCHRP 1-28A, 2004), which are essentially the same as AASHTO T307-99 but specifies internal axial strain measurement and a different set of stresses for testing. Other methods include the European standard (CEN, 2004) and the Australian method '*Determination of permanent deformation and resilient modulus characteristics of unbound granular materials under drained conditions*' (Vuong and Brimble, 2000 as quoted by Anochie-Boateng *et al*., 2009). Individual researchers have also made use of revised or proposed test procedures for determining resilient modulus of unbound material (Andrei *et al*., 2004 as quoted by Anochie-Boateng *et al*., 2009).

Table 3.1 summarises the main differences between the various resilient modulus test procedures. The characteristic differences between the test procedures show the emergence of different resilient modulus test procedures during the past decade. As part of the revision of the current mechanistic-empirical pavement design practice in South Africa, CSIR (through a Strategic Research Project) is developing test protocols for pavement materials characterisation including geomaterials (Anochie-Boateng *et al*., 2009).

Table 3.1: **Summary of main differences among resilient modulus tri-axial test methods (Anochie-Boateng *et al.*, 2009).**

Property	EN 13286-7 (2004)	AASHTO T307-99 (2005)	NCHRP I-28A (2004)	CSIR Transportek (2002)	University of Stellenbosch (2007)	University of Illinois (1998)	Australia AG:PT/053 (2007)
Material types	Max aggregate size < 0.2 sample diameter	1. (Max size < 70% < 2.0 mm < 20% < 0.075 mm, PI < 10%) 2. All others	1. (Max size > 9.5; > 25.4 scalped) 2. (Max size > 9.5; < 10%<0.075) 3. (Max size <9.5; >10%<0.075) 4. Thin wall undisturbed	No details – Borrow pit or test pit Max size 37.5 mm	Unbound & bound granular materials Max size 19 mm duplicate specimens	Unbound aggregates & subgrade soils Max size 25 mm	Max size 19 mm – oversize discarded (not more than 5%)
Specimen preparation	Vibro-compression (1 layer) Vibratory hammer (6-7 lifts)	1. Vibratory hammer (6 lifts) 2. Static (5 lifts) or pneumatic kneading (5 lifts)	Type 1: Impact (Proctor)/ Vibratory hammer (or rotary) Type 2: Vibratory Type 3: Impact/kneading	Vibratory table 3-lifts in split mould	Not finalised	Standard pneumatic concrete vibratory compactor 3-lifts in split mould	Standard & modified Proctor methods at (5 or 8 lifts)
Specimen compaction state	Moisture content & density reps of field conditions 6 specimens (OMC – 4,2,1% & 100,97,95% density)	Insitu wet density & moisture content or standard modified Proctor	Desired density & moisture content	Two levels of density 995-98% & 102-105% Mod) and moisture content (Sr 45, 75%)	Specified moisture content and density	Optimum moisture content and max dry density	Optimum moisture content and max dry density
Height : diameter	2 ± 2% Diam > 5 times max particle size (160 x 320 mm)	2.0 70 mm diam (subgrade); Min diam = 5 times max size (base/subbase)	2.0 70 mm diam (fine-grained), 100-150 mm diam (coarse-grained)	2.0 150 mm x 300-305 mm high	2.0 150 mm diam x 300 mm high	2.0 50 mm diam (subgrade soils); 150 mm diam (base/subbase)	2.0 100 diam x 200 mm high for fine- & coarse-grained
Response measurement	Load cell internal 3 axial LVDTs measuring centre 100 mm of sample at 120°, attached to membrane	Load cell external 2 external axial LVDTs	Load cell internal 2 internal axial LVDTs	Load cell On sample full length	Load cell On specimen LVDTs over middle third	Load cell internal 2 external axial LVDTs	Load cell external or internal 2 axial LVDTs
Confining pressure	Variable & constant (vacuum	Constant up to 140 kPa	Constant up to 140 kPa	Constant up to 200 kPa	Constant up to 200 kPa	Constant up to 140 kPa	Constant up to 500 kPa

3-5

Property	EN 13286-7 (2004)	AASHTO T307-99 (2005)	NCHRP I-28A (2004)	CSIR Transportek (2002)	University of Stellenbosch (2007)	University of Illinois (1998)	Australia AG:PT/053 (2007)
	option) up to 600 kPa						
Chamber medium	Water, air or silicon oil	Air	Air	Air	Air or water	Air	Silicon oil or water covering sample, together with air for pressure
Specimen conditioning	70 kPa confining; axial deviator stress of 200-340 kPa; 20 000 reps	103.4 kPa confining; axial deviator stress of 103.4 kPa; 500-1000 reps	27.6-103.5 kPa confining for subgrade, base/subbase at 1000 reps; axial deviator stress of 50.8-227.7 kPa	200 kPa confining; axial deviator stress of $0.45 \times \sigma_d$ at failure; 500-1000 reps	200 kPa confining; axial deviator stress of 20 kPa; 5000 reps	103.4 kPa confining; axial deviator stress of 310.5 kPa; 1000 reps	50 kPa confining; axial deviator stress of 100 kPa; 1000 reps
Load type	Frequency of axial load (0.2-10 Hz)	Haversine, 0.1s load & 0.9s rest (hydraulic); 0.9 to 3s rest (pneumatic)	Haversine, 0.1s load & 0.9s rest (base/subbase); 0.2s load & 0.8s rest (subgrade)	Haversine, 0.2s load & 0.8s rest period	Haversine, 0.5s load & 0.5s rest period	Haversine, 0.1s load & 0.9s rest period	3s vertical force wave length with load of 1s and rise & fall of 0.3s
Test sequence	100 reps at 29 stress states; confining of 20-150 kPa and axial deviator stress of either 30-475 kPa or 20-300 kPa	100 reps at 15 stress states; confining of 20.7-138 kPa and max axial deviator stress of 20.7-276 kPa	Type 1: 100 reps at 30 stress states; Type 2: at 20 stress states; Type 3: 16 stress states; confining of 20.7-138 kPa and deviator of 20.7-993 kPa cyclic	100 reps at 14 stress states; confining of 20-200 kPa and axial deviator stress of 0.08 to 0.81 times the failure stress	100 reps at 15 stress states; confining of 20-200 kPa (coarse), 140 kPa (fine) and axial deviator stress of 0.1 to 0.9 times the failure stress	100 reps at 8 stress states; confining of 34.5-207 kPa and axial deviator stress of 69-414 kPa	At least 50 reps at 66 stress states; confining of 20-150 kPa and axial deviator stress of 100-600 kPa
Results	Average of last 10 cycles use to compute M_R Stress, strain & MR for each stress path	Average of last 5 cycles use to compute M_R Standard forms	Average of last 5 cycles use to compute M_R Standard forms to calculate MR	Average of all load cycles use to compute M_R Standard spreadsheet	Average of all load cycles use to compute M_R Ave axial deformation per cycle, elastic axial strain, ave MR, bulk stress	Average of last 50 cycles use to compute M_R Not stated	Average of last 6 cycles use to compute M_R For each combination (66) N, Ave s3 & sd, ave MR

3.3.1.3   Development of protocol for SAPDM projects

Equipment setup

The NCHRP 1-28A and EN13286-7 require the use of a load cell inside the tri-axial cell allowing for more accurate reading of the load on the sample. However, the load cells for the available tri-axial machines at the CSIR and University of Stellenbosch are mounted outside the tri-axial cell, similar to AASHTO-T307 and AG:PT/T053 requirements. It should be mentioned that the AASHTO-T307 is being replaced by the NCHRP 1-28A. For the proposed protocol, testing will be conducted using the current equipment set up, but the location of the load cell is indicated in the test conditions when reporting test results (Anochie-Boateng *et al.*, 2009). Tri-axial tests results reported on in this thesis were conducted at the CSIR and therefore the load cell was located outside the tri-axial cell for all tests reported.

Vertical deformation measurement

For the measurement of the vertical deformation, the AASHTO-T307, NCHRP 1-28A and the AG:PT/T053 all require no more than two Linear Variable Displacement Transducers (LVDTs), while the EN13286-7 requires at least two LVDTs. In the AASHTO-T307 the vertical deformation measurement devices are mounted outside the tri-axial cell, while in the NCHRP 1-28A procedure the LVDTs are inside the tri-axial chamber. In the previous CSIR tri-axial test protocol, two LVDTs were specified, while in the proposed protocol the deformation measurement device will consist of three LVDTs diametrically spaced at 120º supported by two plastic collar clips 100 mm apart. The LVDTs shall be placed vertically and, attached to the sample over the middle section of the sample (Anochie-Boateng *et al.*, 2009). Figure 3.2 illustrates the CSIR tri-axial set-up that was used in this thesis with the three LVDTs inside the tri-axial cell.
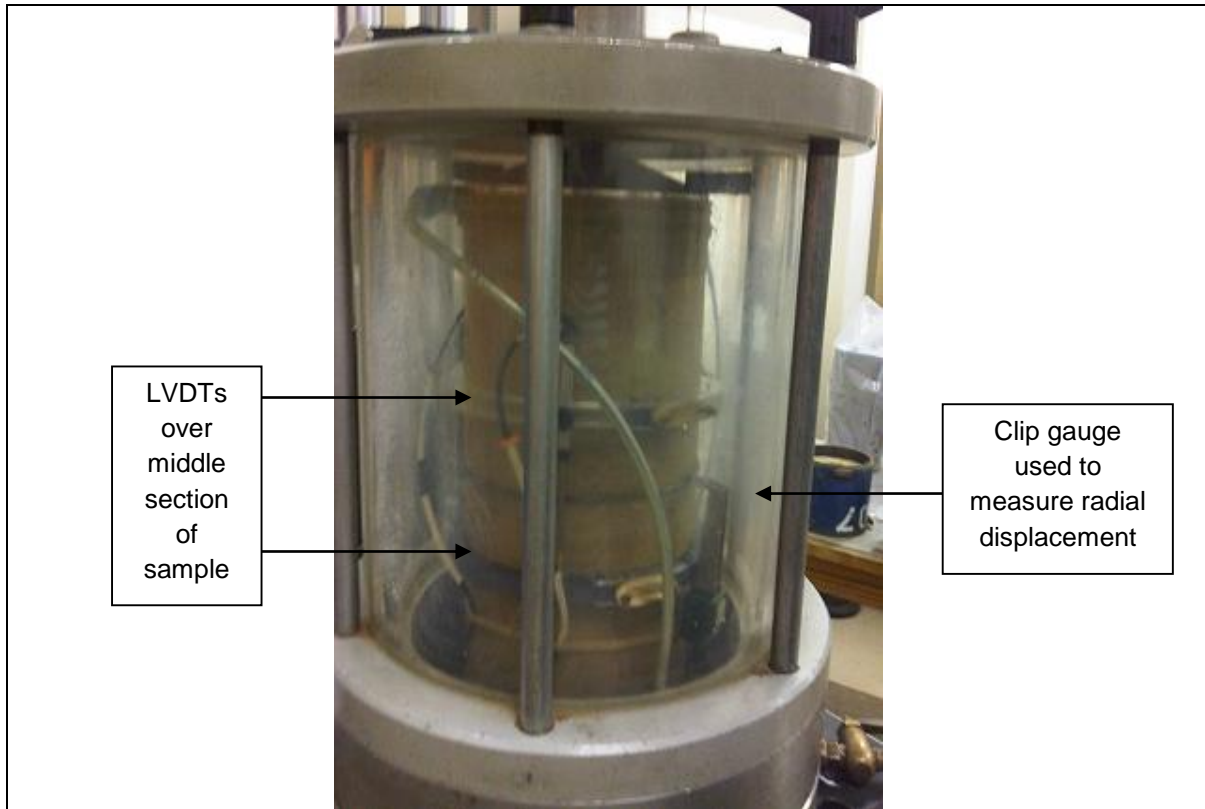
Figure 3.2: **Resilient modulus tri-axial test set-up at the CSIR.**

Measuring radial displacement

Radial displacement was measured and used to calculate Poisson's ratio for each test reported on in this thesis. The radial displacement of the sample was measured with a wire connected to a clip gauge situated in the middle of the sample, between the plastic collars of the LVDTs (Figure 3.2).

Load pulse

The application of the load for the resilient modulus requires a closed-loop electro-hydraulic system capable of generating haversine loading waveform. NCHRP 1-28A uses a haversine load pulse with a 0.1 second duration followed by 0.9 second rest. This loading waveform is deemed to simulate the passing of an axle over a pavement section. It is applicable to base and subbase layers, while a load pulse with a 0.2 second duration followed by 0.8 second rest is applicable to subgrade layers. A haversine load pulse according to NCHRP 1-28A will be used in the proposed protocol. However, it may be necessary to adjust both the pulse duration and rest period depending on the material response (Anochie-Boateng *et al.*, 2009). Tests conducted for this thesis used a haversine load pulse of 0.1 second duration followed for 0.9 second rest.

Specimen size

Data in Table 3.1 reveal that the specimen sizes range from 100 mm to 152.4 mm in diameter and 200 mm to 305 mm in height. The dimensions are mostly dependent on the maximum particle size of the sample being tested. Most protocols require that the length to diameter ratio (L/D) be equal or greater

than 2:1 (Anochie-Boateng *et al.*, 2009). All specimens tested and reported on in this thesis was 152.4 mm (±0.5 mm) in diameter and 305 mm in height (± 5 mm).

Method of compaction

There are several methods for the compaction of specimen in the laboratory and their effect is considered to be different. The application of a static load and the dynamic hammer are the most common methods. Compaction of samples is also achieved by a kneading action or using vibration compaction methods, e.g. vibratory table or vibratory hammer. The vibratory hammer is the recommended compaction method for bitumen stabilized materials (BSM) according to the TG2 Guideline. However, experience has shown that the method may not be appropriate for some materials. The alternative method of compaction is the vibratory table as described in Method A11T in the TMH1 (1985). The vibratory table is the recommended method of compaction in the proposed protocol. It is critical that the method of compaction achieve targeted density or volumetric density as required (Anochie-Boateng *et al.*, 2009). The compaction method used in this thesis was the vibratory table and the actual volumetric density was determined after compaction of each specimen to ensure the required volumetric density was achieved.

Confining pressure during resilient modulus testing

Almost all methods, except for EN13286-7, use constant confining pressure for a given load sequence with different deviator stress levels during the resilient modulus testing. In the EN13286-7 method, both constant and variable confining pressure application are included. In the proposed protocol the constant confining pressure method during the resilient modulus testing shall apply (Anochie-Boateng *et al.*, 2009). A constant confining pressure was used in testing which is reported on in this thesis. The confining pressure was varied during the test and this will be described in Section 3.3.2.3.

Conditioning and resilient modulus testing of specimens

A comparison among the existing protocols reveals that the required cycles for conditioning a specimen ranges between 500 and 20 000, the load pulse is generally haversine with a duration of 0.10 seconds. Application of 1000 cycles is the most common. The required cycles during the resilient modulus testing range between 50 and 200. The most common number of load repetitions is 100. In the proposed protocol, the recommended number of load cycles during specimen conditioning is 1000 and 100 load cycle application for the resilient modulus determination at each load/stress level (Anochie-Boateng *et al.*, 2009). The aforementioned proposed conditioning and load cycle application was followed for testing.

3.3.2   Data

Data for this thesis were obtained through laboratory testing. Appendix D contains all the data obtained through laboratory testing. Only summaries of data will be given where relevant to discussion in Chapters 4 to 6.

Continued quality control was done throughout the period of laboratory testing to ensure that no errors due to operator error or equipment failure were translated into the data obtained.

3.3.2.1   *Material*

Apart from the two materials used by Theyse (2012) for the cord modulus model development, several other unbound granular materials were sourced from in-service roads around South Africa. Table 3.2 lists the bulk samples and Figure 3.3 indicates the location of the bulk sample sites against Thornthwaite's Moisture Index. Bulk samples were taken in four of the five climatic areas in South Africa, therefore attempting to include varying material characteristics, especially material that is known to be moisture sensitive. Route S191 (located in a dry sub-humid area), N4 extension (located in a moist sub-humid area), P10-2 (located in a humid area) and route D804 (located in a semi-arid area). It should be noted that for the NCHRP MEPDG, Thornthwaite's Moisture Index (I_m) was introduced as a climatic variable for use in the base material models (Zapata and Houston, 2008).

Table 3.2:   **Bulk sampled materials and description.**

Sample no.	Sample ID	Description
1*	N4 Ext. B	Crushed norite from the base layer of N4 extension
2	N4 Ext. USel	Weathered chert from the selected layer of N4 extension
3	S191 B	Crushed dolerite from the base layer of S191 near Bethlehem
4	P10-2 B	Weathered shale from the base layer of P10-2 near Bergville
5	D804 B	Weathered calcrete andesite from the base layer of D804 near Slurry, Mafikeng

*Material results used in cord modulus formulation by Theyse (2012)
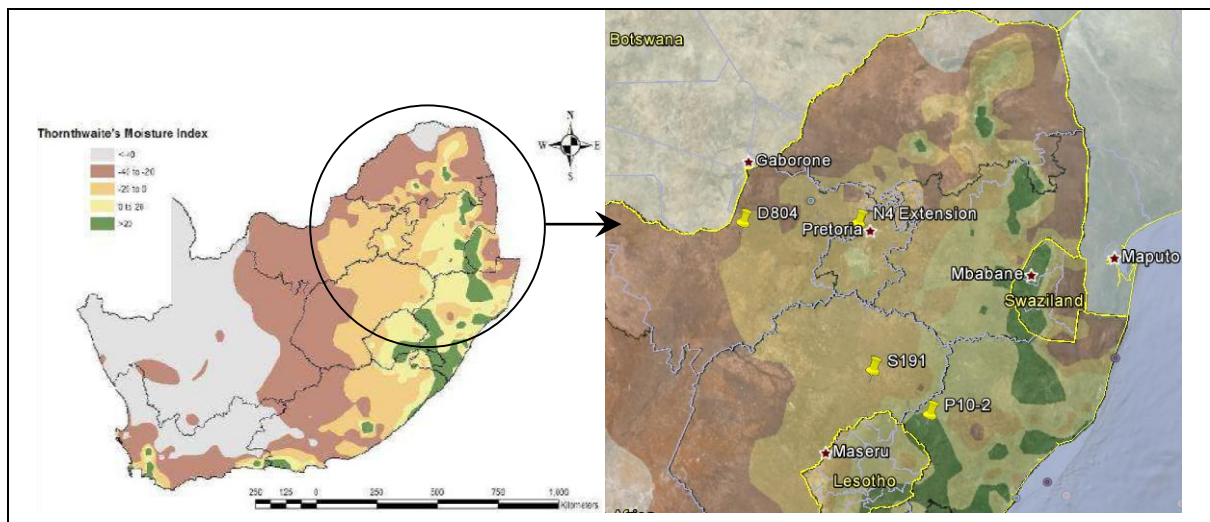
Figure 3.3:   **Location of bulk sample sites.**

3.3.2.2 Routine testing

Standard laboratory testing was done to characterise the material sampled. These routine tests were done in triplicate to ensure correct characterisation of the material and included the following tests:

1. Sieve analysis to determine the particle size distribution of the material;
2. Atterberg indicator tests to characterise the fine fraction of the material;
3. Compaction characteristics:
4. Volumetric properties characterised through Apparent Relative Density and Bulk Relative Density (ARD & BRD) and water absorption;
5. Gravimetric properties characterised through maximum dry density and optimum moisture content (OMC & MDD) using both the Mod AASHTO and vibratory table compaction methods;
6. California Bearing Ratio (CBR) of the material to indicate the materials bearing capacity; and
7. Durability mill to indicate the durability of the material.

Although not routine, suction tests were also conducted on selected materials to indicate the suction pressure which can be expected in the material at various degrees of saturation.

3.3.2.3 Tri-axial testing (Static and Resilient testing)

The most important variables to be considered for testing under the SAPDM project, and which also applies to this thesis is indicated in Table 3.3.

Table 3.3: **Variables to be considered for testing the resilient modulus of unbound granular material (Theyse, 2008b).**

Test variables	Yield strength (Static tri-axial)	Density (D)	• Effect confined to relatively narrow band of density values depending on the material type. • Test at two levels and approximate effect with a linear model.
		Saturation (S)	• Effect highly non-linear over a range of saturation values from 10 to 100%. • Test at least 3 levels (low, medium, high). Exact levels to be determined by material type, but low level always below 20% saturation.
		Confinement (C)	• Effect non-linear. • Test at least 3 levels (low, medium, high). Exact levels to be determined by material type, but low level always equal to 0 kPa.
	Resilient modulus	Density (D)	• Effect confined to relatively narrow band of density values depending on the material type. • Test at two levels and approximate effect with a linear model.

© University of Pretoria

	(Resilient modulus tri-axial)	Saturation (S)	• Effect highly non-linear over a range of saturation values from 10 to 100%. • Test at least 3 levels (low, medium, high). Exact levels to be determined by material type, but low level always below 20% saturation.
		Confinement (C)	• Effect non-linear. • Test at least 3 levels (low, medium, high). Exact levels to be determined by material type, but low level always equal to 0 kPa.
		Stress ratio (SR)	• Planned at 10, 30, 50, 70, and 90 percent of yield strength • 100 load cycles per stress ratio all done on the same specimen

Static tri-axial testing

The testing combinations for static tri-axial or monotonic loading tests, from which the yield/shear/failure strength was determined for this thesis, are set out in Table 3.4 and are similar to those indicated by Theyse (2008b). Density was either high or low, depending on the material characteristics. Saturation was tested as low (smaller than 20 per cent saturation); intermediate (between 40 and 60 per cent saturation) or high (greater than 60 per cent saturation but preferably 80 per cent or greater). Saturation smaller than 20 per cent generally converts to moisture contents of between 1 and 2 per cent, which is dry, while saturation of 80 per cent has been indicated by Savage (2006) to be the OMC of compacted material, i.e. the wet condition for testing.

Confinement was 0, 100 and 200 kPa. Only one repeat was tested at each combination of density, saturation and confinement, since the test is not as variable in nature as the resilient modulus tri-axial test and therefore resulting in 18 static tri-axial tests per bulk material sample. For static tri-axial tests, elements such as the density of the sample, the moisture content, loading rate and level of confinement is fixed for the duration of the test.

Table 3.4:   Test variable combinations for failure strength testing (Theyse, 2008b).

Density (D)	Saturation (S)	Confinement (C)		Test ID	Repeat
High (*H*)	Low (< 20%) (*L*)	Low (*0*)	(0 kPa)	D(*H*), S(*L*), C(*0*)	1
		Intermediate (*I*)	(100 kPa)	D(*H*), S(*L*), C(*I*)	1
		High (*H*)	(200 kPa)	D(*H*), S(*L*), C(*H*)	1
	Intermediate (40 – 60%) (*I*)	Low (*0*)	(0 kPa)	D(*H*), S(*I*), C(*0*)	1
		Intermediate (*I*)	(100 kPa)	D(*H*), S(*I*), C(*I*)	1
		High (*H*)	(200 kPa)	D(*H*), S(*I*), C(*H*)	1
	High (> 60%) (*H*)	Low (*0*)	(0 kPa)	D(*H*), S(*H*), C(*0*)	1
		Intermediate (*I*)	(100 kPa)	D(*H*), S(*H*), C(*I*)	1
		High (*H*)	(200 kPa)	D(*H*), S(*H*), C(*H*)	1

Density (D)	Saturation (S)	Confinement (C)			Test ID	Repeat
Low (L)	Low (< 20%) (L)	Low	(0)	(0 kPa)	D(L), S(L), C(0)	1
		Intermediate	(I)	(100 kPa)	D(L), S(L), C(I)	1
		High	(H)	(200 kPa)	D(L), S(L), C(H)	1
	Intermediate (40 – 60%) (I)	Low	(0)	(0 kPa)	D(L), S(I), C(0)	1
		Intermediate	(I)	(100 kPa)	D(L), S(I), C(I)	1
		High	(H)	(200 kPa)	D(L), S(I), C(H)	1
	High (> 60%) (H)	Low	(0)	(0 kPa)	D(L), S(H), C(0)	1
		Intermediate	(I)	(100 kPa)	D(L), S(H), C(I)	1
		High	(H)	(200 kPa)	D(L), S(H), C(H)	1

Resilient modulus tri-axial testing

Resilient testing was done according to Table 3.5, which is similar to what was proposed by Theyse (2008b). A single specimen was required for testing the effect of confinement and stress ratio. Given the variable nature of the resilient modulus tri-axial test, three repeats were tested at each combination of density and saturation, resulting in 18 resilient tests per bulk material sample.

Table 3.5: **Test variable combinations for resilient modulus testing (Theyse, 2008b).**

Density (D)	Saturation (S)	Confinement (C) (kPa)	Stress ratio (%)	Test ID	Repeat
High (H)	Low (< 20%) (L)	25, 50, 100, 150, 200	10, 30, 50, 70	D(H), S(L)	3
	Intermediate (40 – 60%) (I)	25, 50, 100, 150, 200	10, 30, 50, 70	D(H), S(I)	3
	High (> 60%) (H)	25, 50, 100, 150, 200	10, 30, 50, 70	D(H), S(H)	3
Low (L)	Low (< 20%) (L)	25, 50, 100, 150, 200	10, 30, 50, 70	D(L), S(L)	3
	Intermediate (40 – 60%) (I)	25, 50, 100, 150, 200	10, 30, 50, 70	D(L), S(I)	3
	High (> 60%) (H)	25, 50, 100, 150, 200	10, 30, 50, 70	D(L), S(H)	3

From the discussion in this section, it is clear that sufficient data will be obtained for each material and through constant quality control the quality of the data should not be in doubt.

3.3.3   Analysis

Data obtained were analysed using statistical methods. Regression analysis were utilised in calibration of the cord modulus model where the correlation coefficient (R^2), Root Mean Square Error (RMSE),

Standard Error of Estimate (SEE) and average error were used as indicators of the accuracy of the analysis.

R^2 gives an indication of the linearity of the relationship between Y and X (Van As, 2003), i.e. how well a regression line fits the data. For linear regression, R^2 is simply the square of the sample correlation coefficient between the outcomes and their predicted values, or in the case of simple linear regression, between the outcome and the values being used for prediction. In such cases, the values vary from 0 to 1, with 1 indicating a line fitting the data perfectly. In this thesis R^2 will be calculated using the following equation in the processing of the measured data in MS Excel spreadsheets, which is described in Section 4.2.3.

$$R^2 = 1 - \frac{SS_{err}}{SS_{tot}} = 1 - \frac{\sum((y_i - f_i)^2)}{\sum((y_i - \bar{y})^2)} = 1 - \frac{\sum(M_{obs} - M_{pred})^2}{\sum((M_{obs} - Ave_{obs})^2)} \tag{3.1}$$

Where

SS_{err} = residual sum of squares;

SS_{tot} = total sum of squares;

y_i = observed values of the data set;

f_i = associated modelled values;

$\bar{y}$ = mean of the observed data (Draper and Smith, 1998; Everitt, 2002).

However, R^2 does not indicate whether:

- the independent variables are a true cause of the changes in the dependent variable;
- omitted-variable bias exists;
- the correct regression was used;
- the most appropriate set of independent variables has been chosen;
- there is co-linearity present in the data; or
- the model might be improved by using transformed versions of the existing set of independent variables (Draper and Smith, 1998; Everitt, 2002).

Negative values of R^2 may occur when fitting non-linear trends to data. In these instances, the mean of the data provides a fit to the data that is superior to that of the trend under this goodness of fit analysis (Cameron and Windmeijer, 1997) (Appendix E).

RSME is used in cross-validation, sometimes called rotation estimation, which is a technique for assessing how the results of a statistical analysis will generalize to an independent data set. It is mainly used in settings where the goal is prediction, and one wants to estimate how accurately a predictive model will perform in practice. Cross-validation is important in guarding against testing hypotheses suggested by the data, especially where further samples are hazardous, costly or impossible to collect.

When the value being predicted is continuously distributed, the mean squared error, root mean squared error or median absolute deviation could be used to summarize the errors (Draper and Smith, 1998; Everitt, 2002).

SEE indicates the difference between the estimate and the true value. Correlation between observed data and predicted data were also evaluated using the afore-mentioned indicators. A more detailed description of the analysis on the relevant data will be given in each chapter as it is utilised.

3.4 LIMITATIONS

This study has a number of limitations which will be discussed briefly.

3.4.1 Material

Only seven different materials could be sampled to be included in this thesis due to time and financial constraints. The materials obtained were also dictated by the site selection of other SAPDM projects, since results from one SAPDM project will be used to supplement those required in other SAPDM projects. Ideally a more comprehensive range of the most commonly used natural material in pavement construction over South Africa should be tested to ensure the data obtained through testing is as comprehensive as possible. However, the seven different materials represent a good spread of typically used road building material and its properties.

3.4.2 Laboratory testing

Apart from being limited to only five different materials, each could only be tested at a low, medium and high saturation level, with only a high and low density level. Data obtained through tri-axial testing would be more complete if the levels of saturation could have been tested at intervals of 10 per cent of saturation. Unfortunately this could not be done due to financial and time constraints. The same limitations apply to the density levels, as the matrix of specimens to be tested at the aforementioned saturation levels and additional density levels would grow exponentially.

Suction tests performed on selected materials proved problematic. The suction test method used by University of Witwatersrand (WITS), where testing was conducted, consisted of a gypsum block inserted into a laboratory prepared sample. After the gypsum block was inserted, the disturbed material was compacted over the block. The testing consisted of cycles of wetting and drying of the samples. This was a lengthy process as the duration of one test was 3 to 4 months. Although the same trend can be observed, the results obtained from the tests were highly variable when compared to the suction model developed and refined by Theyse (2009). Matric suction is plotted on a log scale and even a small difference could result in order of magnitude differences (Figure 3.4). Therefore the testing and

incorporation of suction pressure in this thesis was abandoned and it is recommended that the testing of suction pressure should be investigated and refined to improve the accuracy of results.
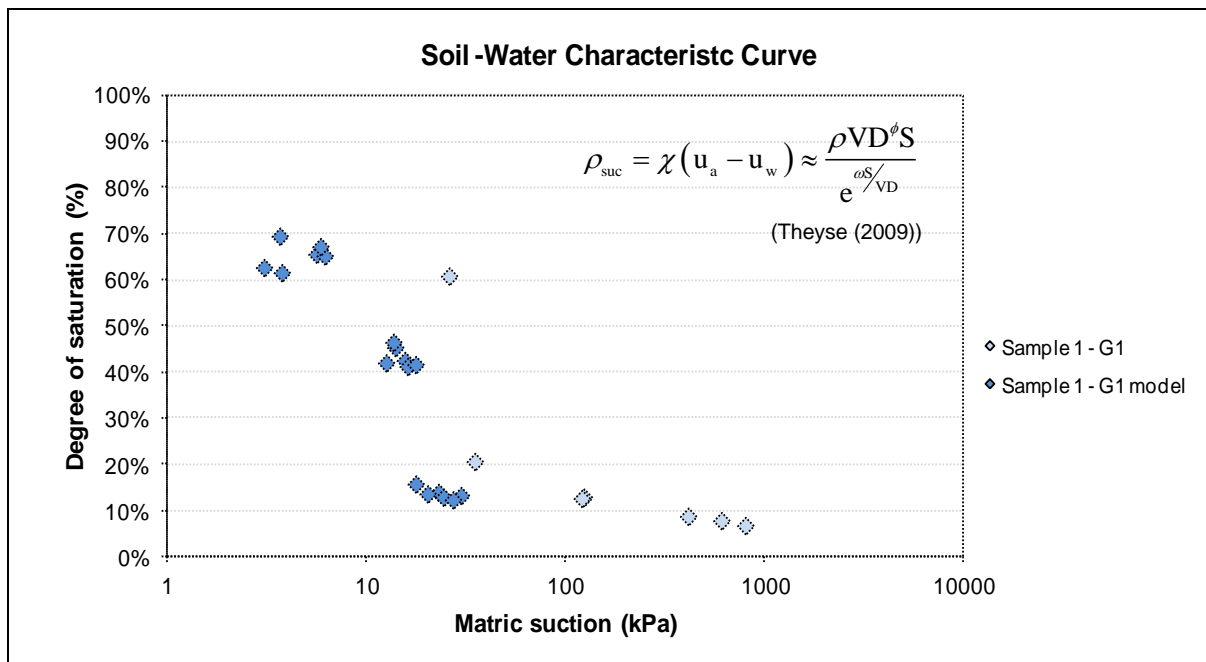
Figure 3.4:   **Matric suction measured versus suction model.**

3.4.3   Analysis

Analysis through statistical methods is widely recognised. However, the extent to which obtained results can be used to generalise conclusions is limited, since it is only applied to a limited set of data. With more comprehensive data available, the analysis could be more refined and more general conclusions can be reached. Nonetheless, the range of materials, saturation levels, density levels and suction values for each material was sufficient for adequate analysis to reach a conclusion in terms of the problem statement and objectives.

3.4.4   Conclusion

The methodology described in this chapter was used in the remainder of the thesis. Data obtained through the research instruments was analysed according to the methods described. More detail of analysis will be given as relevant in each chapter to follow.

3.5 REFERENCES

AASHTO T-307, (2005). '*Standard method of test for determining the resilient modulus of soils and aggregate materials*', U.S.A.

Anochie-Boateng, J.; Paige-Green, P. and Mgangira, M.B. (2009). '*Evaluation of test methods for estimating resilient modulus of modules of pavement geomaterials*', Paper presented at the 28th Annual Southern African Transport Conference 6 - 9 July 2009, CSIR International Convention Centre, Pretoria, South Africa.

Cameron, A.C., Windmeijer, F.A.G. (1997). '*An R-squared measure of goodness of fit for some common non-linear regression models*', Journal of Econometrics, Volume 77, Issue 2, April 1997, pp. 329-342.

Draper, N.R. and Smith, H. (1998). '*Applied regression analysis*', 3rd Edition, Wiley-Interscience, New York, U.S.A.

Everitt, B.S. (2002). '*Cambridge dictionary of statistics*', 2nd Edition, Cambridge University Press, U.K.

National Cooperative Highway Research Program (NCHRP) (2004). '*Project 1-37A: Guide for Mechanistic-Empirical Design of New and Rehabilitated Pavement Structures*', National Cooperative Highway Research Program, Transportation Research Board, of the National Research Council, USA.

National Cooperative Highway Research Program (NCHRP), (2004). '*Project 1-28A: Recommended standard method for routine resilient modulus testing of unbound granular base/subbase materials and subgrade soils*', NCHRP Research Results Digest No 285, Laboratory determination of resilient modulus for flexible pavement. January 2004, U.S.A.

Puppala, A.J. (2008). '*Estimating stiffness of subgrade and unbound materials for pavement design*', NCHRP Synthesis 382, Transportation Research Board, U.S.A.

Savage, P.F. (2006). '*Insights into pavement material density and strength*', Proceedings of the 25th Southern African Transport Conference (SATC), 10 – 13 July 2006, Pretoria, RSA.

Theyse, H L (2009). '*Soil-water characteristic curves and suction pressure models for partially saturated unbound material*', Report No SANRAL/SAPDM/D2/2008-01, Pretoria: Pavement Modelling Corporation, RSA.

Theyse, H.L. (2008b). '*The revision of the South African pavement design method (SAPDM): Detail planning for project SAPDM/B1-a*', Technical note PMC/TN/2008-007, 6 November 2008, RSA.

TMH 1 (1985). '*Technical Methods Highways 1 : Standard test methods for roadbuilding materials*', Department of Transport, Pretoria, RSA.

Van As, S.C. (2003). '*Applied statistics for Civil Engineers*', B.Eng (Honours) course material, University of Pretoria, Pretoria, RSA.

Zapata, C.E. and Houston, W.N. (2008) '*Calibration and validation of the Enhanced Integrated Climatic Model for pavement design*', NCHRP Report 602, Transportation Research Board, Washington, D.C, USA.

4   VERIFICATION OF RESILIENT RESPONSE MODEL

4.1   INTRODUCTION

In Section 2.3.3.3, the cord modulus model formulated by Theyse (2012) was identified as a formulation which can be refined further and calibrated through the data accumulated by resilient modulus tri-axial testing in this thesis. In this chapter the verification of the model through the data available will be explored.

4.2   MATERIAL TEST RESULTS

Sections 4.2.1 to 4.2.3 contain summaries of the results obtained. Complete result sets are contained in the Appendices referred to in the relevant sections.

4.2.1   Routine test results

The aim was to sample a sufficient variety of material types, specifically including moisture sensitive materials. Table 4.1 summarise the average of three repeat tests per bulk material sampled on selected tests and Figure 4.1 depicts the grading of all the materials. All test results are contained in Appendix D. The results appear reasonable and within the expected limits for the type of material tested.
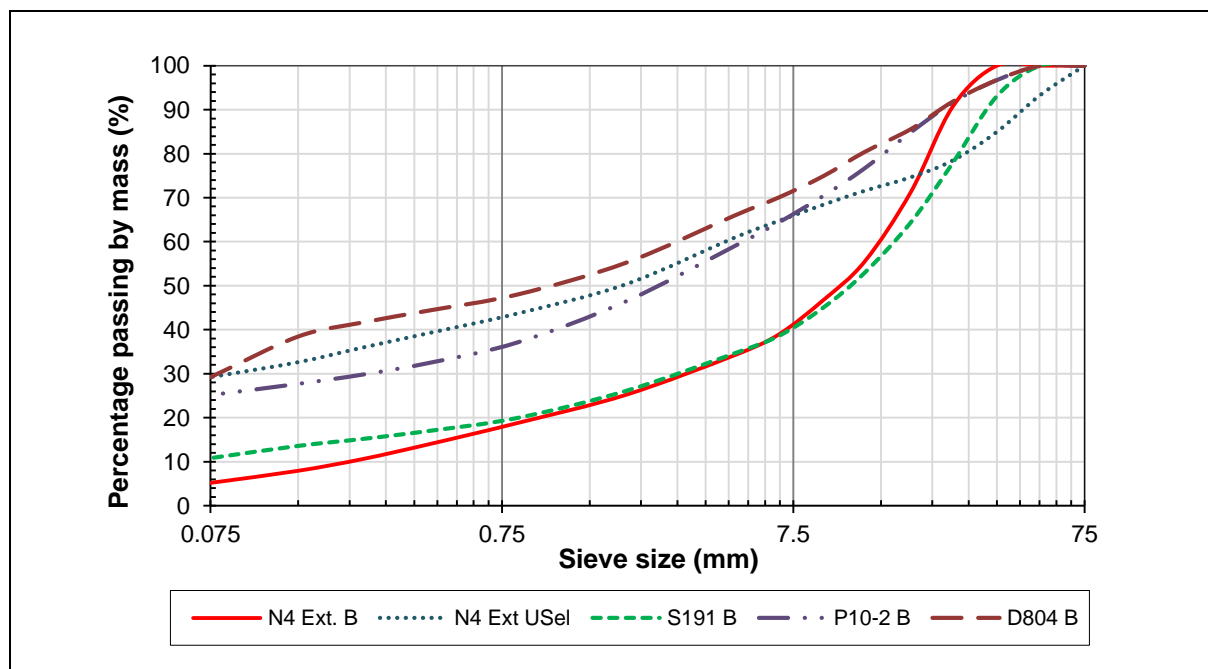
Figure 4.1:   Summary of experimental materials' grading.

Table 4.1: Summary of routine test results.

Material type	Source (Layer)	GM	P_{max} (%)	% Passing 0,425 mm	% Passing 0,075 mm	LL (%)	PL (%)	PI (%)	LS (%)	MDD_{mod} (kg/m³)	OMC_{mod} (%)	MDD_{vib} (kg/m³)	OMC_{vib} (%)	ARD (kg/m³)	TRH 14	AASHTO	DMAC Method
			Grading			**Atterberg limits**				**Mod AASHTO**						**Classification**	
Norite	N4 Ext B	2.60	37.5	14.0	5.2	-	-	-	-	2 465	4.6	2 610	5.0	2 949	G1	A-3	G4 (45%)
Chert	N4 Ext USel	1.90	75.0	37.5	28.3	31.8	19.6	12.3	5.6	2 063	10.6	2 037	11.2	2 895	G5	A-2-6	G5 (49%)
Dolerite	S191 Base	2.50	53.0	17.0	10.8	30.6	22.5	8.1	5.1	2 343	6.9	2 400	8.1	2 907	G6	A-2-4	G4 (45%)
Shale	P10-2 B	1.96	53.0	32.5	25.1	26.5	18.8	7.7	5.2	2 133	8.3	2 130	9.5	2 743	G8	A-4	G3 (41%)
Calcrete	D804 B	1.70	53.0	44.4	29.2	28.1	18.4	9.6	6.6	2 037	9.4	2 018	10.6	2 706	G7	A-4	G6 (49%)

P_{max} — Maximum particle size (mm)

LL — Liquid Limit

PI — Plasticity Index

LS — Linear Shrinkage

GM — Grading Modulus

ARD — Apparent Relative Density

MDD_{mod} — mod AASHTO maximum dry density

OMC_{mod} — mod AASHTO optimum moisture content

MDD_{vib} — vibratory table maximum dry density

OMC_{vib} — vibratory table optimum moisture content

When the Coefficient of Variation (CoV) is calculated for each of the bulk samples' routine tests listed in Table 4.1 (three repeats per routine test), the CoV varies between 25.2 per cent and 0.7 per cent, indicating the variability in routine laboratory tests per material.

When the variability per routine test is assessed with the results available, PI tests indicate the highest variability and MDD the lowest, as is summarised in Table 4.2. Jacobsz and Day (2008) compared the results of basic soil tests from four different laboratories and concluded that for Atterberg Indicators, the LL varied from 53 to 78 per cent, PL from 30 to 42 per cent, PI between 15 to 45 per cent and LS between 9 and 18 per cent for a clayey material. The variability in test results was also identified and addressed in the DMAC classification method (TG 2, 2009) by linking a Certainty Factor (CF), a value equal or below 0.4, to each test considered significant to characterise a material. The CoV calculated indicate clearly that there is inherent variability within any material and the testing of that material.

Table 4.2: **Variability per routine test.**

Constant	Coefficient of Variation (CoV)
LL (%)	4.9%
PL (%)	1.9%
PI (%)	14.3%
LS (%)	4.4%
GM	3.1%
MDD (kg/m^3)	1.3%
OMC (%)	6.5%

Table 4.3 summarises the variability per bulk material sample.

Table 4.3:   Variability per bulk sample per routine test.

Constants	N4 Extension Base layer			N4 Extension Upper Selected layer			S191 Base layer		
	Average	Standard deviation	Coefficient of Variance	Average	Standard deviation	Coefficient of Variance	Average	Standard deviation	Coefficient of Variance
LL (%)	-*	-*	-	30.9	1.9	6.2%	30.6	0.6	1.8%
PL (%)	-*	-*	-	19.5	0.2	1.2%	22.5	0.1	0.7%
PI (%)	NP*	NP*	-	11.4	1.8	15.6%	8.1	0.6	7.8%
LS (%)	-*	-*	-	5.8	0.5	9.0%	5.1	0.2	3.8%
GM	2.6	0.02	0.9%	1.8	0.15	8.5%	2.5	0.03	1.4%
MDD (kg/m³)	2 446	19.00	0.8%	2 056	15.70	0.8%	2 306	53.50	2.3%
OMC (%)	6.0	0.55	9.2%	10.7	0.36	3.4%	7.2	0.49	6.8%

Constants	P10-2 Base layer			D804 Base layer		
	Average	Standard deviation	Coefficient of Variance	Average	Standard deviation	Coefficient of Variance
LL (%)	26.5	2.3	8.7%	28.1	1.1	3.8%
PL (%)	18.8	0.8	4.3%	18.4	0.3	1.5%
PI (%)	7.7	2.0	25.2%	9.6	1.3	13.2%
LS (%)	5.2	N/A		6.6	0.2	2.9%
GM	2.0	0.04	1.9%	1.7	0.07	4.0%
MDD (kg/m³)	2 133**	-	-	2 037**	-	-
OMC (%)	8.3**	-	-	9.4**	-	-

* Material classified as Non Plastic and results not reported by laboratory

** Only one test was conducted

4.2.2   Shear tri-axial data processing and modelling

Processing and modelling of results was refined by using shear tri-axial test results obtained from N4 Extension and N2-33 base layer material. The theory, on which processing and modelling is based, was presented in an interim project report for SAPDM/B1-a by the author and co-supervisor (Van Aswegen and Theyse, 2011). The interim report is not publicly available and was distributed to a select group of researchers involved in the SAPDM project for comment. The refined method of processing and modelling of test results was applied to test results reported on in this thesis. Sections 4.2.2 to 4.2.3.4 contains extracts of the theory contained in the interim report with graphs depicting results from material evaluated in this thesis.

Theyse (2008b) derived a stress-strain model, which combined Kondner and German and Lytton's models to represent the response of unbound granular material in the static tri-axial test below the failure strength of the material. The combined model is formulated as:

$$\sigma_d = \frac{c\varepsilon}{e^{d\varepsilon}\left[1+\left(\frac{c\varepsilon}{a}\right)^b\right]^{\frac{1}{b}}} \qquad (4.1)$$

Where

σ_d	=	deviator stress (kPa)
ε	=	axial strain
e	=	base of the natural logarithm
a, b, c, d	=	model parameters

Theyse's model was fitted to the results from the individual static tri-axial tests. Adjustment was made to the results of individual static tri-axial tests where the loading ram was not in contact with the specimen when the test commenced. The adjustment ensures that the initial linear portion of the load-displacement data aligns with the zero intercept. The failure or yield stress is obtained directly from the model and is represented by the 'a' model parameter. Figure 4.2 illustrates the model from Equation 4.1 fitted to the data from a typical static tri-axial test.
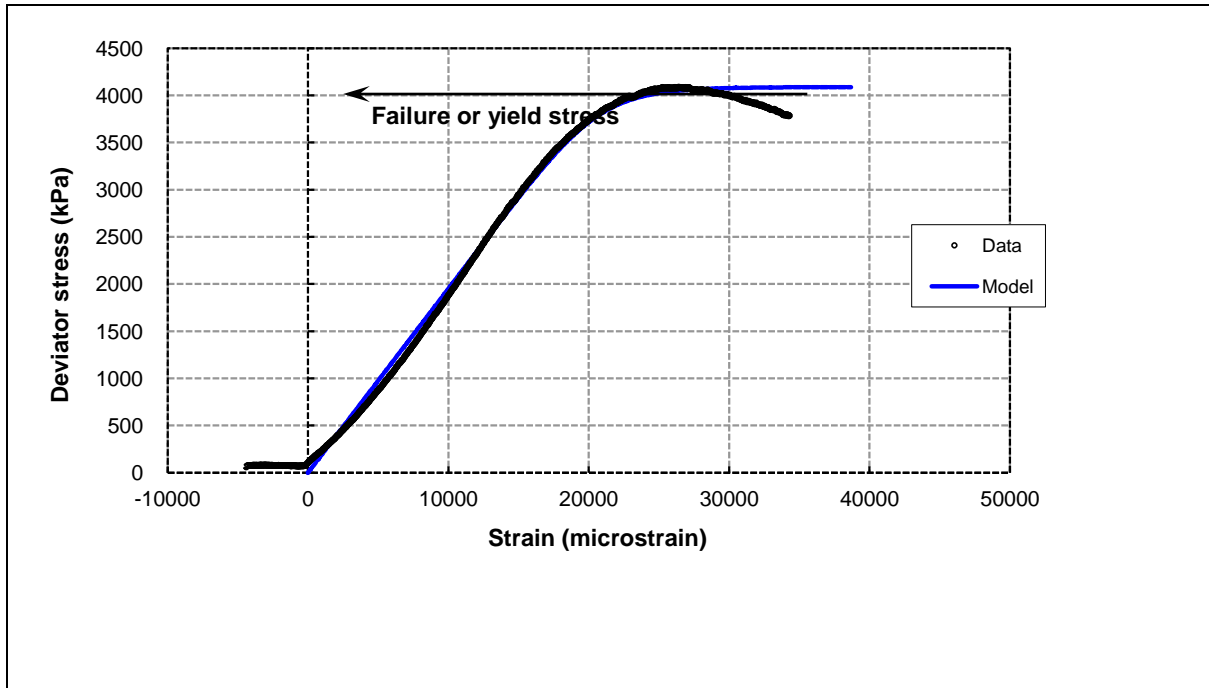
Figure 4.2: **Example of stress-strain model fitted to the data of S191 B (Sample no. 11726-03).**

Once the model from Equation 4.1 is fitted to the data from each individual tri-axial test, the volumetric density, saturation, confinement pressure and failure strength are summarised per material. Static tri-axial result summaries are contained in Appendix D. The failure strength model provided by Equation 4.2 (Theyse, 2008) is calibrated using the summary data per material. The failure stress and confining pressure of each sample were used to calibrate a yield or failure strength model developed by Theyse that incorporates suction pressure. The calibrated failure strength model parameters per material are also contained in Appendix D. The failure strength model is formulated as follows:

$$\sigma_1^f = e^{aVD-bS} \left(\sigma_3 + p_{suc} \right)^c - p_{suc}$$ (4.2)

Where

σ_1^f =   major principal failure stress (kPa)

σ_3 =   minor principal stress or confinement pressure in the tri-axial test (kPa)

VD =   volumetric density (decimal fraction)

S =   degree of saturation (decimal fraction)

p_{suc} =   suction pressure (kPa)

a, b, c =   model parameters

With the suction pressure expressed as:

4-6

$$p_{suc} = \chi\left(u_a - u_w\right) \approx \frac{\rho VD^{\varphi} S}{e^{\omega S/VD}} \qquad\qquad (4.3)$$

Where

p_{suc} =   suction pressure (kPa)

χ =   Bishop parameter

$(u_a - u_w)$ =   matric suction i.e. air-water pressure differential (kPa)

VD =   volumetric density (decimal fraction)

S =   degree of saturation (decimal fraction)

ρ, φ, ω =   suction pressure model parameters

Table 4.4 summarises the failure strength parameters obtained from the calibration of the failure strength model. The correlation coefficient (R^2), Standard Error of Estimate (SEE) and the Root Mean Square Error (RMSE) for all are acceptable for the planning of the stress levels for the resilient modulus tests.

Table 4.4:   **Failure strength model calibration results for unbound material.**

Material	Model parameters						Model fit		
	φ	ω	ρ	a	b	c	R^2	SEE	Avg. error (%)
N4 Ext B	7.5	5.1	1.5e3	4.8	0.14	0.74	0.975	195	11.8
N4 Ext USel	10.5	0.01	7.3e4	0.0	3.19	1.39	0.955	206	13.7
S191 B	0.0	7.1	2.4e3	7.3	1.66	0.46	0.966	248	15.0
P10-2 B	30.0	3.3	2.7e6	6.3	1.63	0.61	0.978	130	11.6
D804 B	25.0	3.8	8.3e6	3.5	1.38	0.97	0.966	186	14.9

These calibration results will be used to determine the loading schedules for the resilient modulus tri-axial testing on these materials.

4.2.3   Resilient modulus tri-axial results

The same processing and modelling was followed in this thesis as described by Van Aswegen and Theyse (2011). Van Aswegen and Theyse (2011) reported on processing and modelling, which was applied on the N4 Extension and N2-33 base layer material that was used to refine the process for application on the test results from material reported on in this thesis.

4.2.3.1 Theoretical considerations for data processing

The protocol for resilient modulus testing calculates the resilient modulus from 1-dimensional axial considerations in such a manner to eliminate plastic strain. However, 3-dimensional stress and strain conditions are induced during tri-axial testing as shown in Figure 4.3. Confinement pressure is applied firstly resulting in the volumetric compression of the specimen as shown in Figure 4.3(a) followed by the application of the axial load shown in Figure 4.3(b). The axial load results in axial deformation of the specimen, which is also accompanied by lateral expansion of the specimen.

(a)   Confinement pressure loading   (b)   Axial loading
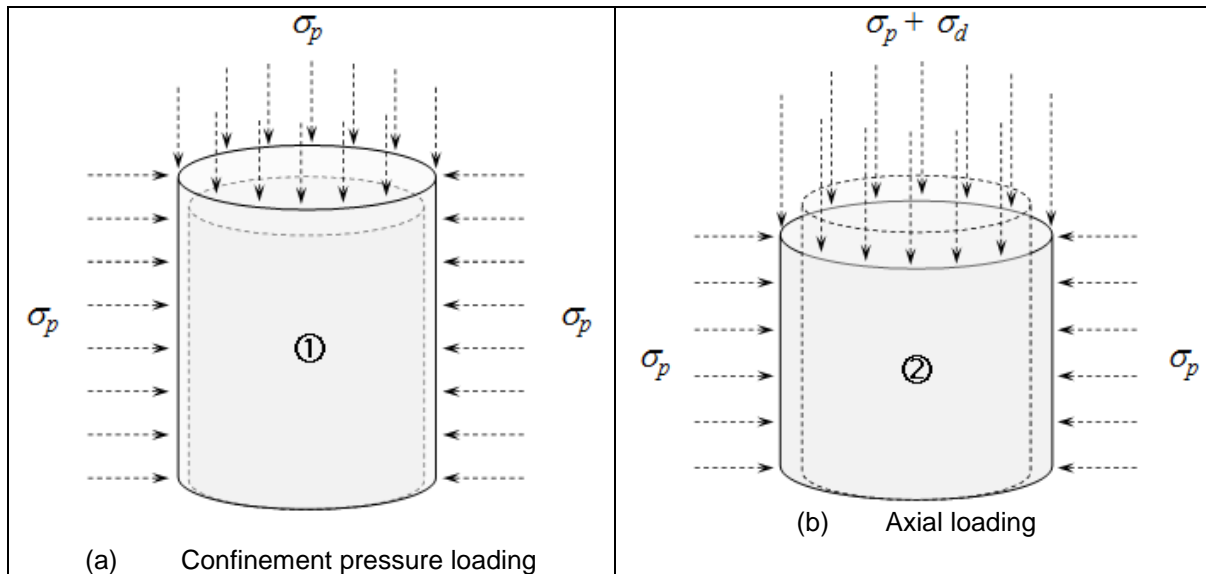
Figure 4.3:   Loading and deformation during a tri-axial test (Van Aswegen and Theyse, 2011).

Figure 4.4 illustrates the stress and strain paths in the principal stress and strain space associated with the initial application of the confinement pressure and subsequent application of the axial deviator stress. Although the final stress and strain condition is represented by principal stress (σ_3, σ_1) and strain (ε_3, ε_1) respectively, it has to be considered that the displacement and hence the strain is calculated relative to the condition at rest (ε_3^p, ε_1^p) after the application of the confinement pressure. The stress that causes the recorded axial and radial deformation is only the deviator stress, σ_d in this case. The following convention is therefore used:

- $\Delta\varepsilon_1$ represents the axial or vertical strain of the specimen associated with the application of the deviator stress and using an engineering convention of positive strain for contraction, and
- $\Delta\varepsilon_3$ represents the radial or horizontal strain of the specimen associated with the application of the deviator stress and using an engineering convention of negative strain for extension.

4-8
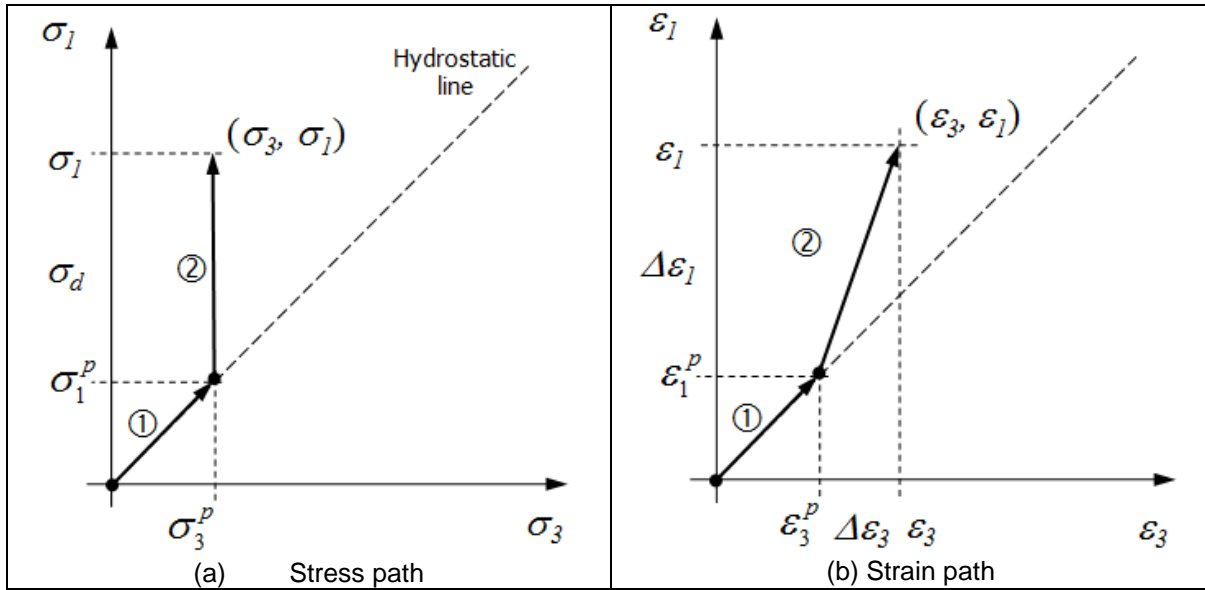
Figure 4.4: Principal stress and strain paths in a tri-axial test (Van Aswegen and Theyse, 2011).

Given the circumferential sensor used in this thesis, the radial strain $\Delta\varepsilon_3$ and subsequently the Poisson's Ratio are calculated from the change in circumference of the specimen as illustrated in Figure 4.5.

$$C_1 = 2\pi r_1 \Rightarrow r_1 = \frac{C_1}{2\pi}$$

$$C_2 = 2\pi r_2 \Rightarrow r_2 = \frac{C_2}{2\pi}$$

$$\Delta r = r_2 - r_1$$

$$= \frac{C_2 - C_1}{2\pi}$$

$$\Delta\varepsilon_3 = \varepsilon_r$$

$$= -\frac{\Delta r}{r}$$

$$= -\left(\frac{C_2 - C_1}{C_1}\right)$$
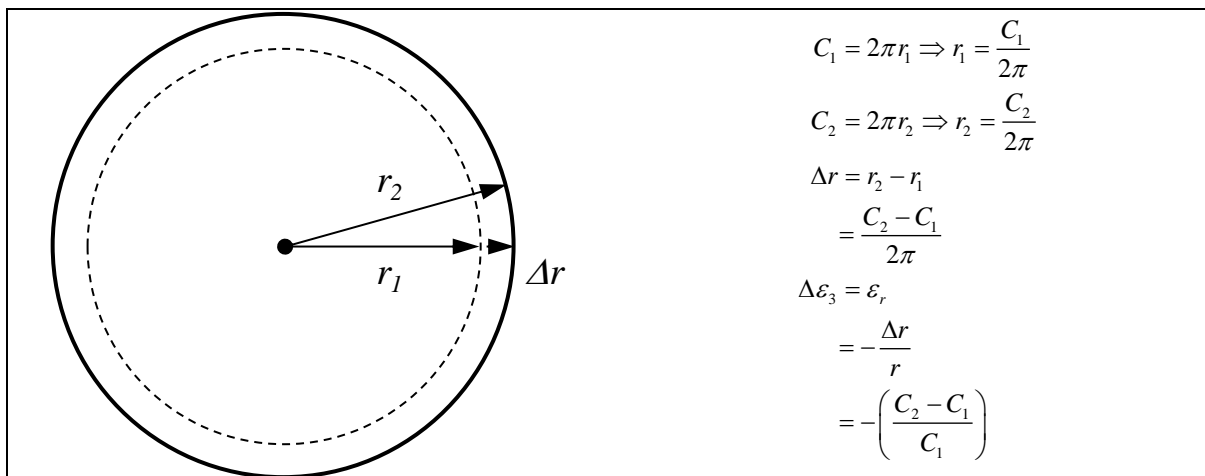
Figure 4.5: Circumferential and radial displacement in a tri-axial test (Van Aswegen and Theyse, 2011).

Hooke's law for an isotropic material in Cartesian coordinates is as follows:

$$
\begin{pmatrix} \sigma_x \\ \sigma_y \\ \sigma_z \\ \tau_{xy} \\ \tau_{yz} \\ \tau_{zx} \end{pmatrix} = \frac{E}{(1+\nu)(1-2\nu)} \begin{pmatrix} (1-\nu) & \nu & \nu & 0 & 0 & 0 \\ \nu & (1-\nu) & \nu & 0 & 0 & 0 \\ \nu & \nu & (1-\nu) & 0 & 0 & 0 \\ 0 & 0 & 0 & \left(\frac{1}{2}-\nu\right) & 0 & 0 \\ 0 & 0 & 0 & 0 & \left(\frac{1}{2}-\nu\right) & 0 \\ 0 & 0 & 0 & 0 & 0 & \left(\frac{1}{2}-\nu\right) \end{pmatrix} \begin{pmatrix} \varepsilon_x \\ \varepsilon_y \\ \varepsilon_z \\ \gamma_{xy} \\ \gamma_{yz} \\ \gamma_{zx} \end{pmatrix} \tag{4.4}
$$

Where

σ_i =   normal stress in the direction of i-axis

τ_{ij} =   shear stress in direction j perpendicular to direction i

ε_i =   normal strain in the direction of i-axis

γ_{ij} =   shear strain in direction j perpendicular to direction i

E =   Young's modulus is the same units as stress

ν =   Poisson's ratio

The following stresses and strains occur under tri-axial conditions:

- $\sigma_x = \sigma_y = \sigma_h = \sigma_3^p$;

- $\varepsilon_x = \varepsilon_y = \varepsilon_r = \Delta\varepsilon_3$;

- $\sigma_z = \sigma_d$;

- $\varepsilon_z = \varepsilon_a = \Delta\varepsilon_1$;

- $\tau_{xy} = \tau_{yz} = \tau_{zx} = \gamma_{xy} = \gamma_{yz} = \gamma_{zx} = 0$

Keeping in mind that the radial strain is negative (extension), the Poisson's ratio is given by Equation 4.5. The stiffness (Young's modulus) may then be obtained from solving the equation for vertical stress σ_z from Equation 4.4 considering only the deviator stress as causing the deformation of the specimen. The resulting formulation for Young's modulus is then given by Equation 4.6.

$$
\nu = -\left(\frac{\varepsilon_r}{\varepsilon_a}\right) \tag{4.5}
$$

$$
\sigma_d = \frac{E}{(1+\nu)(1-2\nu)}\left[\nu(\varepsilon_r) + \nu(\varepsilon_r) + (1-\nu)\varepsilon_a\right]
$$
$$
E = \frac{\sigma_d(1+\nu)(1-2\nu)}{2\nu\varepsilon_r + (1-\nu)\varepsilon_a} \tag{4.6}
$$

The stiffness of the specimen is therefore derived from the vertical deviator stress in combination with the distortion of the specimen. Using the compliance matrix instead of the stiffness matrix from Equation 4.4, a simpler expression may be derived for Young's modulus in the general case as given in Equation 4.7. Under tri-axial conditions with only the deviator stress causing the distortion of the specimen, Young's modulus is given by Equation 4.8 indicating that the resilient modulus may be calculated directly from the deviator stress and axial strain as recommended by the tri-axial protocol.

$$\varepsilon_z = -v\frac{\sigma_x}{E} - v\frac{\sigma_y}{E} + \frac{\sigma_z}{E}$$

$$E = \frac{\sigma_d - v\sigma_x - v\sigma_y}{\varepsilon_z}$$

(4.7)

$$\varepsilon_a = -v\frac{\sigma_h}{E} - v\frac{\sigma_h}{E} + \frac{\sigma_d}{E}$$

$$E = \frac{\sigma_d - 2v\sigma_h}{\varepsilon_a}$$

(4.8)

$$E = \frac{\sigma_d}{\varepsilon_a} \quad \text{as } \sigma_h \text{ does not contribute to the distortion during the load-unload cycle}$$

Also note that the shear stress is only related to the shear strain in Equation 4.4 resulting in the general expression for shear stress given by Equation 4.9. However, as indicated previously, the shear stress for a tri-axial test in Cartesian coordinates is zero and the shear modulus (G) cannot be derived directly.

$$\tau_{ij} = \frac{E\left(\frac{1}{2} - v\right)}{(1+v)(1-2v)}\gamma_{ij}$$

$$= \frac{E}{2(1+v)}\gamma_{ij}$$

$$= G\gamma_{ij}$$

(4.9)

The principal stresses from a tri-axial test may, however, be converted into a mean or equal, all-round octahedral stress and an octahedral shear stress given by Equations 4.10 and 4.11.

$$\sigma_{oct} = \frac{1}{3}\left(\sigma_1 + \sigma_2 + \sigma_3\right)$$

$$= \frac{1}{3}\left(\sigma_d + 2\sigma_3^p\right)$$

$$= \frac{1}{3}\sigma_d \quad \text{as } \sigma_3^p \text{ does not contribute to the distortion during the load-unload cycle}$$

(4.10)

$$\begin{aligned}
\tau_{oct} &= \frac{1}{3}\left[\left(\sigma_1 - \sigma_3\right)^2 + \left(\sigma_2 - \sigma_3\right)^2 + \left(\sigma_3 - \sigma_1\right)^2\right] \\
&= \frac{\sqrt{2}}{3}\left(\sigma_1 - \sigma_3\right) \\
&= \frac{\sqrt{2}}{3}\sigma_d
\end{aligned} \tag{4.11}$$

The corresponding formulations for strain are given by Equations 4.12 and 4.13 with the volumetric strain $\varepsilon_v = \varepsilon_1 + \varepsilon_2 + \varepsilon_3$.

$$\begin{aligned}
\varepsilon_{oct} &= \frac{1}{3}\left(\varepsilon_1 + \varepsilon_2 + \varepsilon_3\right) \\
&= \frac{1}{3}\varepsilon_v
\end{aligned} \tag{4.12}$$

$$\begin{aligned}
\gamma_{oct} &= \frac{2}{3}\left[\left(\varepsilon_1 - \varepsilon_3\right)^2 + \left(\varepsilon_2 - \varepsilon_3\right)^2 + \left(\varepsilon_3 - \varepsilon_1\right)^2\right] \\
&= \frac{2\sqrt{2}}{3}\left(\varepsilon_1 - \varepsilon_3\right)
\end{aligned} \tag{4.13}$$

The octahedral stress given by Equation 4.10 represents an increase in the equal, all-round mean stress on the tri-axial specimen during the application of the deviator stress. Equations 4.6, 4.10, 4.13 and 4.13 were coded in a spreadsheet for the processing of the data from the resilient modulus tri-axial test. The same spreadsheet template was used to analyse the tri-axial results referred to in this thesis.

4.2.3.2   Data processing

Each resilient modulus tri-axial test is done at a number of combinations of confinement pressure and deviator stress. The load sequence used for materials reported on in this thesis are given in Appendix D. Axial displacement is recorded by three on-sample LVDTs mounted over the middle third of the specimen and circumferential displacement is measured by a clip-gauge at the mid-height of the specimen. Cell pressure is recorded by a pressure transducer and the load by a load-cell connected to the actuator that enters the tri-axial pressure cell through a phosphor-bronze sleeve to reduce friction. The following combinations of confinement pressure and deviator loads are applied during the test:

- Conditioning cycles
    - 1 000 cycles at 100 kPa confinement pressure and deviator stress at 20 to 25 per cent of the yield strength of the specimen;
- Confinement pressure at 200 kPa;
    - 100 cycles with the deviator stress at 10 per cent of the yield strength of the specimen. Cycles 1 to 5 and 95 to 100 are recorded;
    - 100 cycles with the deviator stress at 30 per cent of the yield strength of the specimen. Cycles 1 to 5 and 95 to 100 are recorded;

- ○ 100 cycles with the deviator stress at 50 per cent of the yield strength of the specimen. Cycles 1 to 5 and 95 to 100 are recorded;
- ○ 100 cycles with the deviator stress at 70 per cent of the yield strength of the specimen. Cycles 1 to 5 and 95 to 100 are recorded;

The above process is repeated at confinement pressures of 100, 150, 50 and 25 kPa.

The data are recorded in electronic format and arranged according to the above loading sequence with the data for the conditioning cycles at the bottom of the file. This electronic data file is imported into a spreadsheet template that was created for basic data processing. The same spreadsheet template was used to analyse the tri-axial results referred to in this thesis.

4.2.3.3 *Consistency test*

Two aspects are important to monitor during the resilient modulus tri-axial test. The first is the consistency in axial displacement recorded by the three on-sample LVDTs and specifically the ratio between these displacements. If this ratio changes during the test it indicates that the mounting rings have slipped or rotated. Figure 4.6 shows an example of the consistency plot using the axial displacement from LVDT 1 as a reference. Ideally the ratio for LVDTs 2 and 3 should remain close to one. It is clear from this plot that the initial displacement data during the early stages of the conditioning cycles (up to 1 000 cycles) are particularly erratic.
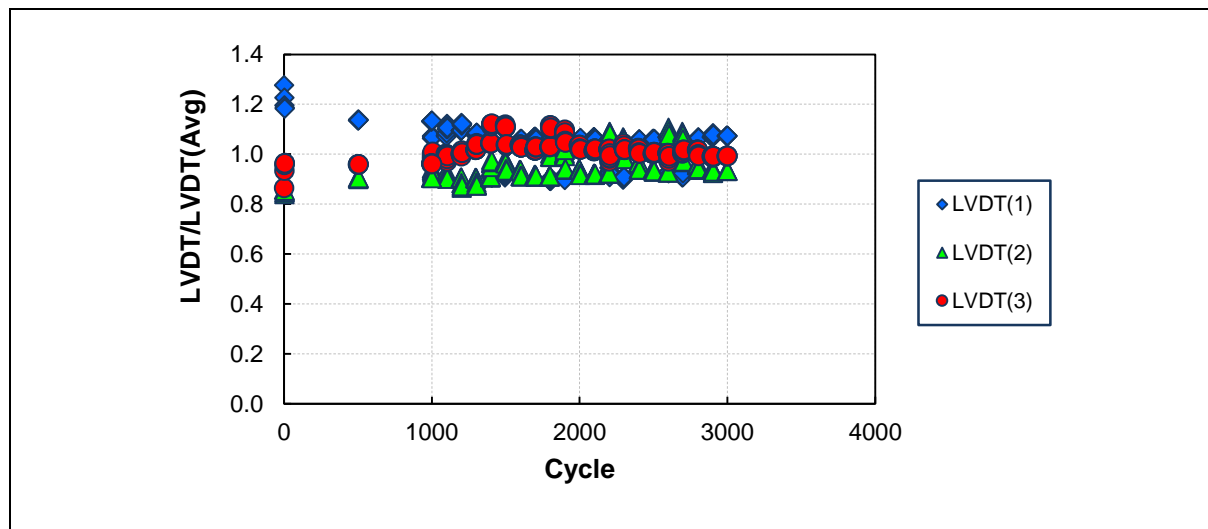
Figure 4.6:   **Axial displacement consistency test for P10-2 B (Sample no. 11721-23).**

Secondly, the amount of plastic strain during the resilient modulus test should remain small and the rate of plastic strain should preferably reduce dramatically after initial bedding-in of the specimen. Figure 4.7 shows a plot of acceptable plastic strain accumulation during a resilient modulus test.
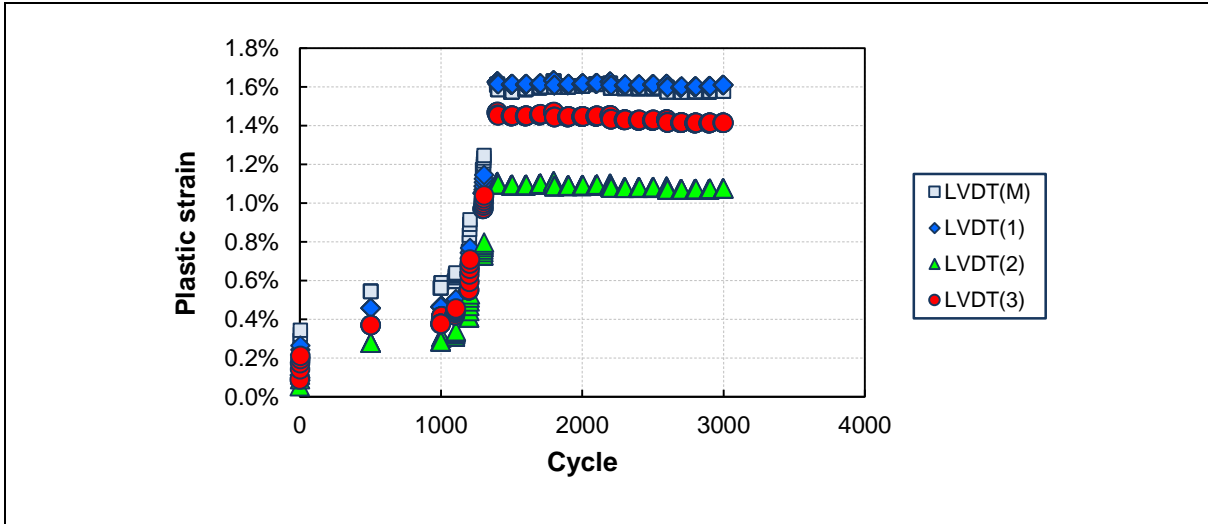
Figure 4.7: **Plastic strain evolution during the resilient modulus tri-axial test for P10-2 B (Sample no. 11721-23).**

The spreadsheet also produces plots of the axial stress, axial and radial strain, but these are merely intended as visual checks to ensure that the test sequence was correct. Examples of these plots are shown in Figure 4.8.

(a)   Axial stress

(b)   Axial strain

(c)   Radial strain
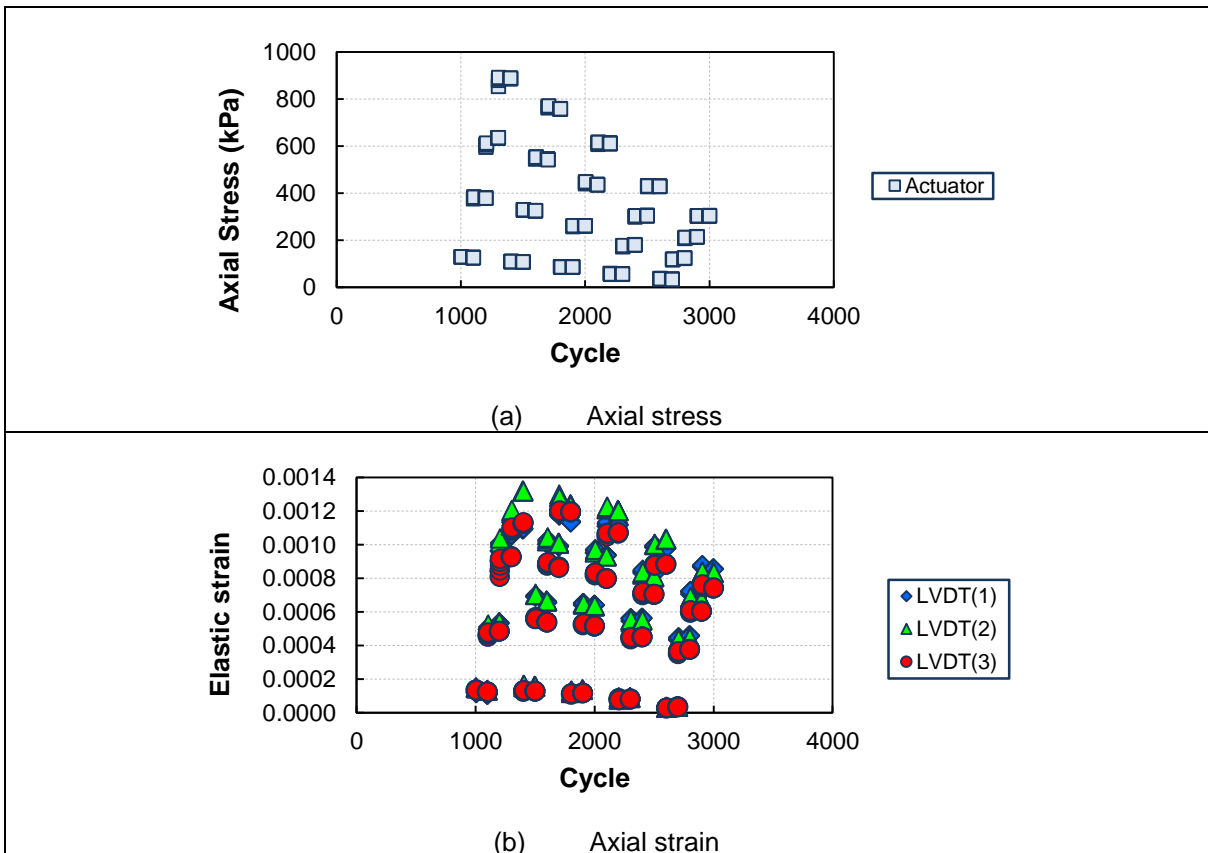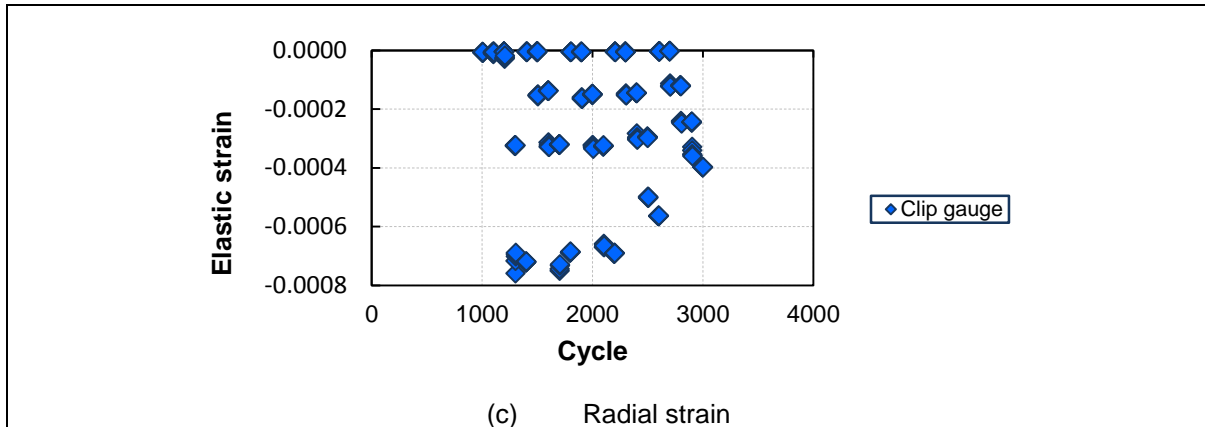
Figure 4.8:   **Stress and strain recorded during a resilient modulus tri-axial test for S191 B (Sample no. 11726-35).**

In the analysis of data in this thesis, the same method of consistency checking was conducted on each sample tested.

4.2.3.4   Processing of test data

In addition to the plots produced for quality control purposes, the spreadsheet also produces plots for each combination of confinement pressure and shear stress during the resilient modulus tri-axial test. These plots are produced for the first five and last six load cycles (the recorded load cycles) of each 100 load cycle sequence. Figure 4.9 shows an example of the axial load recorded for a combination of 200 kPa confinement pressure and an axial stress at 50 per cent of the yield strength of the material. Figure 4.10 shows the corresponding displacement recorded by the on-sample LVDTs. The increase in permanent deformation is clearly visible during the first five load cycles. The circumferential displacement is shown in Figure 4.11, also indicating an increase in the diameter of the specimen during the initial five load cycles.

(a)   First five cycles

4-15

(b)   Last six cycles
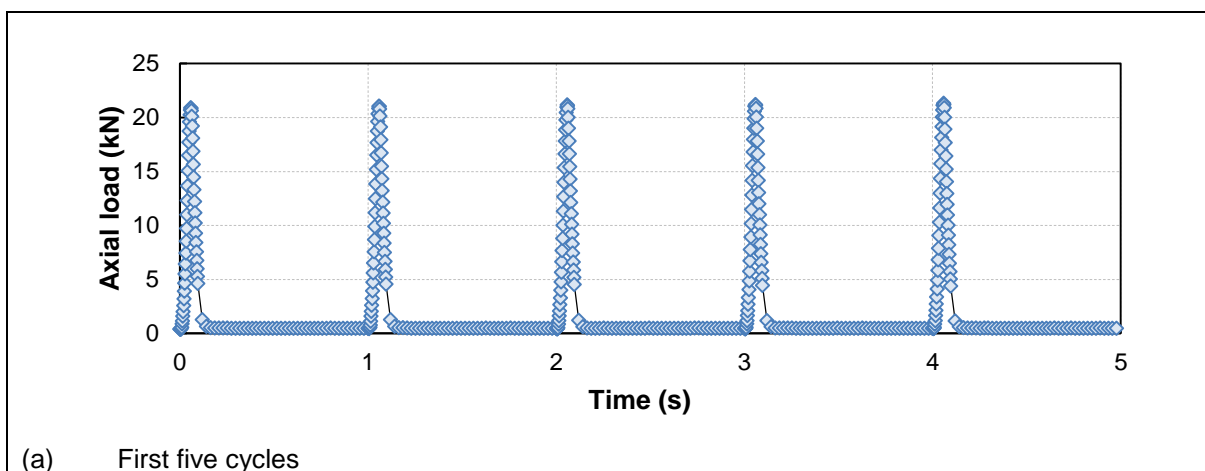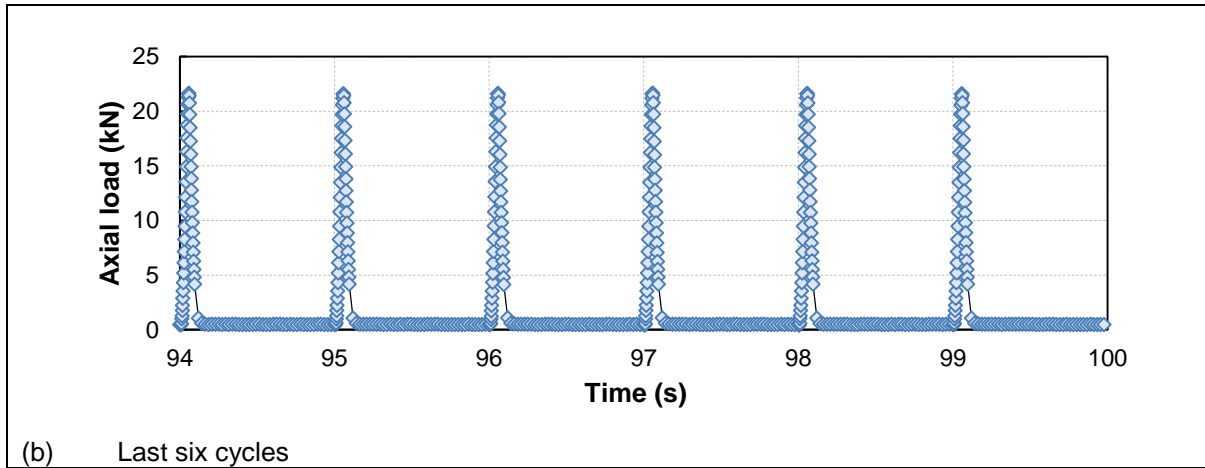
Figure 4.9:   **Axial load cycles recorded during a 100 load cycle sequence for D804 B (Sample no. 11728-28).**

(a)   First five cycles

(b)   Last six cycles
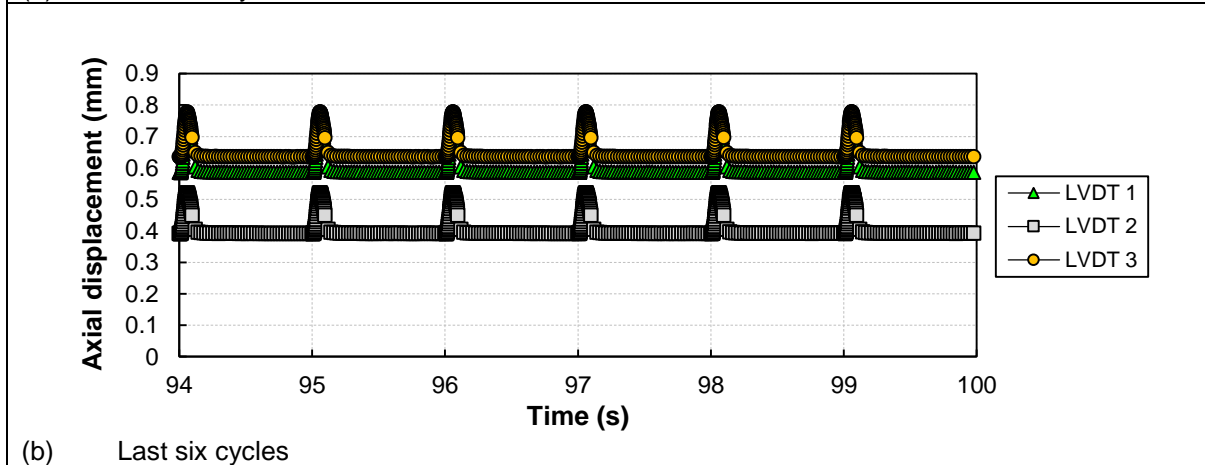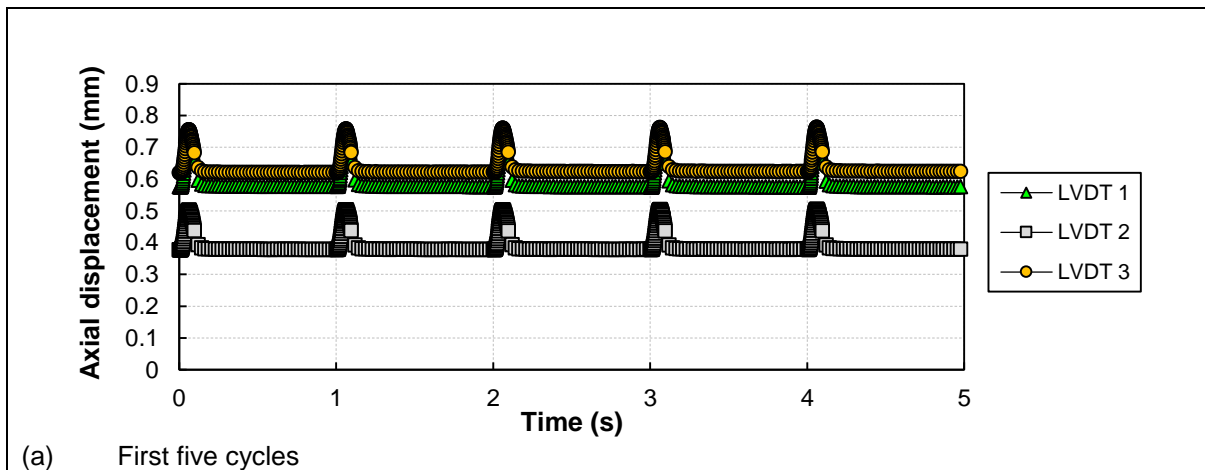
Figure 4.10:   **Axial displacement recorded during a 100 load cycle for D804 B (Sample no. 11728-28).**
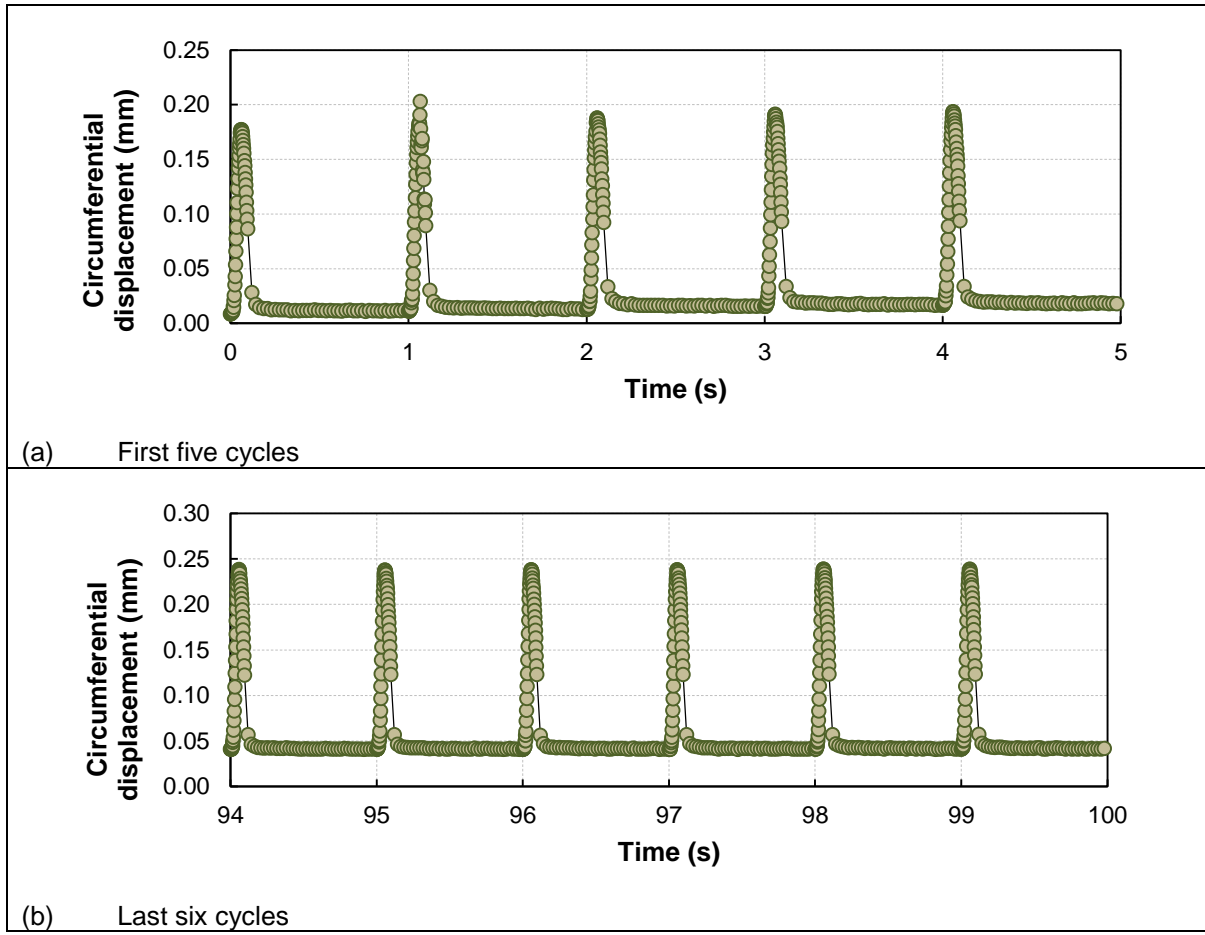
Figure 4.11: **Circumferential displacement recorded during a 100 load cycle sequence for D804 B (Sample no. 11728-28).**

Combining the axial load and displacement data produces the hysteresis loops shown in Figure 4.12, while the combination of axial load and circumferential displacement produces the graphs shown in Figure 4.13. It is clear that only the data from the last six cycles should be used for determining the stiffness moduli of the specimen as the hysteresis loops of the first five cycles are irregular, but seems to have stabilised by the last six cycles of the test.

(a)   First five cycles

(b)   Last six cycles
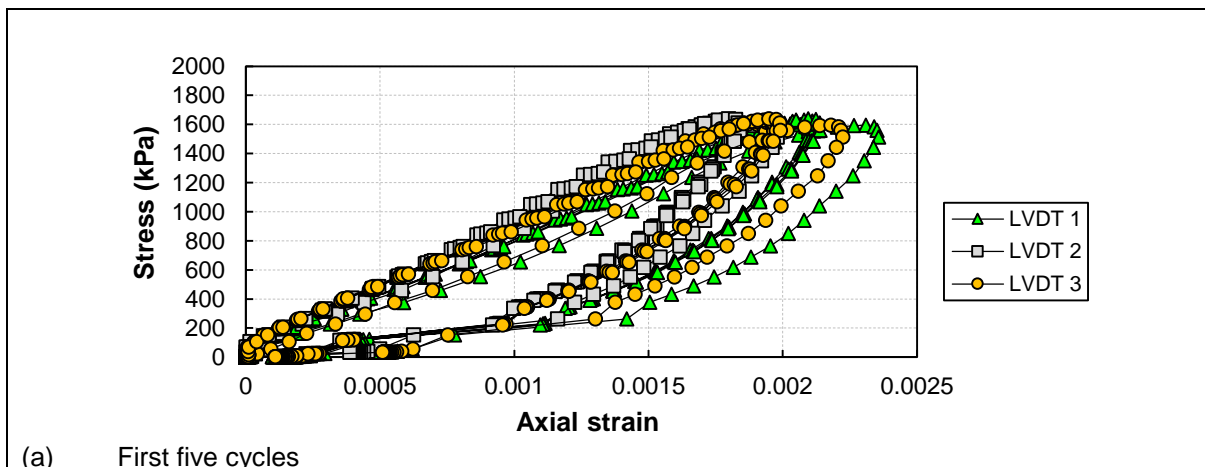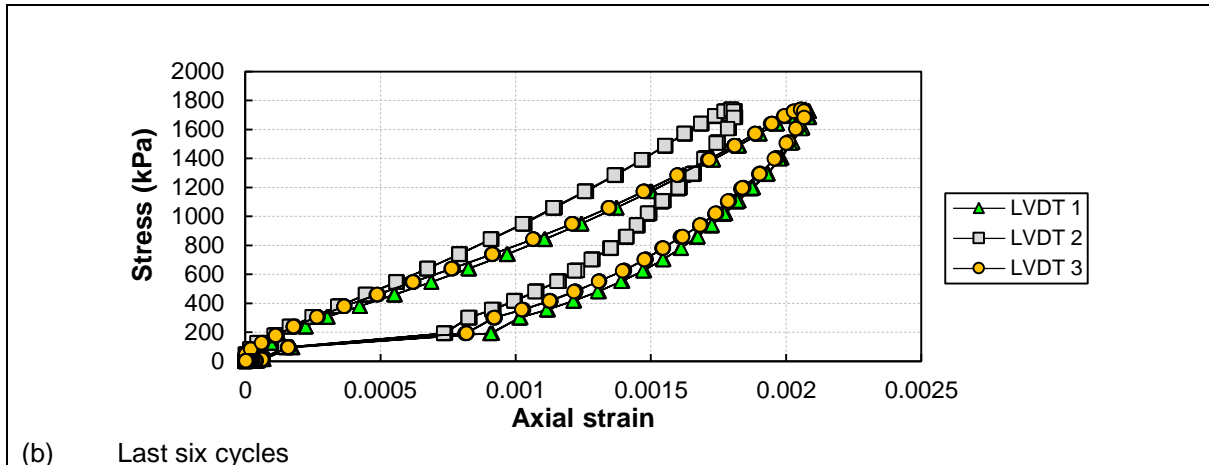
Figure 4.12:   Axial load-displacement hysteresis loops recorded during a 100 load cycle sequence for D804 B (Sample no. 11728-28).

(a)   First five cycles

(b)   Last six cycles
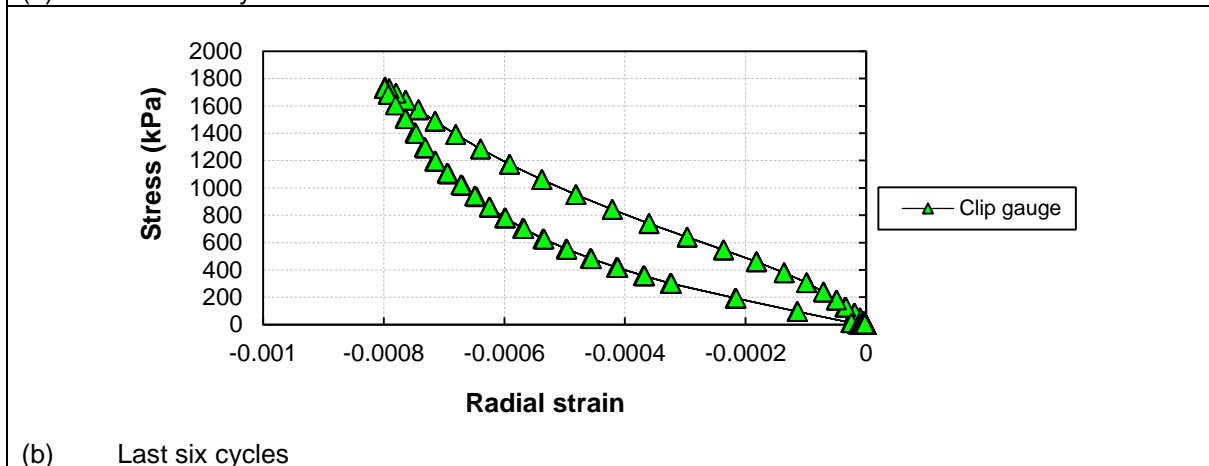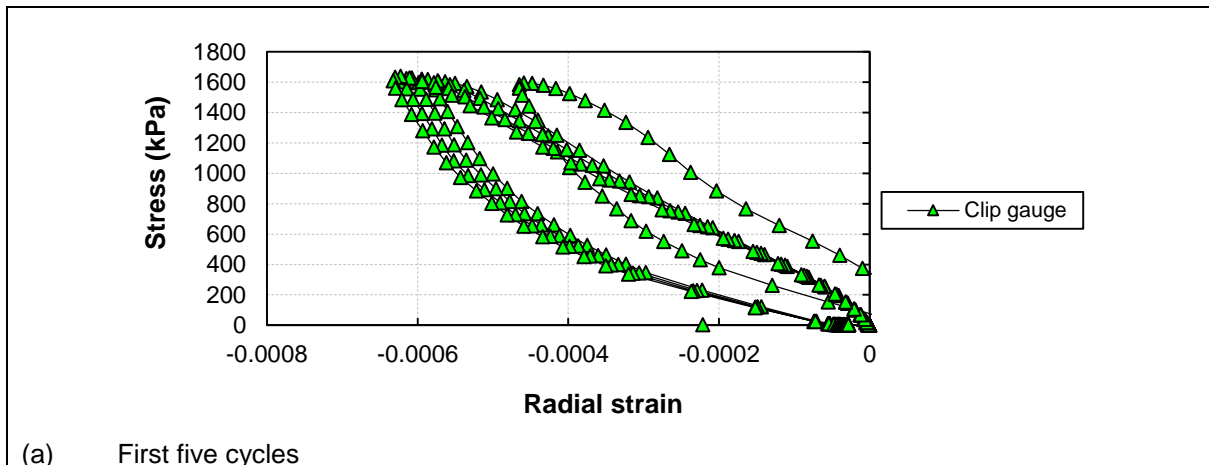
Figure 4.13:   Circumferential load-displacement hysteresis loops recorded during a 100 load cycle sequence for D804 B (Sample no. 11728-28).

The plots shown in Figure 4.9 to Figure 4.13 should be used in addition to the consistency test plots for visual inspection of the data. Figure 4.14 illustrate incorrect data that should not be used in further analysis.

(a) Load data

(b) Load-displacement hysteresis loops
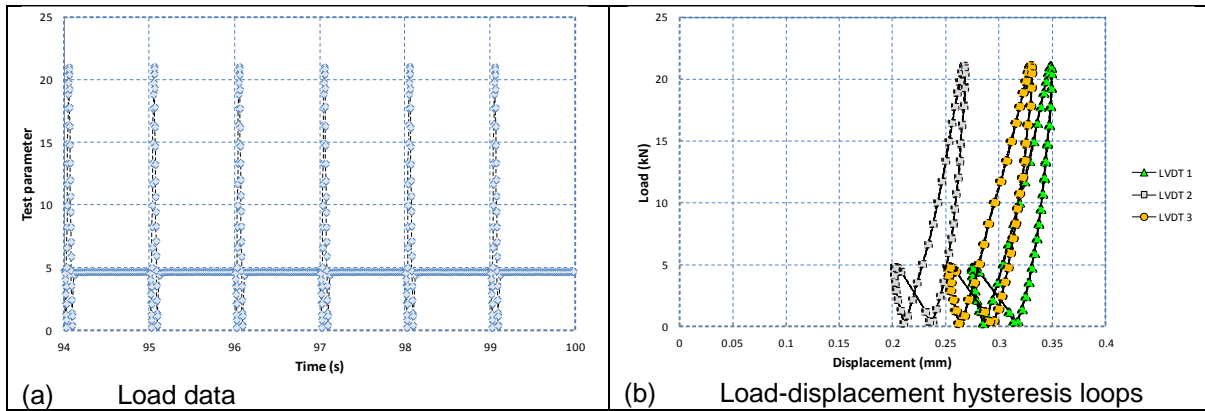
Figure 4.14:   Example of incorrect data that should be discarded (Van Aswegen and Theyse, 2011).

Calculating the axial stress and strain from the load and displacement data, as well as the radial displacement, the spreadsheet also calculates the Poisson's ratio and cord modulus, which is shown in the summary plots of Figure 4.15.

(a)   Resilient modulus

4-19

Loading Phase

(b)   Poisson's ratio
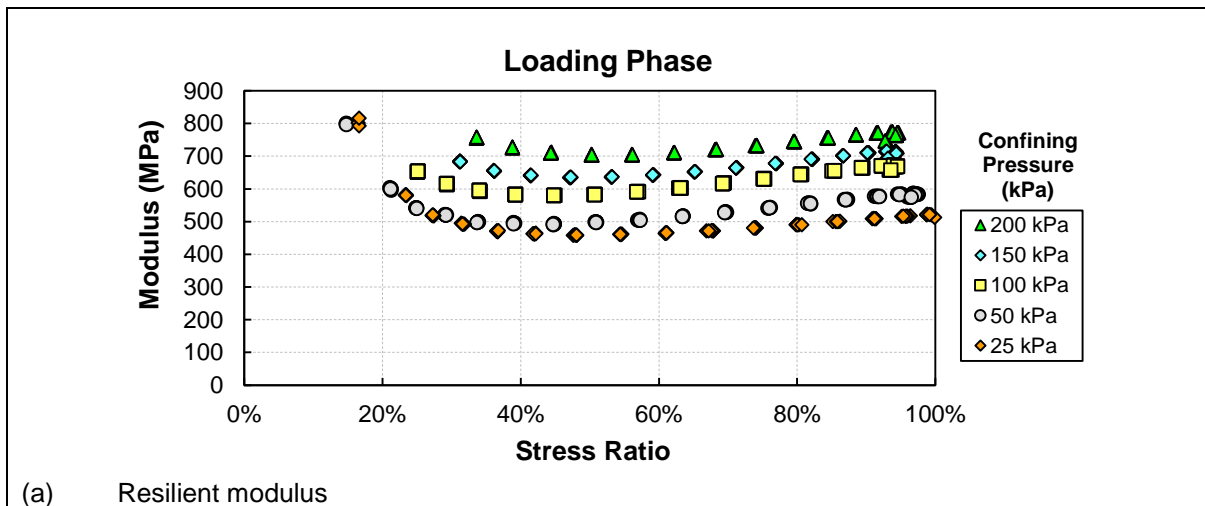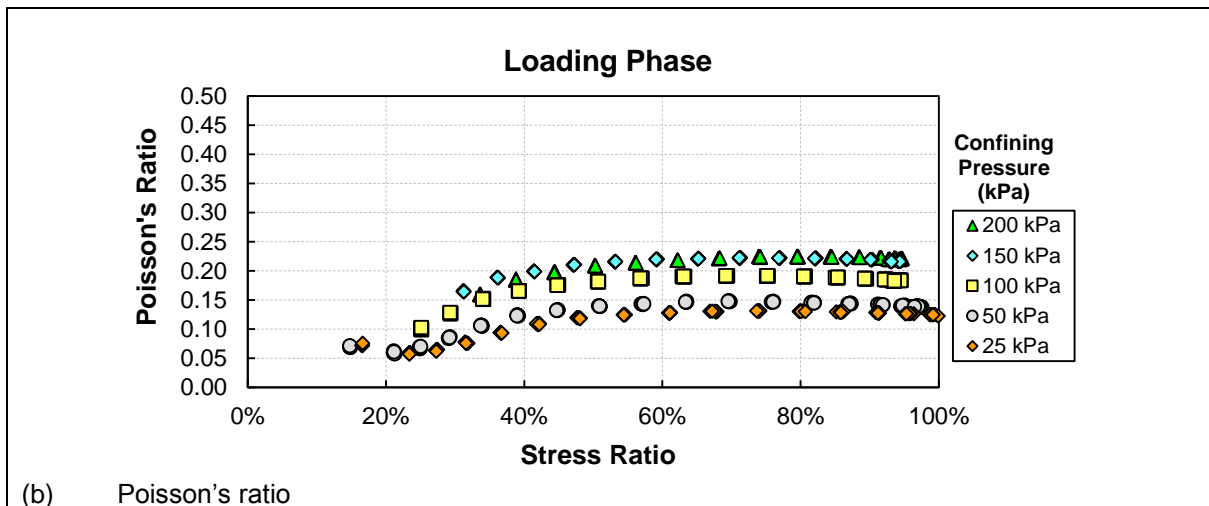
Figure 4.15:   Example of elastic properties calculated from the resilient modulus test results for P10-2 B (Sample no 11721-28).

To the authors' knowledge, the preliminary data presented from N4 Extension and N2-33 base layer material was the first set of comprehensive resilient response properties including the Poisson's ratio and cord modulus that were recorded successfully for unbound granular material in South Africa. The system produces acceptable data given the extremely high sensitivity of the resilient response properties to very small measurement errors. The successful measurement of circumferential or radial strain for the first time enables the investigation of the Poisson's ratio of unbound material in South Africa. The same method described above was used in this thesis to process the test data.

4.3   CALIBRATION OF CORD MODULUS MODEL VARIABLES

The cord modulus model referred to in Section 2.3.3.4 is further investigated in this section. The cord modulus is required for a MLLE solution where non-zero initial stress and strain conditions cannot be accommodated.

4.3.1   Formulation of the Cord Modulus Model

The cord modulus is derived by integrating the tangent modulus given in Section 2.3.3.3. The model consists of a hyperbolic function in combination with a linear function, where the linear function has a non-zero intercept (Figure 4.16).

Where

M_c = cord modulus (MPa)

SR_d = deviator Stress Ratio (SR)

$= \dfrac{(\sigma_d + \sigma_3)}{\sigma_d^f}$

a, b, c = regression coefficients found from regression analysis

$$M_c = a + bSR_d + \frac{c}{SR_d}$$
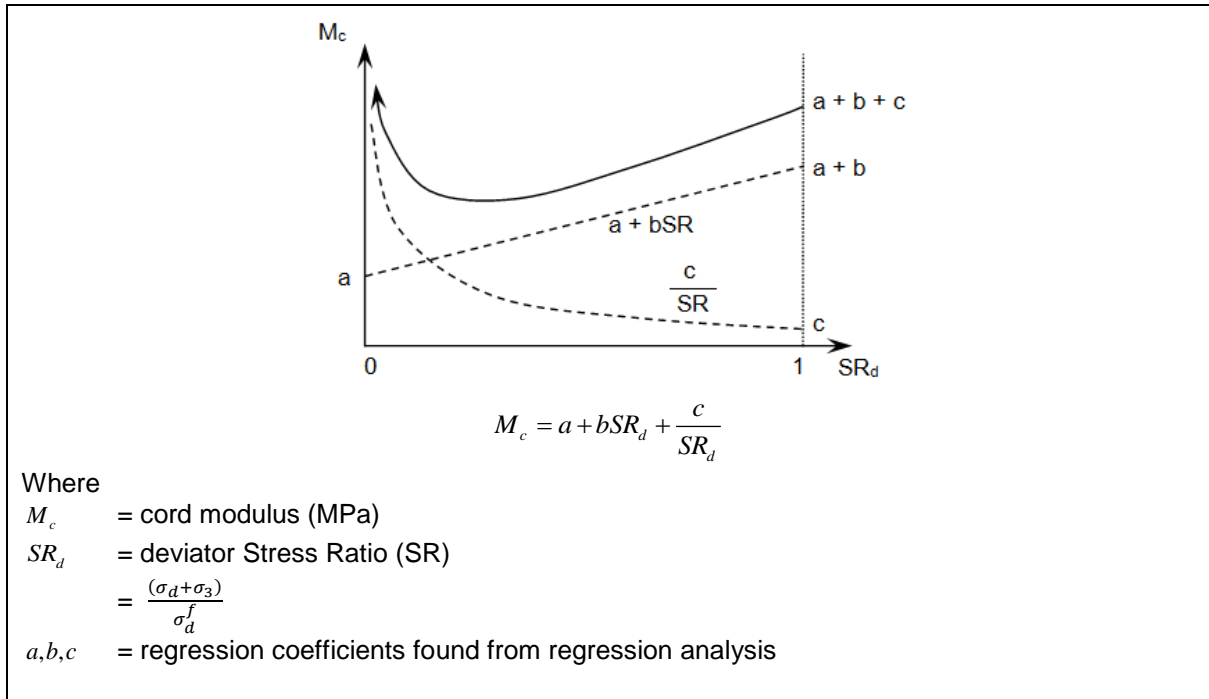
Figure 4.16:   Cord modulus model.

Considering the formulation of the cord modulus model, it is apparent that none of the variables 'a', 'b' or 'c' can be allowed to be negative values. Negative variable values would result in the following:

1.   A negative 'a' value will force 'c' to be a negative value;

2.   A negative 'c' value results in the hyperbolic portion of the model switching and having a negative asymptote; which will result in negative predicted stiffness values that is counter intuitive;

3.   Although the line formed by 'a' and 'b' is allowed to have a negative slope, a negative 'b' value is not allowed, as it might force 'c' to be negative when 'a' is not large enough, resulting in negative predicted stiffness values.

As illustrated by Figure 4.17, the model successfully predicts the stress-dependency of material with regard to stiffness, where an initial modulus value increase with increasing confinement pressure, as well as the initial stress-softening with increasing stress ratio followed by stress-stiffening.
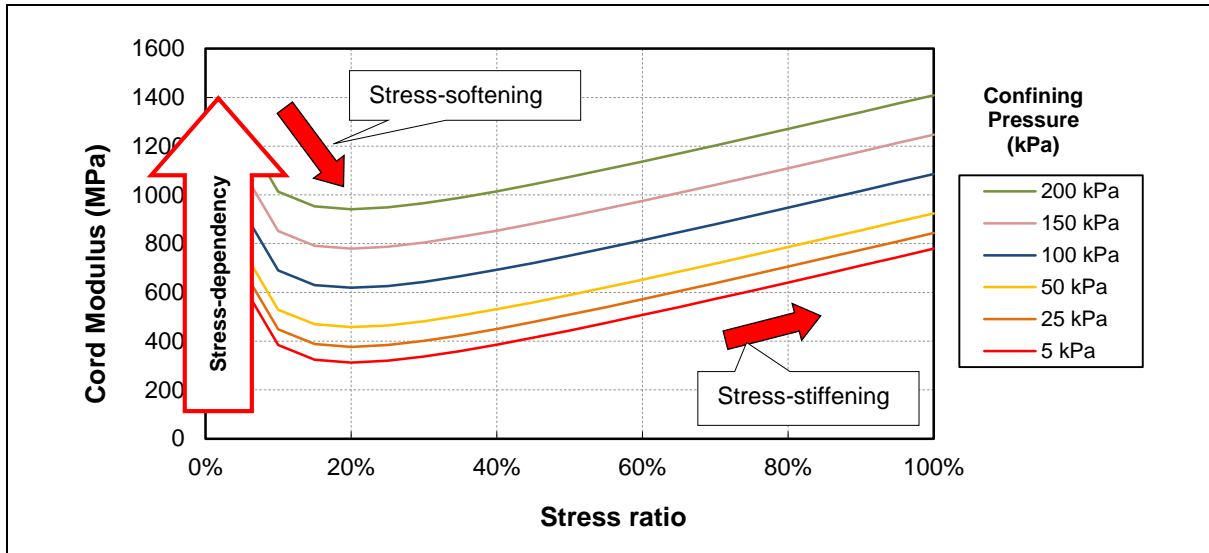
Figure 4.17: Stress-dependent behaviour of material.

From the literature (Section 2.2.2.3 and 2.2.3.2) and Section 4.3 it is evident that moisture has a significant influence on the stiffness and shear strength of unbound granular material. Therefore the cord modulus model formulation had to be extended to include the effect of moisture content or degree of saturation on the stiffness of the material. Figure 4.18 illustrate three different material responses to the increasing effect of degree of saturation (from top to bottom in each of the three columns).

4-22
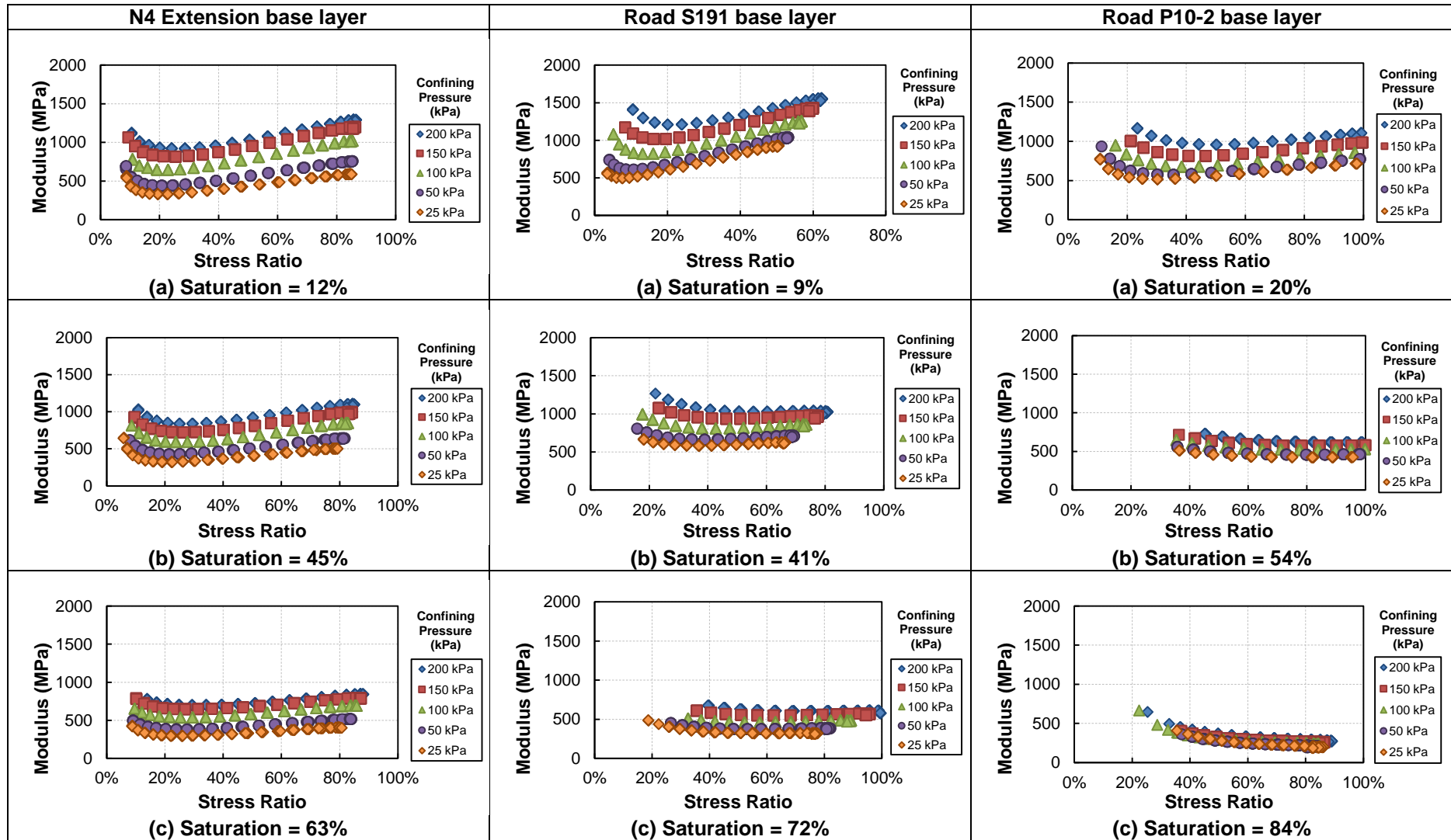
Figure 4.18: Change in cord modulus calculated from tri-axial results with increasing degree of saturation.

The following observations can be made regarding the behaviour depicted in Figure 4.18:

- There is a general reduction in the magnitude of the cord modulus with increasing degree of saturation for the materials depicted;
- Stress-stiffening behaviour with increasing confinement pressure but also with increasing stress ratio above 20 per cent at all levels of saturation is observed for the N4 Extension base layer material. (This material is a crushed stone, while the others depicted are natural unbound granular material);
- Road S191 base layer material indicate stress-stiffening behaviour with increasing confinement pressure at the three saturation levels, but the effect of increasing confinement pressure reduced with increasing saturation level. Stress-stiffening occurred with increasing stress ratio at low and intermediate levels of saturation, but not at the highest level of saturation where the cord modulus remained almost constant with increasing stress ratio; and
- Stress-stiffening behaviour with increasing confinement pressure at the three levels of saturation was observed for Road P10-2 base layer material. However, the effect of increasing confinement pressure became negligible at the highest saturation level. Stress-stiffening occurred with increasing stress ratio only at the low level of saturation. The cord modulus showed stress softening with increasing stress ratio at the intermediate and high levels of saturation with the cord modulus reducing consistently with increasing stress ratio.

These observations appear sensible when the material characteristics are considered as given in Table 4.5, with Road P10-2 base layer material having being classified as a weaker, lower quality material than N4 Extension base layer material.

Table 4.5:   Material characteristics for behaviour depicted in Figure 4.18.

Sample	GM	$P_{0.075}$ (%)	PI	Classification
N4 Ext. Base	2.6	5.2	NP	G1
S191 Base	2.5	10.8	8	G6
P10-2 Base	2.0	25.1	8	G8

Section 4.3.2 describes how the variables of the cord modulus model are linked to mathematical functions which take the observations from this section into consideration.

4.3.2   Selection of mathematical functions approximating variables

After the processing of the test data was complete, the data were copied to a template where the cord modulus values '*a*', '*b*' and '*c*' were calibrated for each specimen tested for each of the bulk sampled materials, i.e. eighteen samples per bulk sample. Calibration of the model was done in MS Excel using the solver function after identifying a mathematical function that best fit the data. Various combinations of mathematical functions were tested, expressed as accuracy of the complete model using RMSE, before a function was assigned to a variable. Variable '*a*' and '*c*' is approximated by a linear equation

fitted to data for all the specimens. However, the constants of the linear approximation may differ from sample to sample. The same method was followed for variable '*b*' which is approximated by a constant value, which may differ from sample to sample (Figure 4.19).
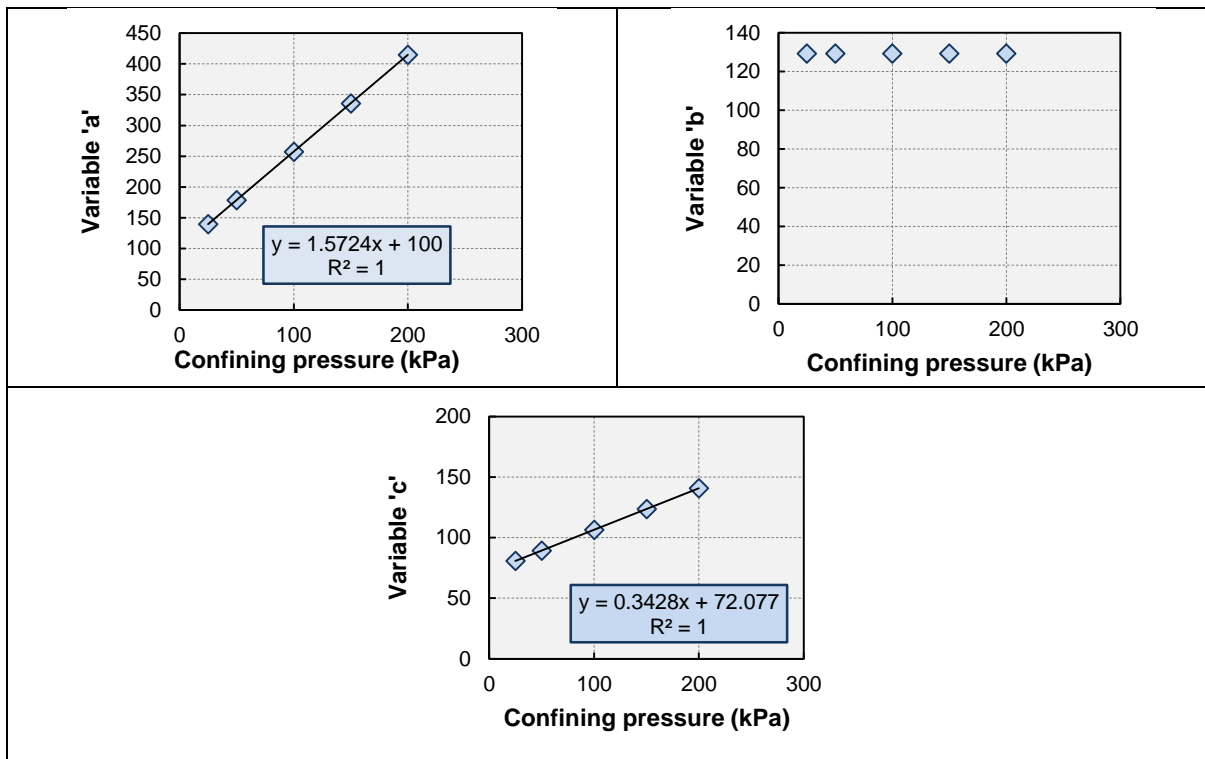
Figure 4.19:   Mathematical functions approximating variables for S191 B (Sample no. 11726-36).

Figure 4.20 illustrate how the mathematical functions are linked to the cord modulus model variables.

$$M_c = a + bSR_d + \frac{c}{SR_d}$$

$$M_c = \left(\alpha_1 + \beta_1\sigma_3\right) + \left(\alpha_2\right)\left(\frac{\sigma_1 - \sigma_3}{\sigma_1^f - \sigma_3}\right) + \frac{\left(\alpha_3 + \beta_1\sigma_3\right)}{\left(\dfrac{\sigma_1 - \sigma_3}{\sigma_1^f - \sigma_3}\right)}$$

Where

M_c = cord modulus (MPa)

SR_d = deviator Stress Ratio (SR)

$\alpha_1, \beta_1, \alpha_2, \alpha_3, \beta_3$ = regression coefficients found from regression analysis
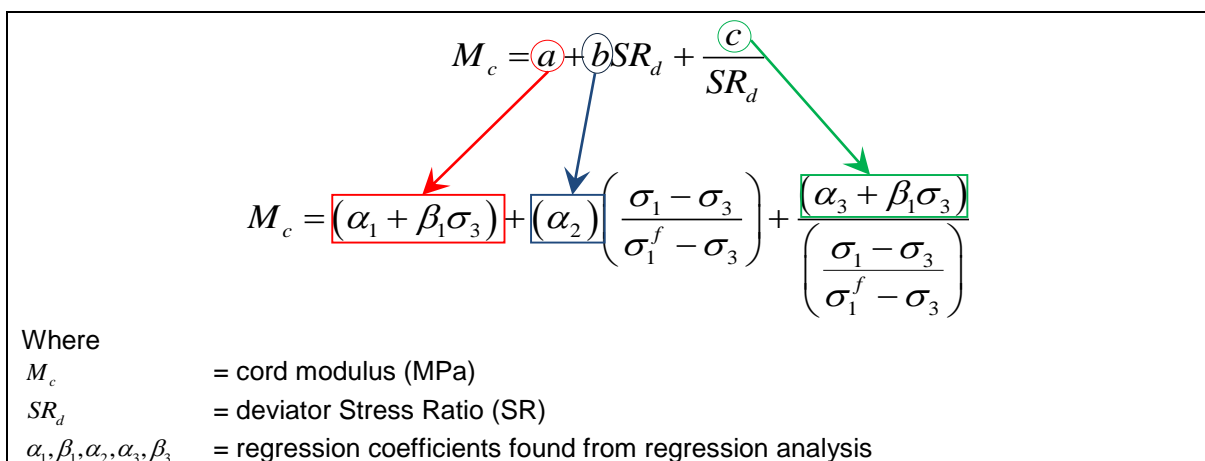
Figure 4.20:   Hierarchy of variables and mathematical functions approximating the variables.

4-25

4.3.3 Identification of sub-variable relationships within variables

After the calibration process described in Section 4.3.2 for variables '*a*', '*b*' and '*c*', the sub-variables (α_1, β_1, α_2, (β_2=0), α_3 and β_3) were evaluated against saturation, distinguishing between 'high (HD)' and 'low (LD)' density samples. Figure 4.21 depicts the graphs for Road P10-2. Similar graphs were generated for all the material samples which are contained in Appendix F. The limitation that none of the variables are allowed to be a negative value was kept in mind during the identification of mathematical equations describing the observed trends.
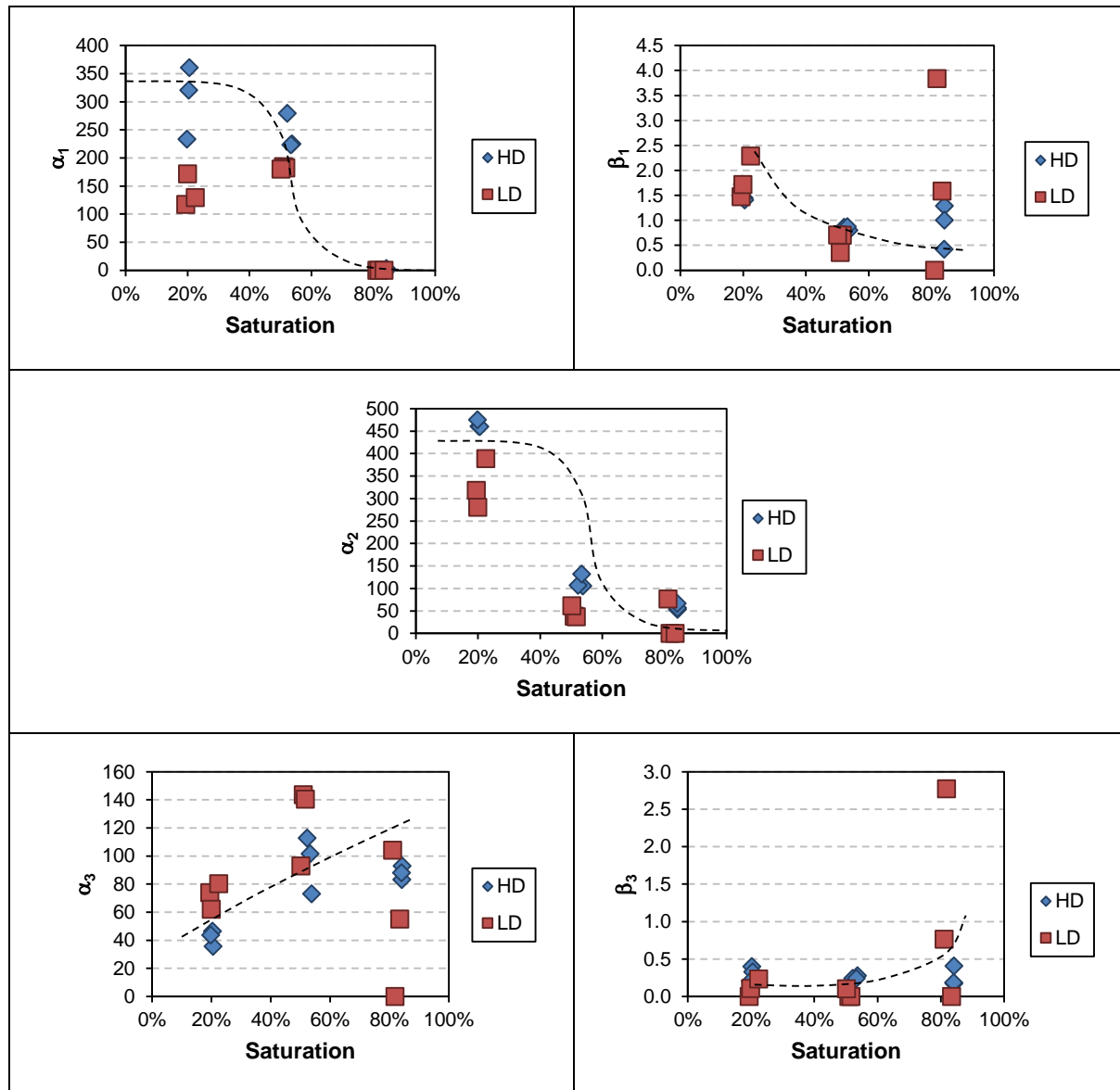
Figure 4.21:   Calibrated sub-variable values of Road P10-2 plotted against saturation.

The following mathematical equations were linked to the observed trends:

- Sub-variable 'α_1': The sub-variable appears to reach a plateau for saturation levels below 40 per cent and then rapidly decrease to a lower level plateau at saturation levels above 60 per

4-26

cent saturation. This ties in with the observations made in Section 4.3.1 where the cord modulus approached zero at high saturation levels. Theyse (2009) reported that the stiffness of partially saturated unbound granular material reaches a ceiling value below a certain threshold value of saturation. Theyse (2009) used a sigmoidal curve (Figure 4.22) which was also identified to predict the trend of sub-variable 'α_1'.

- Sub-variable 'β_1': A logarithmic curve was selected as it predicts the trend in data best.

- Variable 'b' or sub-variable 'α_2': The sub-variable appears to reach a plateau for saturation levels below 40 per cent and then rapidly decrease to a lower level plateau at saturation levels above 60 per cent saturation. Therefore a sigmoidal curve was selected to predict the trend in the data.

- Sub-variable 'α_3': No obvious trend could be identified for 'α_3' and linear, exponential and power curves were evaluated. The accuracy of the complete model using RMSE was used to evaluate which trend to link to 'α_3'. A linear curve was selected to predict 'α_3' values, as in combination with 'β_3' it yielded acceptable accuracy for the complete model.

- Sub-variable 'β_3': No obvious trend could be identified for 'β_3' and linear, exponential, logarithmic and power curves were evaluated. The accuracy of the complete model using RMSE was used to evaluate which trend to link to 'β_3'. An exponential curve was selected to predict 'β_3' values, as in combination with 'α_3' it yielded acceptable accuracy for the complete model.
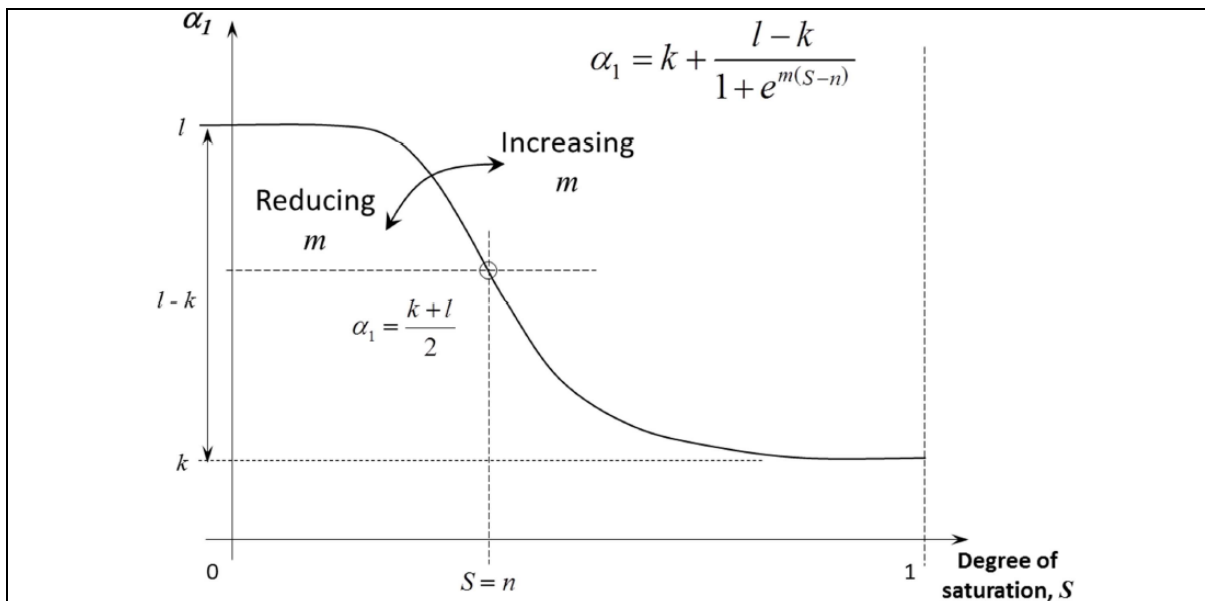
Figure 4.22:   Sigmoid curve fitted to α_1 and α_2 data.

Based on the aforementioned evaluations, mathematical relationships in terms of saturation were used to describe each sub-variable which in turn is used to describe variables 'a', 'b' and 'c', as depicted in Figure 4.23. This combination results in a saturation and stress dependent cord modulus model formulation.

4-27

$$M_c = a + b\$R_d + \frac{c}{SR_d}$$

$$M_c = \left(\alpha_1 + \beta_1 \sigma_3 \right) + \left(\alpha_2 \right)\left(\frac{\sigma_1 - \sigma_3}{\sigma_1^f - \sigma_3} \right) + \frac{\left(\alpha_3 + \beta_3 \sigma_3 \right)}{\left(\frac{\sigma_1 - \sigma_3}{\sigma_1^f - \sigma_3} \right)}$$

$$\alpha_1 = k_{\alpha_1} + \frac{l_{\alpha_1} - k_{\alpha_1}}{1 + e^{m_{\alpha_1}(S - n_{\alpha_1})}}$$

$$\beta_1 = k_{\beta_1} \ln(S) + l_{\beta_1}$$

$$\alpha_2 = k_{\alpha_2} + \frac{l_{\alpha_2} - k_{\alpha_2}}{1 + e^{m_{\alpha_2}(S - n_{\alpha_2})}}$$

$$\alpha_3 = k_{\alpha_3} S + l_{\beta_3}$$

$$\beta_3 = k_{\beta_3} e^{(S \cdot l_{\beta_3})}$$

Where

M_c	= cord modulus (MPa)
SR_d	= deviator Stress Ratio (SR)
$\alpha_1, \beta_1, \alpha_2, \alpha_3, \beta_3$	= regression coefficients found from regression analysis
k_i, l_i, m_i, n_i	= regression coefficients found from regression analysis
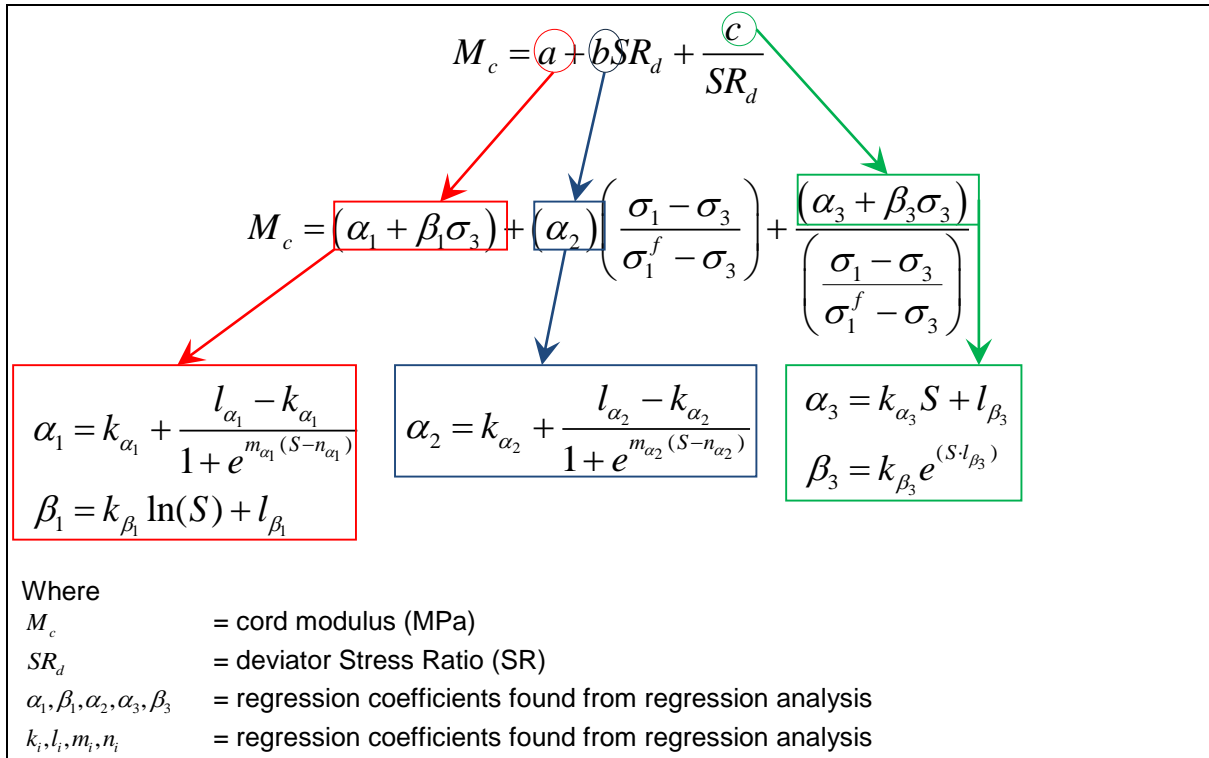
Figure 4.23:   Hierarchy of variables and sub-variables.

4.3.4   Model calibration per bulk material sample

The aforementioned saturation and stress dependent cord modulus model was calibrated using the model formulation depicted in Figure 4.23 for all the material samples. Figure 4.25 to Figure 4.32 illustrate the prediction accuracy of the model for the two different levels of volumetric density at which samples were prepared. Individual test results for all the materials are depicted in Appendix G, as well as statistical parameters which were calculated when the calibrated variables (α_1, β_1, α_2, α_3, β_3, k_i, l_i, m_i and n_i) were used as input to calculate the cord modulus value per individual test sample.

4.3.4.1   N4 Extension base layer

The model appears to have good prediction accuracy for the material from N4 Extension base layer on material and individual test result level. This is indicated by the statistical parameters listed in Table 4.6 for the high (HD) and low volumetric density (LD) samples.

Table 4.6:   Statistical data for high and low volumetric density samples from N4 Ext. base layer.

N4 Ext. Base	R^2 (ratio)	RMSE (%)	SEE (MPa)	% Error
HD	0.85	0.44%	84.24	9.55%
LD	0.72	0.63%	99.31	12.81%

Two high density test results appear to have slightly lower prediction accuracy than the rest of the high density samples (Figure 4.24 and Table 4.7). Sample 11306_21 deviate from the perfect fit line, due to slight over prediction of the resilient response at 200, 50 and 25 kPa confining pressure. The SEE for the results from this sample is 162 MPa (R^2 = 0.59), while the results for the remaining two repeat samples are 55 MPa (R^2 = 0. 96) and 64 MPa (R^2 = 0.95) respectively. Sample 11306_25 also slightly deviate from the perfect fit line due to under estimation of the model for resilient response at 200 kPa confining pressure. The SEE for the results from this sample is 160 MPa (R^2 = 0.68), while the results from the remaining two repeat samples are 71 MPa (R^2 = 0.88) and 71 MPa (R^2 = 0.97) respectively. Since three repeat tests at a specific saturation level was conducted and two of the three samples at the low and high saturation level indicate accurate prediction by the model, the individual test results with lower accuracy can be discarded.

Table 4.7: **Statistical data for HD samples from N4 Ext. base layer.**

Sample no.	VD (ratio)	S (ratio)	R^2 (ratio)	RMSE (%)	SEE (MPa)	% Error
11306_19	0.82	0.14	0.96	0.27%	55.0	5.6%
11306_20	0.83	0.16	0.95	0.27%	63.9	5.7%
11306_21	0.82	0.14	0.59	0.89%	161.8	20.8%
11306_22	0.82	0.43	0.94	0.33%	53.4	7.0%
11306_23	0.83	0.45	0.96	0.26%	45.4	5.3%
11306_24	0.82	0.41	0.89	0.39%	76.6	8.5%
11306_25	0.82	0.66	0.68	0.69%	159.8	17.4%
11306_26	0.82	0.65	0.83	0.48%	71.3	7.4%
11306_27	0.82	0.67	0.88	0.42%	70.9	8.3%
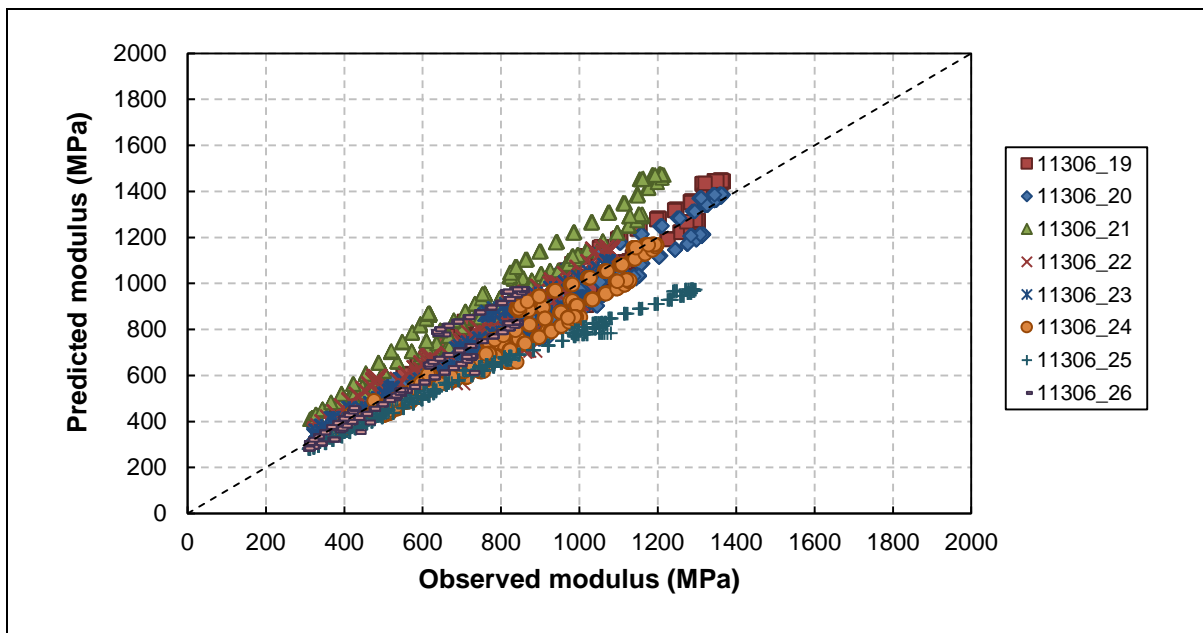
Figure 4.24: **Prediction accuracy for high volumetric density samples from N4 Extension base layer.**

Three results of the low density samples appear to have lower prediction accuracy than the other samples (Figure 4.25 and Table 4.8). The predicted modulus for samples 11306_28, 29, 32 and 33 is slightly lower than the observed modulus. The remaining individual results of the set of three indicate a good fit. These results can be discarded as the remaining individual results from the set at the specific saturation level indicate accurate prediction by the model. Sample 11306_30s results were discarded due to an error during testing.

Table 4.8: **Statistical data for LD samples from N4 Ext. base layer.**

Sample no.	VD (ratio)	S (ratio)	R^2 (ratio)	RMSE (%)	SEE (MPa)	% Error
11306_28	0.80	0.13	0.25	1.00%	157.4	20.0%
11306_29	0.81	0.13	0.26	0.88%	150.7	19.2%
11306_30	0.80	0.12				
11306_31	0.79	0.42	0.81	0.53%	80.5	11.2%
11306_32	0.80	0.42	0.74	0.71%	125.2	14.6%
11306_33	0.80	0.46	0.82	0.56%	97.0	13.0%
11306_34	0.80	0.69	0.88	0.46%	85.3	10.0%
11306_35	0.79	0.62	0.95	0.51%	51.2	9.6%
11306_36	0.79	0.63	0.90	0.41%	53.9	8.7%
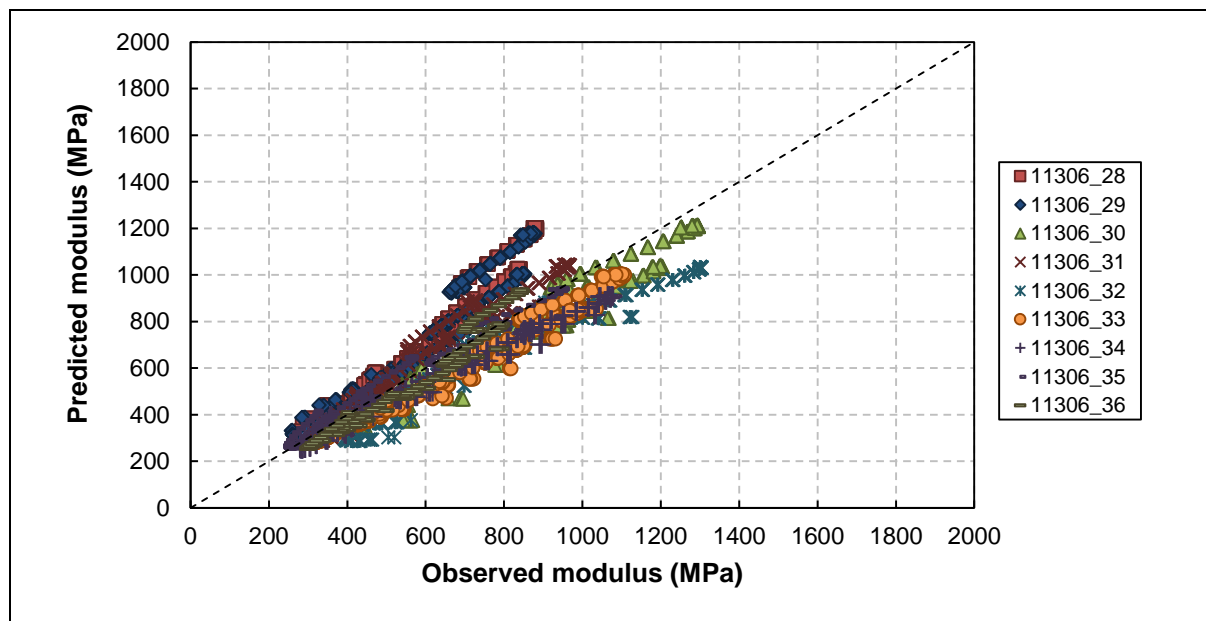
Figure 4.25: **Prediction accuracy for low volumetric density samples from N4 Extension base layer.**

4.3.4.2   *N4 Extension upper selected layer*

The model appears to have good prediction accuracy for the material from N4 Extension upper selected layer on material and individual test result level, especially for the high volumetric density samples. This is indicated by the statistical parameters listed in Table 4.9 for the high (HD) and low volumetric density (LD) samples.

Table 4.9:   **Statistical data for high and low volumetric density samples from N4 Ext.**
upper selected layer.

N4 Ext. USEL	R^2 (ratio)	RMSE (%)	SEE (MPa)	% Error
HD	0.82	0.34%	41.20	6.49%
LD	0.25	0.69%	123.04	13.87%

The SEE for the HD test results varies between 17 MPa and 81 MPa with R^2 between 0.53 and 0.99, which is acceptable considering inherent material variability and that these results are obtained at material level (Figure 4.26 and Table 4.10).

Table 4.10:   **Statistical data for HD samples from N4 Ext. upper selected layer.**

Sample no.	VD (ratio)	S (ratio)	R^2 (ratio)	RMSE (%)	SEE (MPa)	% Error
11307_19	0.70	0.18	0.99	0.09%	16.9	1.7%
11307_20	0.70	0.18	0.86	0.29%	58.7	6.8%
11307_21	0.70	0.18	0.96	0.17%	35.0	3.5%
11307_22	0.70	0.46	0.70	0.42%	80.5	8.7%
11307_23	0.70	0.46	0.80	0.36%	54.1	7.6%
11307_24	0.70	0.46	0.92	0.19%	39.8	3.8%
11307_25	0.69	0.74	0.79	0.40%	21.1	6.5%
11307_26	0.69	0.73	0.81	0.44%	30.0	5.8%
11307_27	0.69	0.74	0.53	0.73%	34.8	14.1%
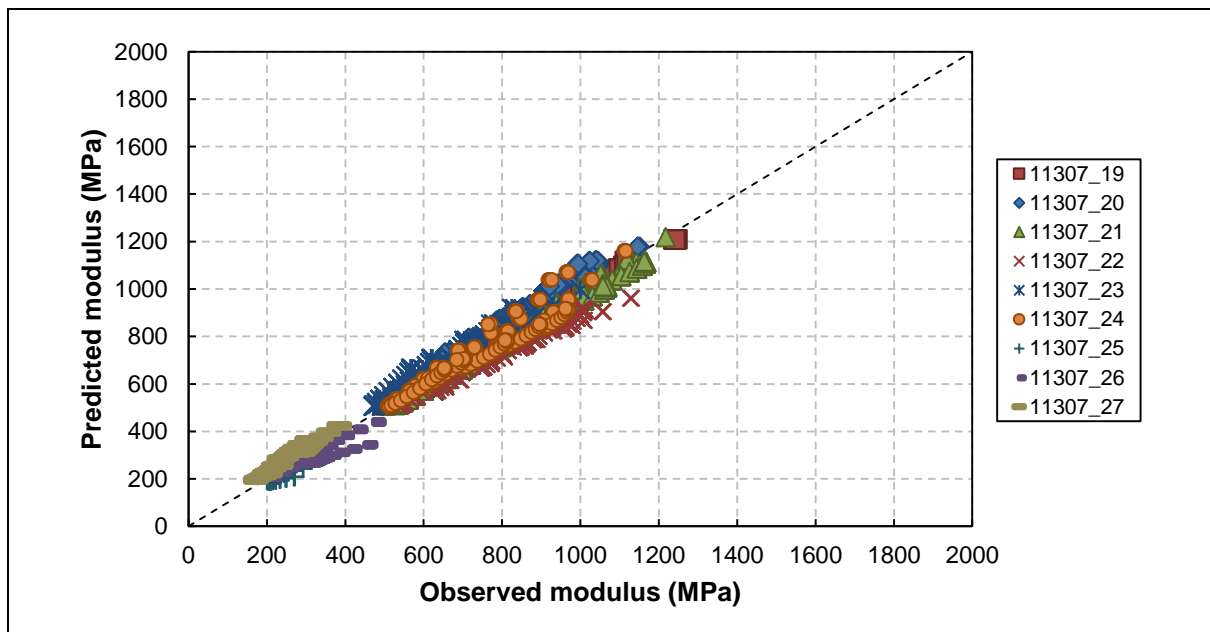
Figure 4.26:   **Prediction accuracy for high volumetric density samples from N4 Extension**
upper selected layer.

Samples 11306_28, 30, 32 and 36 appears to have lower prediction accuracy than the remaining samples (Figure 4.27 and Table 4.11). The observed trend in modulus results for these samples all appear to lack a stress-stiffening component and the observed modulus decrease rapidly at all confining pressure levels without reaching a constant modulus at higher saturation levels. Therefore the model cannot model the behaviour accurately as it differs from the general trends identified in Figure 4.18. The SEE for the remaining samples varies between 17 MPa and 136 MPa with R^2 between 0.40 and 0.96, which is acceptable considering inherent material variability and that these results are obtained at material level. The results from samples 11307_31 and 34 were discarded due to an error during testing.

Table 4.11:   Statistical data for LD samples N4 Ext. upper selected layer.

Sample no.	VD (ratio)	S (ratio)	R^2 (ratio)	RMSE (%)	SEE (MPa)	% Error
11307_28	0.68	0.16	0.10	0.98%	257.7	19.6%
11307_29	0.69	0.16	0.75	0.25%	136.1	6.2%
11307_30	0.69	0.16	-0.62	1.65%	254.2	33.4%
11307_31	0.68	0.49				
11307_32	0.68	0.48	-0.08	0.73%	110.9	15.6%
11307_33	0.69	0.47	0.96	0.15%	17.2	2.6%
11307_34	0.68	0.73				
11307_35	0.68	0.70	0.40	0.56%	31.5	11.2%
11307_36	0.68	0.69	0.25	0.54%	53.5	8.5%
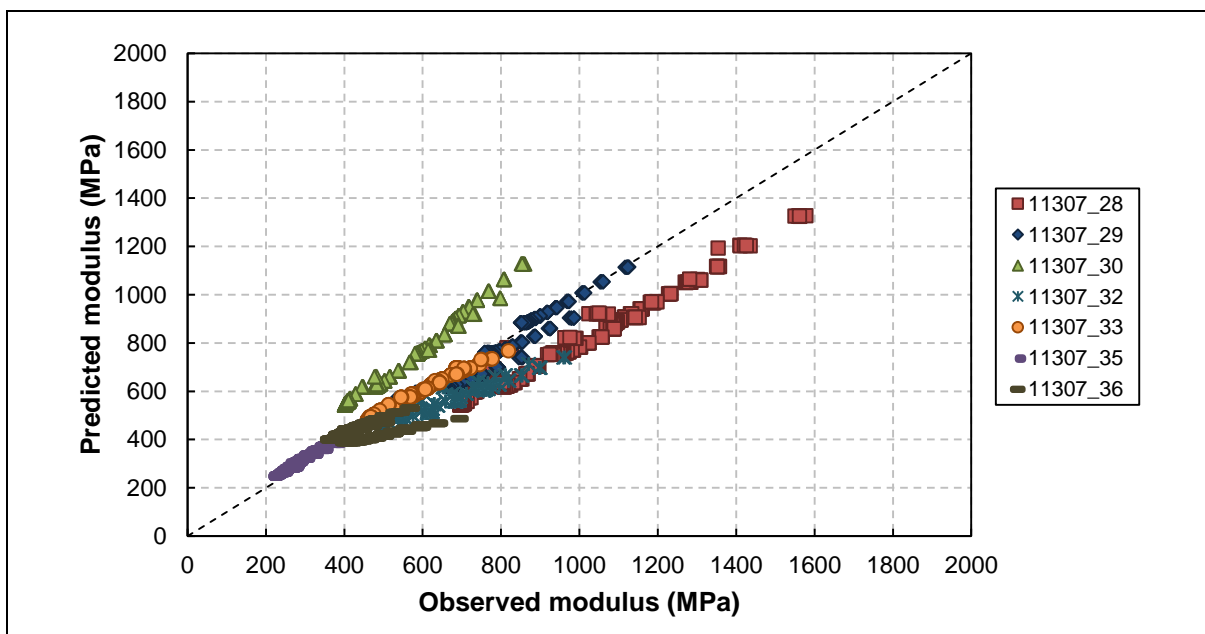
Figure 4.27:   Prediction accuracy for low volumetric density samples from N4 Extension upper selected layer.

4.3.4.3 Road S191 base layer

The model appears to have good prediction accuracy for the material from Road S191 base layer on material, as well as on individual test result level. This is indicated by the statistical parameters listed in Table 4.12 for all the samples combined. The samples were evaluated without a split between high and low density as the high and low volumetric density values in this case differed with only one per cent.

Table 4.12: Statistical data for high and low volumetric density samples from Road S191 base layer.

S191 Base	R^2 (ratio)	RMSE (%)	SEE (MPa)	% Error
All	0.92	0.33%	85.61	7.78%

Samples 11726_20, 21, 24, 25, 28 and 29 appears to have slightly lower prediction accuracy than the remaining high volumetric density samples (Figure 4.28 and Table 4.13). Some isolated data points of sample 11726_20 and 21 seem to indicate a poor fit, but the general fit of the model appears good when the individual test results are considered. The initial observed modulus at 200 kPa confining pressure for samples 11726_24 and 25 is higher than the initial modulus for the other samples in the same level of saturation set, which explains why the prediction accuracy for these samples are slightly poorer. The SEE varies between 15 MPa and 99 MPa with R^2 between 0.55 and 0.99 which is acceptable considering that these results are obtained at material level. The results from sample 11726_31 were discarded due to an error during testing.

Table 4.13: Statistical data for all samples from Road S191 base layer.

Sample no.	VD (ratio)	S (ratio)	R^2 (ratio)	RMSE (%)	SEE (MPa)	% Error
11726_19	0.80	0.09	0.89	0.33%	99.2	7.0%
11726_20	0.80	0.09	0.92	0.40%	85.6	7.8%
11726_21	0.80	0.09	0.94	0.28%	76.2	5.8%
11726_22	0.80	0.43	0.87	0.28%	43.8	4.1%
11726_23	0.80	0.41	0.95	0.23%	36.5	3.8%
11726_24	0.80	0.40	0.58	0.50%	120.3	10.1%
11726_25	0.80	0.71	0.46	0.85%	121.6	17.0%
11726_26	0.80	0.72	0.77	0.43%	51.5	8.3%
11726_27	0.80	0.73	0.97	0.21%	21.3	3.6%
11726_28	0.79	0.10	0.98	0.18%	41.8	3.1%
11726_29	0.79	0.11	0.95	0.28%	67.6	5.2%
11726_30	0.79	0.11	0.91	0.31%	77.4	6.2%
11726_31	0.79	0.42				
11726_32	0.79	0.43	0.91	0.26%	46.7	4.6%
11726_33	0.79	0.43	0.96	0.22%	32.3	3.6%
11726_34	0.79	0.77	0.99	0.12%	14.5	2.1%
11726_35	0.79	0.77	0.96	0.20%	27.7	3.8%
11726_36	0.79	0.75	0.55	0.60%	67.9	12.5%
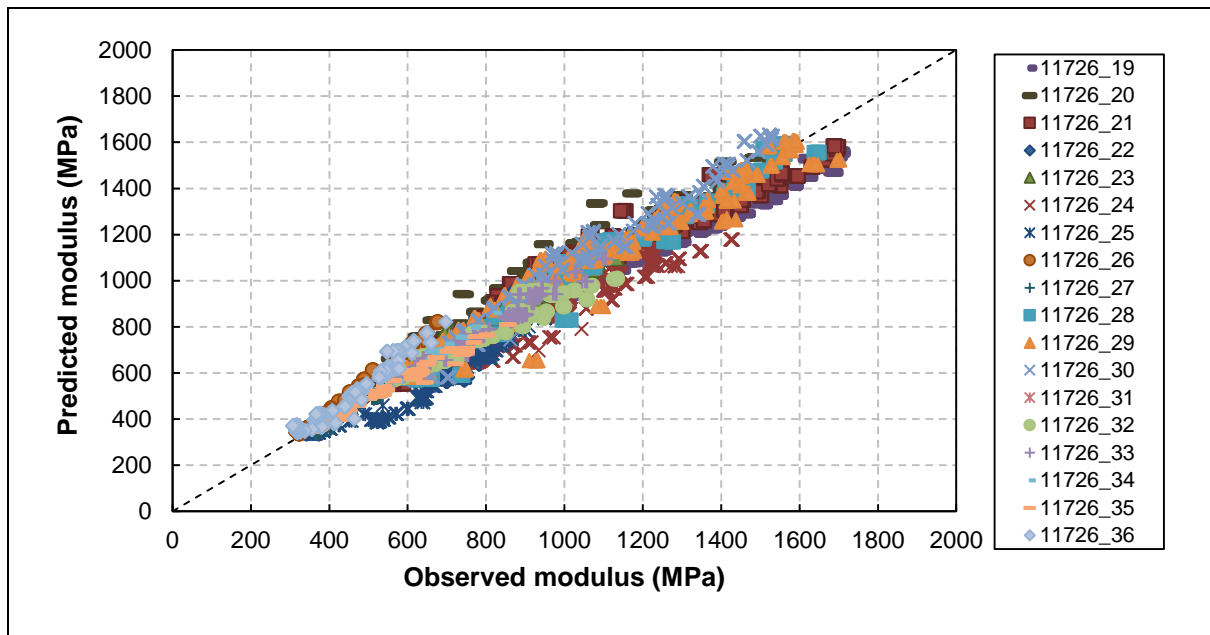
Figure 4.28: **Prediction accuracy for all samples from Road S191 base layer.**

4.3.4.4   Road P10-2 base layer

The model appears to have good prediction accuracy for the material from Road P10-2 base layer on material and individual test result level. This is indicated by the statistical parameters listed in Table 4.14 for the high (HD) and low volumetric density (LD) samples.

Table 4.14: **Statistical data for high and low volumetric density samples from Road P10-2 base layer.**

P10-2 base	R^2 (ratio)	RMSE (%)	SEE (MPa)	% Error
HD	0.68	0.34%	34.72	6.93%
LD	0.33	0.50%	75.85	10.13%

For samples at high density (Figure 4.29 and Table 4.15), the SEE varies between 11 MPa and 62 MPa with R^2 between 0.77 and 0.98 which is acceptable considering that these results are obtained at material level. The results from sample 11721_27 were discarded due to an error during testing.

Table 4.15:   Statistical data for HD samples from Road P10-2 base layer.

Sample no.	VD (ratio)	S (ratio)	R^2 (ratio)	RMSE (%)	SEE (MPa)	% Error
11721_19	0.76	0.20	0.86	0.34%	61.6	7.6%
11721_20	0.76	0.20	0.91	0.22%	44.0	4.5%
11721_21	0.76	0.20	0.98	0.11%	23.4	2.1%
11721_22	0.76	0.54	0.91	0.21%	22.8	3.9%
11721_23	0.76	0.52	0.82	0.25%	33.8	4.0%
11721_24	0.76	0.53	0.77	0.27%	36.5	5.2%
11721_25	0.76	0.84	0.83	0.38%	24.6	7.7%
11721_26	0.76	0.84	0.91	0.22%	11.3	3.5%
11721_27	0.76	0.84				
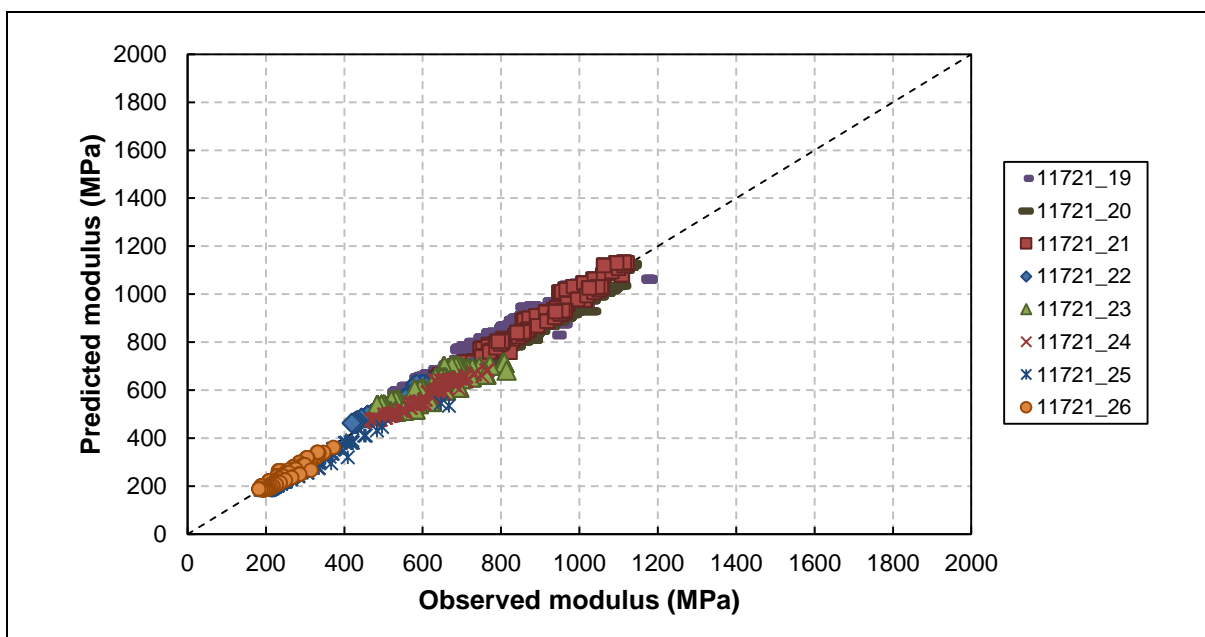
Figure 4.29:   Prediction accuracy for high volumetric density samples from Road P10-2 base layer.

The model appears to have good prediction accuracy for samples at low density (Figure 4.30 and Table 4.16). However, samples 11721_30 and 32 depict poor prediction accuracy due to under estimation of the modulus. The remaining samples in the specific saturation level set have better prediction accuracy and therefore the two sample results can be discarded. The SEE of the remaining samples varies between 21 MPa and 34 MPa with R^2 between 0.60 and 0.95 which is acceptable considering inherent material variability and that these results are obtained at material level. The results from samples 11721_34, 35 and 36 were discarded due to an error during testing.

Table 4.16: **Statistical data for LD samples Road P10-2 base layer.**

Sample no.	VD (ratio)	S (ratio)	R² (ratio)	RMSE (%)	SEE (MPa)	% Error
11721_28	0.73	0.19	0.88	0.22%	32.6	4.3%
11721_29	0.73	0.20	0.95	0.18%	27.4	3.5%
11721_30	0.73	0.22	-0.366	0.97%	207.8	22.2%
11721_31	0.74	0.51	0.60	0.33%	33.5	5.2%
11721_32	0.73	0.52	-0.96	0.97%	132.6	21.0%
11721_33	0.74	0.50	0.86	0.24%	21.2	4.6%
11721_34	0.74	0.81				
11721_35	0.74	0.82				
11721_36	0.73	0.83				
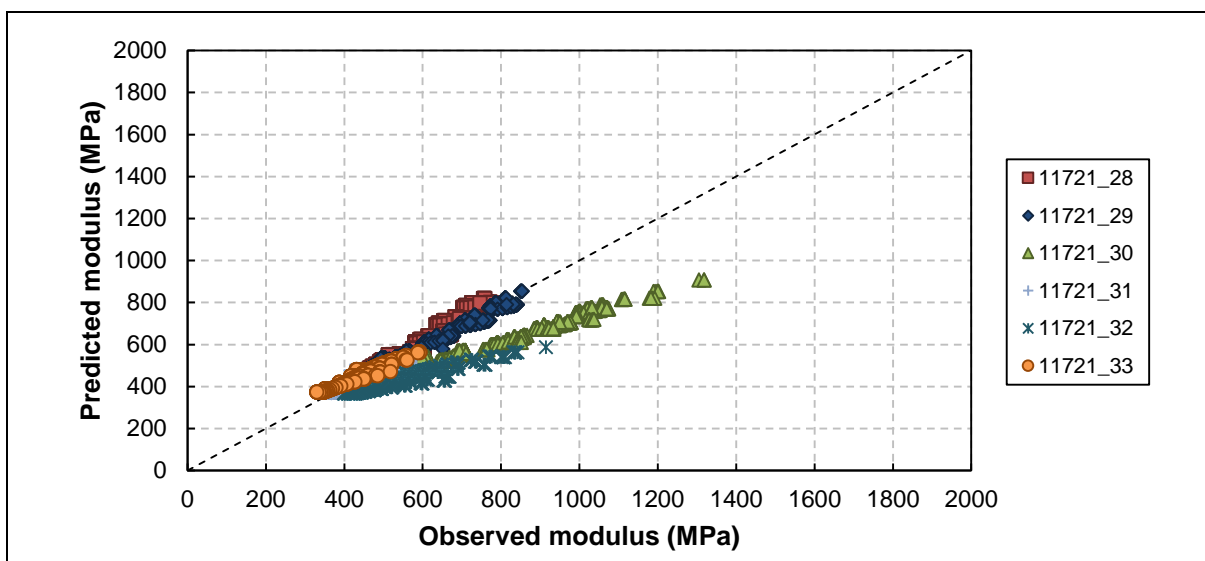
Figure 4.30: **Prediction accuracy for low volumetric density samples from Road P10-2 base layer.**

4.3.4.5 *Road D804 base layer*

The model appears to have relatively good prediction accuracy for the material from Road D804 base layer on material level. This is indicated by the statistical parameters listed in Table 4.17 for the high (HD) and low volumetric density (LD) samples.

Table 4.17: **Statistical data for high and low volumetric density samples from Road D804 base layer.**

D804 base	R² (ratio)	RMSE (%)	SEE (MPa)	% Error
HD	0.81	0.26%	37.73	5.00%
LD	0.62	0.40%	46.19	7.38%

However, some of the individual test results appear to not predict the material behaviour as accurately. Based on SEE only individual test results from two samples (11728_20 and 21) with SEE 85 MPa and

94 MPa can be regarded as poor as depicted in Figure 4.31 and Table 4.18. The SEE for the remaining individual results varies between 15 MPa and 33 MPa with R^2 between 0.74 and 0.96 which is acceptable considering that these results are obtained at material level. The result for sample 11728_19 was discarded due to an error during testing.

Table 4.18: **Statistical data for HD samples from Road D804 base layer.**

Sample no.	VD (ratio)	S (ratio)	R^2 (ratio)	RMSE (%)	SEE (MPa)	% Error
11728_19	0.73	0.21				
11728_20	0.73	0.20	0.52	0.43%	85.3	9.7%
11728_21	0.73	0.21	0.57	0.35%	93.5	8.0%
11728_22	0.73	0.43	0.74	0.23%	33.3	3.8%
11728_23	0.73	0.43	0.94	0.13%	20.6	2.0%
11728_24	0.73	0.43	0.93	0.14%	23.4	2.3%
11728_25	0.72	0.77	0.89	0.30%	17.5	5.3%
11728_26	0.73	0.80	0.96	0.21%	12.9	3.4%
11728_27	0.73	0.79	0.93	0.29%	15.4	5.5%
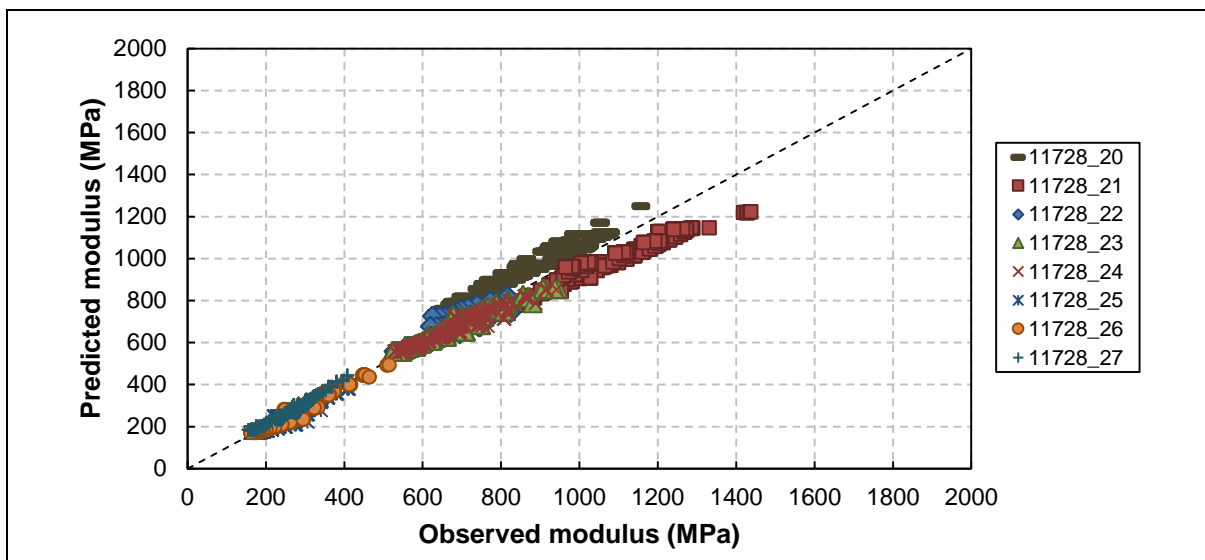
Figure 4.31: **Prediction accuracy for high volumetric density samples from Road D804 base layer.**

The model appears to have relatively good prediction accuracy for the low density material from Road D804 base layer on material level (Figure 4.32 and Table 4.19). Individual test results for sample 11728_31, 32 and 33 indicate poor prediction accuracy with the SEE 60 MPa, 42 MPa and 47 MPa respectively. R^2 is 0.33, 0.68 and 0.17 respectively. The observed trend in modulus results for these samples all appear to lack a stress-stiffening component and the observed modulus decrease rapidly at all confining pressure levels without reaching a constant modulus at higher saturation levels. Therefore the model cannot model the behaviour accurately as it differs from the general trends identified in Figure 4.18 and can be discarded. The remaining samples yield SEEs of between 26 MPa

and 61 MPa, with R^2 ranging from 0.65 to 0.86, which is acceptable considering that these results are obtained at material level. The result for sample 11728_34 was discarded due to an error during testing.

Table 4.19:   Statistical data for LD samples Road D804 base layer.

Sample no.	VD (ratio)	S (ratio)	R^2 (ratio)	RMSE (%)	SEE (MPa)	% Error
11728_28	0.70	0.21	0.86	0.20%	37.0	3.9%
11728_29	0.70	0.20	0.78	0.31%	61.0	6.1%
11728_30	0.70	0.20	0.77	0.40%	57.3	7.8%
11728_31	0.70	0.40	0.33	0.40%	59.8	6.7%
11728_32	0.70	0.41	0.68	0.29%	41.7	4.5%
11728_33	0.70	0.41	0.17	0.40%	46.6	7.1%
11728_34	0.71	0.79				
11728_35	0.71	0.77	0.65	0.65%	40.2	12.7%
11728_36	0.71	0.78	0.69	0.52%	25.9	10.3%
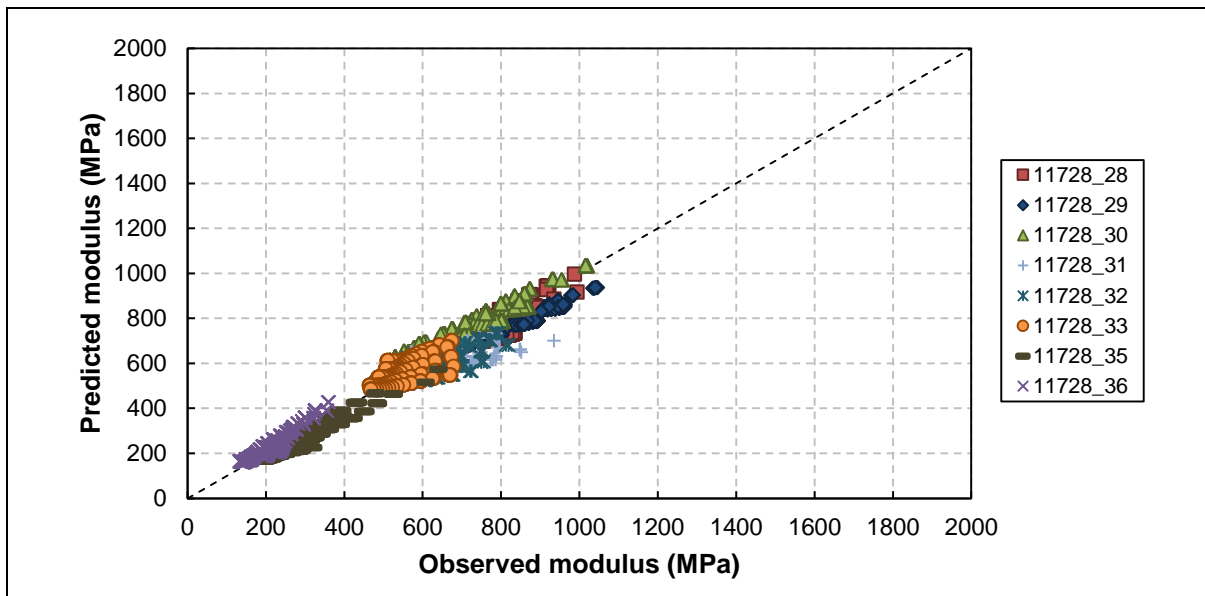
Figure 4.32:   Prediction accuracy for low volumetric density samples from Road D804 base layer.

4.3.5   Parametric analysis per bulk material sample

The model was further assessed by investigating parametric plots of the model. The high and low volumetric density scenarios were assessed individually. The difference between high and low volumetric densities is between 1 and 3 per cent. The stress dependency of the model reflects the trends observed in the data. In terms of the parametric plot for saturation, the model realistically reflects trends observed in the data as it extrapolates from the three levels of saturation tests were conducted at in this thesis.

4.3.5.1   N4 Extension base layer

The stress dependent behaviour of the material is realistically reflected in the parametric plots for both the high and low density resilient modulus samples tested as explained in Figure 4.17, Section 4.3.1. At 80 per cent saturation, the predicted modulus does not differ significantly between high and low volumetric densities as can be observed in Figure 4.33.

High density (VD = 82 %)

Low density (VD = 80 %)
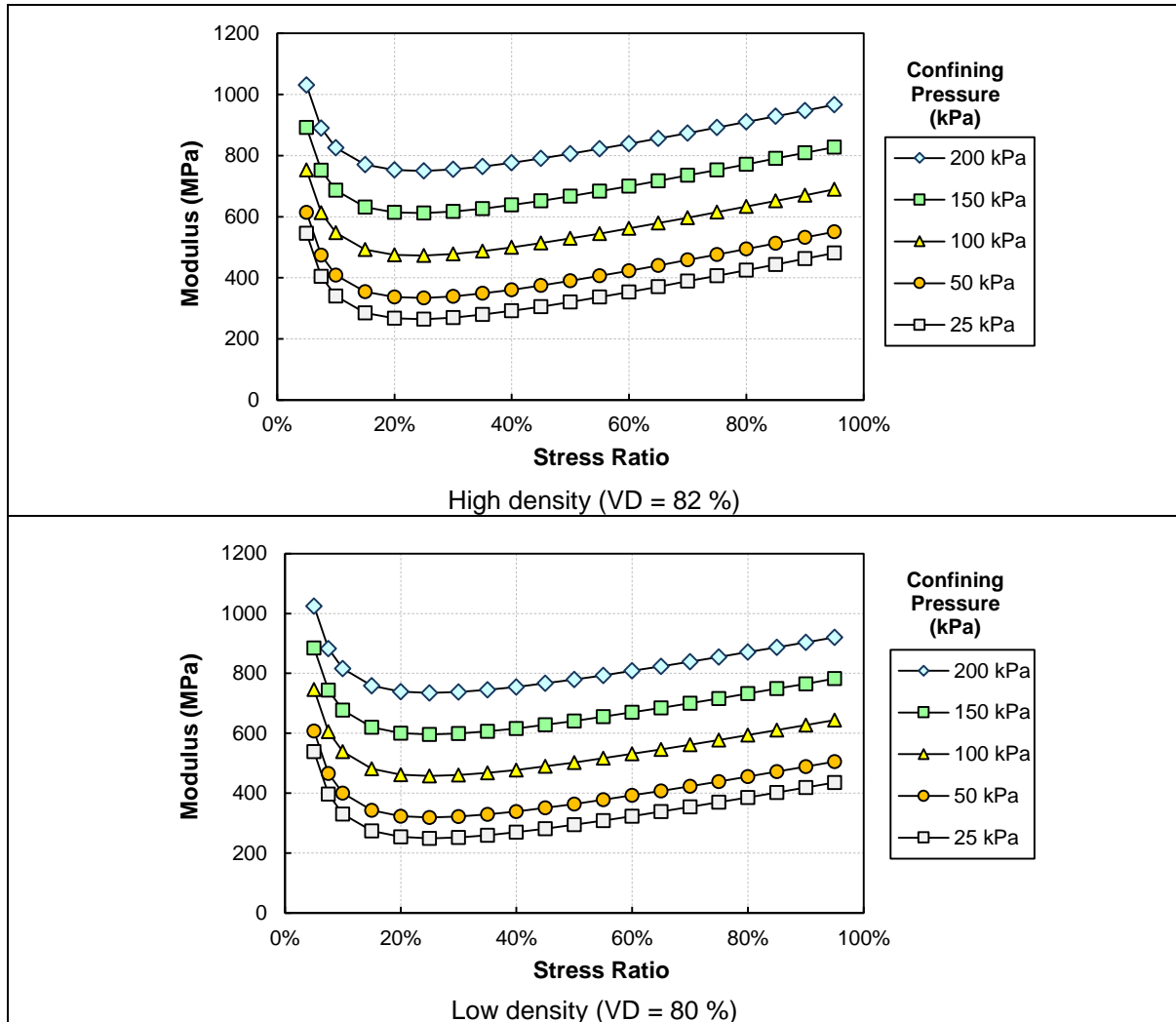
Figure 4.33:   Parametric plots of the stress-dependent behaviour for N4 Extension base layer.

The parametric plots for saturation realistically reflect the decrease of modulus with increasing saturation level at 50 kPa confining pressure (Figure 4.35). The low deviator stress of 20 kPa appears to reflect the influence of suction pressure on the material strength, before the increasing deviator stress over shadows the influence of suction pressure. The failure or yield strength at 0 kPa confinement predicted by using Theyse's suction model (2009), as described in Section 2.2.7.3, in essence depicts the influence of suction pressure. Figure 4.34 illustrates the failure or yield strength at 0 kPa, i.e. influence of suction pressure for this material.
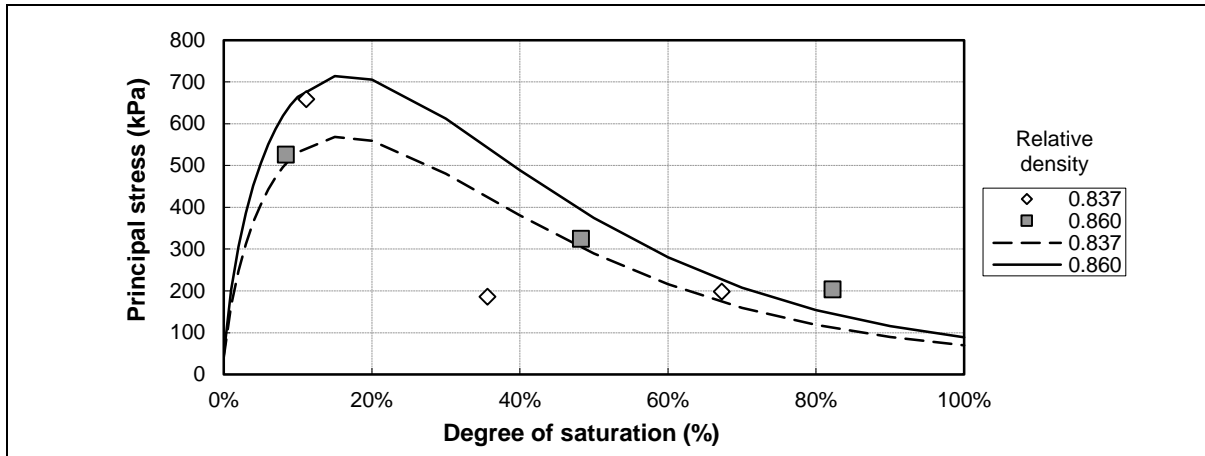
Figure 4.34: Failure or yield strength at 0 kPa confinement.

High density (VD = 82 %)

Low density (VD = 80 %)
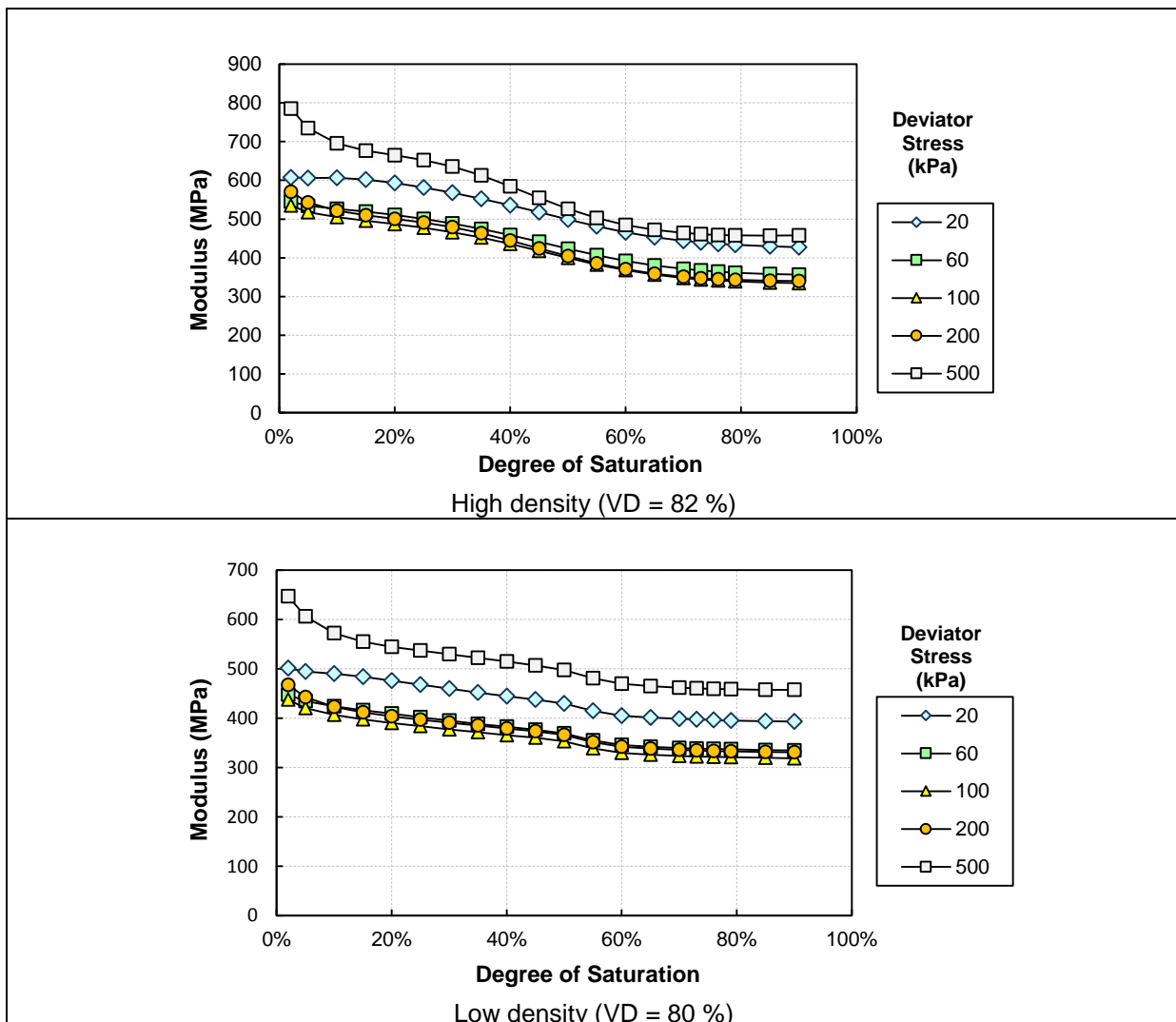
Figure 4.35: Parametric plots of saturation at different deviator stress levels for N4 Extension base layer.

4.3.5.2 N4 Extension upper selected layer

The stress dependent behaviour depicted by the model at 20 per cent saturation appears to be realistic as depicted in Figure 4.36. The higher initial modulus at lower density can be explained by the hyperbolic part of the model, which predicts high initial modulus values. These values might not be as unrealistic when the high PI of the material is considered (PI = 11), which at low saturation and low density levels may provide additional strength.

High density (VD = 70 %)

Low density (VD = 68 %)
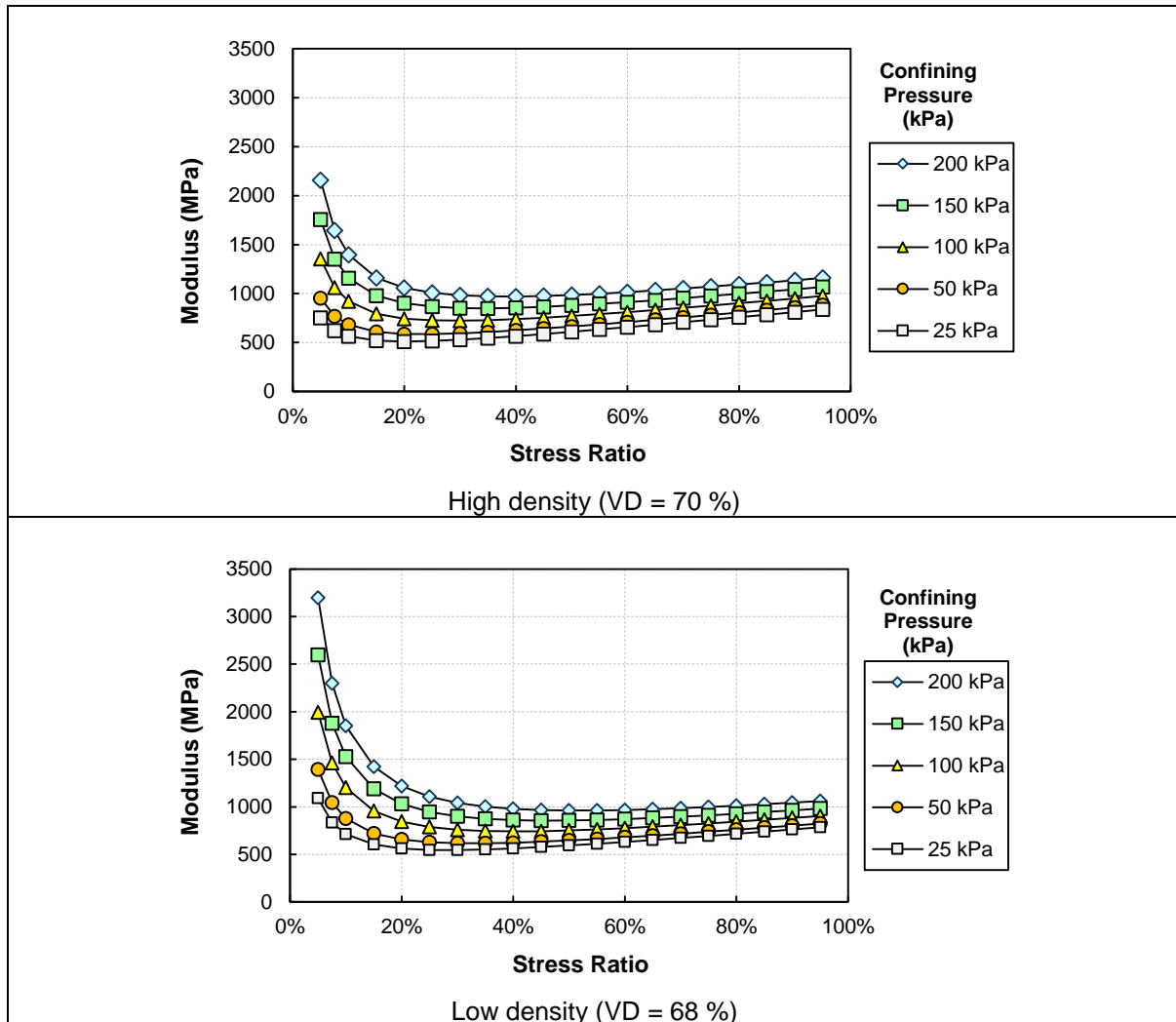
Figure 4.36:   Parametric plots of the stress-dependent behaviour for N4 Extension upper selected layer.

The influence of high fines content and PI can also be seen in the parametric plots for saturation (Figure 4.37). The influence of suction pressure on the material strength can be seen up to 100 kPa deviator stress at 25 kPa confining pressure. This trend of high predicted modulus values was also observed applying Theyse's suction model (2009) and comparing it to the principle stress measured at 0 kPa confinement. Deviator stress of 200 kPa and 500 kPa indicate a decrease in modulus with increasing saturation up to 20 per cent saturation, remaining constant to approximately 40 per cent saturation with

a marked decrease in modulus at 40 and 60 per cent saturation. This trend can be seen in all five materials to varying extents.

High density (VD = 70 %)
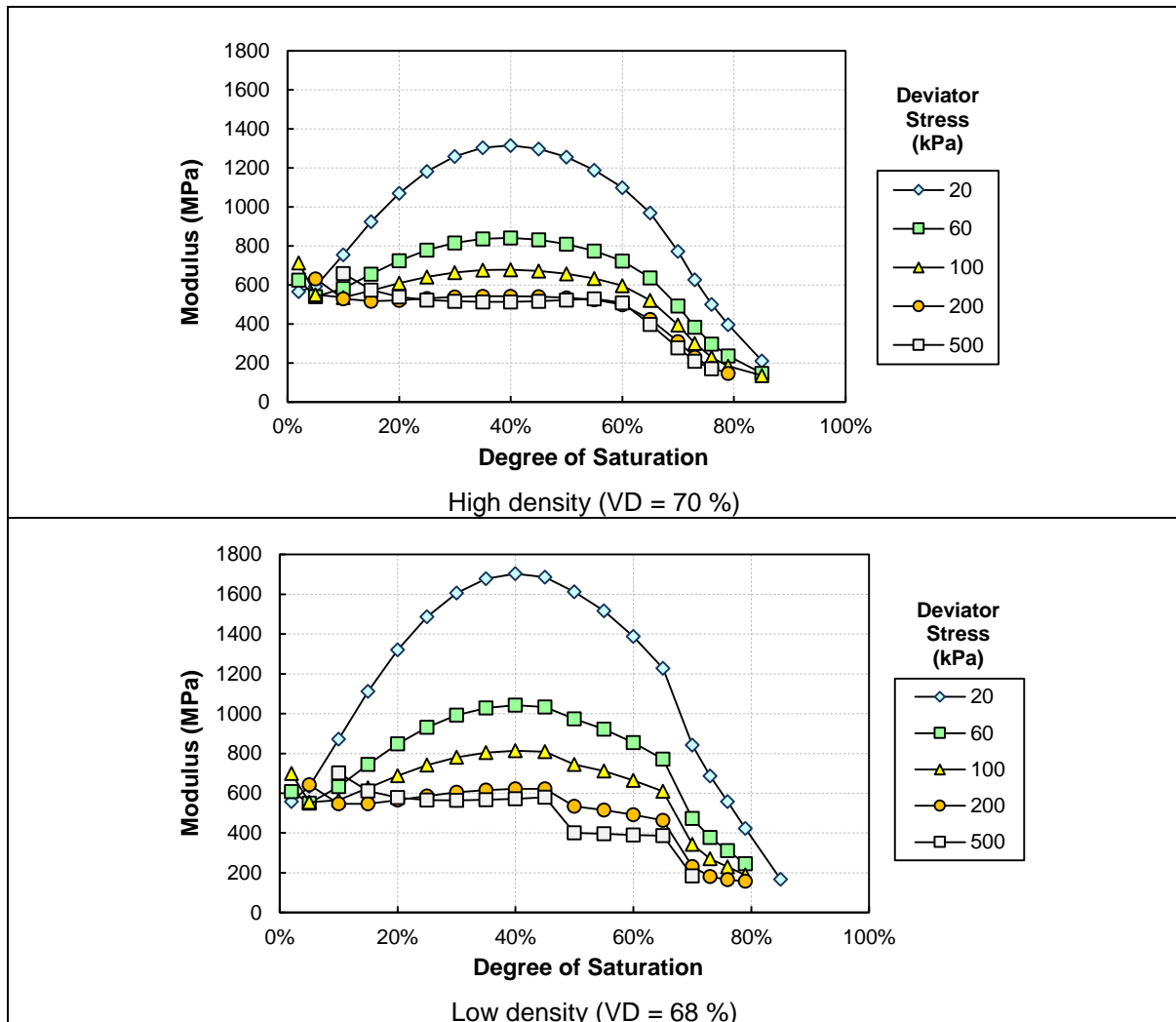
Low density (VD = 68 %)

Figure 4.37: **Parametric plots of saturation at different deviator stress levels for N4 Extension upper selected layer.**

4.3.5.3 Road S191 base layer

The difference between the high and low density was so small, that all 18 samples are evaluated at a single average volumetric density of 79 per cent. The model realistically predicts the stress-dependent behaviour at 30 per cent saturation observed in the data (Figure 4.38). Although this material does not have as high a PI and fines content as material from N4 Extension upper selected layer, it has a very good GM of 2.46. Therefore the high modulus values predicted are not unrealistic for the material.

The modulus values predicted by the parametric plots for saturation at 100 kPa confining pressure appear to be realistic when the strength of the material at 0 kPa confinement is considered. At 0 kPa confinement and 79 per cent density, values of between 2000 and 2500 kPa was measured for saturation levels lower than 20 per cent.
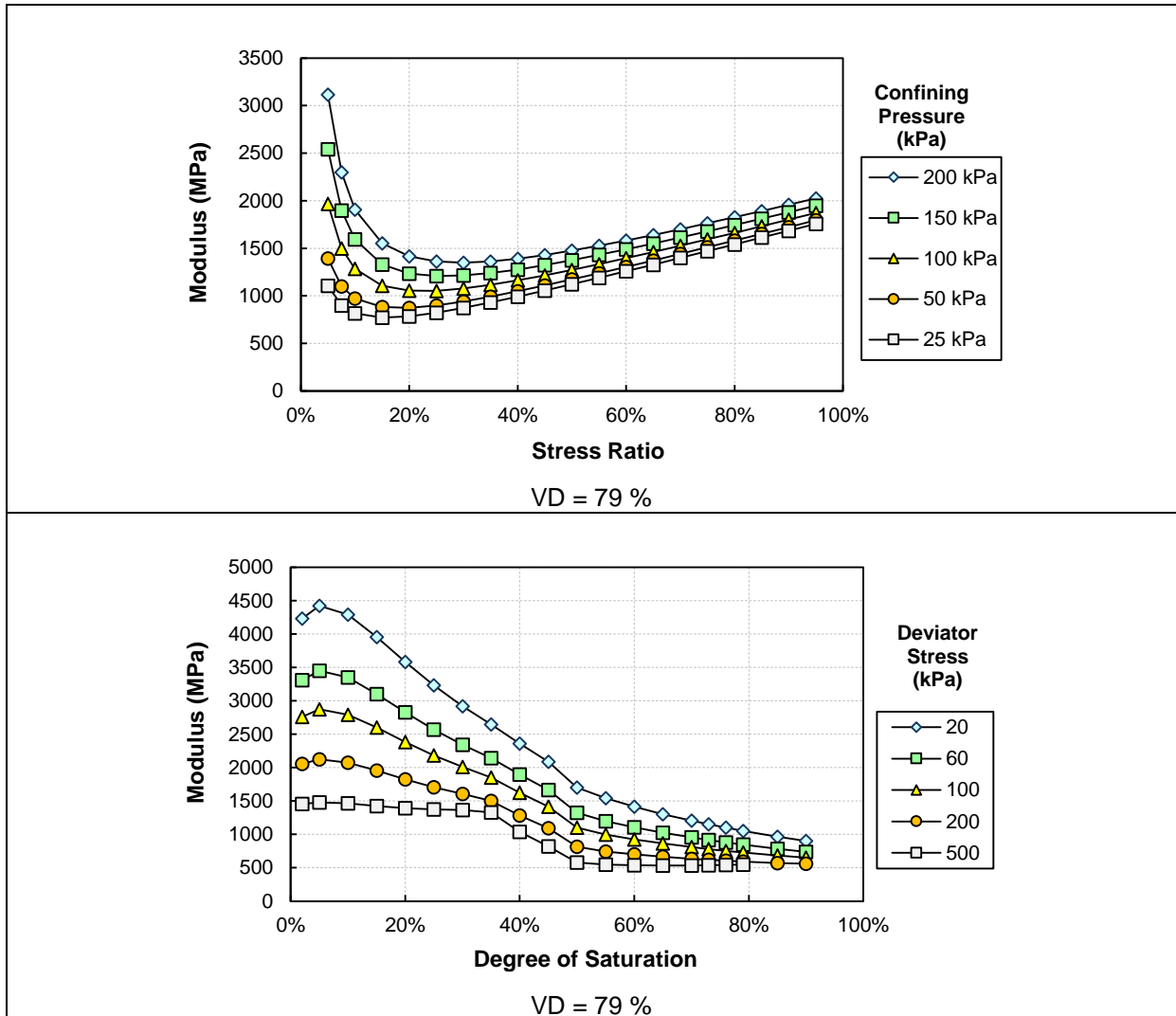
Figure 4.38: **Parametric plots of the saturation and stress-dependent cord modulus model for RoadS191 base layer.**

4.3.5.4 Road P10-2 base layer

The stress-dependent behaviour predicted for the material at 40 per cent saturation at both high and low density levels appear realistic when compared with the trends observed in the data (Figure 4.39). The observed modulus also did not indicate distinct stress-stiffening behaviour as depicted in Figure 4.18.
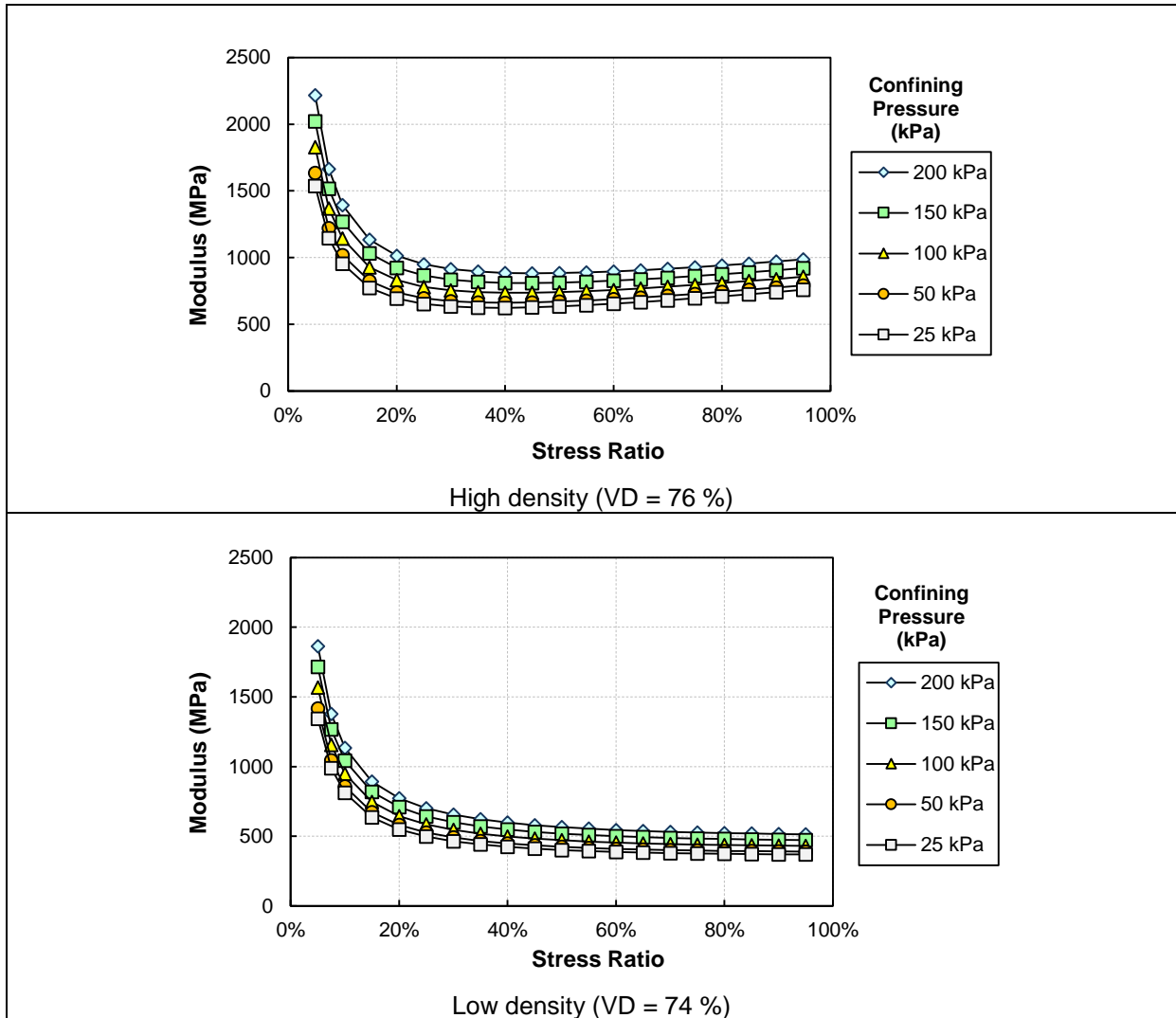
Figure 4.39: **Parametric plots of the stress-dependent behaviour for Road P10-2 base layer.**

The parametric plots for saturation at 25 kPa confining pressure realistically predict the behaviour of the material with increasing degree of saturation (Figure 4.40). The trend of two distinct decreases in modulus at 40 and 60 per cent saturation can be seen in this material as well. Although the model at a high density predict a slight increase in modulus at 500 kPa deviator stress instead of a constant or decreasing modulus, it must be kept in mind that the parametric plots extrapolate from three saturation levels at which tests were conducted to the entire saturation spectrum. The slight increase is not observed when the low density plot is evaluated.
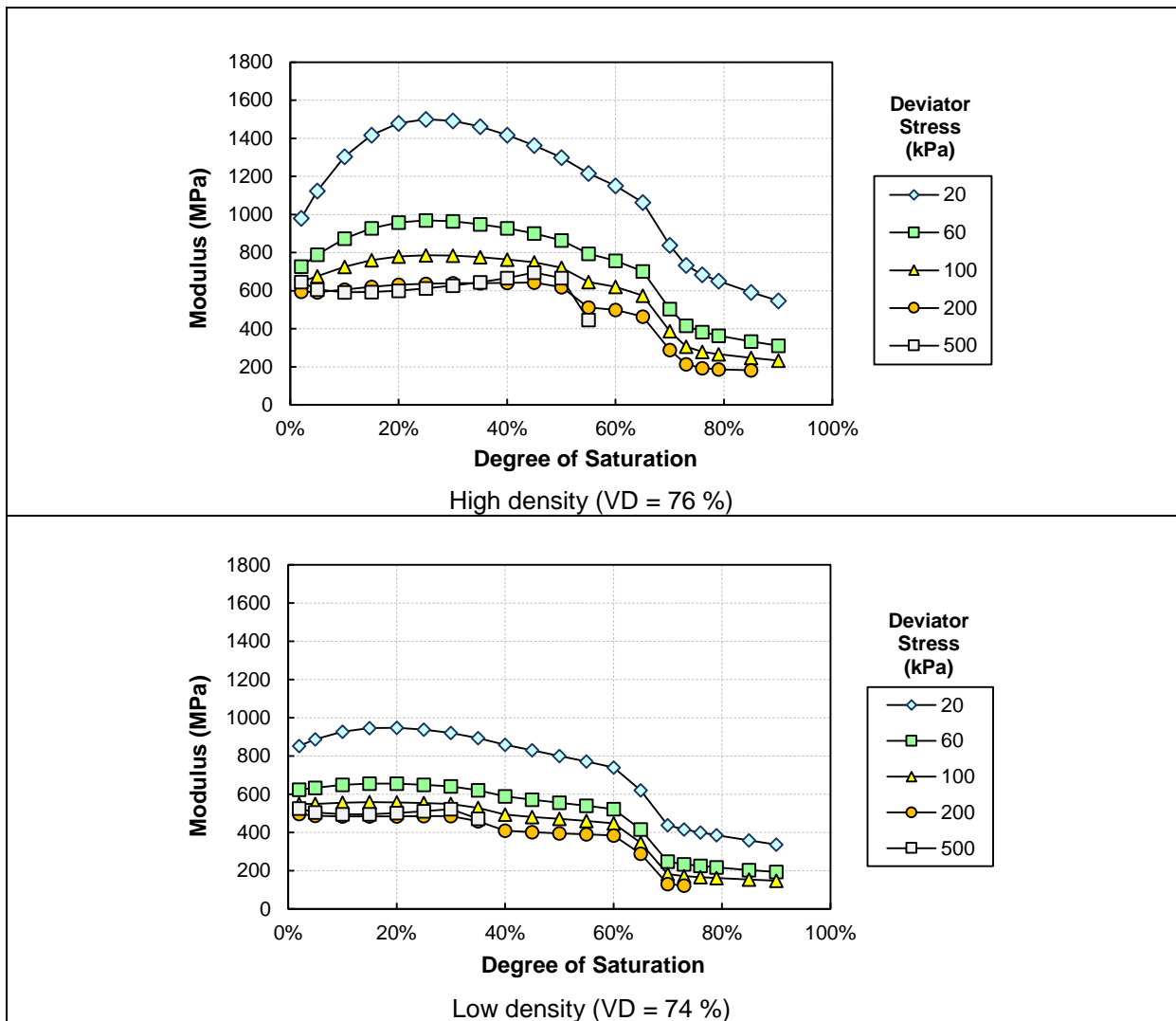
Figure 4.40: **Parametric plots of saturation at different deviator stress levels for Road P10-2 base layer.**

4.3.5.5 *D804 base layer*

Figure 4.41 illustrates the stress-dependent model parametric plots for high and low density at 20 per cent saturation. The parametric plots realistically models the behaviour observed in the data trends. Similar to the modulus behaviour of Road P10-2 base layer material, Road D804 base layer material do not have a distinct stress-stiffening component with increasing stress ratio. Both the aforementioned materials have low GM values of 1.96 and 1.71 respectively.
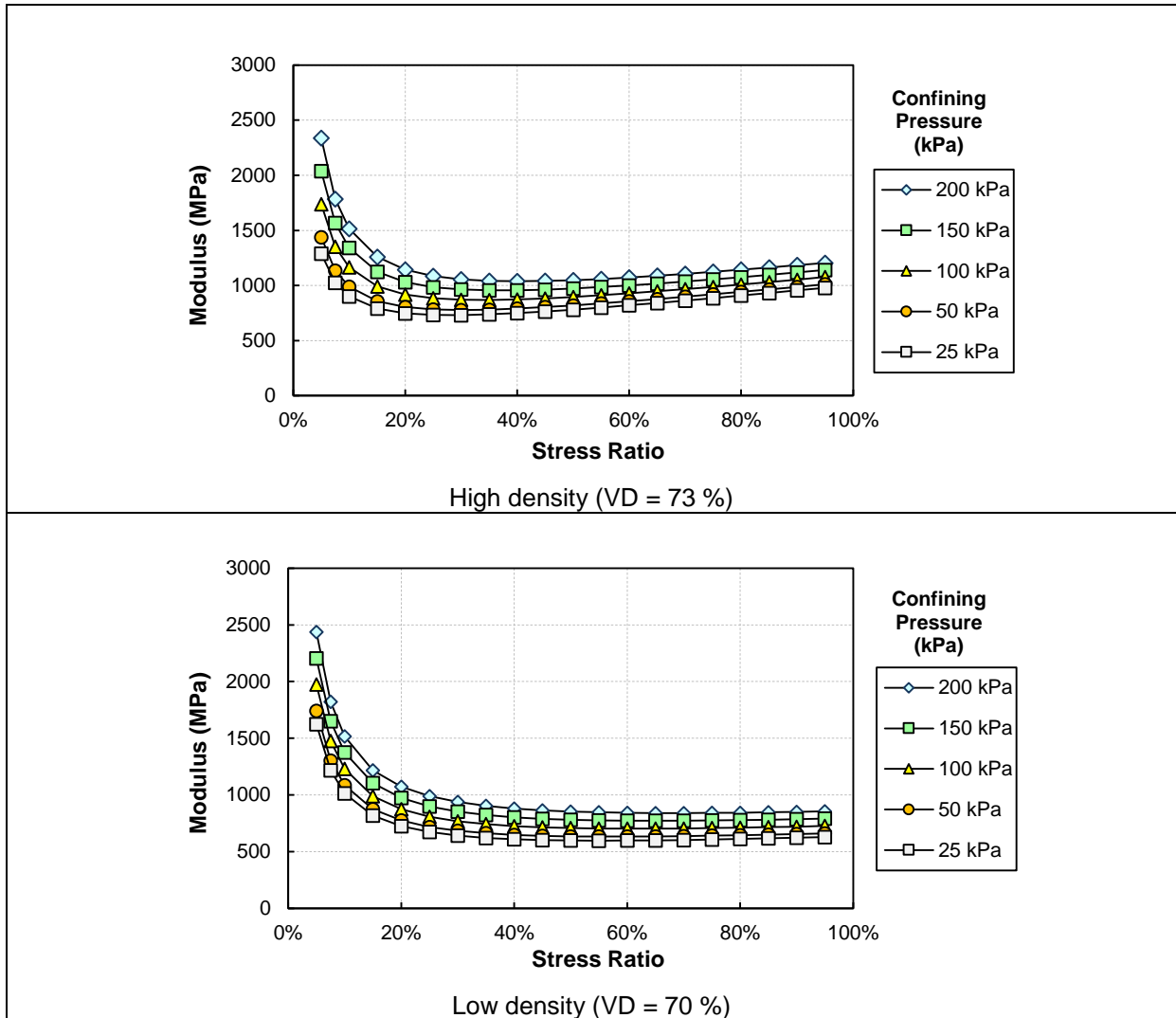
Figure 4.41:   Parametric plots of the stress-dependent behaviour for Road D804 base layer.

As for N4 Extension upper selected layer material, the influence of high fines content and PI can also be seen in the parametric plots for saturation (Figure 4.42). The influence of suction pressure on the material strength can be seen up to 100 kPa deviator stress at 25 kPa confining pressure. This trend of high predicted modulus values was also observed at 0 kPa confinement where values of between 2000 kPa and 1800 kPa were observed.
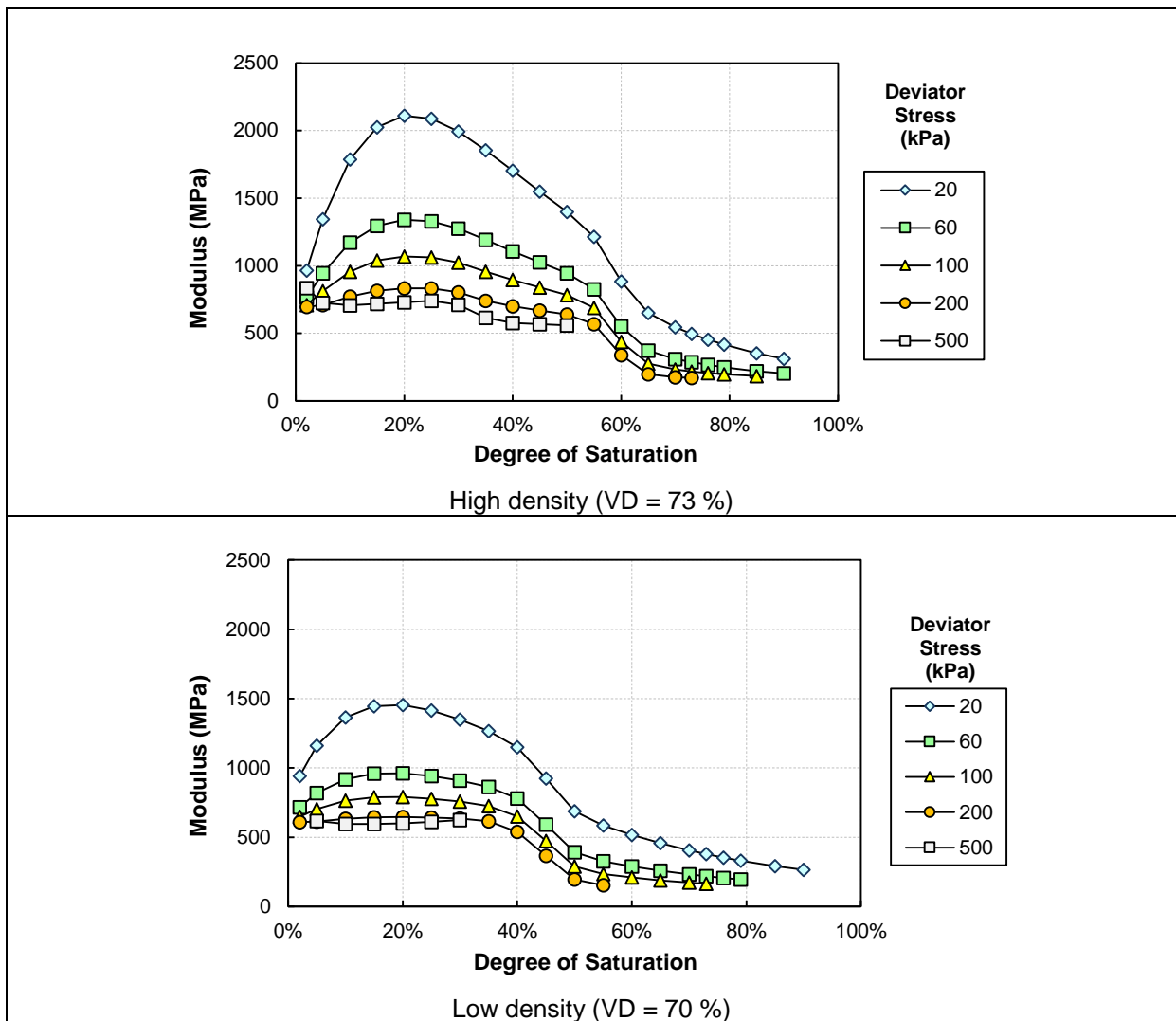
Figure 4.42:   **Parametric plots of saturation at different deviator stress levels for Road D804 base layer.**
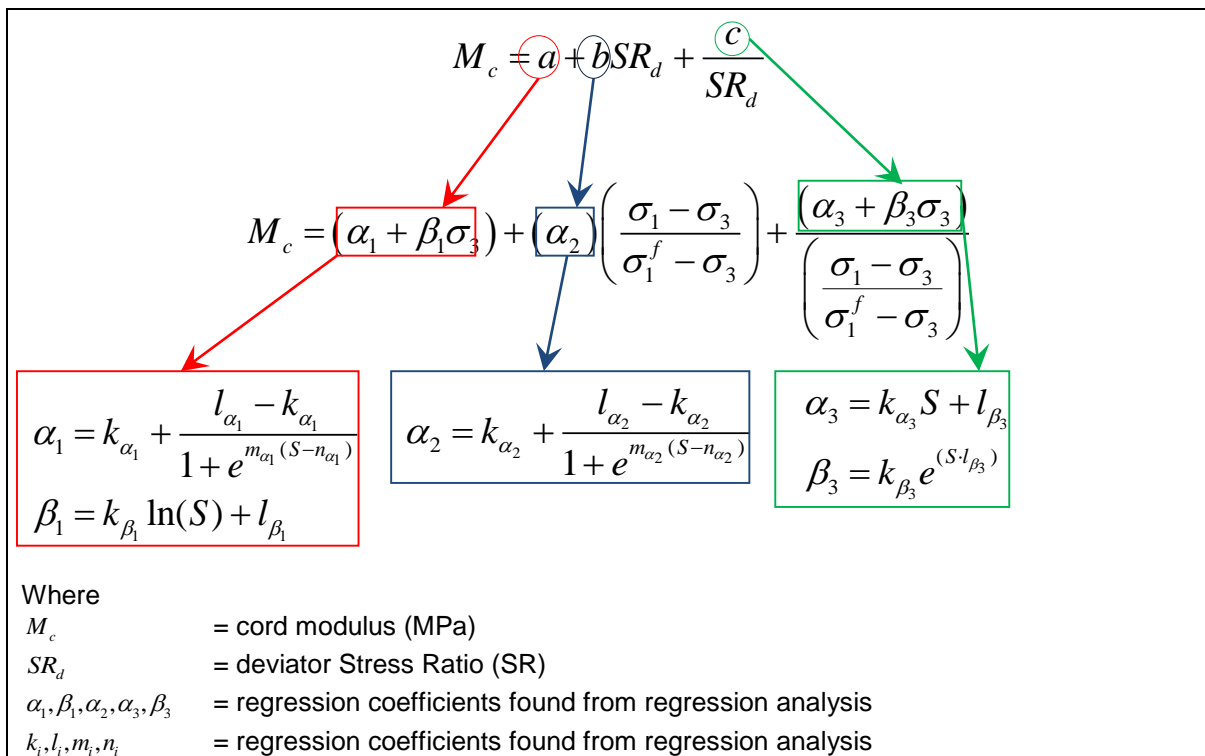
Plots depicting the behaviour of each material at 0 kPa confining pressure are contained in Appendix D.

4.4   CONCLUSIONS

In Section 4.2.1 it was shown that there is inherent variability in the routine test results of fundamental properties which is used to classify a material sample. This variability is carried through in any subsequent tests conducted on a material. Section 4.2.3 indicated how the data from resilient modulus tri-axial tests were processed to eliminate test errors in an attempt to limit more variability incorporated into the test results used to calculate a cord modulus.

A cord modulus model was identified in Section 2.3.3.4 and elaborated on in Section 4.3. The cord modulus calculated for five different unbound granular materials illustrated the complex interaction

4-47

between moisture and stress condition. The effect of density was not as clear as expected, but that may be due to the experimental design which only allowed for two different volumetric density levels. These volumetric density levels only differed between 1 and 3 per cent and it is recommended that future research work allow for a wider range of volumetric density levels to be tested. Section 4.3.1 illustrated the formulation of a simple model that consistently captures the complex stress dependent behaviour of the selection of materials. Sections 4.3.2 to 4.3.4 showed that to model the saturation dependency, multiple model components had to be introduced based on trends that could be observed from the data. A saturation and stress dependent cord modulus model was formulated and calibrated for all five bulk material samples. The model generally has good prediction accuracy. The final model formulation of the saturation and stress dependent cord modulus model is as depicted in Figure 4.43.

$$M_c = a + bSR_d + \frac{c}{SR_d}$$

$$M_c = \left(\alpha_1 + \beta_1\sigma_3\right) + \left(\alpha_2\right)\left(\frac{\sigma_1 - \sigma_3}{\sigma_1^f - \sigma_3}\right) + \frac{\left(\alpha_3 + \beta_3\sigma_3\right)}{\left(\frac{\sigma_1 - \sigma_3}{\sigma_1^f - \sigma_3}\right)}$$

$$\alpha_1 = k_{\alpha_1} + \frac{l_{\alpha_1} - k_{\alpha_1}}{1 + e^{m_{\alpha_1}(S - n_{\alpha_1})}}$$

$$\beta_1 = k_{\beta_1}\ln(S) + l_{\beta_1}$$

$$\alpha_2 = k_{\alpha_2} + \frac{l_{\alpha_2} - k_{\alpha_2}}{1 + e^{m_{\alpha_2}(S - n_{\alpha_2})}}$$

$$\alpha_3 = k_{\alpha_3}S + l_{\beta_3}$$

$$\beta_3 = k_{\beta_3}e^{(S \cdot l_{\beta_3})}$$

Where
M_c = cord modulus (MPa)
SR_d = deviator Stress Ratio (SR)
$\alpha_1, \beta_1, \alpha_2, \alpha_3, \beta_3$ = regression coefficients found from regression analysis
k_i, l_i, m_i, n_i = regression coefficients found from regression analysis

Figure 4.43:   Saturation and stress dependent cord modulus model.

Parametric analysis of the saturation and stress dependent cord modulus model indicated that the material behaviour with increasing stress ratio is reflected realistically for each bulk material sample and that the effect of increasing saturation is also reflected realistically. It is recommended that future studies should conduct testing at more than three levels of saturation, as was the case in this thesis. The parametric plots for saturation were extrapolated from the three levels of saturation tested to the entire saturation spectrum. Although the results appear realistic, more data points could verify the distinct decrease in modulus at 40 and 60 per cent saturation that was observed in the parametric plots.

Section 2.2.5.1 refers to the concept of levels of technology, which was adopted in the MEPDG (NCHRP, 2004). For a Level 1 investigation, resilient modulus tri-axial tests as described in this thesis

on bulk material samples can be conducted and the results used in the pavement design. For Level 2 (where a higher level of uncertainty is still acceptable) the simple saturation and stress dependent cord modulus model can be utilised. It is recommended that a database of resilient modulus tri-axial results of various bulk material samples from all areas of South Africa should be populated and the saturation and stress dependent cord modulus model calibrated for each material in the database. From this database engineers can select sub-variable constants calibrated on material similar to material on site and by utilising the model, modulus values can be calculated. This concept compares well with the MEPDG (NCHRP, 2004) and SAPDM (Theyse, 2006) objectives of utilising databases with material results for pavement design.

4.5   REFERENCES

Jacobsz, S.W. and Day, P. (2008). '*Are we getting what we pay for from geotechnical laboratories*', SAICE Civil Engineering Magazine, Volume 16, Number 4, April, pp. 8-11, South African Institute for Civil Engineering (SAICE), Johannesburg, RSA.

National Cooperative Highway Research Program (NCHRP) (2004). '*Project 1-37A: Guide for Mechanistic-Empirical Design of New and Rehabilitated Pavement Structures*', National Cooperative Highway Research Program, Transportation Research Board, of the National Research Council, USA

TG 2, Appendix A (2009). '*Technical Guideline: Bitumen Stabilised Materials*', Second Edition, May 2009, Asphalt Academy, Pretoria, RSA.

Theyse, H.L (2006). '*An improved pavement design method for Southern Africa: Research and development framework*', Report No. CSIR/BE/IE/IR/2006/0042/B, Pretoria, CSIR Built Environment Unit, RSA.

Theyse, H.L. (2008). '*A mechanistic-empirical design model for unbound granular pavement layers*', PhD dissertation, University of Johannesburg, Johannesburg, RSA.

Theyse, H L. (2009). '*Resilient modulus models for partially saturated unbound granular material*'. Pavement Modelling Corporation, Pretoria, South Africa. (Report Number: SANRAL/SAPDM/B1A-2009-01).

Theyse, H.L. (2012). '*Stress-dependent Resilient Response Model Formulation for Unbound Granular Material based on Repeated Load Tri-axial Test Results*', Pavement Modelling Corporation, Pretoria, RSA. (Report Number: SANRAL/SAPDM/B1A-2012-01)

Van Aswegen, E and Theyse, H L. (2011). '*Resilient response testing – Unbound material*'. Ndodana Consulting Engineers and Pavement Modelling Corporation, Pretoria, South Africa. (Report Number: SANRAL/SAPDM/B1A-2011-04).

5 THE CORD MODULUS MODEL FOR CRUSHED AND NATURAL UNBOUND MATERIAL

To link to the Level 2 input discussed in Chapter 4, where the saturation and stress dependent cord modulus model is utilised and calibrated per bulk material sample, Chapter 5 considers Level 3 input into a design method. This will be achieved by calibrating a single model for crushed unbound material and a single model for natural unbound material. One step further will be linking basic material properties to the saturation and stress dependent cord modulus models for crushed and natural material. A similar approach was discussed in Section 2.2.6.4 where George (2004) reported on a LTPP-FHWA study program where the relationship between the resilient modulus and physical properties of unbound sub-grade materials were investigated.

5.1 DISTINCTION BETWEEN CRUSHED AND NATURAL UNBOUND MATERIAL

When the bulk samples in this thesis is considered, the N4 Extension base layer and Road S191 base layer appears to consist of a crushed unbound material. Figure 5.1 depicts the bulk samples during sampling in which the crushed material can be seen. Grading analysis indicated that the Grading Modulus (GM) of the two bulk samples is 2.60 and 2.50 respectively. No crushed material was visible in the remainder of the bulk material samples. This is also reflected in lower GM values ranging between 1.70 and 1.96.

| N4 Extension base layer in test pit | Road S191 base layer in test pit |

Figure 5.1: Bulk samples of base layer material from N4 Extension and Road S191.

When the variables calibrated in Section 4.3.4 for each bulk material sample is compared with saturation level, it appears as if the crushed material and natural material group together. This is illustrated by the lines in Figure 5.2 which indicates the possible groupings. However, such a grouping could not be clearly identified for variable 'β_3'.
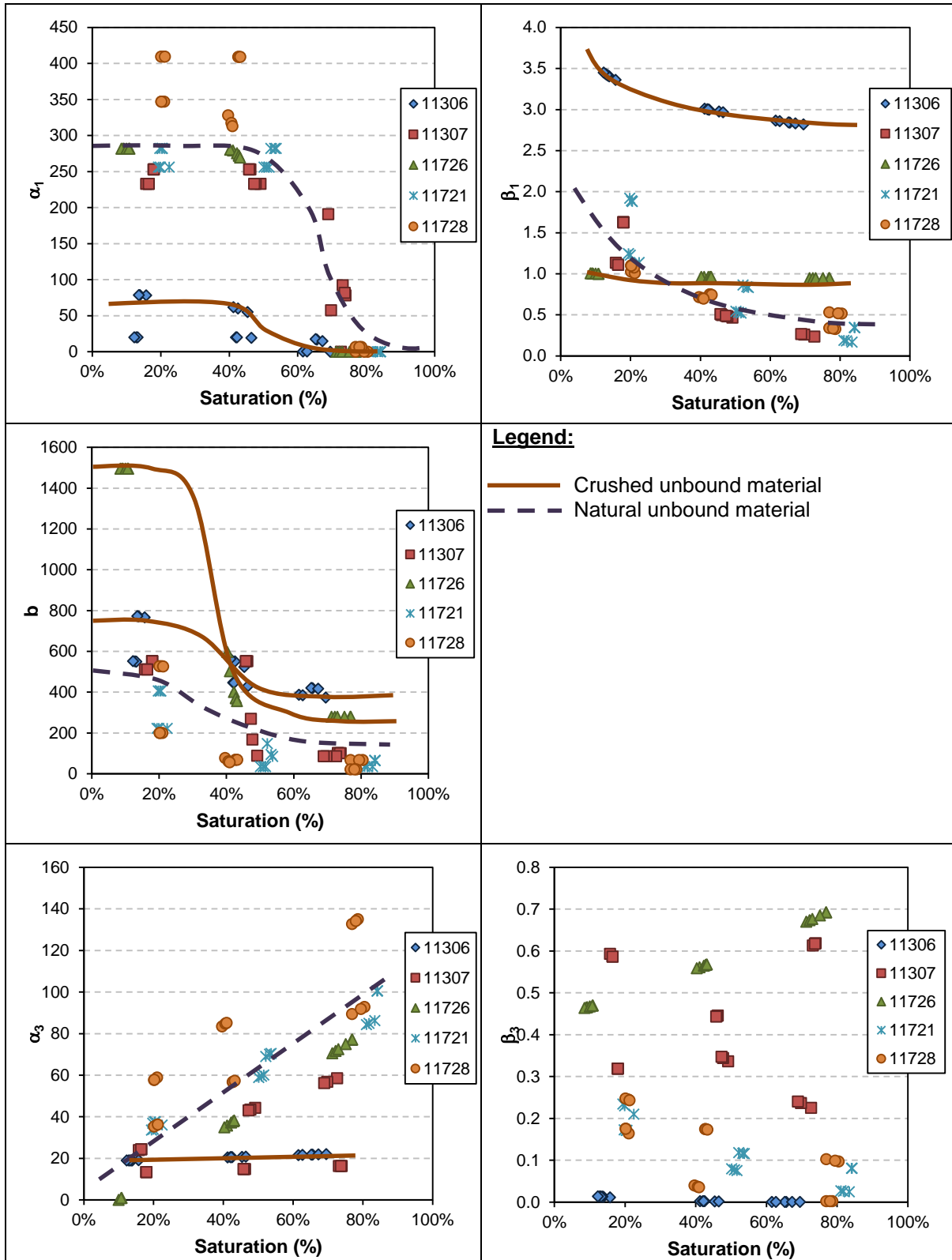
Figure 5.2:   Relationship between saturation and stress-dependent cord modulus model variables.

Considering the differences in physical appearance during sampling and the difference in GM, it appears as the saturation and stress dependent cord modulus can be divided into two groups consisting

of crushed material and natural material. Therefore the bulk material sample results were split into two groups and calibration of the variables repeated for each group.

5.2 CALIBRATION OF CORD MODULUS MODEL VARIABLES FOR CRUSHED AND NATURAL UNBOUND MATERIAL

The bulk material sample results were divided into two groups based on the appearance during sampling and the difference in GM of the samples. The crushed unbound material group consisted of N4 Extension base layer and Road S191 base layer material. Further to Section 2.2.1.4, where the difference between crushed and natural unbound material was explored, the Standard Specifications for Road and Bridge Works for State Road Authorities (COLTO, 1998), specifies grading envelopes for G1 to G4 material. When these envelopes are used to calculate the GM envelopes for G1 to G4 material, GM values between 2.70 and 2.05 are calculated. The natural unbound material group consisted of N4 Extension upper selected, Road P10-2 base and Road D804 base layer material. COLTO (1998) provide broad envelope values for GM for natural unbound materials (G5 to G9). Although the two material groups only consists of two and three bulk material samples respectively, the basic material properties as defined and listed in Section 2.2.1.3, indicate that the materials comprising the two groups are not similar and still includes a range of variability. The basic material properties for each of the bulk material samples are repeated in Table 5.1.

Table 5.1: Summary of routine test results.

| Group | Material type | Source (Layer) | GM | Grading | | Atterberg limits | | | | Mod AASHTO | | Class TRH14 |
				% Passing 0,425 mm	% Passing 0,075 mm	LL (%)	PL (%)	PI (%)	LS (%)	MDD_{mod} (kg/m³)	OMC_{mod} (kg/m³)	
Crushed material	Norite	N4 Ext B	2.60	14.0	5.2	*-	*-	*NP	*-	2 465	4.6	G1
	Dolerite	S191 B	2.50	17.0	10.8	30.6	22.5	8.1	5.1	2 343	6.9	G6
Natural material	Shale	P10-2 B	1.96	32.5	25.1	26.5	18.8	7.7	5.2	2 133	8.3	G8
	Calcrete	D804 B	1.70	44.4	29.2	28.1	18.4	9.6	6.6	2 037	9.4	G7
	Chert	N4 Ext USEL	1.90	37.5	28.3	31.8	19.6	12.3	5.6	2 063	10.6	G5

Note *:

Material classified as Non-Plastic (NP) and other results not reported by laboratory

5.2.1 Model calibration for crushed unbound material

The model appears to have relatively good prediction accuracy for crushed unbound material considering that two different materials are now combined. This is indicated by the statistical parameters listed in Table 5.2 for the high (HD) and low volumetric density (LD) samples. Negative R^2 values indicate that non-linear trends were fitted to the data (Cameron and Windmeijer, 1997). The error values observed are acceptable when variability inherent in materials is considered.

Table 5.2: **Statistical data for high and low volumetric density samples of crushed unbound material.**

Crushed material	R^2 (ratio)	RMSE (%)	SEE (MPa)	% Error
HD	-0.26	0.41%	187.16	24.7%
LD	-1.57	0.43%	204.32	30.4%

However, some of the individual test results appear to not predict the material behaviour as accurately. Table 5.3 lists the statistical parameters for individual test results. The sample numbers highlighted in yellow, indicate the individual test results that were identified in Section 4.3.4 to have a poorer fit than the rest of the individual samples. The values highlighted in pink indicate samples yielding a negative R^2 value or high SEE or high error results. From the highlighted values it appears that the calibrated values generally fit the material from N4 Extension base layer worse than for Road S191 base layer material. This may be due to the inherent difference between the two materials as illustrated in Table 5.1, where, for example, material from Road S191 base layer has a PI and N4 Extension base layer is classified as non-plastic.

Table 5.3: **Statistical data for crushed unbound material samples.**

Sample no.	VD (ratio)		S (ratio)	R^2 (ratio)	SEE (MPa)	% Error
11306-19	HD	0.82	0.14	0.69	161.0	21.0%
11306-20	HD	0.83	0.16	0.79	126.8	14.6%
11306-21	HD	0.82	0.14	-0.28	286.6	42.1%
11306-22	HD	0.82	0.43	-0.91	299.8	41.9%
11306-23	HD	0.83	0.45	-1.28	324.4	45.9%
11306-24	HD	0.82	0.41	-0.16	249.3	29.0%
11306-25	HD	0.82	0.66	-0.81	380.7	51.8%
11306-26	HD	0.82	0.65	-2.62	324.7	57.9%
11306-27	HD	0.82	0.67	-7.03	579.5	70.2%
11306-28	LD	0.80	0.13	-14.52	714.9	121.7%
11306-29	LD	0.81	0.13	-13.58	668.6	112.7%
11306-30	LD	0.80	0.12			
11306-31	LD	0.79	0.42	-2.20	328.5	57.1%
11306-32	LD	0.80	0.42	0.48	178.7	24.3%
11306-33	LD	0.80	0.46	-0.51	280.0	33.5%
11306-34	LD	0.80	0.69	-0.31	281.3	33.0%
11306-35	LD	0.79	0.62	-0.21	242.8	34.0%
11306-36	LD	0.79	0.63	-1.56	268.0	34.8%
11726-19	HD	0.80	0.09	0.87	109.6	8.2%
11726-20	HD	0.80	0.09	0.97	51.3	5.0%
11726-21	HD	0.80	0.09	0.98	46.2	3.8%
11726-22	HD	0.80	0.43	0.76	59.0	6.4%
11726-23	HD	0.80	0.41	0.96	32.3	3.4%
11726-24	HD	0.80	0.40	0.04	182.3	17.4%
11726-25	HD	0.80	0.71	0.81	72.4	11.4%
11726-26	HD	0.80	0.72	0.66	62.4	11.7%

Sample no.	VD (ratio)		S (ratio)	R² (ratio)	SEE (MPa)	% Error
11726-27	HD	0.80	0.73	0.97	20.5	3.7%
11726-28	LD	0.79	0.10	0.98	35.6	2.7%
11726-29	LD	0.79	0.11	0.98	38.6	3.0%
11726-30	LD	0.79	0.11	0.98	39.5	2.9%
11726-31	LD	0.79	0.42			
11726-32	LD	0.79	0.43	0.90	50.3	4.7%
11726-33	LD	0.79	0.43	0.96	32.0	3.6%
11726-34	LD	0.79	0.77	0.99	14.7	2.3%
11726-35	LD	0.79	0.77	0.94	32.6	4.8%
11726-36	LD	0.79	0.75	0.61	63.1	11.2%

Figure 5.3 and Figure 5.4 depicts the relationship between predicted and observed modulus values of which the statistical parameters is provided in Table 5.3.
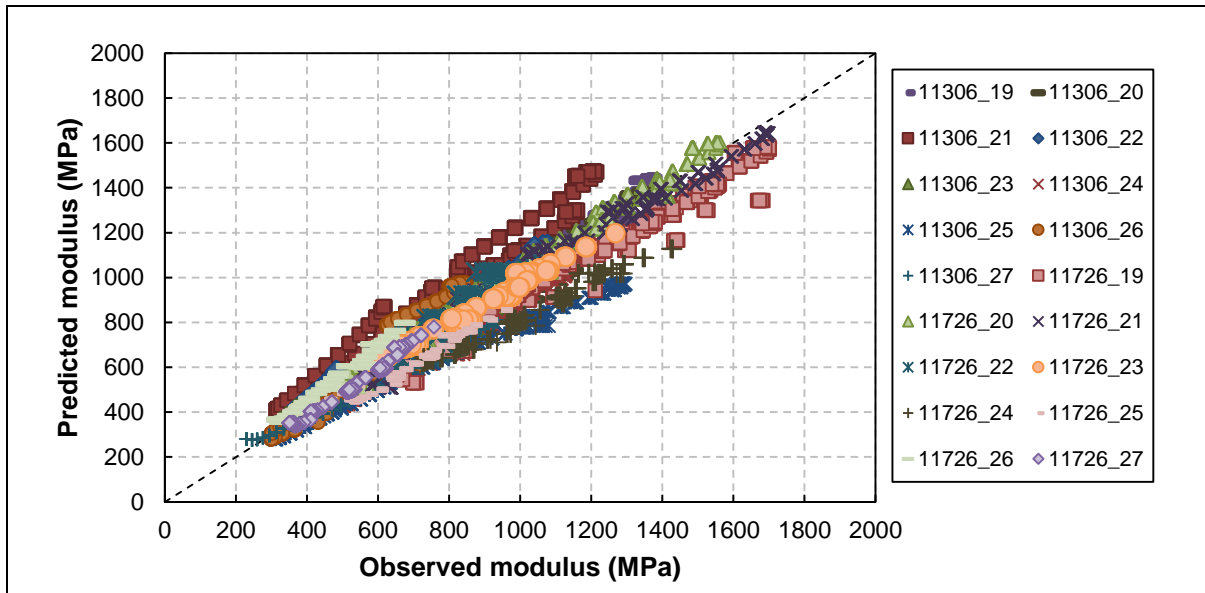
Figure 5.3: **Prediction accuracy for high volumetric density samples for crushed unbound material.**
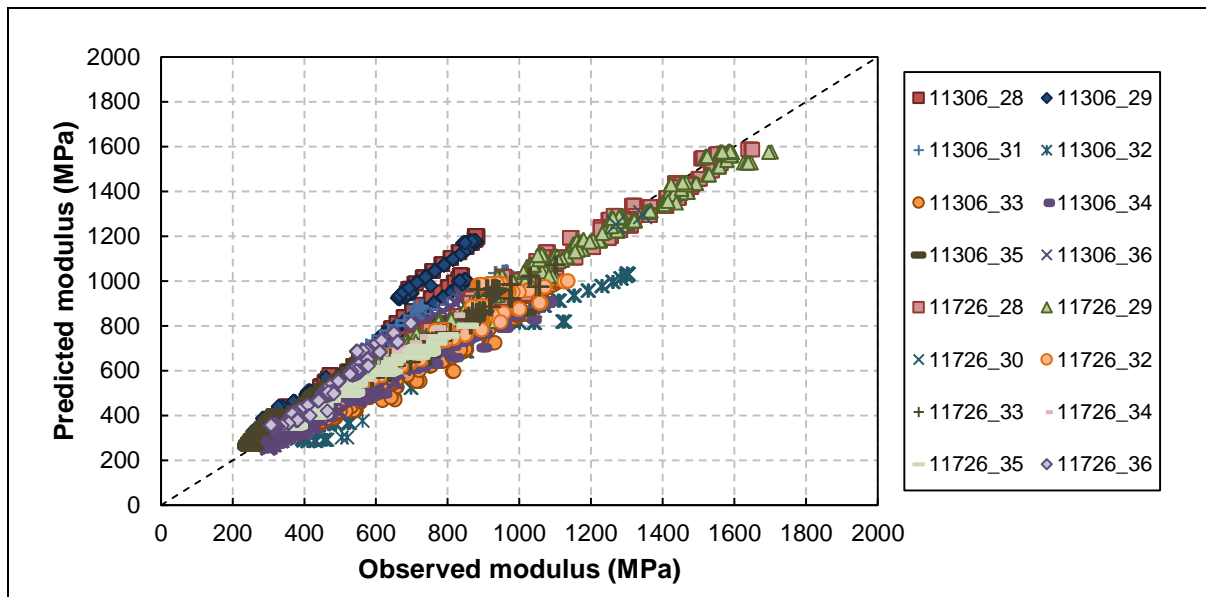
Figure 5.4:   **Prediction accuracy for low volumetric density samples for crushed unbound material.**

When the average of the model variables calibrated for HD and LD are calculated and used in the saturation and stress dependent cord modulus model, the model retains relatively good prediction accuracy as indicated by the statistical parameters listed in Table 5.4. This was done, since the HD and LD were arbitrarily determined for this study and it does not constitute universally accepted high or low density values. The statistical parameters per individual sample did not improve or worsen significantly and is therefore not listed again. Table 5.5 contains the model variables proposed when the model is applied to crushed unbound materials.

Table 5.4:   **Statistical data for all samples of crushed unbound material.**

Crushed material	R^2 (ratio)	RMSE (%)	SEE (MPa)	% Error
	-1.46	0.48%	241.03	32.07%

Table 5.5:   **Model variables for crushed unbound material.**

	k	l	m	n
α_1	0.00	285.95	102.00	0.65
β_1	-0.33	1.13		
b or α_2	247.96	1473.60	44.28	0.26
α_3	118.30	-7.21		
β_3	0.31	0.72		

5.2.2 Model calibration for natural unbound material

The model appears to have relatively good prediction accuracy for natural unbound material considering that three different materials are now combined. This is indicated by the statistical parameters listed in Table 5.6 for the high (HD) and low volumetric density (LD) samples. Negative R^2 values indicate that non-linear trends were fitted to the data (Cameron and Windmeijer, 1997). The error values observed are excellent when variability inherent in materials is considered.

Table 5.6: Statistical data for high and low volumetric density samples of natural unbound material.

Natural material	R^2 (ratio)	RMSE (%)	SEE (MPa)	% Error
HD	0.62	0.42%	56.42	7.78%
LD	-0.09	0.67%	90.31	12.89%

However, some of the individual test results appear to not predict the material behaviour as accurately. Table 5.8 list the statistical parameters for individual test results. The sample numbers highlighted in yellow, indicate the individual test results that were identified in Section 4.3.4 to have a poorer fit than the rest of the individual samples. The values highlighted in pink indicate samples yielding a negative R^2 value or high SEE or high error results. Unlike for the crushed unbound material, the calibrated values generally fit all three of the materials equally well. The same individual samples that were identified in Section 4.3.4 to have a worse fit generally also yielded higher SEE and error results. When all the highlighted individual samples are removed from the data set, the statistical data for high and low volumetric density samples improve, especially for the low density samples (Table 5.7).

Table 5.7: Statistical data for revised set of high and low volumetric density samples of natural unbound material.

Natural material	R^2 (ratio)	RMSE (%)	SEE (MPa)	% Error
HD	0.71	0.39%	48.22	7.18%
LD	0.51	0.47%	61.45	9.58%

Table 5.8: Statistical data for natural unbound material samples.

Sample no.	VD (ratio)		S (ratio)	R^2 (ratio)	SEE (MPa)	% Error
11307-19	HD	0.70	0.18	0.95	41.7	4.9%
11307-20	HD	0.70	0.18	0.74	81.4	10.2%
11307-21	HD	0.70	0.18	0.97	31.2	3.0%
11307-22	HD	0.70	0.46	0.05	142.8	14.9%
11307-23	HD	0.70	0.46	0.58	79.3	10.0%
11307-24	HD	0.70	0.46	0.25	125.1	14.3%
11307-25	HD	0.69	0.74	0.64	27.5	8.7%
11307-26	HD	0.69	0.73	0.43	51.3	14.1%
11307-27	HD	0.69	0.74	0.75	25.2	9.5%
11307-28	LD	0.68	0.16	0.13	253.7	22.9%

Sample no.	VD (ratio)		S (ratio)	R² (ratio)	SEE (MPa)	% Error
11307-29	LD	0.69	0.16	0.85	105.0	8.5%
11307-30	LD	0.69	0.16	0.24	174.0	24.2%
11307-31	LD	0.68	0.49			
11307-32	LD	0.68	0.48	0.03	104.9	13.6%
11307-33	LD	0.69	0.47	0.69	49.2	6.5%
11307-34	LD	0.68	0.73			
11307-35	LD	0.68	0.70	0.75	20.3	6.0%
11307-36	LD	0.68	0.69	-7.16	176.4	37.3%
11721-19	HD	0.76	0.20	0.83	67.6	7.8%
11721-20	HD	0.76	0.20	0.86	55.6	5.3%
11721-21	HD	0.76	0.20	0.93	40.1	3.2%
11721-22	HD	0.76	0.54	0.89	26.0	4.3%
11721-23	HD	0.76	0.52	0.84	31.8	3.9%
11721-24	HD	0.76	0.53	0.81	33.0	4.4%
11721-25	HD	0.76	0.84	0.78	28.0	6.5%
11721-26	HD	0.76	0.84	0.65	22.8	7.1%
11721-27	HD	0.76	0.84			
11721-28	LD	0.73	0.19	0.15	86.8	13.2%
11721-29	LD	0.73	0.20	0.73	64.2	9.4%
11721-30	LD	0.73	0.22	0.23	155.8	15.6%
11721-31	LD	0.74	0.51	0.34	43.0	7.9%
11721-32	LD	0.73	0.52	-0.84	128.5	20.7%
11721-33	LD	0.74	0.50	0.02	57.0	12.6%
11721-34	LD	0.74	0.81			
11721-35	LD	0.74	0.82			
11721-36	LD	0.73	0.83			
11728-19	HD	0.73	0.21			
11728-20	HD	0.73	0.20	0.64	74.0	7.4%
11728-21	HD	0.73	0.21	-1.56	227.6	21.8%
11728-22	HD	0.73	0.43	0.25	56.2	6.3%
11728-23	HD	0.73	0.43	0.78	40.8	4.3%
11728-24	HD	0.73	0.43	0.76	42.4	3.9%
11728-25	HD	0.72	0.77	0.80	23.7	7.7%
11728-26	HD	0.73	0.80	0.89	20.2	6.1%
11728-27	HD	0.73	0.79	0.93	15.5	4.8%
11728-28	LD	0.70	0.21	0.52	68.6	7.5%
11728-29	LD	0.70	0.20	0.54	87.6	10.1%
11728-30	LD	0.70	0.20	0.94	29.7	3.6%
11728-31	LD	0.70	0.40	-0.38	85.8	9.4%
11728-32	LD	0.70	0.41	0.35	59.4	7.4%
11728-33	LD	0.70	0.41	-1.23	76.4	11.7%
11728-34	LD	0.71	0.79			
11728-35	LD	0.71	0.77	0.48	49.0	14.1%
11728-36	LD	0.71	0.78	0.80	21.1	8.6%

Figure 5.6 and Figure 5.6 depicts the relationship between predicted and observed modulus values of which the statistical parameters is provided in Table 5.8. The accuracy depicted in Figure 5.6 does not appear to be as good, but when the SEE and error is considered, it appears acceptable.
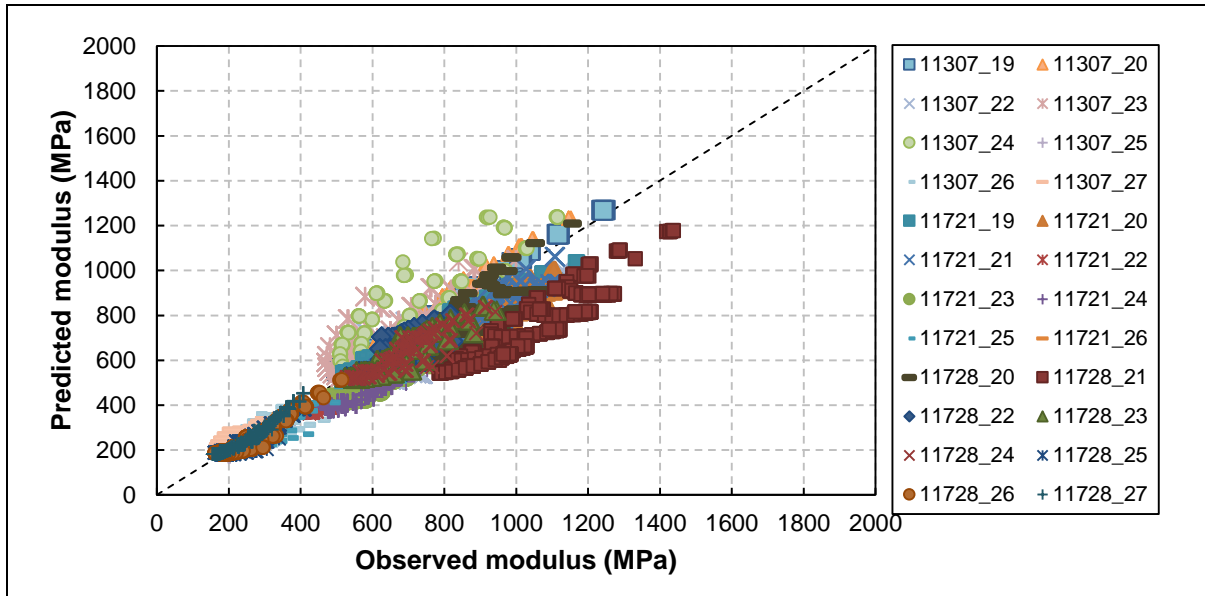
Figure 5.5: Prediction accuracy for high volumetric density samples for natural unbound material.
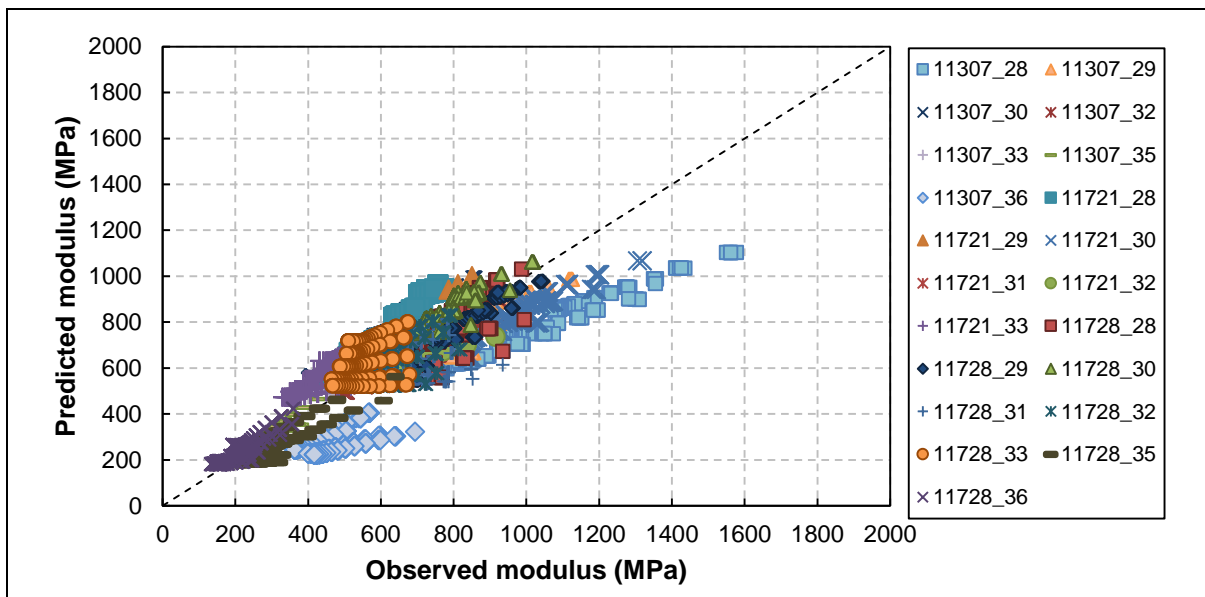
Figure 5.6: Prediction accuracy for low volumetric density samples for natural unbound material.

When the average of the model variables calibrated for HD and LD are calculated and used in the saturation and stress dependent cord modulus model, the model retains relatively good prediction accuracy as indicated by the statistical parameters listed in Table 5.9. This was done, since the HD and LD were arbitrarily determined for this study and it does not constitute universally accepted high or low density values. The statistical parameters per individual sample did not improve or worsen significantly

and is therefore not listed again. Table 5.10 contains the model variables proposed when the model is applied to natural unbound materials.

Table 5.9: **Statistical data for all samples of natural unbound material.**

Natural material	R^2 (ratio)	RMSE (%)	SEE (MPa)	% Error
	-0.21	0.67%	91.09	13.05%

Table 5.10: **Model variables for natural unbound material.**

	k	l	m	n
α_1	27.70	386.47	44.69	0.54
β_1	-0.82	-0.07		
b or α_2	79.28	516.15	12.70	0.14
α_3	90.62	-8.84		
β_3	0.38	-0.09		

5.3   PARAMETRIC ANALYSIS OF CALIBRATED CRUSHED AND NATURAL UNBOUND MATERIAL CORD MODULUS MODELS

The two calibrated models were further assessed by investigating parametric plots of the models. The stress dependency of the model reflects the trends observed in the data. In terms of the parametric plot for saturation, the model realistically reflects trends observed in the data as it extrapolates from the three levels of saturation at which tests were conducted in this thesis.

5.3.1   Crushed unbound material

The stress dependent behaviour of the material is realistically reflected in the parametric plots even when the two materials are combined. The parametric plots for saturation appear distorted. Stress and saturation parametric plots are depicted in Figure 5.7. The apparent distortion from parametric plots for the individual materials might be explained when the Atterberg Limits of the two materials is considered. Road S191 base layer material has a high fines content and PI whereas the N4 Extension base layer material has low fines content and was classified as non-plastic. The influence of fines content and PI is distinguishable at low deviator stress levels and saturation levels below 20 per cent, where suction pressure appears to provide material strength. For deviator stress levels higher than 100 kPa and saturation levels between 20 and 60 per cent, the modulus decrease and or remain constant, where after it decrease for saturation levels higher than 60 per cent.
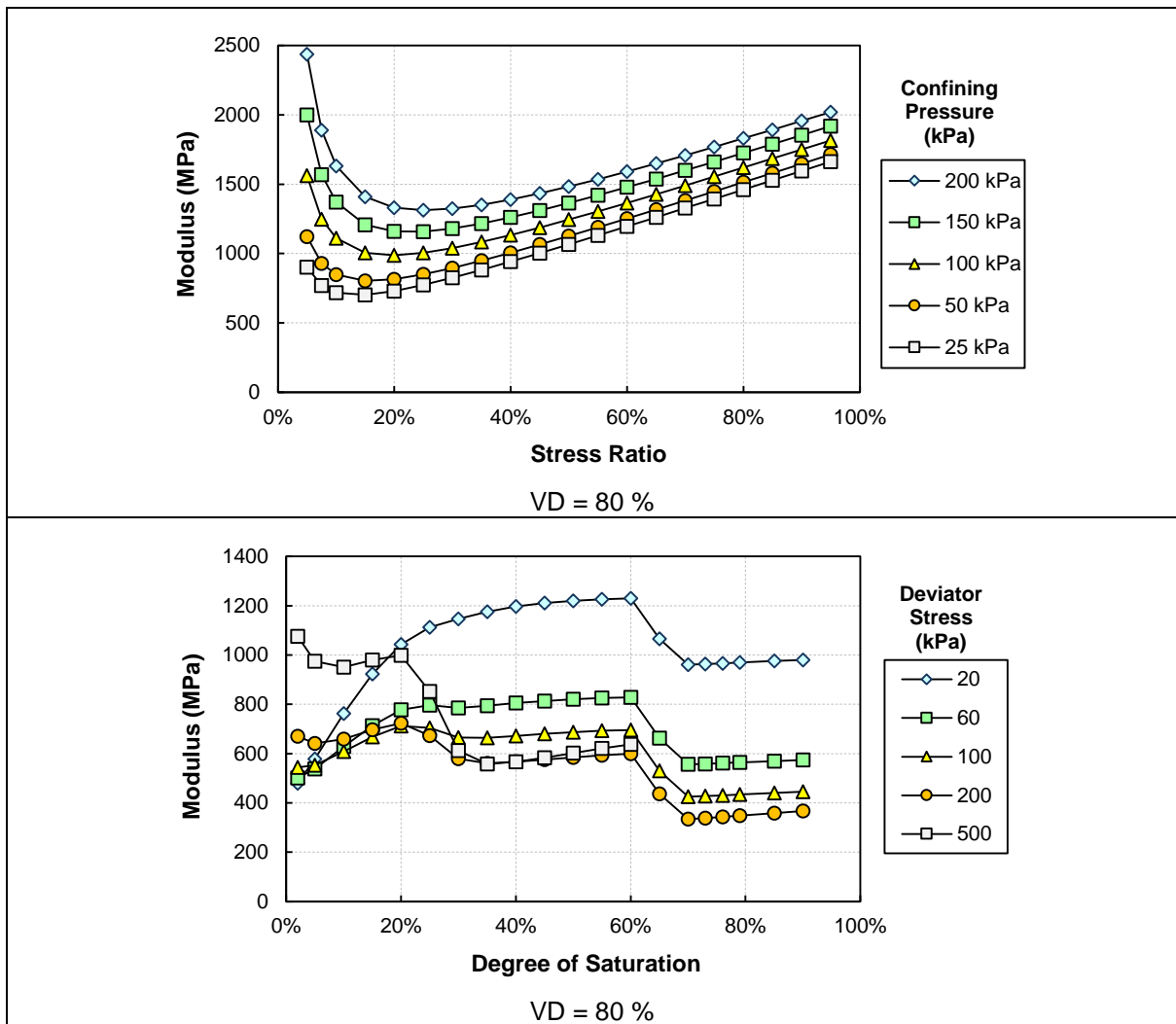
Figure 5.7:   **Parametric plots for crushed unbound material depicting stress dependent behaviour and behaviour in terms of level of saturation.**

5.3.2   Natural unbound material

The stress dependent behaviour of the material is realistically reflected in the parametric plots even with the combination of three materials. The parametric plots for saturation appear consistent with plots of the individual materials. Stress and saturation parametric plots are depicted in Figure 5.8. The influence of high fines contents and PI is clear at low deviator stress levels (up to 100 kPa), where suction pressure appears to provide material strength. At deviator stress levels above 100 kPa the influence of suction pressure is overshadowed by the influence of confinement and the level of saturation.
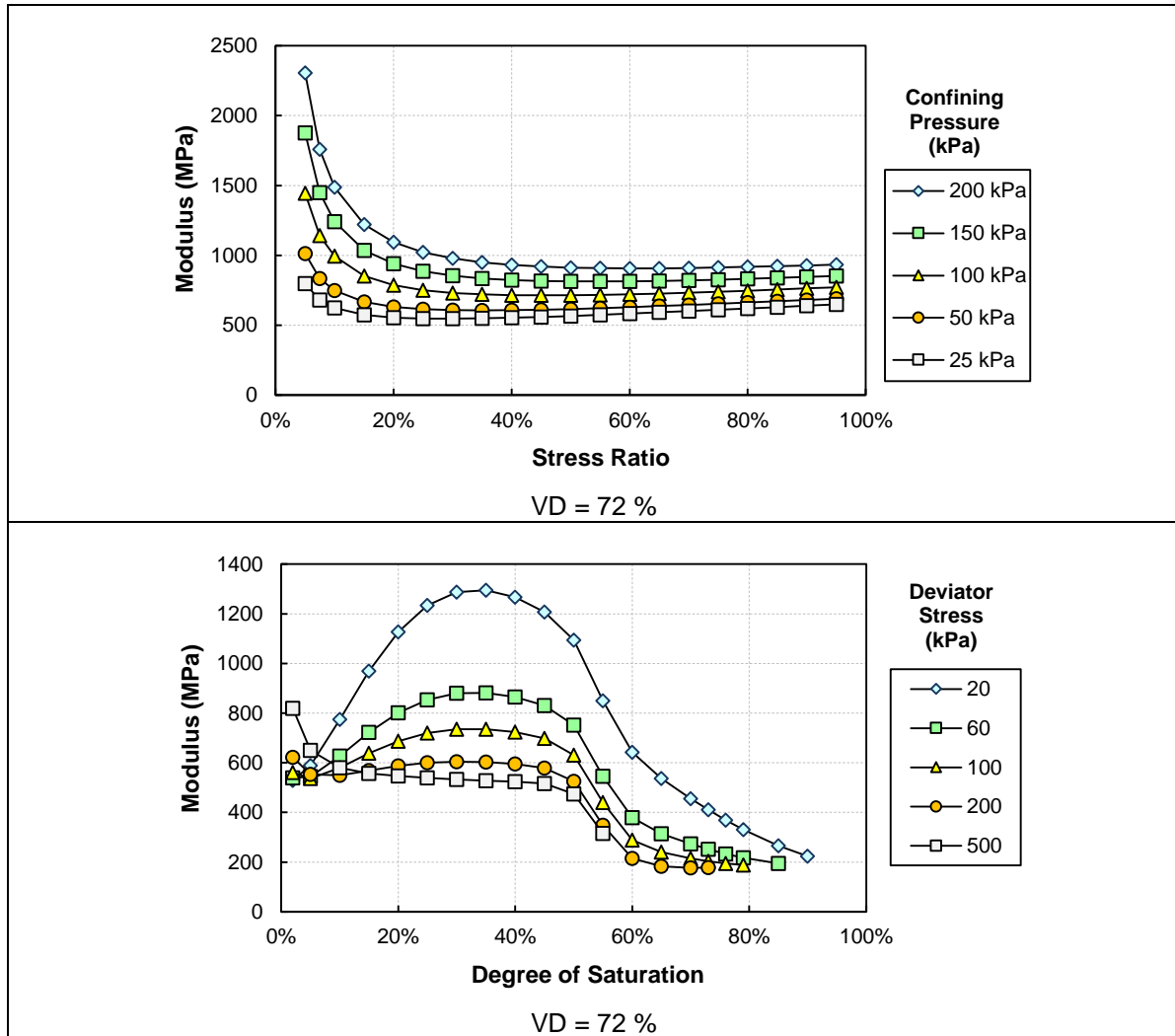
Figure 5.8: **Parametric plots for natural unbound material depicting stress dependent behaviour and behaviour in terms of level of saturation.**

5.4 LINK MODEL TO BASIC MATERIAL PROPERTIES

At Level 3, the accuracy of the model can be lower and the input into the model as basic as possible. Therefore, to link basic material properties to the model variables listed in Table 5.5 and Table 5.10 was considered.

5.4.1 Basic material properties to model variables

No clear trend or relationship could be observed between basic material properties and calibrated model variables. Figure 5.9 depicts the relationship between the 'k' variable (calibrated number) for the natural unbound material model and the percentage passing the 0.425 mm sieve ($P_{0.425mm}$). The relationship between the remaining variables and basic material properties depict similar trends, as well as for the crushed unbound material model. Figure 5.10 depicts the relationship between the 'k' variable for each individual bulk material sample at high (HD) and low density (LD) against $P_{0.425mm}$. The relationship

between the remaining variables and basic material properties depict similar trends, as well as for the crushed unbound material model. From the figures no trend or relationship can be observed.
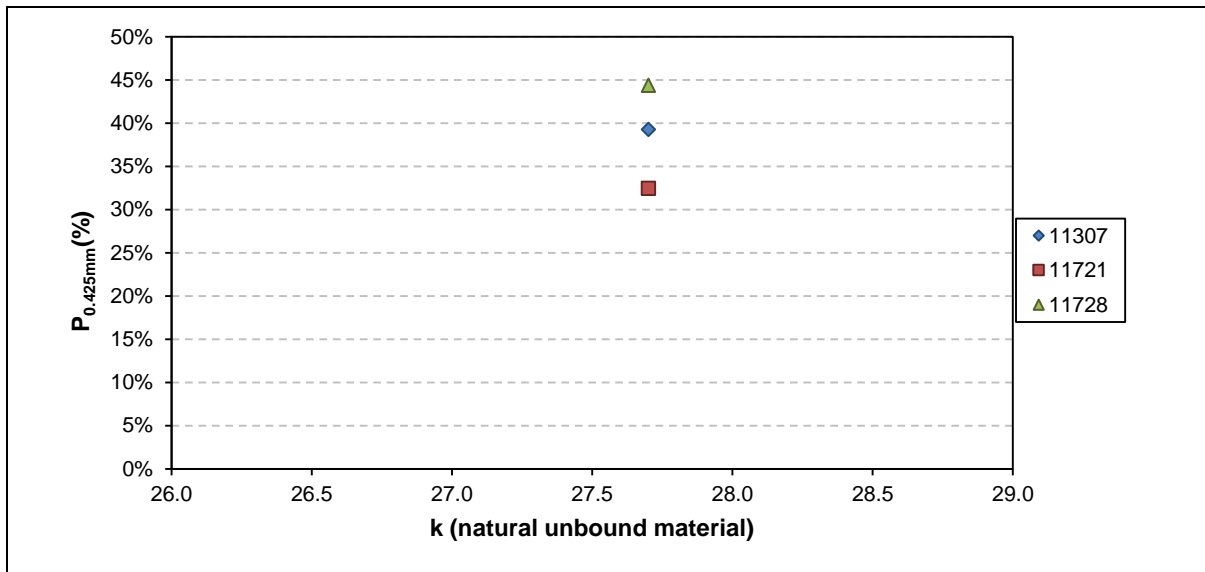
Figure 5.9: **Natural unbound material model: variable 'k's relationship to $P_{0.425mm}$.**
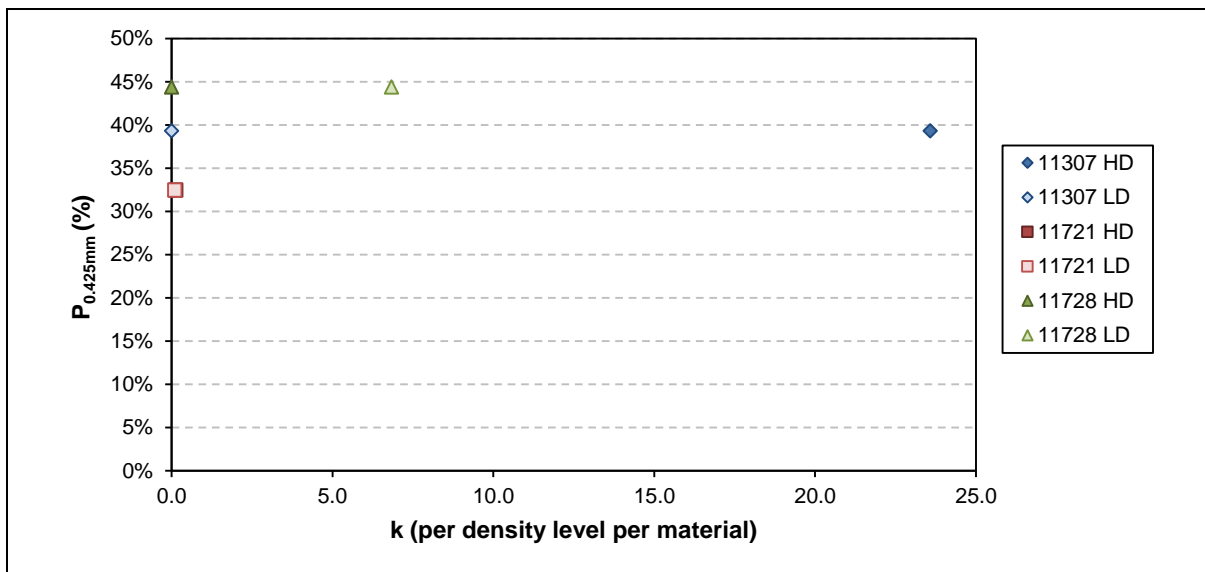
Figure 5.10: **Individual bulk sample material model: variable 'k's relationship to $P_{0.425mm}$.**

5.4.2   Regression analysis to link basic material properties to model variables

Linear regression was considered to obtain a link between basic material properties and the two models' variables, but the equations developed did not predict the values of the variables satisfactorily. Figure 5.11 depicts the results of the linear regression analysis for variable 'k' of the natural unbound material model. The R^2 value is 0.5 with error of 10 (number value) and when the predicted values as opposed to the observed values are evaluated, the fit is considered poor.

Summary Output

	$k_{observed}$	$P_{0.425mm}$ (ratio)	$P_{0.075mm}$ (ratio)	LL (ratio)	PL (ratio)	LS (ratio)	MDD (kg/m³)	OMC (ratio)	$k_{predicted}$
11307 HD	23.57	0.39	0.29	0.31	0.20	0.06	2056	0.11	11.79
11307 LD	0.00	0.39	0.29	0.31	0.20	0.06	2056	0.11	11.79
11721 HD	0.12	0.32	0.25	0.27	0.19	0.05	2133	0.08	0.11
11721 LD	0.10	0.32	0.25	0.27	0.19	0.05	2133	0.08	0.11
11728 HD	0.00	0.44	0.29	0.28	0.18	0.07	2037	0.09	3.42
11728 LD	6.83	0.44	0.29	0.28	0.18	0.07	2037	0.09	3.42

Figure 5.11: Linear regression analysis results for variable '*k*' of natural unbound material model.

In light of the above, it is the authors' opinion that with the set of results from this thesis, no reliable consistent link between model variables and basic material parameters can be obtained. However, if the number of results could be increased by incorporating more bulk samples to be tested as described in this thesis, a link may be obtained. Increasing the number of bulk samples will however have a large cost and time implication, as all of the tests, processing of data and calibration phases described thus

far in the thesis must be the same to have comparative results. Unfortunately it was not possible to increase the number of bulk samples tested during this study.

5.5 LINK MODULUS TO BASIC PROPERTIES THROUGH STATISTICAL DISTRIBUTIONS

After no direct link to basic material properties and the variables of the calibrated saturation and stress dependent cord modulus models for crushed and natural unbound materials could be established, the observed resilient behaviour of the bulk material samples and the basic properties of the materials were evaluated statistically.

5.5.1 Selected statistical distributions

Based on previous studies by Steyn (2011) and Van Aswegen and Steyn (2012), where the Kolmogorov-Smirnov (K-S) value was used to evaluate observed resilient behaviour to determine which statistical distribution fits the resilient behaviour the best, the Weibull and Log-normal distributions were selected. The best-fit distribution is defined as the distribution with the best K-S value (Steyn, 2011). The K-S test quantifies the distance between the empirical distribution function of the sample and the cumulative distribution function selected as the reference distribution (in this case the Weibull and Log-normal). The Weibull and Log-normal distributions were selected because these distributions only allow non-negative outputs as would be expected for the resilient behaviour of an unbound granular material (Steyn, 2011). Figure 5.12 depicts the statistical distributions and the observed resilient data histograms, irrespective of stress ratio and confining pressure for all materials analysed in this thesis.
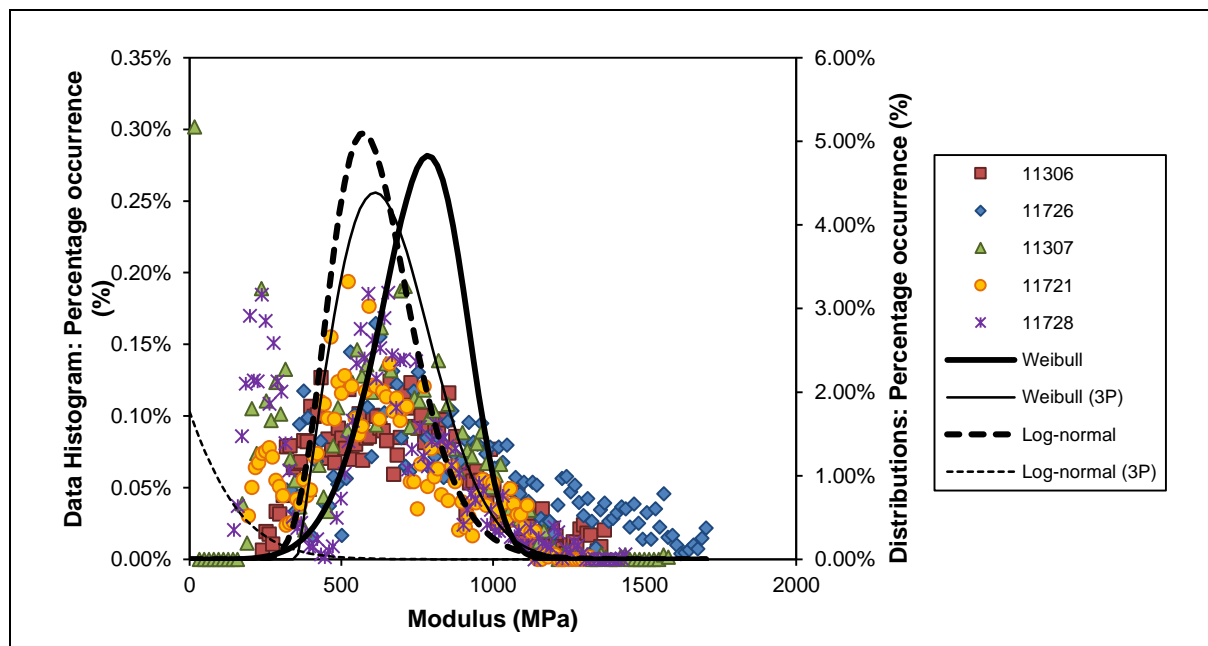
Figure 5.12:   **Statistical distributions and observed cord modulus data.**

Figure 5.13 and Figure 5.14 depicts the two groups of materials (crushed and natural unbound material). It is evident that even when the distributions are compared against a cloud of data, the majority of the data lies well within one or both of the statistical distributions.
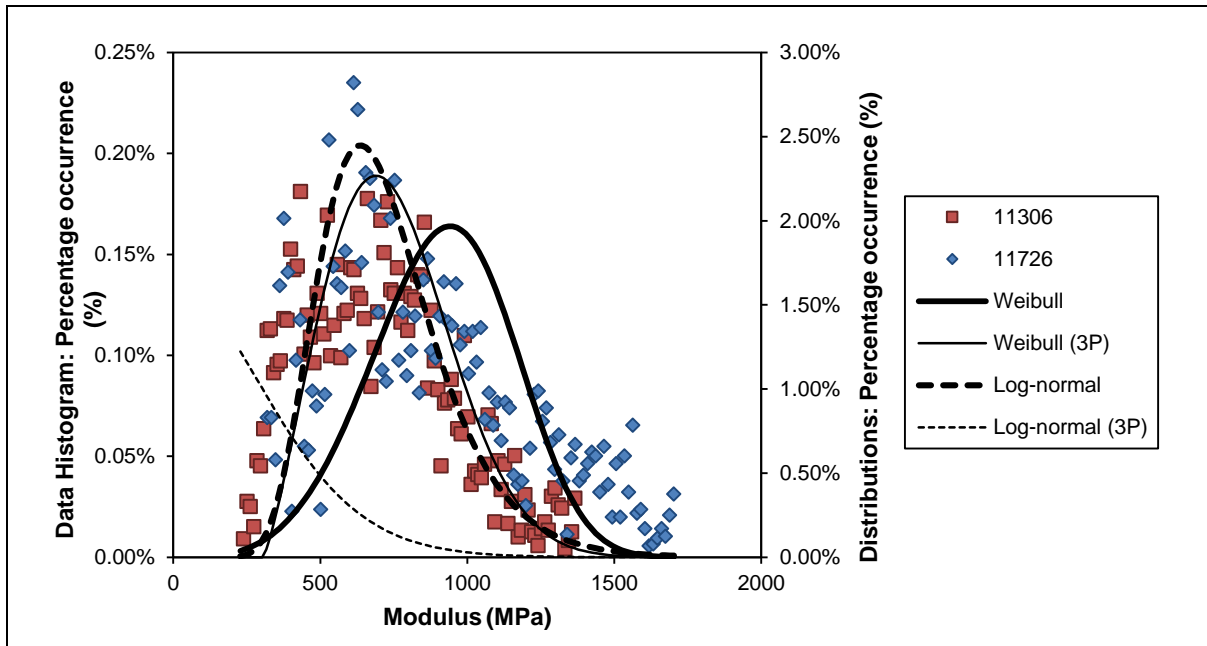
Figure 5.13: Statistical distributions and observed cord modulus data for crushed unbound material.
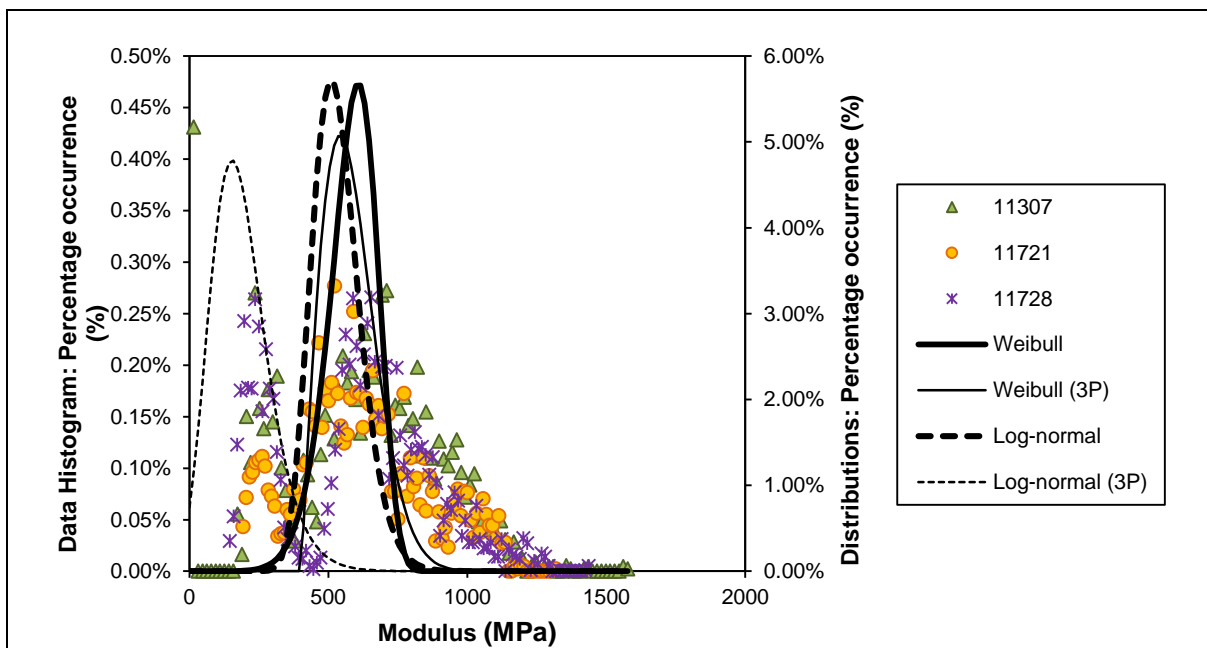
Figure 5.14: Statistical distributions and observed cord modulus data for natural unbound material.

5.5.2   Analysis of Parameters to Develop Statistical Parameter Equations

The parameters of the statistical distributions were analysed to develop equations that can be used to generate the statistical parameters for the Weibull and Log-normal distributions by using basic engineering properties of material as input. The Weibull and Log-normal distributions are described by Equations 5.1 and 5.2.

$$f(x) = \frac{\alpha}{\beta}\left(\frac{x}{\beta}\right)^{\alpha-1} e^{\left(-\left(\frac{x}{\beta}\right)^{\alpha}\right)} \qquad \text{or} \qquad f(x) = \frac{\alpha}{\beta}\left(\frac{x-\gamma}{\beta}\right)^{\alpha-1} e^{\left(-\left(\frac{x-\gamma}{\beta}\right)^{\alpha}\right)} \tag{5.1}$$

Where:

α = continuous shape parameter ($\alpha > 0$);

β = continuous scale parameter ($\beta > 0$);

γ = continuous location parameter ($\gamma \equiv 0$ yields the two-parameter Weibull distribution).

$$f(x) = \frac{e^{\left(-\frac{1}{2}\left(\frac{lnx-\mu}{\sigma}\right)^2\right)}}{x\cdot\sigma\cdot\sqrt{2\pi}} \qquad \text{or} \qquad f(x) = \frac{e^{\left(-\frac{1}{2}\left(\frac{ln(x-\gamma)-\mu}{\sigma}\right)^2\right)}}{(x-\gamma)\cdot\sigma\cdot\sqrt{2\pi}} \tag{5.2}$$

Where:

σ = continuous shape parameter ($\sigma > 0$);

μ = continuous scale parameter;

γ = continuous location parameter ($\gamma \equiv 0$ yields the two-parameter Log-normal distribution).

The parameters of the statistical distributions were determined for each bulk material sample which is summarized in Table 5.11.

Table 5.11:   Parameters of statistical distributions as determined for each bulk material sample.

	Weibull		Weibull (3P)			Log-normal		Log-normal (3P)		
	α	β	α	β	γ	σ	μ	σ	μ	γ
N4 Ext B	3.53	1107.95	2.31	523.54	209.80	0.35	6.45	0.18	7.59	-2108.14
S191 B	5.14	893.23	2.23	468.50	399.93	0.24	6.63	0.09	7.79	-2197.73
N4 Ext USEL	6.30	648.40	1.42	204.91	367.35	0.19	6.29	0.24	6.29	-409.52
P10-2 B	7.59	634.06	1.95	219.04	398.63	0.16	6.31	0.19	6.35	-447.53
D804 B	8.20	602.47	1.98	181.94	406.12	0.16	6.21	0.25	5.93	-130.74

In order to determine which basic engineering properties of the material to incorporate as parameters in the equations to generate the statistical parameters, the correlation between properties was analysed (Table 5.12). A good correlation exists between variables if the correlation coefficient is close to or inclusive of one, whether positive or negative (Van As, 2003). All the values reported in Table 5.12 were

satisfactory, except those highlighted, which indicated a poor correlation. However, to keep the number of variables as small as possible, only four properties were selected to be utilised in further analysis.

Table 5.12: **Correlation analyses output for all data.**

	$P_{0.425mm}$ (ratio)	$P_{0.075mm}$ (ratio)	GM (ratio)	*LL* (ratio)	PL (ratio)	PI (ratio)	LS (ratio)	MDD (kg/m³)	OMC (ratio)
$P_{0.425mm}$ (ratio)	1.00								
$P_{0.075mm}$ (ratio)	0.98	1.00							
GM (ratio)	-1.00	-0.99	1.00						
LL (ratio)	*-0.30*	*-0.33*	*0.35*	1.00					
PL (ratio)	-0.91	-0.93	0.94	0.65	1.00				
PI (ratio)	0.62	0.61	-0.59	0.55	*-0.28*	1.00			
LS (ratio)	0.85	0.71	-0.79	*-0.06*	-0.62	0.60	1.00		
MDD (kg/m³)	-0.97	-0.99	0.98	*0.27*	0.91	-0.65	-0.79	1.00	
OMC (ratio)	0.90	0.93	-0.91	*0.20*	-0.61	0.92	0.66	-0.94	1.00

The general format for the equations to be developed is given in Equation 5.3.

Statistical parameter = $A_1 \cdot GM + A_2 \cdot LS + A_3 \cdot MDD + A_4 \cdot OMC$ (5.3)

Linear regression analysis was used to derive the equations for the statistical parameters of the Weibull and Log-normal distributions, using the basic engineering properties as indicated (GM, LS, MDD and OMC). Table 5.13 gives the constants for A_1 to A_4 to calculate the statistical parameters of the Weibull and Log-normal distributions, as well as the SEE and R^2 for each of the parameters. In this analysis all the materials were utilised and the materials were not divided into two groups. Relatively large standard errors for the Weibull 'β' parameter were recorded, which is the parameter which gives an indication of the scale of the distribution, as well as for the Weibull and Log-normal 'γ' parameter, which gives an indication of the location of the distribution. The R^2 values recorded for all the parameters are above 0.95.

Table 5.13: **Constants for equations to determine statistical input for distributions.**

Weibull	α	β	(3P) α	(3P) β	(3P) γ
GM (A_1)	-10.11	412.57	-1.19	515.84	-29.72
LS (A_2)	69.74	-3959.19	10.78	-1072.93	4495.32
MDD (A_3)	1.39E-02	-0.03	0.00	-0.33	0.15
OMC (A_4)	-74.65	1753.89	-27.20	175.40	-1497.32
SEE	0.53	76.46	0.11	52.78	23.04
R^2	0.98	0.99	0.98	0.99	0.99

Log-normal	σ	μ	(3P) σ	(3P) μ	(3P) γ
GM (A_1)	0.16	0.01	-0.32	3.16	-4435.55
LS (A_2)	-2.34	8.84	-1.78	5.83	2025.56
MDD (A_3)	-7.29E-05	2.48E-03	3.64E-04	-4.83E-04	3.92
OMC (A_4)	1.74	6.06	1.65	11.52	-5251.08
SEE	0.03	0.04	0.02	0.08	277.19
R^2	0.96	0.99	0.98	0.99	0.99

The constants reported in Table 5.13 were used to calculate the statistical parameters for the distributions using the average of the basic properties for all the materials as input. Figure 5.15 depicts the derived distributions as opposed to the observed data. The derived distributions will not accurately predict the extreme modulus values at the lower and upper end of the scale, but should fairly accurately predict the bulk of the modulus values.
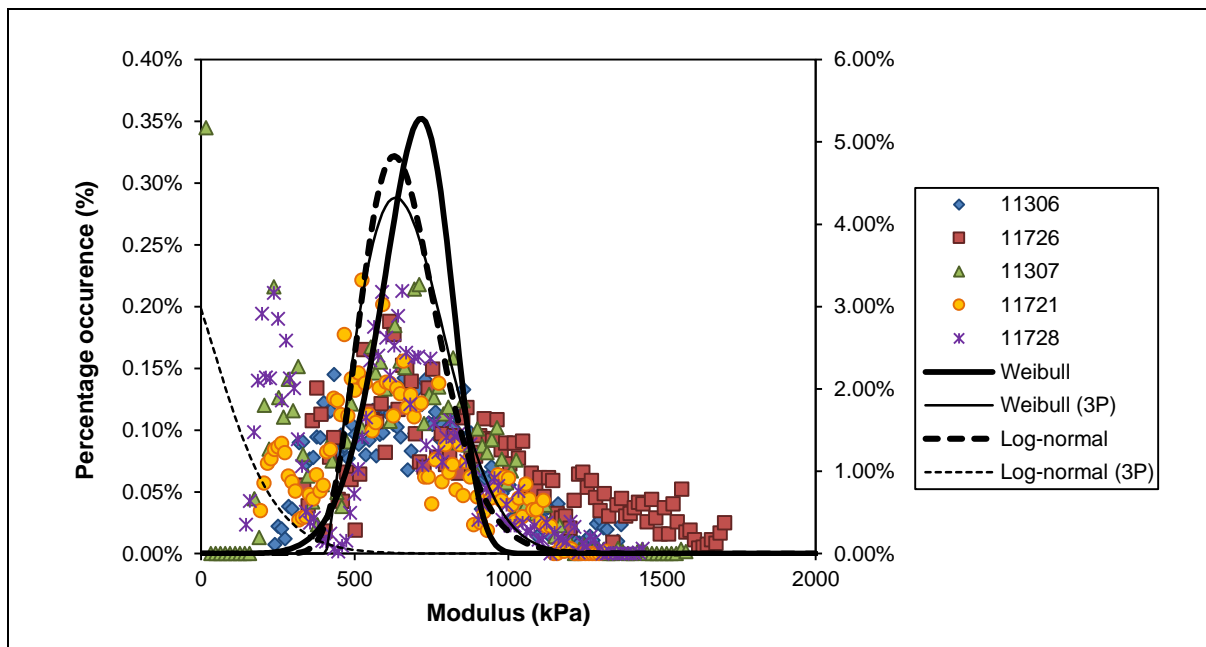
Figure 5.15:   **Predictive statistical distributions and observed cord modulus data.**

5.5.3   Verification of Equations to Estimate Statistical Parameters for Distributions

A parametric study was conducted to determine how the various basic engineering properties affect the resilient behaviour. In this study, for example, GM was varied through reasonable values, while LS, MDD and OMC were given average values. This was repeated for each of the properties used in the equations which estimated statistic parameters. The variables A_1 to A_4 was the same as derived through the regression analysis.

5.5.3.1   Grading Modulus (GM)

GM was varied between 1.5 and 2.5 with 2 used as an average value. The range of GM values could be modelled by the distributions throughout the range and it seems as though GM influence the location and width of spread of the distribution. Figure 5.16 depicts the Weibull distribution when GM values

range from 1.5 to 2.5. The distribution is bell shaped. The literature indicates that GM influences resilient behaviour when moisture is introduced and well-graded materials yield higher modulus values because these materials can hold water in the pores (Lekarp *et.al.*, 2000).
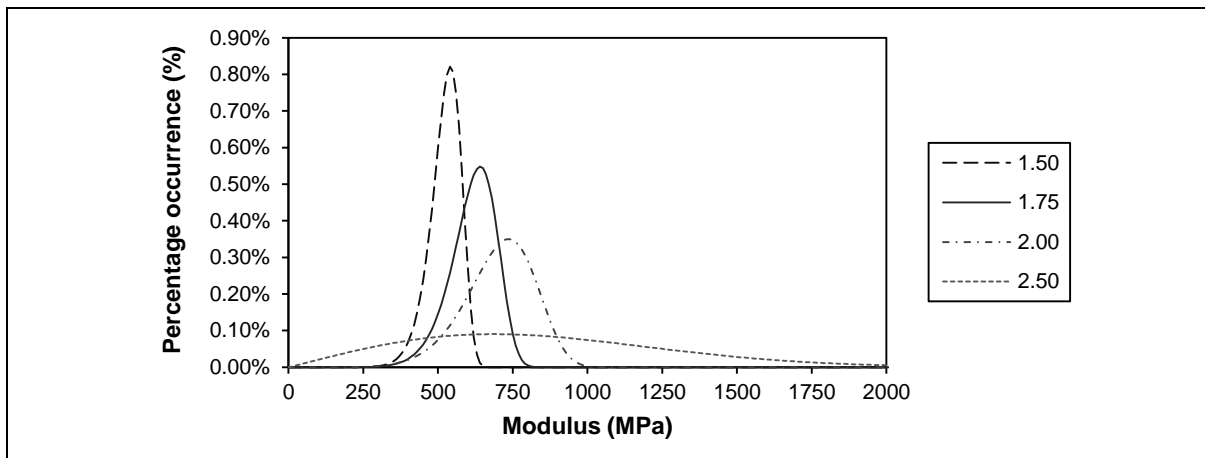
Figure 5.16:   Effect of variable GM on modulus prediction.

5.5.3.2   *Linear shrinkage (LS)*

LS were varied between 0 per cent and 8 per cent with an average of 4 per cent. This range of values represents the limits set in the TRH14 (1985) for material up to a G5 and to include the results obtained in this study. The highest modulus values were predicted by the smallest LS value analysed, while the smallest modulus values were predicted by the highest LS value analysed. These observations are in line with the TRH14 limits where higher LS are associated with a material class of lower bearing capacity. Theyse (2008a) concurred with other researchers that LS is a good indicator of material performance. Figure 5.17 illustrates the Weibull distribution for four values evaluated.
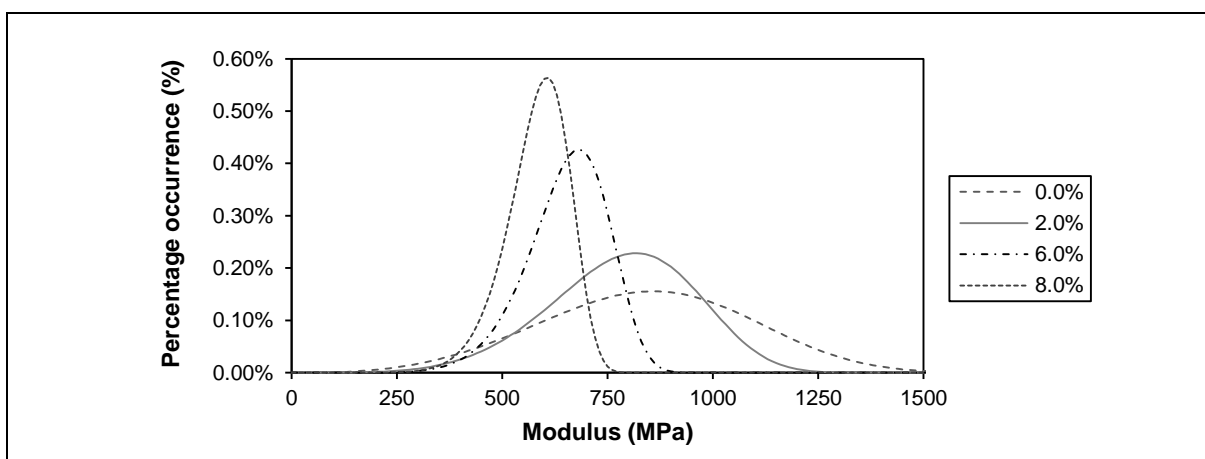
Figure 5.17:   Effect of variable LS on modulus prediction.

5.5.3.3 Maximum Dry Density (MDD)

MDD was varied between 2 000 kg/m^3 and 2 800 kg/m^3 with an average of 2 200 kg/m^3. The influence of density on modulus values has been well documented and a number of studies indicate a high density correlates to a high modulus value (Lekarp *et.al.*, 2000). The distributions of the variable MDD is bell shaped to slightly positively skew. Figure 5.18 illustrates the Log-normal distribution of various densities.
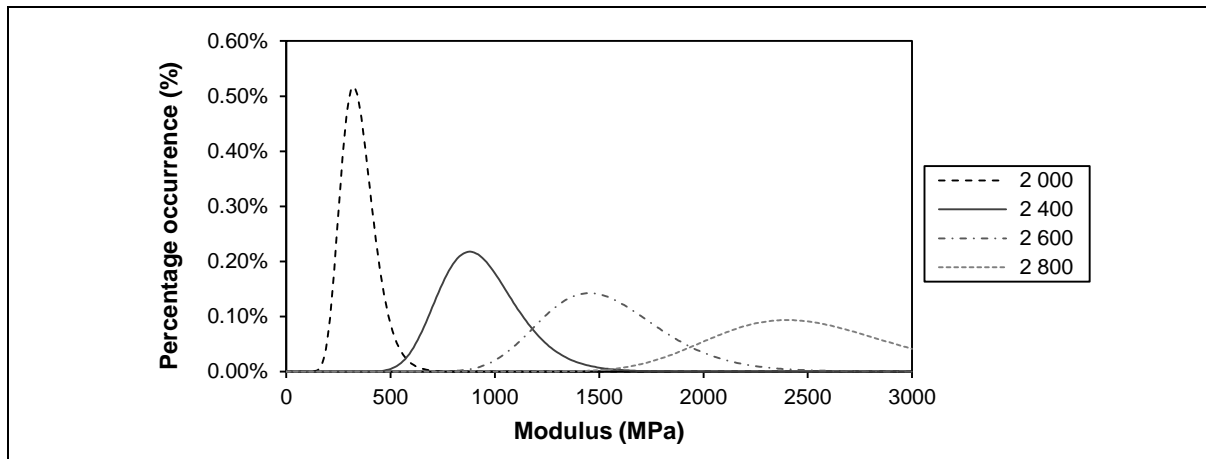
Figure 5.18:   Effect of variable MDD on modulus prediction.

5.5.3.4 Optimum Moisture Content (OMC)

OMC was varied between 4 per cent and 12 per cent with an average of 8 per cent. The spread of the distributions increased as the OMC increased. The lowest OMC value predicted the highest modulus value. The influence of moisture content on modulus values has been well documented and correlates with what is indicated in Figure 5.19 which is illustrated by the Weibull (3P) distribution.
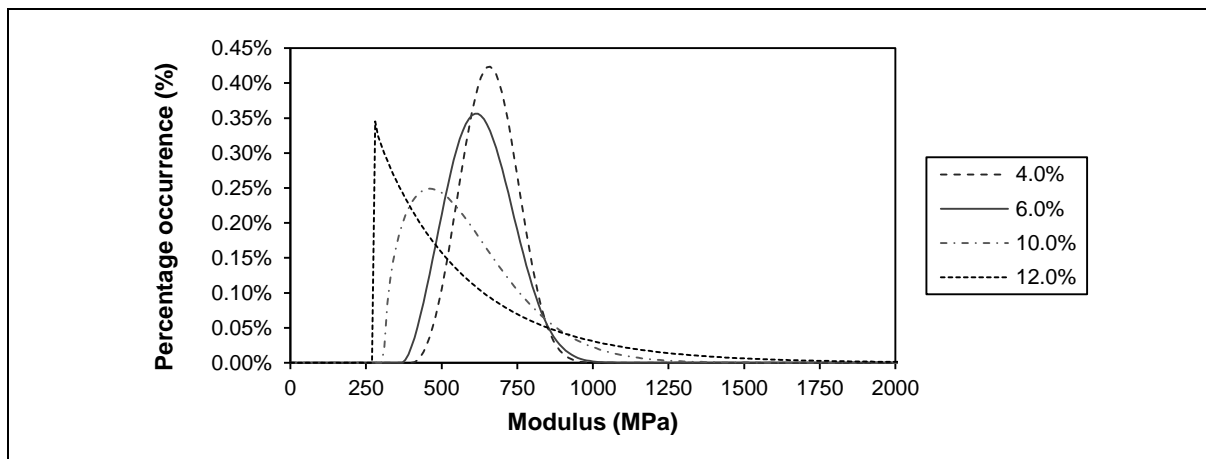
Figure 5.19:   Effect of variable OMC on modulus prediction.

From the relatively successful verification of the equations to estimate statistical parameters for distributions and confirmation by the parametric study that realistic results can be obtained, the investigation was taken a step further.

5.5.4 Development of a family of distributions predicting resilient behaviour

Using Equation 5.3 and applying it to a material with a GM of 2.0, LS of 5 per cent, MDD of 2 200 kg/m^3 and varying the OMC ratio between 0 and 18 per cent, a family of distributions can be generated estimating the modulus obtainable at each OMC. Figure 5.20 depicts this family of distributions.
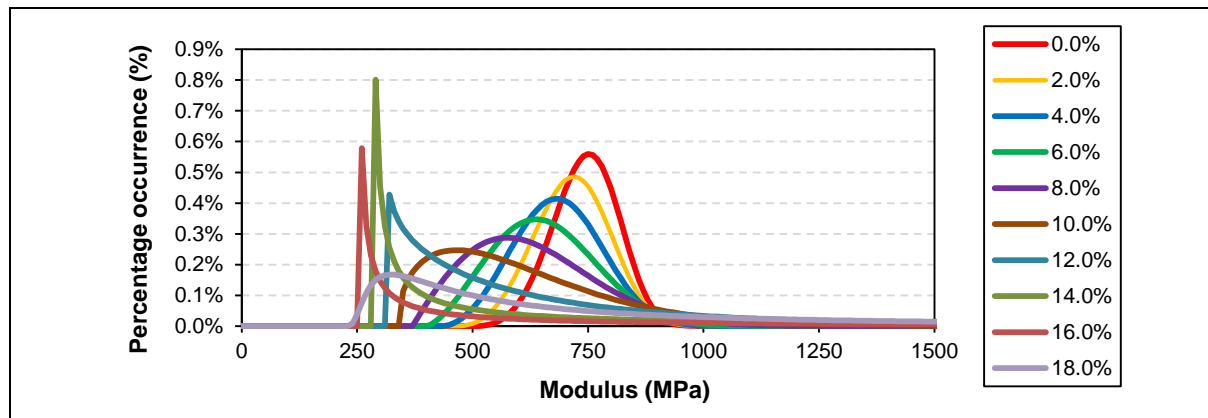
Figure 5.20: **Family of Weibull (3P) distributions when OMC is varied.**

When the modulus estimated in Figure 5.20 by the Weibull (3P) distribution at each OMC is evaluated as indicated in Figure 5.21, a graph is generated from which the modulus can be estimated for that material, given the specific OMC used as input. The shape of the graph resembles that of a sigmoid curve which was used in Section 4.3.2 and correlates with findings by Theyse (2008a). Figure 5.22 depicts a plot of a selection of modulus data from Theyse (2008a), ranging from G1 to G7 material, opposed to saturation. The same sigmoid curve can be observed in the data even though the moisture condition of the data is expressed in terms of saturation and not OMC.
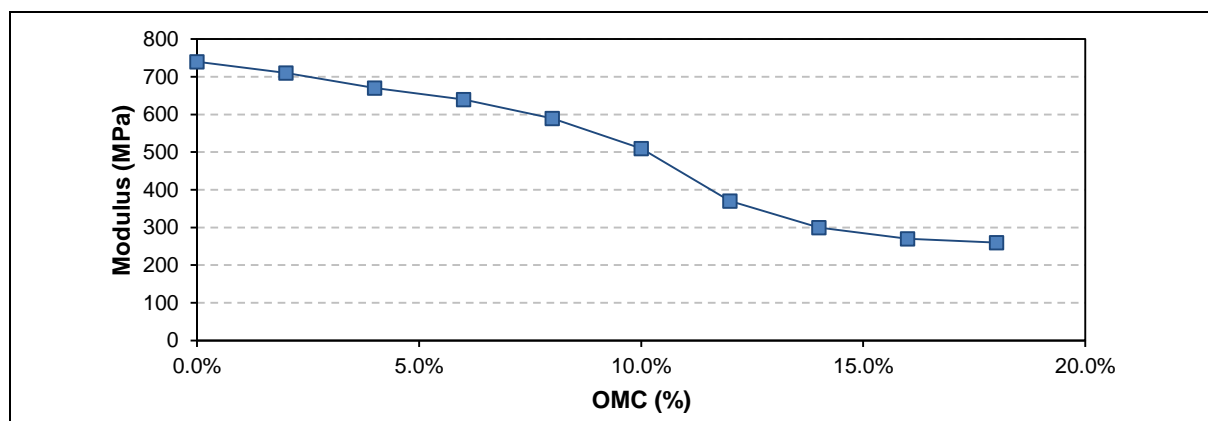
Figure 5.21: **Modulus versus OMC relationship for a specific material.**
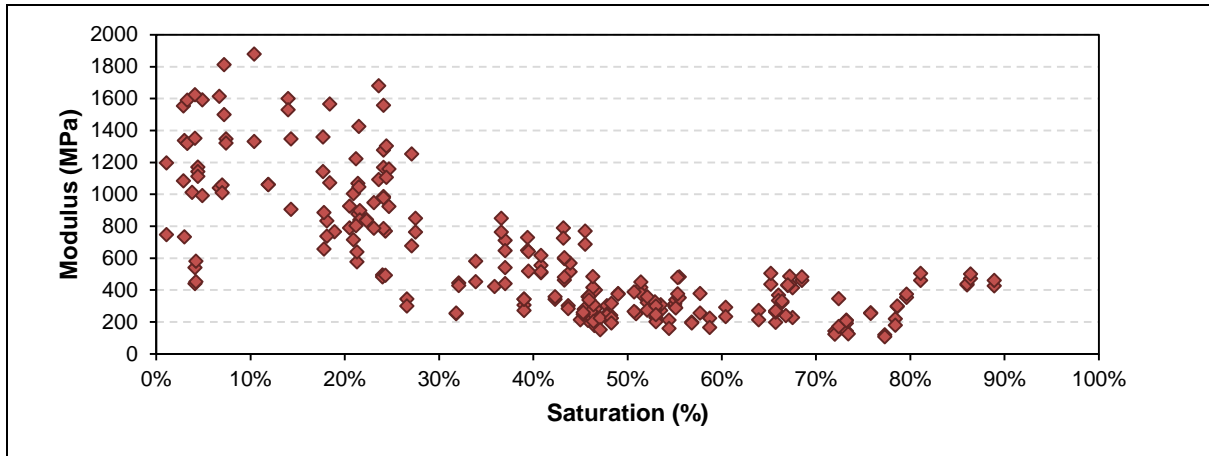
Figure 5.22: **Modulus versus saturation relationship for data published by Theyse (2008a).**

5.5.5 Proposed use of predictive statistical distributions and family of curves

Previously in South Africa, modulus values had to be determined through tri-axial testing (Level 1) or through the use of tables containing suggested upper and lower modulus limits for a specific material classification, taking into account a wet or dry condition (Level 2 and/or 3) (Theyse *et.al.*, 1996).

The application of predictive statistical distributions are illustrated by using Equation 5.3 and constants listed in Table 5.13 to determine the distributions for a sample not included in this thesis, but that was tested and processed according to the same protocols as reported in this thesis. The material from Sample 11727 was classified as a G6 class material. Table 5.14 contains the basic properties used as input into Equation 5.3 along with the constants of Table 5.13. Figure 5.23 depicts the distributions generated against the observed modulus values.

Table 5.14: **Basic properties of Sample 11727 used as input.**

Basic property	Value
GM (ratio)	2.20
LS (ratio)	0.06
MDD (kg/m³)	2 267.00
OMC (ratio)	0.08

5-23
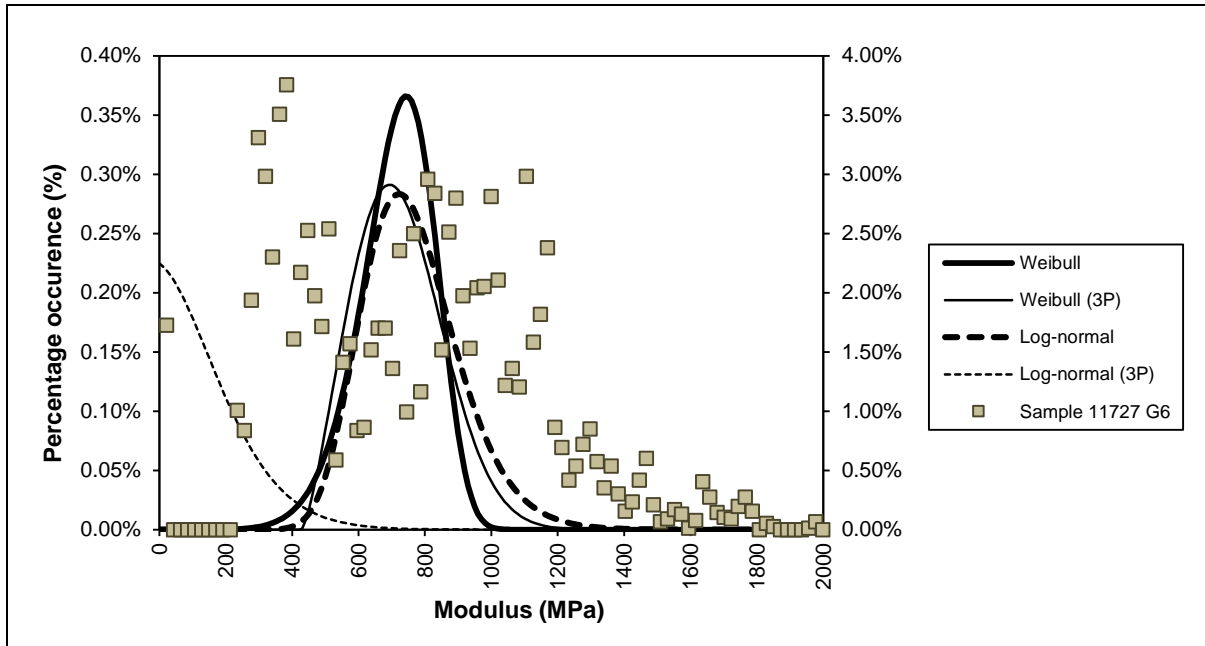
Figure 5.23:   Predictive statistical distributions for Sample 11727 data.

The fit of the predictive statistical distributions is not as accurate as would be preferred. Figure 5.24 depicts the maximum suggested modulus to be used for a Level 2 and/or 3 analyses for a G6 class material (Theyse *et.al.*, 1996). From this it appears that the predictive statistical distributions are more in line with observed data than the suggested ranges currently used in practice.
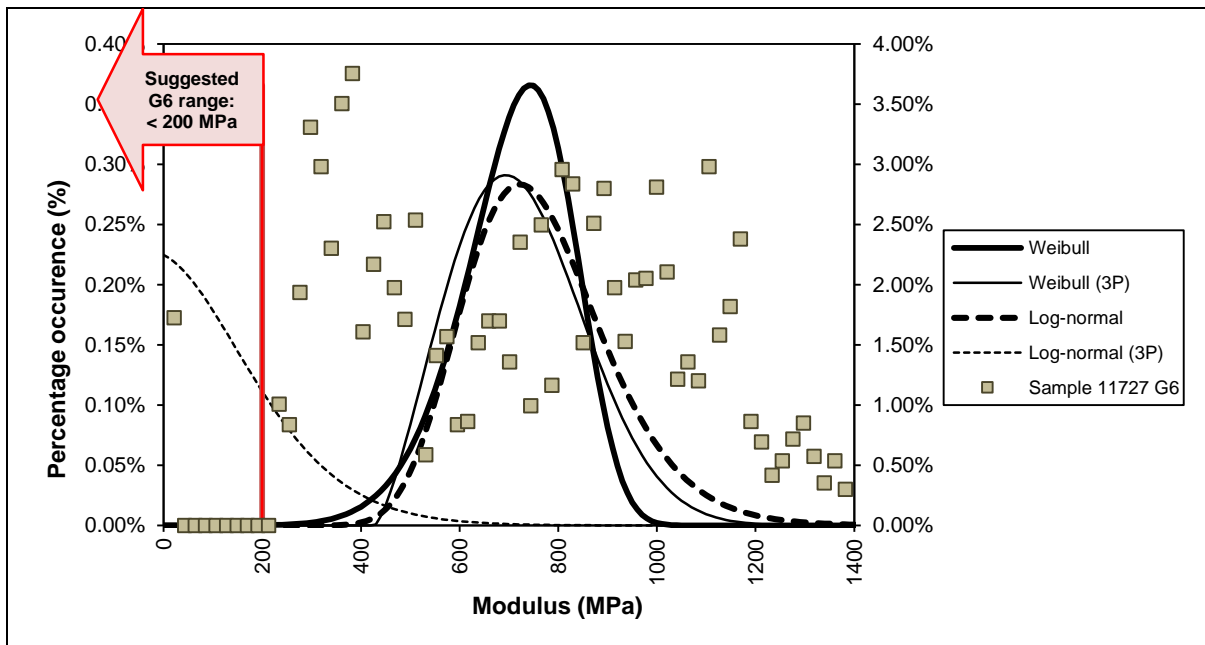
Figure 5.24:   Predictive statistical distributions and suggested range for Sample 11727 data.

Figure 5.25 depicts the family of distributions that can be generated for Sample 11727 when the moisture content is varied.
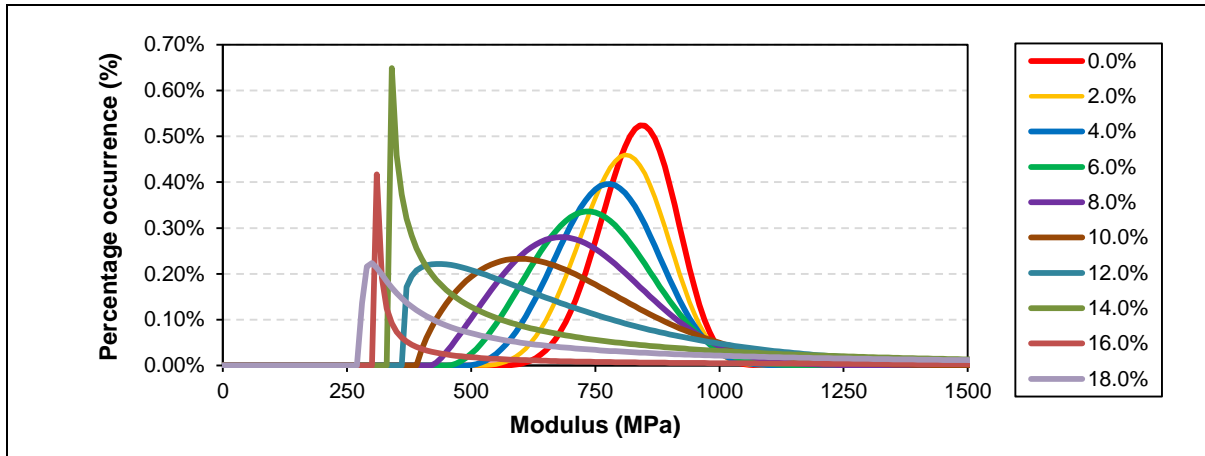
Figure 5.25: Family of Weibull (3P) distributions for Sample 11727 data.

When the maximum modulus value predicted by the distributions are plotted against moisture content (Figure 5.26), the variability of modulus due to change in moisture content can be seen.
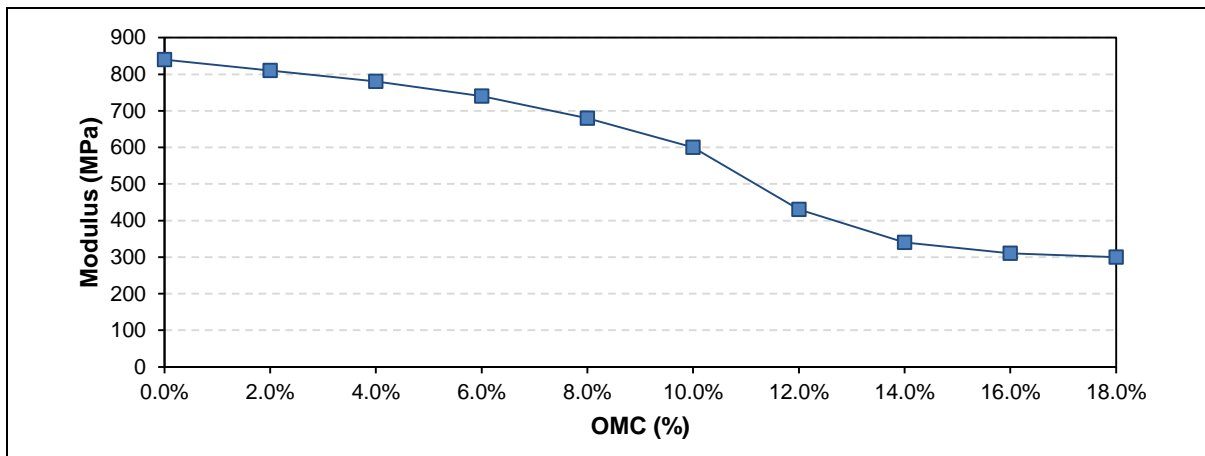
Figure 5.26: Modulus versus OMC relationship for Sample 11727 data.

It is proposed that the method of predictive statistical distributions be utilised as a tool in Level 2 and/or 3 analyses, as it appears to be more realistic than the suggested ranges for modulus in use currently.

5.6 CONCLUSION

In Section 5.1 to Section 5.3 the grouping of bulk material samples considered in this thesis into two groups were evaluated. Based on physical appearance and grading modulus results were grouped into a crushed unbound gravel or natural unbound gravel group. It is proposed that materials with a GM > 2.0 should be modelled as crushed unbound gravel and material with a GM < 2.0 as natural unbound gravel. In Section 5.2 the saturation and stress dependent cord modulus model developed in Section 4

was calibrated for crushed and natural unbound material. Two sets of constant variables to be used as input in the model was derived. These are given in Table 5.15 and Table 5.16.

Table 5.15:   Model variables for crushed unbound material.

Crushed unbound	k	l	m	n
α_1	0.00	285.95	102.00	0.65
β_1	-0.33	1.13		
b or α_2	247.96	1473.60	44.28	0.26
α_3	118.30	-7.21		
β_3	0.31	0.72		

Table 5.16:   Model variables for natural unbound material.

Natural unbound	k	l	m	n
α_1	27.70	386.47	44.69	0.54
β_1	-0.82	-0.07		
b or α_2	79.28	516.15	12.70	0.14
α_3	90.62	-8.84		
β_3	0.38	-0.09		

Parametric analysis of the two models indicated that the saturation and stress dependency of the materials are realistically reflected by the models.

As stated in the objectives of this thesis, linking of basic material properties to the model was explored in Section 5.4. With the limit set of results, this was not successful and it is recommended that future research conducted in line with the protocol and processing of data used in this thesis should be used to explore this objective further. It is the author's opinion that with a large set of results, linking to basic material properties is possible.

Section 5.5 explored an alternative link between modulus and basic material properties. The use of predictive statistical distributions based on the Weibull and Log-normal distributions were evaluated. Weibull or Log-normal distributions were evaluated as these distributions do not allow non-negative results, which is in line with observed modulus values. In Section 5.5.2 selected basic material properties were used to develop equations that estimate the statistical parameters used to calculate the aforementioned distributions. Only GM, LS, MDD and OMC were used, since an equation consisting with as little as possible variables and constants is preferred, as it limits compensating by variables for one another. Equation 5.4 to 5.6 and Table 5.17 constitutes the predictive statistical distributions.

Weibull:

$$f(x) = \frac{\alpha}{\beta}\left(\frac{x}{\beta}\right)^{\alpha-1} e^{\left(-\left(\frac{x}{\beta}\right)^{\alpha}\right)} \qquad \text{or} \qquad f(x) = \frac{\alpha}{\beta}\left(\frac{x-\gamma}{\beta}\right)^{\alpha-1} e^{\left(-\left(\frac{x-\gamma}{\beta}\right)^{\alpha}\right)} \qquad (5.4)$$

Log-normal:

$$f(x) = \frac{e^{\left(-\frac{1}{2}\left(\frac{\ln x - \mu}{\sigma}\right)^2\right)}}{x \cdot \sigma \cdot \sqrt{2\pi}} \qquad \text{or} \qquad f(x) = \frac{e^{\left(-\frac{1}{2}\left(\frac{\ln(x-\gamma)-\mu}{\sigma}\right)^2\right)}}{(x-\gamma) \cdot \sigma \cdot \sqrt{2\pi}} \qquad (5.5)$$

Statistical parameter $(\alpha / \beta / \gamma / \sigma / \mu / \gamma) = A_1 \cdot GM + A_2 \cdot LS + A_3 \cdot MDD + A_4 \cdot OMC$ (5.6)

Table 5.17:   **Constants for equations to determine statistical input for distributions.**

Weibull	α	β	(3P) α	(3P) β	(3P) γ
GM (A$_1$)	-10.11	412.57	-1.19	515.84	-29.72
LS (A$_2$)	69.74	-3959.19	10.78	-1072.93	4495.32
MDD (A$_3$)	1.39E-02	-0.03	0.00	-0.33	0.15
OMC (A$_4$)	-74.65	1753.89	-27.20	175.40	-1497.32
Log-normal	α	β	(3P) α	(3P) β	(3P) γ
GM (A$_1$)	0.16	0.01	-0.32	3.16	-4435.55
LS (A$_2$)	-2.34	8.84	-1.78	5.83	2025.56
MDD (A$_3$)	-7.29E-05	2.48E-03	3.64E-04	-4.83E-04	3.92
OMC (A$_4$)	1.74	6.06	1.65	11.52	-5251.08

Verification of the developed equations indicated that the results obtained are not counter-intuitive. From the predictive statistical distributions, a family of distributions can be developed over a range of moisture conditions. Section 5.5.4 indicated that this can give an indication of the modulus values that can be expected at various moisture conditions. Section 5.5.5 evaluated the developed equations of Section 5.5 by applying it to an independent data set. Although the application of the predictive statistical distributions did not yield an exceptionally accurate estimation of the data, it was shown to be more realistic than the ranges used in practice.

The analysis in Chapter 5 indicated that there is potential for linking basic material properties to the saturation and stress dependent cord modulus model or the use of predictive statistical distributions at Level 2 and/or 3. The aforementioned ties in with the MEPDG (NCHRP, 2004) and SAPDM (Theyse, 2006) concept of levels of design according to the level of accuracy in pavement design that is required. It is recommended that future research incorporate a similar analysis or that the analyses of Chapter 5 be updated with additional results when available to refine the equation's accuracy for more materials.

5.7 REFERENCES

George, K.P. (2004). '*Prediction of resilient modulus form soil index properties*', Final Report, Mississippi Department of Transportation, Research Division, Jackson, Mississippi, USA.

Lekarp, F., Isacsson, U. & Dawson, A. (2000). '*State of the art I: Resilient response of unbound aggregates*', Journal of Transportation Engineering, Volume 126, No. 1, January/February, 2000, pp 66-75.

NCHRP (2004). '*Project 1-37A: Guide for Mechanistic-Empirical Design of New and Rehabilitated Pavement Structures*', National Cooperative Highway Research Program, Transportation Research Board, of the National Research Council, USA.

Steyn, W.J.vdM. (2011). '*Vehicle Dynamics – Development of statistical distributions for selected Rigid vehicle case studies*', Report no. SANRAL/SAPDM/A-4/2011-01, University of Pretoria, Pretoria, RSA.

Theyse, H.L (2006). '*An improved pavement design method for Southern Africa: Research and development framework*', Report No. CSIR/BE/IE/IR/2006/0042/B, Pretoria, CSIR Built Environment Unit, RSA.

Theyse, H.L, De Beer, M. and Rust, F.C. (1996). '*Overview of the South African Mechanistic Pavement Design Analysis Method*', In Transportation Research Record: Journal of the Transportation Research Board, No 1539, Transportation Research Board of the National Academies, Washington, D.C., 2003, pp 6-17.

Theyse, H.L. (2008a). '*A mechanistic-empirical design model for unbound granular pavement layers*', PhD dissertation, University of Johannesburg, Johannesburg, RSA.

TRH 14 (1985). '*TRH 14: Guidelines for road construction materials*', Dept. Of Transport, Pretoria, RSA.

Van As, S.C. (2003). '*Applied statistics for Civil Engineers*', B.Eng. Honours course material, University of Pretoria, Pretoria, RSA.

Van Aswegen, E. and Steyn, W.J.vdM. (2012). '*Statistical Modeling of Resilient Behavior of Unbound Granular Material*'. Peer-reviewed paper presented at the 91st TRB meeting, Washington D.C., USA.

6   CONCLUSIONS AND RECOMMENDATIONS

6.1   CONCLUSIONS

Unbound granular material is used in the pavement structure and usually comprises the bulk of the structural and foundation layers of a typical South African pavement. The term '*unbound granular material*' refers to the classification of natural material, which has not been modified in any way. Unbound granular material is classified from a G1 to G10 quality according to its fundamental behaviour and strength characteristics (TRH4, 1996, TRH14, 1985). This thesis focussed on unbound granular material.

Various mechanistic-empirical models for the resilient response of unbound granular material have been developed over the years. However, few have incorporated important influencing parameters such as moisture or density on the basic stress-strain relationship or linked variables of the models to basic engineering properties of unbound granular material.

Theyse (2008a) has considered unbound granular material and developed a resilient response model taking moisture and density into account. Theyse (2008a) incorporated materials ranging from G1 to G10, but could only calibrate a single resilient modulus successfully for crushed aggregate (G1 to G3) due to a lack of data over a wider range of saturation levels. It was recommended that future research should focus on G4 to G10 material to calibrate a single model for these materials and that a wider range of moisture conditions should be evaluated.

There is currently a comprehensive project underway which is jointly sponsored by the South African National Roads Agency Ltd (SANRAL) and the Council for Scientific and Industrial Research (CSIR). The project entails the revision of the South African Mechanistic-Empirical Design Method (SAMEDM) which has been one of the primary pavement design tools in South Africa since the early 1970s (Theyse, 2006). One of the research areas of the South African Pavement Design Method (designated SAPDM as opposed to SAMEDM), focus on material resilient response models, which is particularly relevant to this thesis. Data collected in the Project SAPDM/B1-a were utilised in this thesis and reference is made to unpublished, continuing research work done under Project SAPDM/B1-a since 2011 (Section 2.3). The work is not publicly available, but has been presented to a panel of researchers on a three monthly basis and internal reports have been distributed to all researchers involved in the overall project for review.

Material for Project SAPDM/B1-a was selected that was deemed moisture sensitive and an experimental design adopted which included three levels of saturation and two levels of volumetric density. Basic engineering properties were determined through routine testing that included sieve analysis and Atterberg indicator tests. Analysis of the variability in Atterberg indicator test results indicated variability between 0.7 and 25 per cent. This variability is carried through in any subsequent

tests conducted on the materials. However, the test results yielded expected results for the materials under consideration and were deemed acceptable. Following the experimental design, static and resilient modulus tri-axial testing was conducted on the bulk material samples. The data from resilient modulus tri-axial tests were processed to eliminate test errors in an attempt to limit more variability incorporated into the test results used to calculate a cord modulus. The data set utilised after processing was deemed acceptable with as little inherent variability as practically possible.

A cord modulus model was identified in Section 2.3.3.4 and elaborated on in Section 4.3. The cord modulus calculated for five different unbound granular materials illustrated the complex interaction between moisture and stress condition. The effect of density was not as clear as expected, but that may be due to the experimental design which only allowed for two different volumetric density levels. These volumetric density levels only differed between 1 and 3 per cent and it is recommended that future research work allow for a wider range of volumetric density levels to be tested. Section 4.3.1 illustrated the formulation of a simple model that consistently captures the complex stress dependent behaviour of the selection of materials. Sections 4.3.2 to 4.3.4 showed that to model the saturation dependency, multiple model components had to be introduced based on trends that could be observed from the data. A saturation and stress dependent cord modulus model was formulated and calibrated for all five bulk material samples. The model generally has good prediction accuracy. The final model formulation of the saturation and stress dependent cord modulus model is as depicted in Figure 6.1 (as per Figure 4.43).

$$M_c = a + bSR_d + \frac{c}{SR_d}$$

$$M_c = \left(\alpha_1 + \beta_1\sigma_3\right) + \left(\alpha_2\right)\left(\frac{\sigma_1 - \sigma_3}{\sigma_1^f - \sigma_3}\right) + \frac{\left(\alpha_3 + \beta_3\sigma_3\right)}{\left(\frac{\sigma_1 - \sigma_3}{\sigma_1^f - \sigma_3}\right)}$$

$$\alpha_1 = k_{\alpha_1} + \frac{l_{\alpha_1} - k_{\alpha_1}}{1 + e^{m_{\alpha_1}(S - n_{\alpha_1})}}$$
$$\beta_1 = k_{\beta_1}\ln(S) + l_{\beta_1}$$

$$\alpha_2 = k_{\alpha_2} + \frac{l_{\alpha_2} - k_{\alpha_2}}{1 + e^{m_{\alpha_2}(S - n_{\alpha_2})}}$$

$$\alpha_3 = k_{\alpha_3}S + l_{\beta_3}$$
$$\beta_3 = k_{\beta_3}e^{(S \cdot l_{\beta_3})}$$

Where
M_c = cord modulus (MPa)
SR_d = deviator Stress Ratio (SR)
$\alpha_1, \beta_1, \alpha_2, \alpha_3, \beta_3$ = regression coefficients found from regression analysis
k_i, l_i, m_i, n_i = regression coefficients found from regression analysis
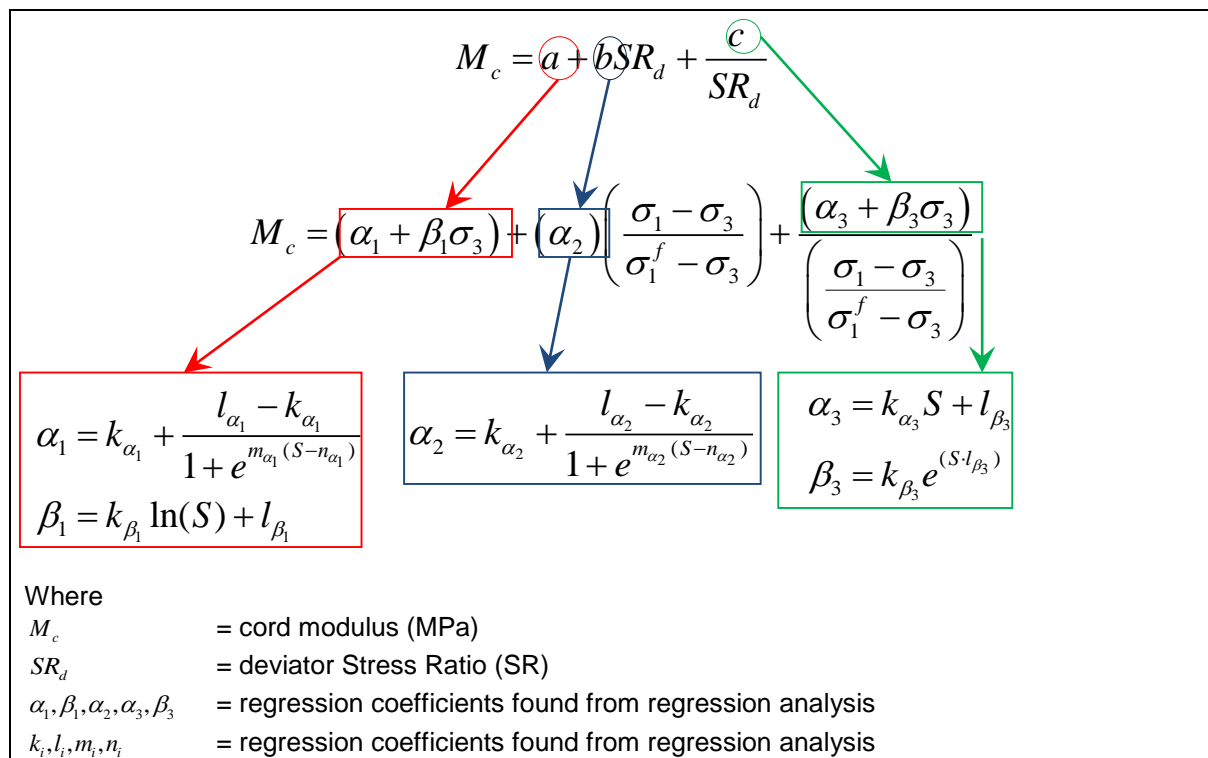
Figure 6.1: **Saturation and stress dependent cord modulus model.**

Parametric analysis of the saturation and stress dependent cord modulus model indicated that the material behaviour with increasing stress ratio is reflected realistically for each bulk material sample and that the effect of increasing saturation is also reflected realistically. It is recommended that future studies should conduct testing at more than three levels of saturation, as was the case in this thesis. The parametric plots for saturation were extrapolated from the three levels of saturation tested to the entire saturation spectrum. Although the results appear realistic, more data points could verify the distinct decrease in modulus at 40 and 60 per cent saturation that was observed in the parametric plots.

Based on physical appearance and grading modulus, the grouping of results was considered. It is proposed that materials with a GM > 2.0 should be modelled as crushed unbound gravel and material with a GM < 2.0 as natural unbound gravel. The saturation and stress dependent cord modulus model developed in Chapter 4 was calibrated for crushed and natural unbound material. Two sets of constant variables to be used as input in the model was derived. These are given in Table 6.1 and Table 6.2.

Table 6.1: **Model variables for crushed unbound material.**

Crushed unbound	k	l	m	n
α_1	0.00	285.95	102.00	0.65
β_1	-0.33	1.13		
b or α_2	247.96	1473.60	44.28	0.26
α_3	118.30	-7.21		
β_3	0.31	0.72		

Table 6.2: **Model variables for natural unbound material.**

Natural unbound	k	l	m	n
α_1	27.70	386.47	44.69	0.54
β_1	-0.82	-0.07		
b or α_2	79.28	516.15	12.70	0.14
α_3	90.62	-8.84		
β_3	0.38	-0.09		

Parametric analysis of the two models indicated that the saturation and stress dependency of the materials are realistically reflected by the models.

As stated in the objectives of this thesis, linking of basic material properties to the model was explored further. With the limited set of results, this was not successful. An alternative link between modulus and basic material properties was explored. The use of predictive statistical distributions based on the Weibull and Log-normal distributions were evaluated as these distributions do not allow non-negative results, which is in line with observed modulus values. Selected basic material properties were used to develop equations that estimate the statistical parameters used to calculate the aforementioned

distributions. Only GM, LS, MDD and OMC were used. Equation 6.1 to 6.3 and Table 6.3 constitutes the predictive statistical distributions.

Weibull:

$$f(x) = \frac{\alpha}{\beta}\left(\frac{x}{\beta}\right)^{\alpha-1} e^{\left(-\left(\frac{x}{\beta}\right)^{\alpha}\right)} \qquad \text{or} \qquad f(x) = \frac{\alpha}{\beta}\left(\frac{x-\gamma}{\beta}\right)^{\alpha-1} e^{\left(-\left(\frac{x-\gamma}{\beta}\right)^{\alpha}\right)} \qquad (6.1)$$

Log-normal:

$$f(x) = \frac{e^{\left(-\frac{1}{2}\left(\frac{lnx-\mu}{\sigma}\right)^{2}\right)}}{x\cdot\sigma\cdot\sqrt{2\pi}} \qquad \text{or} \qquad f(x) = \frac{e^{\left(-\frac{1}{2}\left(\frac{ln(x-\gamma)-\mu}{\sigma}\right)^{2}\right)}}{(x-\gamma)\cdot\sigma\cdot\sqrt{2\pi}} \qquad (6.2)$$

Statistical parameter $(\alpha / \beta / \gamma / \sigma / \mu / \gamma) = A_1 \cdot GM + A_2 \cdot LS + A_3 \cdot MDD + A_4 \cdot OMC$ (6.3)

Table 6.3: **Constants for equations to determine statistical input for distributions.**

Weibull	α	β	(3P) α	(3P) β	(3P) γ
GM (A₁)	-10.11	412.57	-1.19	515.84	-29.72
LS (A₂)	69.74	-3959.19	10.78	-1072.93	4495.32
MDD (A₃)	1.39E-02	-0.03	0.00	-0.33	0.15
OMC (A₄)	-74.65	1753.89	-27.20	175.40	-1497.32
Log-normal	α	β	(3P) α	(3P) β	(3P) γ
GM (A₁)	0.16	0.01	-0.32	3.16	-4435.55
LS (A₂)	-2.34	8.84	-1.78	5.83	2025.56
MDD (A₃)	-7.29E-05	2.48E-03	3.64E-04	-4.83E-04	3.92
OMC (A₄)	1.74	6.06	1.65	11.52	-5251.08

Verification of the developed equations indicated that the results obtained are not counter-intuitive. From the predictive statistical distributions, a family of distributions can be developed over a range of moisture conditions, which gives an indication of the modulus values that can be expected at various moisture conditions. Although the application of the predictive statistical distributions did not yield an exceptionally accurate estimation of the data, it was shown to be more realistic than the ranges used in practice.

6.2 RECOMMENDATIONS

Both the MEPDG (NCHRP, 2004) and SAPDM (Theyse, 2006) has adopted the concept of levels of design according to the level of accuracy in pavement design that is required. To tie in with this concept it is recommended that for a Level 1 investigation, resilient modulus tri-axial tests as described in this thesis on bulk material samples should be conducted and the results used in the pavement design. For Level 2 (where a higher level of uncertainty is still acceptable) the simple saturation and stress dependent cord modulus model can be utilised. It is recommended that a database of resilient modulus

tri-axial results of various bulk material samples from all areas of South Africa should be populated and the saturation and stress dependent cord modulus model calibrated for each material in the database. From this database engineers can select sub-variable constants calibrated on material similar to material on site and by utilising the model, modulus values can be calculated. The simple saturation and stress dependent cord modulus model calibrated for crushed and natural unbound material can also be utilised for Level 2 analysis. The calibration of the two versions of the model can be refined by input from future research or data accumulated in the proposed database. For Level 3 analysis, the use of the predictive statistical distribution method is proposed. However, it is recommended that this method should be refined by results from future research.

The following recommendations are presented:

1. Future South African research in this field should adopt similar static and resilient modulus tri-axial testing protocols as described in this thesis, as this protocol is also used in the research conducted under the SAPDM Project;
2. Although expensive and time consuming, future research should attempt to include a wider range of bulk material samples which are moisture susceptible;
3. Further to the recommendation above, future research projects should attempt to include a wider range of volumetric density and moisture levels. Alternatively, future research projects can build on the results reported in this thesis and test at volumetric density and moisture levels not covered in this thesis to fill in the gaps;
4. A database of basic engineering properties, static and resilient modulus tri-axial test results should be built up, incorporating more bulk material samples that can be utilised to refine the current model, used to refine the regression equations linking resilient behaviour to basic properties and to be utilised by practitioners and researchers.

7   REFERENCES

Aggregate and Sand Producers Association of Southern Africa (ASPASA) (2006). http://www.aspasa.co.za web home page assessed on 23 April 2010.

American Association for Highway Transportation Officials (AASHTO) (1928), M 145 or ASTM D3282, U.S.A.

American Association for Highway Transportation Officials (AASHTO) T-307, (2005). '*Standard method of test for determining the resilient modulus of soils and aggregate materials*', U.S.A.

Anochie-Boateng, J.K. (2007). '*Advance testing and characterisation of transportation soils and bituminous sands*', PhD dissertation, University of Illinois, Urbana, Illinois, USA.

Anochie-Boateng, J.; Paige-Green, P. and Mgangira, M.B. (2009). '*Evaluation of test methods for estimating resilient modulus of modules of pavement geomaterials*', Paper presented at the 28th Annual Southern African Transport Conference 6 - 9 July 2009, CSIR International Convention Centre, Pretoria, South Africa.

Austin, A. (2009). '*Fundamental characterisation of unbound base course materials under cyclic loading*', Masters dissertation, Louisiana State University & Agricultural and Mechanical College, Louisiana, USA.

Baloyi, R. (2006).'*Producers of sand and aggregate in the Republic of South Africa*', Directorate: Mineral Economics, Directory D14/2006, Department Minerals and Energy, Pretoria, RSA.

Bejarano, M.O. and Thompson, M.R. (1999). '*Subgrade soil evaluation for the design of airport flexible pavements'*. Technical Report, DOT 95-C-001, Federal Aviation Administration, U.S.A.

Brown, S.F. and Pappin, J.W. (1981). '*Analysis of pavements with granular bases*', Transportation Research Record 810, Transportation Research Board, Washington, D.C., USA.

Cameron, A.C., Windmeijer, F.A.G. (1997). '*An R-squared measure of goodness of fit for some common non-linear regression models*', Journal of Econometrics, Volume 77, Issue 2, April 1997, pp. 329-342.

Cary, C.E. and Zapata, C.E. (2010). '*Resilient modulus testing for unsaturated unbound materials*', Proceedings of the 89th Annual Meeting of the Transportation Research Board, January 2010, Washington, D.C., USA.

Cary, C.E. and Zapata, C.E. (2010). '*Comparative study of a mechanistic resilient modulus predictive equation for unbound materials*', Proceedings of the 2nd International Conference on Transport Infrastructure, 4-6 August 2010, Sao Paulo, Brazil.

Constantino, D. (2012). '*Statistics: First-quarter aggregate production up 9.7 percent*', Article published by North Coast Media electronically, 19 June 2012, on web page http://www.pitandquarry.com/economics/statistics/news/first-quarter-aggregate-production-97-percent-3598

Correia, A.G. and De Almeida, J.R. (1998). '*Mechanical behaviour of unbound granular materials for modelling of flexible pavements*', p 1211-1220, Proceedings of the Fifth International Conference on the Bearing Capacity of Roads and Airfields, The Norwegian University of Science and Technology, Trondheim, Norway.

Craciun, O. (2009). '*Matric suction response of unbound granular base material subjected to cyclic loading*', PhD thesis, University of New South Wales, Australia.

Craig, R.F. (1997). '*Soil mechanics*', Sixth Edition, E & FN Spon, London & New York.

Dawson, A. (2009). '*Water in road structures – Movement, drainage and effects*', Geotechnical, Geological and Earthquake Engineering, Volume 5, Springer Science & Business Media B.V. (Based on WATMOVE study reported as COST Action No. 351).

De Beer, M and Maina, J.W. (2008). '*Some fundamental definitions of the elastic parameters for homogeneous isotropic linear elastic materials in pavement design and analysis*', Proceedings of the 27th Southern African Transport Conference (SATC), July 2008, Pretoria, RSA.

Draper, N.R. and Smith, H. (1998). '*Applied regression analysis*', 3rd Edition, Wiley-Interscience, New York, U.S.A.

Ekblad, J. (2006). '*Influence of water on coarse granular road material properties*', KTH, Stockholm, ISSN 1650-867x.

Emery, S.J. (1985). '*Prediction of moisture content for use in pavement design*', PhD Thesis, University of Witwatersrand, Johannesburg, RSA.

Everitt, B.S. (2002). '*Cambridge dictionary of statistics*', 2nd Edition, Cambridge University Press, U.K.

Fredlund, D.G. and Rahardjo, H. (1993). '*Soil mechanics for unsaturated soils*', John Wiley & Sons, Inc.

George, K.P. (2004). '*Prediction of resilient modulus form soil index properties*', Final Report, Mississippi Department of Transportation, Research Division, Jackson, Mississippi, USA.

Gere, J.M. (2001). '*Mechanics of materials*', Fifth Edition, Brooks/Cole, USA

Gudishala, R. (2004). '*Development of resilient modulus prediction models for base and subgrade pavement layers from in situ devices test results*', Masters dissertation, Louisiana State University & Agricultural and Mechanical College, Louisiana, USA.

Hicks, R.G. and Monismith, C.L., (1971). '*Factors influencing the resilient properties of granular materials*', Transportation Research Record 345, Transportation Research Board, Washington, D.C., USA.

Jacobsz, S.W. and Day, P. (2008). '*Are we getting what we pay for from geotechnical laboratories*', SAICE Civil Engineering Magazine, Volume 16, Number 4, April, pp. 8-11, South African Institute for Civil Engineering (SAICE), Johannesburg, RSA.

Jooste, F.J., Long, F.M. and Hefer, A.O. (2007). '*A Method for Consistent Classification of Materials for Pavement Rehabilitation and Design*', Technical Memorandum. Modelling and Analysis Systems, Cullinan, South Africa. SABITA/Gauteng Department of Public Transport, Roads and Works, Pretoria, 2007. (GDPTRW report number: CSIR/BE/IE/ER/2007/0005/B).

Kancherla, A. (2004). '*Resilient modulus and permanent deformation testing of unbound granular materials*', Masters Dissertation, Texas A&M University, Austin, Texas, USA.

Kim, M. (2007). '*Three-dimensional finite element analysis of flexible pavements considering nonlinear pavement foundation behaviour*', PhD Thesis, University of Illinois, Urbana, Illinois, USA.

Kwon, J.; Tutumluer, E.; Al-Qadi, I.L. & Anochie-Boateng, J. (2007). '*Geomaterial characterizations of full scale pavement test sections for mechanistic analysis and design*', proceedings of the Geo-Denver 2007: New Peaks in Geotechnics; Congress, Denver, USA, 18-21 February 2007, pp. 10.

Lekarp, F., Isacsson, U. & Dawson, A. (2000). '*State of the art I: Resilient response of unbound aggregates*', Journal of Transportation Engineering, Volume 126, No. 1, January/February, 2000, pp 66-75.

National Cooperative Highway Research Program (NCHRP) (2004). '*Project 1-37A: Guide for Mechanistic-Empirical Design of New and Rehabilitated Pavement Structures*', National Cooperative Highway Research Program, Transportation Research Board, of the National Research Council, USA

National Cooperative Highway Research Program (NCHRP), (2004). '*Project 1-28A: Recommended standard method for routine resilient modulus testing of unbound granular base/subbase materials and*

subgrade soils', NCHRP Research Results Digest No 285, Laboratory determination of resilient modulus for flexible pavement. January 2004, U.S.A.

Prozzi J.A. and Madanat S.M (2002). '*A non-linear model for predicting pavement serviceability*', Proceedings of the ASCE Conference on Application of Advanced Technology in Transportation, Boston, Massachusetts, USA.

Puppala, A.J. (2008). '*Estimating stiffness of subgrade and unbound materials for pavement design*', NCHRP Synthesis 382, Transportation Research Board, U.S.A.

Savage, P.F. (2006). '*Insights into pavement material density and strength*', Proceedings of the 25th Southern African Transport Conference (SATC), July 2006, Pretoria, RSA.

Seed, H.C., Chan, C.K. and Lee, C.E (1962). '*Resilient characteristics of subgrade soils and their relation to fatigue failures in asphalt pavements*', Proceedings of International Conference on the Structural Design of Asphalt Pavements, University of Michigan, U.S.A.

Steyn, W.J. vdM. (2001). '*Vehicle-Pavement interaction for pavement design*', PhD thesis, University of Pretoria, Pretoria, RSA.

Steyn, W.J. vdM. (2007). '*Applications of observational techniques in pavement engineering*', Proceedings of Southern Africa Transportation Conference (SATC), July 2007, Pretoria, RSA.

Steyn, W.J. vdM. and Paige-Green, P. (2009). '*Evaluation of issues around road materials for sustainable transport*', Proceedings of 28th Southern Africa Transportation Conference (SATC), 6 – 9 July 2009, Pretoria, RSA.

Steyn, W.J.vdM. (2011). '*Vehicle Dynamics – Development of statistical distributions for selected Rigid vehicle case studies*', Report no. SANRAL/SAPDM/A-4/2011-01, University of Pretoria, Pretoria, RSA.

TG 2, Appendix A (2009). '*Technical Guideline: Bitumen Stabilised Materials*', Second Edition, May 2009, Asphalt Academy, Pretoria, RSA.

Theyse, H.L, De Beer, M. and Rust, F.C. (1996). '*Overview of the South African Mechanistic Pavement Design Analysis Method*', In Transportation Research Record: Journal of the Transportation Research Board, No 1539, Transportation Research Board of the National Academies, Washington, D.C., 2003, pp 6-17.

Theyse, H.L (2006). '*An improved pavement design method for Southern Africa: Research and development framework*', Report No. CSIR/BE/IE/IR/2006/0042/B, Pretoria, CSIR Built Environment Unit, RSA.

Theyse, H.L. (2006). '*The suction pressure, yield strength and effective stress of partially saturated unbound granular pavement layers*', CSIR Built Environment, Pretoria, RSA.

Theyse, H.L. (2008). '*A mechanistic-empirical design model for unbound granular pavement layers*', PhD dissertation, University of Johannesburg, Johannesburg, RSA.

Theyse, H.L. (2008). '*The revision of the South African pavement design method (SAPDM): Detail planning for project SAPDM/B1-a*', Technical note PMC/TN/2008-007, 6 November 2008, RSA.

Theyse, H L (2009). '*Soil-water characteristic curves and suction pressure models for partially saturated unbound material*', Report No SANRAL/SAPDM/D2/2008-01, Pretoria: Pavement Modelling Corporation, RSA.

Theyse, H L. (2009). '*Resilient modulus models for partially saturated unbound granular material*'. Pavement Modelling Corporation, Pretoria, South Africa. (Report Number: SANRAL/SAPDM/B1A-2009-01).

Theyse, H.L. and Kannemeyer, L. (2010). '*New directions in the design of unbound granular layers in road pavements*', SAICE Civil Engineering, Volume 18, No. 8, September 2010, RSA.

Theyse, H.L. (2012). '*Stress-dependent Resilient Response Model Formulation for Unbound Granular Material based on Repeated Load Tri-axial Test Results*', Pavement Modelling Corporation, Pretoria, RSA. (Report Number: SANRAL/SAPDM/B1A-2012-01)

Theyse, H.L. (2012). Personal communication on 22 August 2012.

Thom, N.H. and Brown, S.F. (1987). '*Effect of moisture on the structural performance of a crushed-limestone road base*', Transportation Research Record, 1121, Transportation Research Board, Washington, D.C., USA.

TMH 1 (1985). '*Technical Methods Highways 1 : Standard test methods for roadbuilding materials*', Department of Transport, Pretoria, RSA.

Transportation Research Board (TRB), 1990. '*State of the art report 8: Guide to earthwork construction*', Appendix E, p 14, National Research Council, Washington, D.C., USA.

TRH 14 (1985). '*TRH 14 : Guidelines for road construction materials*', Department of Transport, Pretoria, South Africa.

TRH 4 (1996). '*Draft TRH 4 : Structural design of flexible pavements for interurban and rural roads*', Department of Transport, Pretoria, South Africa.

Uzan, J. (1985). '*Characterisation of granular material*', Transportation Research Record 1022, Transportation Research Board, Washington D.C., USA.

Van As, S.C. (2003). '*Applied statistics for Civil Engineers*', B.Eng. Honours course material, University of Pretoria, Pretoria, RSA.

Van Aswegen, E and Theyse, H L. (2011). '*Resilient response testing – Unbound material*'. Ndodana Consulting Engineers and Pavement Modelling Corporation, Pretoria, South Africa. (Report Number: SANRAL/SAPDM/B1A-2011-04).

Van Aswegen, E. and Steyn, W.J.vdM. (2012). '*Statistical Modeling of Resilient Behavior of Unbound Granular Material*'. Peer-reviewed paper presented at the 91st TRB meeting, Washington D.C., USA.

Van Heerden, J.H.F. (2002). '*Direct measurement of pore fluid suction in gold mine tailings*', Masters Dissertation, University of Pretoria, Pretoria, RSA.

Visser, A.T. (1981). '*An evaluation of unpaved road performance and maintenance*', PhD Thesis, University of Texas at Austin, May 1981.

Visser, A.T., Queiroz, C and Hudson, W.R. (1983). '*Study of resilient characteristics of tropical soils for use in low-volume pavement design*', TRB 898, p 133-140, Washington, D.C, 1983.

Yeh, S.T. and Su, C.H. (1989). '*Resilient properties of Colorado soils*', Final report, report no CDOH-DH-SM-89-9, Colorado Dept. of Highways in corporation with FWHA, December 1989, USA.

Yoder, E.J. and Witczak, M.K., (1975). '*Principles of pavement design*', 2nd Edition, John Wiley and Sons.

Zapata, C.E. and Houston, W.N. (2008) '*Calibration and validation of the Enhanced Integrated Climatic Model for pavement design*', NCHRP Report 602, Transportation Research Board, Washington, D.C, USA.

APPENDIX A

TABLE OF CONTENT

LIST OF TABLES

LIST OF FIGURES

A. SOUTH AFRICAN PAVEMENT DESIGN METHOD (SAPDM) PROJECT OVERVIEW

A.1 BACKGROUND

There is currently a comprehensive project underway which is jointly sponsored by the South African National Roads Agency Ltd (SANRAL) and the Council for Science and Industrial Research (CSIR). The project entails the revision of the South African Mechanistic-Empirical Design Method (SAMEDM) which has been one of the primary pavement design tools in South Africa since the early 1970s (SAPDM, 2009). Some improvements were made to the original SAMEDM through the years, but the main components of the SAMEDM were still based on research conducted during the 1970s and 1980s. In May 2005 a workgroup was appointed to initiate the revision of the SAMEDM as it stood at that time (Theyse, 2006).

The focus of the South African Pavement Design Method (SAPDM, as opposed to the SAMEDM), is on improving the structural design model which forms part of the overall pavement design process. Two alternatives will be provided for the structural design model, a Pavement Performance based Information System (PPIS) that uses a Pavement Number (PN) approach and the improved Mechanistic-Empirical (ME) model (Theyse, 2006).

The overall pavement design process will be an iterative one, consisting of input from a traffic volume and axle load -, contact stress -, materials -, spatial and time variation information system. For example, the traffic volume and axle load information system will incorporate traffic volumes and axle load histograms which may be used by the design engineer for a specific project to generate traffic data where it is lacking or incorporate the effect of variability into the analysis (Theyse, 2006).

The functional elements of the design system will consist of three sub-systems, namely:
1. A project level design investigation system where available network level data will be combined with data collected during the design investigation to classify the condition of the pavement, the materials in the existing pavement structure as well as other sources and to derive the inputs required by the design process;
2. A recursive performance simulation system that models functional and structural distress and specifies interventions based on the type of pavement and deterioration of the pavement. This system will allow for the use of two alternative pavement models, the Pavement Number (PN) model the Mechanistic-Empirical (ME) model; and
3. A cost-benefit analysis system assessing different life-cycle strategies (Theyse, 2006).

Figure A.1 illustrate the iterative design process in terms of the functional elements described above in number 1 and 2. Figure A.2 illustrates the complete process.
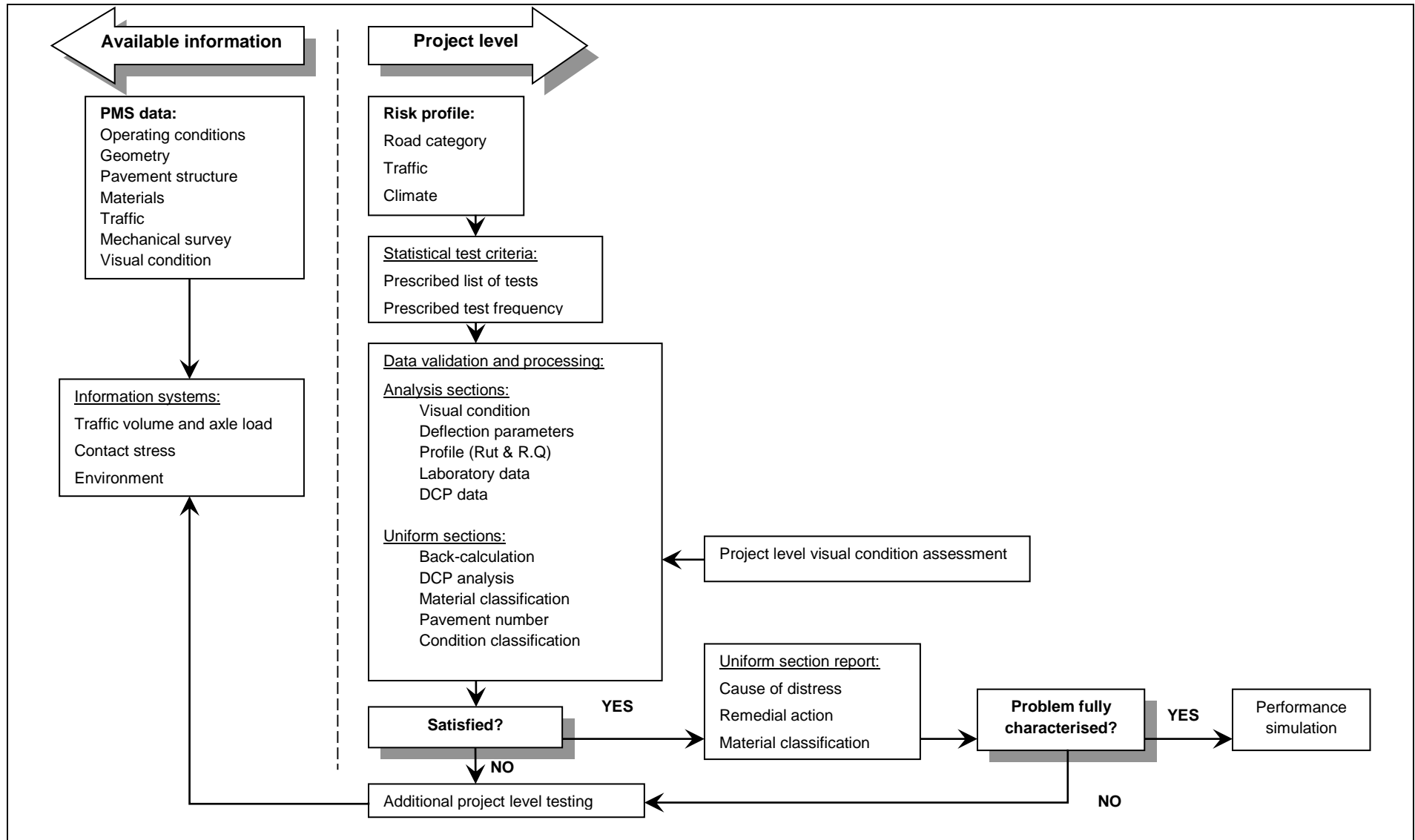
Figure A.1: Iterative design investigation process proposed in the SAPDM (Theyse, 2006).
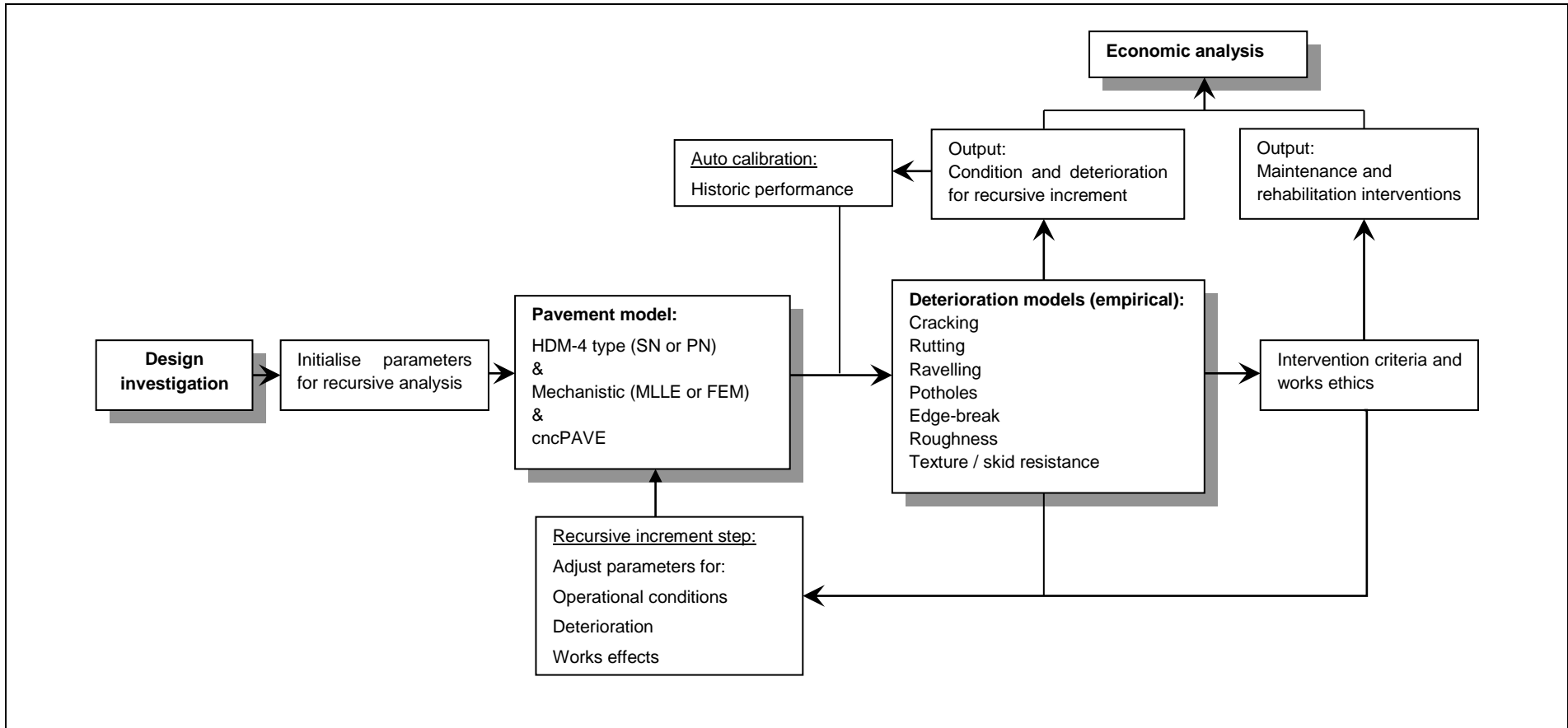
Figure A.2:   **Performance simulation process proposed in SAPDM (Theyse, 2006).**

A-3

The SAPDM project was divided into various research areas which require revision. Table A.1 summarise the research areas, project titles and project leaders (Theyse, 2006). It is clear from the list of research areas that the scope of this project is quite comprehensive, investigating every aspect possible. The list of project leaders consists of knowledgeable and well respected researchers in the field of pavement engineering in South Africa.

The project '*Material resilient response models for unbound material*' (bold in Table A.1) is of special interest to this study, since data collected in that project, will be utilised in this study.

Table A.1: **Summary of SAPDM focus areas.**

Research area	Project title	Project no.	Project leader
Integration project	Integration of design subsystems and methodologies into an integrated design system	SAPDM/ILP	Dr H L Theyse
Pavement Performance Information System	The development and population of a pavement performance information system	SAPDM/PPIS	Dr A Hefer
Traffic demand analysis	A tyre-pavement contact stress information system	SAPDM/A-1	Prof M de Beer
	A traffic volume and axle load information system	SAPDM/A-2	Dr S C van As
	Guidelines on conducting traffic surveys and processing the data for the purpose of pavement design	SAPDM/A-3	Dr S C van As
	The effects of vehicle dynamics and vehicle speed on traffic input to the design method	SAPDM/A-4	Prof W Steyn
Material resilient response models	**Resilient response models for unbound material**	**SAPDM/B-1a**	**Dr H L Theyse**
	Resilient response models for bituminous material	SAPDM/B-1b	Mr B Verhaeghe
	Resilient response models for stabilised material	SAPDM/B-1c	Dr M Mgangira
	Agreement between different methods of calibrating material response models, especially linear-elastic material models.	SAPDM/B-2	Dr J Maina
	Documentation on material testing, the interpretation of results, the derivation of design inputs and model calibration.	SAPDM/B-3	Dr J Maina
Primary pavement response models	Improved modelling of the complex tyre-pavement contact patch in terms of stress magnitude and contact area shape	SAPDM/C-1	Dr J Maina
	A benchmark of measured stresses and strains collected on a variety of pavements for various loading conditions	SAPDM/C-2	Prof W Steyn
	Improved modelling of the primary resilient response of pavement systems	SAPDM/C-3	Dr H L Theyse
Damage models calibrated for the effects of field variables and traffic loads	Improved damage models for bituminous material	SAPDM/D-1	Mr B Verhaeghe
	Improved damage models for unbound material including the pavement subgrade	SAPDM/D-2	Dr H L Theyse
	Improved damage models for stabilised material	SAPDM/D-3	Dr H L Theyse
Cross-cutting topics	An environmental and field variables information system incorporating the effects of spatial and	SAPDM/E-1	Dr P Paige-Green

Research area	Project title	Project no.	Project leader
	time variation		
	Guidelines on the collection and interpretation of statistical information	SAPDM/E-2	Dr S C van As
	Probabilistic, linear recursive and non-linear recursive simulation	SAPDM/E-3	Dr H L Theyse
	A design input information system for pavement materials	SAPDM/B-4	Dr H L Theyse

A.2   SCOPE OF SAPDM/B-1A

The following section summarise what was described in more detail in PMC/TN/2008-007 (Theyse, 2008) to provide further background to the reader on how SAPDM/B-1a relates to other SAPDM projects.

The aim of SAPDM/B1-a is to develop a predictive model for the resilient modulus of unbound granular material based on resilient modulus testing. Under Project SAPDM/B-3, the CSIR and University of Stellenbosch (US) will produce a single test protocol for resilient modulus testing based on various other recognized protocols. Resilient modulus testing under this project will be done according to the aforementioned protocol.

Project SAPDM/B-2 has to compare the stiffness results of different pavement materials using different test methods such as those determined from the Falling Weight Deflectometer (FWD), Multi Depth Deflections (MDD) and seismic testing amongst others. Sites at which tests will be conducted will be identified in coordination with Project SAPDM/E-1, where instrumentation will be installed and material samples for Project SAMPD/B-1a taken. Laboratory stiffness results from the materials sampled and tested under Project SAMPD/B-1a will complete the stiffness data of field and laboratory tests which will be directly compared under Project SAPDM/B-2. At the same time, the selection of unbound material types should be such that a sufficient variety of materials are tested to develop a predictive laboratory based stiffness model.

Within the scope of the SAPDM/B1-a project is:
- Investigate the effect of a wide range of moisture and suction pressure on resilient response of unmodified unbound granular material by conducting tri-axial tests;
- Calibrate the identified resilient response model with the tri-axial test results to more accurate and confidently model resilient response of unbound granular material;

It falls outside the scope of work to analyse:
- The resilient response of modified granular material, since the combinations of modifiers and application rates will be investigated under project SAPDM/B-b and c;

A.3 ACTIVITIES

Most of the activities undertaken as part of this thesis also form part of the SAPDM/B-1a, '*Resilient response models for unbound material*' project. The student was responsible for the management and execution of the SAPDM/B-1a project.

The following activities were undertaken as part of the Project:

- The selection of sites to be sampled for unbound granular material was done in conjunction with Dr Theyse (Pavement Modelling Corporation), Dr Paige-Green (CSIR) and Dr Maina (CSIR), since the tests sites are linked to projects SAPDM/E-1 and SAPDM/B-2 as well, and the results from these three projects will supplement each other. For this project for example, insitu moisture and density results could be obtained from SAPDM/E-1 which instrumented each site.
    - o Site selection was required for both project B-1a and this project. The student was also responsible for project SAPDM/B-1a, liaising between the aforementioned projects to obtain the unbound granular material samples;
- The student was responsible to organise and oversee a total of 9 bulk material samples which processed by the CSIR laboratory. This entailed that the student was present at each site where samples were collected, advising on which layers of the pavement structure to sample;
- A series of tests was conducted at the CSIR laboratory on the sampled material including grading, Atterberg limits, Apparent Relative Density (ARD) determination, Bulk Relative Density (BRD) determination, Optimum Moisture Content (OMC) and Maximum Dry Density (MDD) utilising Modified AASHTO and vibratory compaction methods, California Bearing Ratio (CBR) tests and durability mill tests. The student had to analyse these results critically, for it was the basis of the experimental design prepared for the shear and resilient modulus tri-axial tests;
- Shear strength tri-axial tests, as well as resilient modulus tri-axial tests, was performed at the CSIR laboratory at two density levels and three saturation levels for each unbound granular material sampled. The student was responsible for detailed briefs for the laboratory personnel to ensure the required density and saturation level is obtained for each specific sample as per the experimental design done under the guidance of Dr Theyse. The student was also responsible to ensure that all relevant measurements were taken as and when required and documented;
- The two aforementioned activities required the student to be present at the laboratory for extended periods to ensure that results are correct and tests are conducted according to the detailed briefs;
- The student was responsible for basic data processing of all test results,
- The student was responsible for data presentation and report writing;

A.4 STATUS

At the time of submission of this thesis, the SAPDM/B-1a project was still underway. Interim project reports were submitted and are listed in Table A.2. No interim reports are publicly available and is only distributed to the researchers involved in the SAPDM project (listed in Table A.1).

Table A.2:   Summary of SAPDM/B-1a interim reports.

Report number	Report title	Author	Date
SANRAL/SAPDM/B-1a/2009-01	Resilient modulus models for partially saturated unbound granular material	H.L. Theyse	Jan. 2009
SANRAL/SAPDM/B-1a/2009-03	Density estimates for unbound granular material	H.L. Theyse	Nov. 2010
SANRAL/SAPDM/B-1a/2011-02	Initial subgrade stiffness and stiffness reduction under repeated loading	H.L. Theyse	Mar. 2011
SANRAL/SAPDM/B-1a/2011-03	Tangent and cord modulus models for unbound granular material based on monotonic loading tri-axial test results	H.L. Theyse	May 2011
SANRAL/SAPDM/B-1a/2011-04	Resilient response testing – Unbound material	E. van Aswegen H.L. Theyse	Oct. 2011
SANRAL/SAPDM/B-1a/2012-01	Stress-dependent resilient response model formulation for unbound granular material based on repeated load tri-axial test results	H.L. Theyse	Apr. 2012

Six bulk material samples have been sampled, processed and all tests completed. The three outstanding bulk material samples will be obtained to the end of 2012. Processing and testing will commence thereafter. The student will be responsible for the data processing and presentation of these results, as well as final reporting of the SAPDM/B-1a projects results.

SANRAL and CSIR will publish the results from each focus area once the SAPDM project is completed as a whole.

A.5 REFERENCES

Theyse, H.L. (2006). '*An improved pavement design method for Southern Africa: Research and development framework*', Report no. CSIR/BE/IE/IR/2006/0042/B, CSIR Built Environment Unit, Pretoria, RSA.

Theyse, H.L. (2008). '*The revision of the South African pavement design method (SAPDM): Detail planning for project SAPDM/B1-a*', Technical note PMC/TN/2008-007, Pavement Modelling corporation, Pretoria, RSA.

APPENDIX B

TABLE OF CONTENT

LIST OF FIGURES

B. RESILIENT RESPONSE MODELS

B.1 THEORY OF ELASTICITY

As mentioned, Young's modulus or Modulus of elasticity (E) and Poisson's ratio (ν) are the two constants used to define the elastic properties of a material. For granular material Young's modulus or Modulus of elasticity (E) has been replaced with Resilient modulus (M_R) to indicate the non-linearity of the behaviour, i.e. dependence on stress level (Lekarp *et al.*, 2000). Figure B.1 illustrates the stresses in a pavement structure beneath a rolling wheel. In unbound layers, the vertical and horizontal stresses are positive, whereas the shear stress is reversed as the load passes, thus causing a rotation of the principal stress axes (Lekarp *et al.*, 2000). The strain which develops as a result of a rolling wheel can be defined as a recoverable (resilient) deformation and a residual (permanent) deformation, which is illustrated in Figure B.2 (Lekarp *et al.*, 2000).
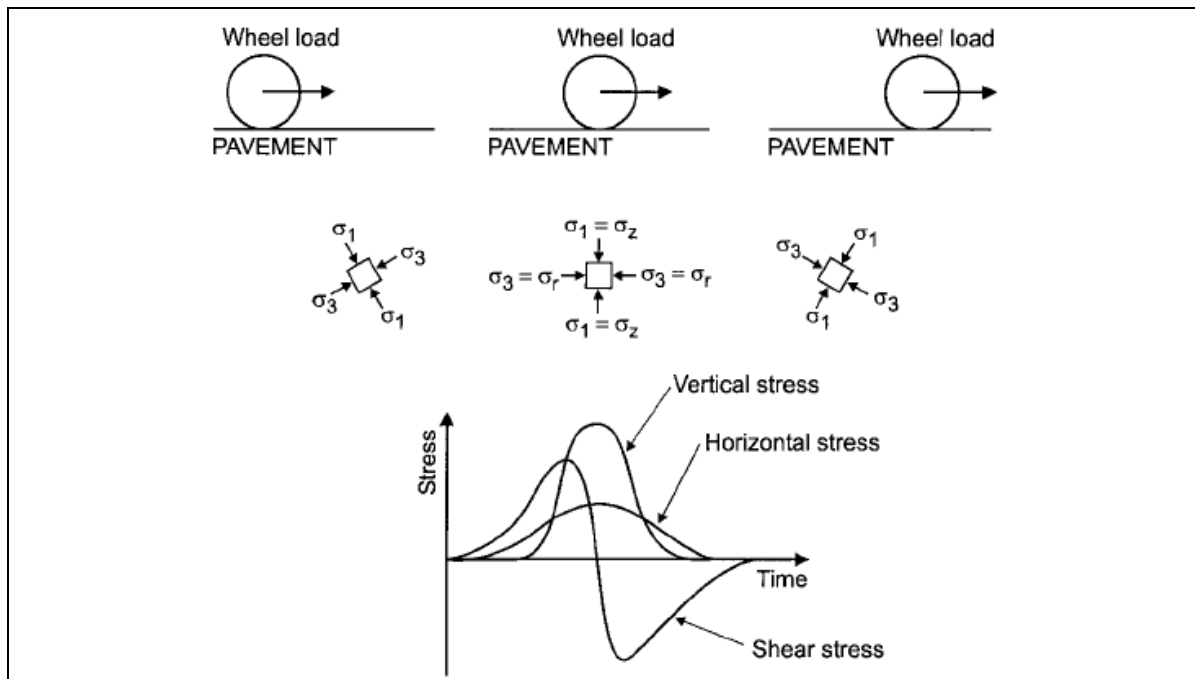
Figure B.1:   Stresses beneath a rolling wheel load (Lekarp *et al.*, 2000).
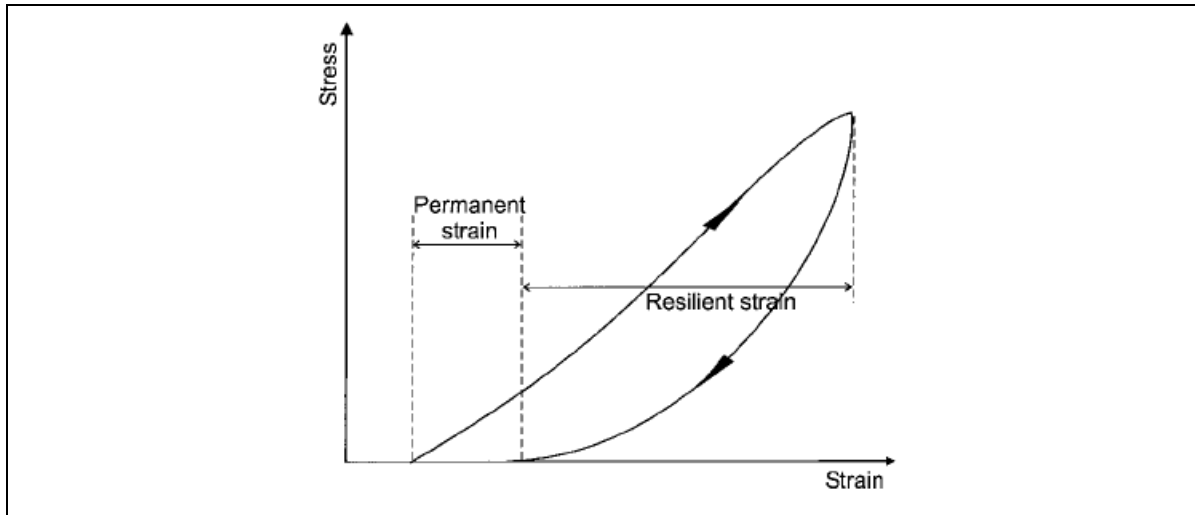
Figure B.2: **Strains in granular materials during one cycle of load application (Lekarp et al., 2000).**

The resilient modulus is defined as follows for a repeated load triaxial test with constant confining pressure (Lekarp *et al.*, 2000):

$$M_R = \frac{\Delta(\sigma_1 - \sigma_3)}{\varepsilon_{1,r}}$$ (B.1)

Where

M_R = resilient modulus;

Δ = 'change in';

$\sigma_1; \sigma_3$ = major and minor principal stress;

$\varepsilon_{1,r}; \varepsilon_{3,r}$ = recoverable axial and horizontal strain.

The same method of calculation as in equation A.1 would apply to an isotropic, linear-elastic material under uni-axial stress conditions. A 3D stress-strain relationship, according to Hooke's Law, is used for an isotropic, linear-elastic material under cyclic confining pressure and the resilient modulus is derived as follows (Lekarp *et al.*, 2000):

$$M_R = \frac{\Delta(\sigma_1 - \sigma_3)\Delta(\sigma_1 + 2\sigma_3)}{\varepsilon_{1,r}\Delta(\sigma_1 + \sigma_3) - 2\varepsilon_{3,r}\Delta\sigma_3}$$ (B.2)

B.2   MOHR-COULOMB FAILURE CRITERION

This model is a widely known strength definition and is mainly utilised for soil stability analysis in geotechnical engineering (Craig, 1997). The model is defined by equation A.3 and illustrated by Figure B.3 below.

$$\tau_{max} = c + \sigma_n \tan\phi \qquad\qquad\qquad\qquad (B.3)$$

Where

τ_{max} = shear strength;

σ_n = normal stress at failure;

c = cohesion intercept;

$\tan\phi$ = slope of the failure envelope;

ϕ = friction angle.
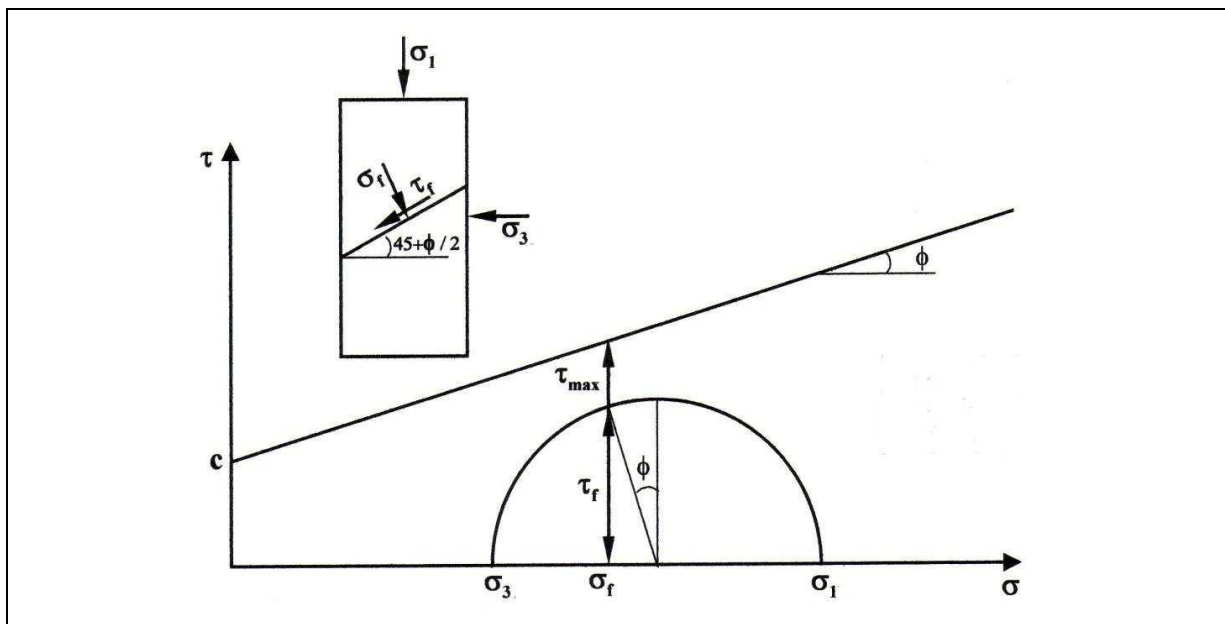
Figure B.3:   **Mohr-Coulomb representation of shear strength and applied stress states (Anochie-Boateng, 2007).**

The Mohr-Coulomb criterion states that the shear stress in a plane at failure is a function of the normal stress in the plane. The failure line is defined by the friction angle and the cohesion. This model is assumes linear elastic and perfectly plastic behaviour of the material until failure occurs (Anochie-Boateng, 2007).

Although this model does not accurately describe the behaviour of granular material, which is stress-dependent, inelastic and non-linear, particularly during dynamic loading, it does address the aspect of shear stress (Anochie-Boateng, 2007).

B.3   CONFINING PRESSURE MODEL

This model is a simple model relating resilient modulus to confining stresses. Researchers (Dunlap, 1963; Monismith *et al.*, 1967 and Seed *et al.*, 1967 as quoted by Kim, 2007 and Lekarp *et al.*, 2000) reported that the resilient modulus increase with increasing confining pressure and is unaffected by the magnitude of repeated deviator stress (deviator stress is defined as $\sigma_d = \sigma_1 - \sigma_3$), provided that the deviator stress does not cause excessive plastic deformation. The following expression was proposed:

$$M_R = K_1(\sigma_3)^{K_2} \qquad \text{or} \qquad M_R = K_1\left(\frac{\sigma_3^{K_2}}{p_0}\right) \tag{B.4}$$

Where

σ_3 = confining pressure;

p_0 = reference pressure, often equal to atmospheric pressure (101,3 kPa)

K_1, K_2 = regression coefficients.

However, this model did not give high correlation coefficients (Kim, 2007). Some variations of the confining pressure model were developed since the 1960's. For example, deviator stress was included into the confining pressure model (Pezo, 1993; Garg and Thompson, 1997 as quoted by Lekarp *et al.*, 2000):

$$M_R = N_1 q^{N_2} \sigma_3^{N_3} \tag{B.5}$$

It was also shown that resilient modulus is dependent on the first invariant of stress and the stress ratio (Johnson *et al.*, 1986 as quoted by Lekarp *et al.*, 2000):

$$M_R = K_1\left(\frac{J_2}{\tau_{oct}}\right)^{K_2} \tag{B.6}$$

And, for routine design and analysis, it was proposed that the resilient modulus be expressed as a function of stress ratio (Lekarp *et al.*, 2000):

$$M_R = K_1\left(\frac{p}{q}\right)^{K_2} \tag{B.7}$$

B.4 K-THETA MODEL

This hyperbolic relationship models resilient modulus as a function of stress, therefore analysing the stress dependence of material stiffness. Various researchers contributed to the development of this model such as Seed *et al.* (1967), Brown and Pell (1967), Hicks (1970) as reported by Lekarp *et al.*, (2000) and Hicks and Monismith (1971). The model is described as simple and extremely useful and is defined as follows (Kim, 2007):

$$M_R = K_1\theta^{K_2} \qquad \text{or} \qquad M_R = K_1\left(\frac{\theta}{p_0}\right)^{K_2} \tag{B.8}$$

Where

θ = bulk stress = $(\sigma_1 + \sigma_2 + \sigma_3)$ or $(\sigma_1 + 2\sigma_3)$ or $(\sigma_d + 3\sigma_3)$ where $\sigma_d = (\sigma_1 - \sigma_3)$ (Kim, 2007 and Theyse, 2007)

p_0 = reference pressure, often equal to atmospheric pressure (101,3 kPa)

K_1, K_2 = regression coefficients

The K-θ model essentially describes stress-stiffening behaviour, as the resilient modulus increase as the minor principle stress (σ_3 = confining pressure in the tri-axial test) or the bulk stress increase (Theyse, 2008). Seed *et al.* (1967) formulated a model combining stress-stiffening and stress-softening behaviour of granular material (Theyse, 2008):

$$M_R = K_1(K_2 - ln\sigma_d)\theta^n \tag{B.9}$$

Where

σ_d = deviator stress = $(\sigma_1 - \sigma_3)$

θ = bulk stress = $(\sigma_1 + \sigma_2 + \sigma_3)$

K_1, K_2, n = regression coefficients

ln = natural logarithm

The K-θ model does have certain shortcomings, such as assuming a constant Poisson's ratio, which is used to calculate radial strain. Research indicated that the model predicts axial strain good, but not radial and volumetric strains and studies have shown that Poisson's ratio is not a constant, but varies depending on applied stresses (Hicks, 1970; Hicks and Monismith, 1971; Brown and Hyde, 1975; Boyce, 1980; Sweere, 1990; Kolisoja, 1997 as quoted by Lekarp *et al.*, 2000). The model is only valid to predict volumetric strains when confining pressure is less than deviator stress (Brown *et al.* 1981 as quoted by Kim, 2007). Additional stress parameters are required, since studies have shown that utilising only the sum of principle stresses is insufficient. Shear stress is neglected, although shear strain or deviator stress impacts on the resilient modulus (Lekarp *et al.*, 2000 and Kim, 2007). The

K-θ model is also not dimensionally satisfied, since the dimension of K is the same as M_R (Nataatmadja, 1989 as quoted by Kim, 2007).

B.5 UZAN AND UNIVERSAL MODELS

Uzan (1985) modified the K-θ model to include shear effects, therefore modelling stress-stiffening and stress-softening behaviour, and is defined as follows:

$$M_R = k_1 \theta^{k_2} \sigma_d^{k_3}$$
(B.10)

This model was later modified by Witczak and Uzan (1992), and in the three-dimensional case, considers the dilation effect that takes place when an element of the material is subjected to a large principal stress ratio, e.g. when large construction equipment moves over soils (Anochie-Boateng, 2007). In the modified model the deviator stress is replaced with the octahedral stress. This was presented as the Universal model:

$$M_R = k_1 \cdot P_a \cdot \left(\frac{\theta}{P_a}\right)^{k_2} \cdot \left(\frac{\tau_{oct}}{P_a}\right)^{k_3}$$
(B.11)

The universal model was shown through a number of studies to be superior to the K-θ model (Lade and Nelson, 1987; Witczak and Uzan, 1988; Kolisoja, 1997 as quoted by Lekarp *et al.*, 2000). However, further studies modified the model to include a failure term (Elliot and Lourdesnathan, 1989) to predict resilient behaviour beyond the static failure condition and the effect of density (Kolisoja, 1997), where density is accounted for by porosity of aggregate (as quoted by Lekarp *et al.*, 2000). Recently, the model was modified to include solidity and saturation of the material (Theyse, 2008). Theyse (2008) also concluded that the variables of the Uzan and universal models, namely θ and τ_{oct} or σ_d are not independent since these are derived from σ_1, σ_2 & σ_3.

B.6 HYPERBOLIC STRESS-STRAIN MODEL

A non-linear tangent modulus model was developed by Kodner (1963) for monotonic tri-axial test results in which the stress-strain response is a function of the initial tangent modulus, axial strain and the ultimate deviator stress, which is defined as follows (Anochie-Boateng, 2007 and Theyse, 2008):

$$\frac{\varepsilon}{\sigma_1 - \sigma_3} = \left[\frac{1}{E_i} + \frac{\varepsilon}{(\sigma_1 - \sigma_3)_u}\right]$$
(B.12)

Where

E_i = initial tangent modulus

$(\sigma_1 - \sigma_3)_u$ = maximum or ultimate stress difference

ε = axial strain

The tangent model is mostly used in geotechnical engineering and not as frequently in pavement engineering (Theyse, 2008). This model is illustrated by Figure B.4 and shows that it can be transformed to a linear model by dividing the axial strain by deviator stress and plotting the result against axial strain. The model parameters may then be obtained directly from the transformed model, with the initial tangent modulus represented by the inverse of the intercept of the transformed model and the ultimate deviator strength of the material represented by the inverse of the slope of the transformed model (Theyse, 2008).
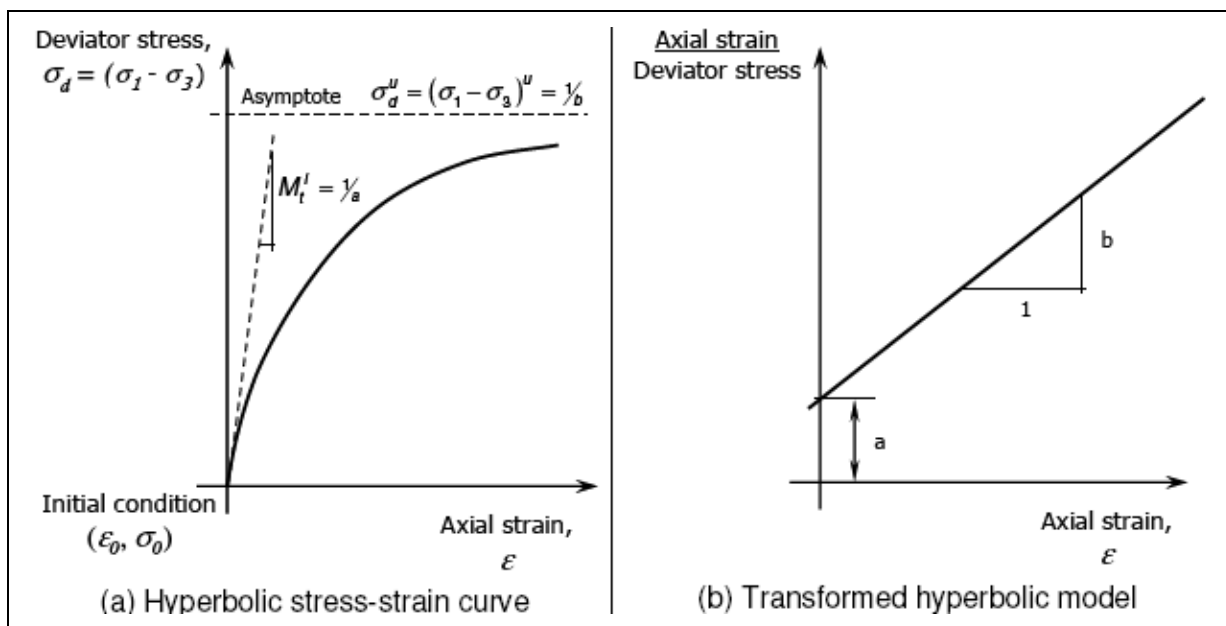
Figure B.4: **Kodner's hyperbolic stress-strain model (Theyse, 2008).**

Duncan and Chang (1970) reported that when this process is applied to experimental data, the ultimate deviator strength normally exceeded the measured failure or yield strength of the material by a small amount (Theyse, 2008). This ultimate stress difference is related to compressive strength, or stress difference at failure, and is defined by a failure ratio:

$$R_f = \frac{(\sigma_1 - \sigma_3)_f}{(\sigma_1 - \sigma_3)_u} \tag{B.13}$$

Variation of $(\sigma_1 - \sigma_3)_f$ with confining pressure, σ_3, can be expressed in terms of the Mohr-Coulomb criterion as follows:

$$(\sigma_1 - \sigma_3)_f = \frac{2c\,cos\emptyset}{1-sin\emptyset} + \frac{2sin\emptyset}{1-sin\emptyset}\sigma_3 \tag{B.14}$$

B-7

Typical values reported for R_f varies between 0.5 - 1.0 and R_f was found to be independent of confining pressure (Anochie-Boateng, 2007).

A stress-dependent hyperbolic model in which Ei varied with σ_3 was developed by Janbu (1963) and was based on primary loading data from tri-axial tests. The model is as defined as follows (Anochie-Boateng, 2007):

$$E_i = kP_a \left(\frac{\sigma_3}{P_a}\right)^n \tag{B.15}$$

Where

P_a = atmospheric pressure expressed in the same units as E_i and σ_3;

k = Young's modulus number;

n = Young's modulus exponent, which determines the rate of variation of E_i with σ_3.

By plotting E_i against σ_3 on a log-log scale as determined from the results of standard laboratory tri-axial tests, the parameters k and n may be derived (Anochie-Boateng, 2007).

Duncan and Chang (1970) derived the hyperbolic model by substituting equation B.13 and B.14 into the derivative of equation 2.x with respect to strain. The model is defined by equation B.12. This model is mainly confining pressure dependent, i.e. stress-dependent (Anochie-Boateng, 2007).

$$E_t = \left[1 - \frac{R_f(1-sin\emptyset)(\sigma_1-\sigma_3)}{2c\,cos\emptyset + 2\sigma_3 sin\emptyset}\right]^2 kP_a \left(\frac{\sigma_3}{P_a}\right)^n \tag{B.16}$$

Another hyperbolic model was proposed by Duncan and Chang (1970) to show the variation of modulus with confining pressure, using the unloading and reloading of tri-axial test data of sand material and is defined as follows (Anochie-Boateng, 2007):

$$E_{ur} = k_{ur}P_a \left(\frac{\sigma_3}{P_a}\right)^n \tag{B.17}$$

Where

E_{ur} = unloading/reloading Young's modulus

k_{ur} = unloading/reloading Young's modulus number

Duncan reported that for stiff soils the value of k_{ur} could be 20% greater than the value of k in equation x.x and for soft soils the value of k_{ur} can be three times as large as k (Anochie-Boateng, 2007). Duncan also proposed that there was a non-linear relationship between the bulk modulus, deviator stress and volumetric strain for tri-axial tests in which the deviator stress $(\sigma_1 - \sigma_3)$ increased from zero at constant confining pressure (Anochie-Boateng, 2007). This is expressed as:

$$K = \left(\frac{\sigma_1 - \sigma_3}{3\varepsilon_v} \right)$$
(B.18)

Where

K   = bulk modulus

ε_v = volumetric strain

The non-linear relationship of equation x.x was expressed in terms of a hyperbolic model:

$$K = k_b P_a \left(\frac{\sigma_3}{P_a} \right)^m$$
(B.19)

Where

k_b = bulk modulus number

m = bulk modulus exponent (between 0 and 1 for most materials)

The hyperbolic models described in this section, however, do not describe the behaviour of soil completely and have certain limitations, namely:

1. The majority of the models do not include volume changes due to shear stress and therefore not predicting deformations accurately;
2. The hyperbolic model is limited to static loading conditions; and
3. The parameters of the hyperbolic model is empirically derived (Anochie-Boateng, 2007).

B.7   SHACKEL'S MODEL

Shackel (1973) developed a model in terms of octahedral shear stress and octahedral normal stress, based on repeated load tri-axial tests on silty-clayey soil. This model was considered one of the early advanced non-linear models, since it was defined in terms of stress invariants. Shackel proposed that he model was valid for both granular and cohesive soils (Kim, 2007). The model is defined as follows:

$$M_R = K_1 \left[\frac{(\tau_{oct})^{K_2}}{(\sigma_{oct})^{K_3}} \right]$$
(B.20)

$$\sigma_{oct} = \frac{1}{3}(\sigma_1 + \sigma_2 + \sigma_3) = \frac{1}{3} I_1$$
(B.21)

$$\tau_{oct} = \frac{1}{3} [(\sigma_1 - \sigma_2)^2 + (\sigma_2 - \sigma_3)^2 + (\sigma_1 - \sigma_3)^2]^{\frac{1}{2}} = \frac{\sqrt{2}}{3}(I_1^2 - 3I_2)^{\frac{1}{2}}$$
(B.22)

Where

K_1 = material regression constants obtained from tri-axial test data;

I_1 = first stress invariant;

I_2 = second stress invariant.

B.8   SHEAR MODULUS AND DAMPING RATIO MODELS

Anochie-Boateng (2007) reported that the standard laboratory cyclic tri-axial and resonant column tests, as described by ASTM D 3999 and ASTM D 4015, can be utilised to determine material properties. From the cyclic tri-axial test, the shear modulus (G) can be indirectly computed from the elastic modulus (E) of the material using an assumed value of Poisson's ratio. The material damping ratio can be determined from the hysteresis loop of deviator stress graphed with axial strain. The slope of the secant line connecting the extreme points on the hysteresis loop is used to define the material's elastic modulus. The material damping ratio (D) is computed as the ratio of the energy dissipated in one cycle to the maximum strain energy stored by the sample. The following equations are utilised in the computational methods described above (Anochie-Boateng, 2007):

$$E = \frac{\sigma_d}{\varepsilon_1}$$
(B.23)

$$\gamma = (1 + \nu)\varepsilon$$
(B.24)

$$G = \frac{E}{2(1+\nu)}$$
(B.25)

$$D = \frac{A_L}{4\pi A_T} \times 100$$
(B.26)

Where

σ_d = deviator stress;

γ = shear strain;

ε_1 = axial strain;

ν = Poisson's ratio;

A_L = area of hysteresis loop which is equivalent to total energy dissipated in one cycle;

A_T = total area representing the maximum strain energy

B.9   BULK-SHEAR MODULUS MODEL (BOYCE'S MODEL)

The influence of mean normal stress to resilient strain was defined by a non-linear mechanistic model based on the secant bulk modulus (K) and the shear modulus (G) by Boyce (1980). These relationships are given as follow (Kim, 2007):

$$K = K_i p^{(1-n)}$$
(B.27)

$$G = G_i p^{(1-n)} \tag{B.28}$$

Where

K_i = initial bulk modulus

G_i = initial shear modulus

n = constant (<1)

This model was updated to satisfy Maxwell's reciprocity theorem (i.e. no net loss of strain energy (Lekarp *et al.*, 2000)). Accordingly, the second order partial derivatives of a stress potential function are independent of the order of differentiation of volumetric and deviatoric stress components (Kim, 2007). The updated model can be defined as follows:

$$K = \frac{K_i p^{(1-n)}}{1 - \beta \left(\frac{q}{p}\right)^2} \tag{B.29}$$

$$G = G_i p^{(1-n)} \tag{B.30}$$

Where

β $= (1-n)\dfrac{K_i}{6G_i}$

p = mean normal stress

q = deviator stress

The volumetric strains and deviatoric strains of the updated model as stated in equation A29 and A.30 are related to the mean normal stress and deviatoric stress as follows:

$$\varepsilon_v = \left(\frac{1}{K_i}\right) p^n \left[1 - \beta \left(\frac{q}{p}\right)^2\right] \tag{B.31}$$

$$\varepsilon_q = \left(\frac{1}{3}G_i\right) p^n \left(\frac{p}{q}\right) \tag{B.32}$$

Where

ε_v = volumetric strain

ε_q = shear strain

Boyce's model is mainly used in Europe (Lekarp *et al.*, 2000). One disadvantage of the model is that it will model the inelastic behaviour of unbound granular material incorrectly, since it is based on the assumption of elasticity (Lekarp *et al.*, 2000). This was overcome by Sweere (1990), who removed the coupling of volumetric and shear strains by the theorem of reciprocity and keeping the relationship between shear and volumetric strains with stresses independent from each other (Lekarp *et al.*, 2000). Sweere achieved this by increasing the material parameters from three in the Boyce's model to four or five independent parameters.

Resilient volumetric and shear strains can be expressed as contours in a p-q stress space (mean normal stress – deviator stress space) from which the magnitudes of strains can be derived. The strains can be derived as the change in contour values from the initial to the final stress state (Lekarp *et al.*, 2000). Contour models was formulated by Brown and Pappin (1981) and the notation associated is with the model is illustrated in Figure B.5.
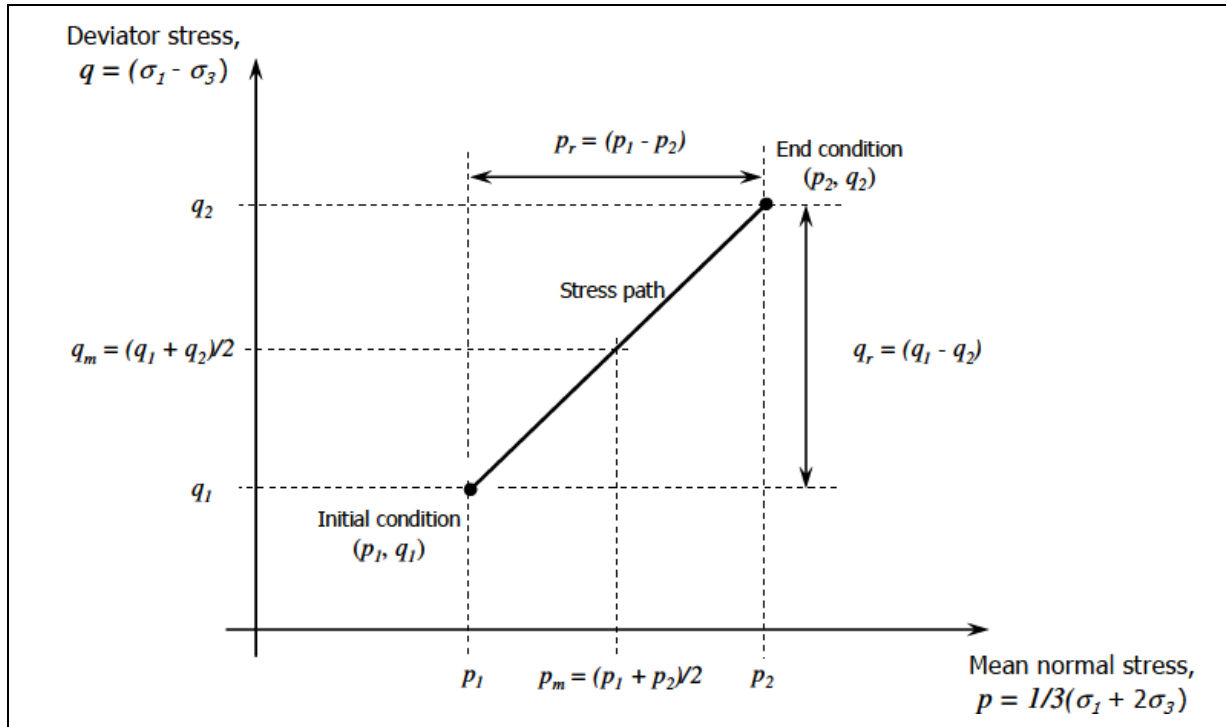
Figure B.5: **Stress path notation used by Brown and Pappin (1981).**

The formulas for the volumetric stain contours in the p-q space are defined in equation A.33 and A34 (Brown and Pappin, 1981). Figure B.6 illustrates the volumetric strain contours and Figure B.7 the shear strain contours in the p-q space (Brown and Pappin, 1981).

$$\varepsilon_v = \delta \left[\left(\frac{p}{A} \right)^B \left(1 - C \left(\frac{p}{q} \right)^2 \right) \right] \tag{B.33}$$

$$\varepsilon_s = D\delta \left[\frac{q}{p+E} \right] \left[\frac{\sqrt{p_r^2 + q_r^2}}{p_m} \right]^F \tag{B.34}$$
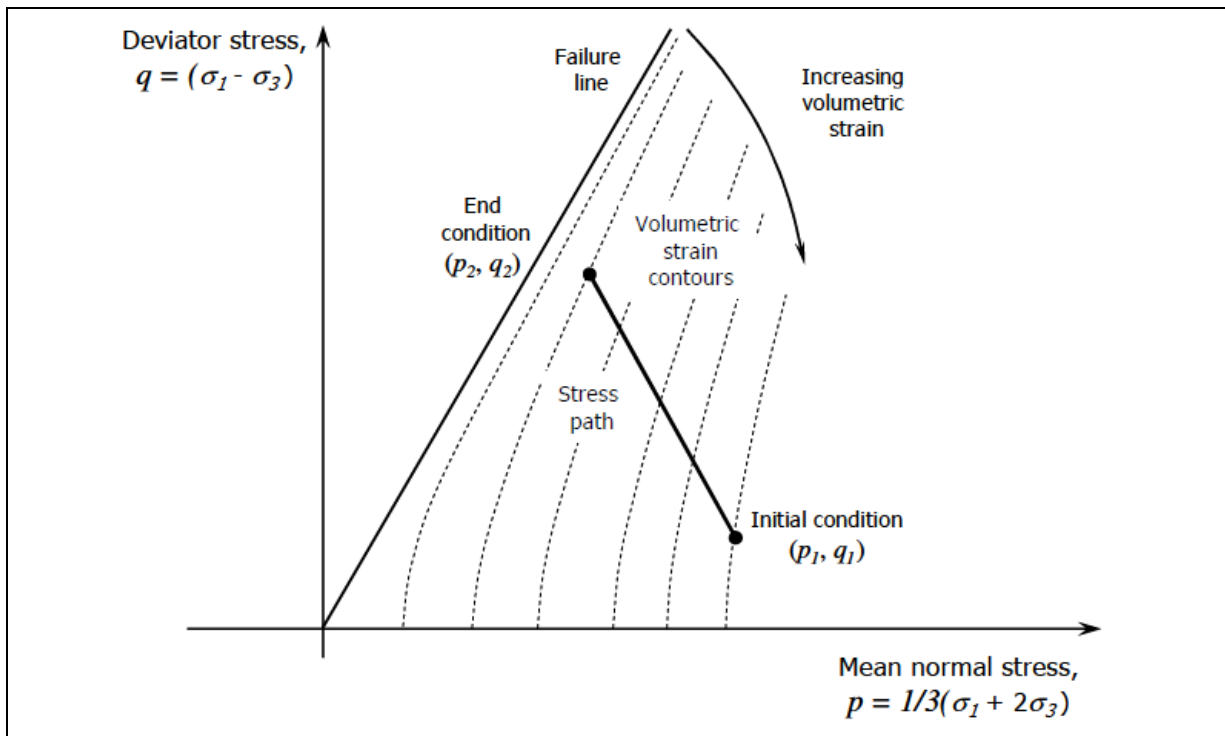
Figure B.6: Volumetric strain contours in p-q space (Brown and Pappin, 1981).
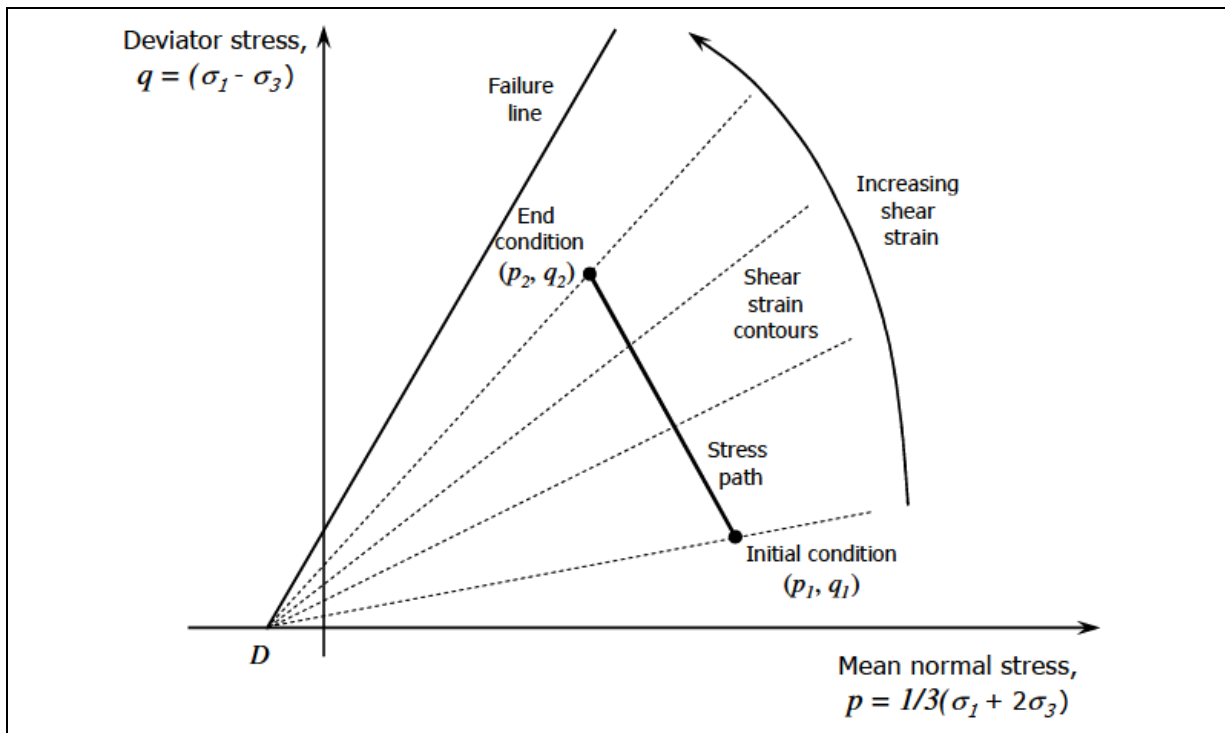
Figure B.7: Shear strain contours in p-q space (Brown and Pappin, 1981).

Brown and Pappin concluded that the length of the stress path influences the shear strain, as well as the maximum stresses, and that the volumetric strain depends only on the maximum values of stresses (Brown and Pappin, 1981).

Their model resembles the Boyce model, but with the difference of independent material parameters leading to better modelling of inelastic behaviour and modelling shear strain by taking account of the length of stress path corresponding to the load cycle (Lekarp *et al.*, 2000). However, in a study by Mayhew (1983), he concluded that the stress path length had no significant influence on the shear strain response. When the stress path dependence is removed from the contour model, it is the equivalent of the inelastic modified Boyce's model proposed by Sweere (1990) (as quoted by Lekarp *et al.*, 2000). Mayhew's model was rewritten by Brown and Selig (1991) to be defined as follows (as quoted by Lekarp *et al.*, 2000):

$$\varepsilon_v = \frac{p^A}{K_a}\left[1 - C\frac{q^2}{p^2}\right] \tag{B.35}$$

$$\varepsilon_s = \frac{p^B}{3G_a}\left(\frac{q}{p}\right) \tag{B.36}$$

Where

ε_v = volumetric strain;

ε_s = shear strain;

p = mean normal stress;

q = deviator stress;

A, B, C, K_a, G_a = model parameter

B.10 CONCLUSION

From the literature quoted in Section B.1 it is clear that the search for a resilient modulus model has been the topic for many research projects and that it is not a new area of research. However, every model has its limitations, with no generally applicable model for unbound granular material. This background study reiterates the need for such a model, granted that it will not be the first attempt at such a model.

B.11 REFERENCES

Anochie-Boateng, J.K. (2007). '*Advance testing and characterisation of transportation soils and bituminous sands*', PhD dissertation, University of Illinois, Urbana, Illinois, USA.

Brown, S.F. and Pappin, J.W. (1981). '*Analysis of pavements with granular bases*', Transportation Research Record 810, Transportation Research Board, Washington, D.C., USA.

Craig, R.F. (1997). '*Soil mechanics*', Sixth Edition, E & FN Spon, London & New York.

Kim, M. (2007). '*Three-dimensional finite element analysis of flexible pavements considering nonlinear pavement foundation behaviour*', PhD thesis, University of Illinois, Urbana, Illinois, USA.

Lekarp, F., Isacsson, U. and Dawson, A. (2000). '*State of the art. I: Resilient response of unbound aggregates*', Journal of Transportation Engineering, Volume 126, No. 1, January/February, 2000.

Seed, H.C., Chan, C.K. and Lee, C.E (1962). '*Resilient characteristics of subgrade soils and their relation to fatigue failures in asphalt pavements*', Proceedings of International Conference on the Structural Design of Asphalt Pavements, University of Michigan, U.S.A.

Theyse, H.L. (2008). '*A mechanistic-empirical design model for unbound granular pavement layers*', PhD dissertation, University of Johannesburg, Johannesburg, RSA.

Uzan, J. (1985). '*Characterisation of granular material*', Transportation Research Record 1022, Transportation Research Board, Washington, D.C., USA.

APPENDIX C

TABLE OF CONTENT

LIST OF TABLES

LIST OF FIGURES

C. PROPOSED TRI-ACIAL TEST PROTOCOL

C.1 BACKGROUND

The following outline sections of the proposed protocol of Mgangira (2011), which applies to tri-axial testing conducted in this thesis. Minor amendments have been made to the proposed protocol which is indicated in Chapter 3.

C.2 SCOPE

C.2.1 The proposed protocol shall provide a means for the determination of the resilient modulus, permanent deformation and shear strength of cylindrical specimens of both unbound and stabilized granular materials.

C.2.2 The protocol shall provide for the measurement of axial and lateral strains of a specimen subjected to repeated axial loading to simulate moving wheel loads. The protocol is applicable to laboratory compacted specimens with a particle-specimen diameter ratio smaller than one fifth.

C.2.3 The development of the proposed test protocol has taken into account factors that are considered critical based on similar testing principles used in existing standard test methods for the determination of resilient modulus, permanent deformation and shear strength. But laboratory test procedures used at Stellenbosch University (Ebels 2008) and the CSIR's Built Environment Advanced Laboratory (reference Theyse 2004) form the basis of the proposed test method.

C.3 REFERENCED DOCUMENTS

The following documents are referenced to in this method.

C.3.1 South African National Standard (SANS 3001: Civil engineering test methods)

SANS 3001-GR2:   Dry preparation and dry particle size analysis of gravels and sands.

SANS 3001-GR20:   Determination of the moisture content by oven-drying.

SANS 3001-GR30:   The determination of the maximum dry density and optimum moisture content.

Method A11T   Tentative method for the determination of the maximum dry density and optimum moisture content of graded crushed stone and cohesionless sand by means of vibratory compaction.

C.3.2 Other standard test methods

NCHRP 1-28 Appendix 2: Recommended Standard Test Method for Routine Resilient Modulus Testing of Unbound Base/Subbase Materials and Subgrade Soils.

C.4 DEFINITIONS

C.4.1. *Maximum Applied Axial Load* (P_{max}) as shown in Figure 1, is the load applied to the specimen and it consists of the seating (contact) load and cyclic load (effect of confining pressure is not included). Units are in kilonewton (kN).

C.4.2 *Contact/Seating Load* ($P_{contact}$) as shown in Figure 1 is the vertical load applied to the specimen to maintain a positive contact between the loading ram and the specimen top cap. Units are in kilonewton (kN).

C.4.3 *Cyclic Load* (P_{cycl}) as shown in Figure 1 is the repetitive axial load applied to the specimen. ($P_{cyclic} = P_{max} - P_{contact}$). Units are in kilonewton (kN).

C.4.4 *Maximum Applied Axial Stress* (σ_{max}) is the axial stress (ratio of maximum applied load to the area of specimen) applied to the specimen and it consists of the seating/contact stress ($\sigma_{contact}$) and the cyclic stress (σ_{cyclic}).

C.4.5 *Contact/seating stress* ($\sigma_{contact}$) is the axial contact or seating stress applied to the specimen to maintain a positive contact between the loading ram and the specimen top cap. Units are in kilopascal (kPa). Contact stress should be maintained at 10% of the confining pressure, 5 kPa being a minimum.

C.4.6 *Confining Stress* (σ_{conf}) is the applied confining pressure applied to the specimen in the tri-axial chamber (i.e. the minor principal stress, σ_3). Units are in kilopascal (kPa). Cyclic Stress (deviatoric stress) is the maximum repetitive applied axial stress. $\sigma_{cyclic} = \sigma_d = (\sigma_{max} - \sigma_{contact})$. Units are in kilopascal (kPa).
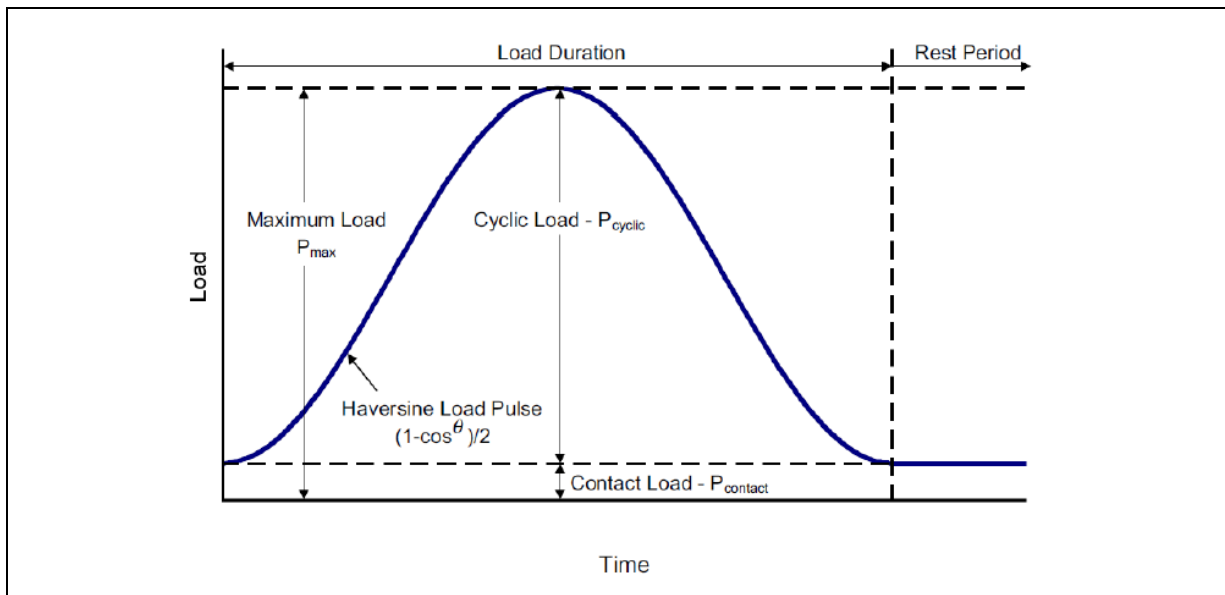
Figure C.1: Definition of resilient modulus terms (NCHRP 1-28)

C.4.7 *Gauge Length* (L_g) is the distance between the measurement points for the axial deformation. Units are in millimetre (mm). A gauge length of 100 mm for a 300 mm specimen length is used in this method.

C.4.8 *Vertical resilient deformation* (δ_a) is the maximum deformation of the specimen length measured during the application of a given cyclic stress in a given cycle. Units are in millimetre (mm).

C.4.9 *Radial resilient deformation* (δ_r) is the maximum deformation of the specimen over its radius measured during the application of a cyclic stress in a given cycle. Units are in millimetre (mm).

C.4.10 *Vertical axial permanent deformation* (δ_p) is the deformation accumulated during the application of a given cyclic stress level, from the first cycle to a given number of loading cycles. Units in millimetre (mm).

C.4.11 *Resilient axial strain* (ε_a) is the recovered axial deformation over the gauge length (δ_a/L_g). Expressed as a percentage.

C.4.12 *Resilient radial strain* (ε_r) is the recovered radial deformation measured at the mid-section of the specimen over its radius (ε_r/R). Expressed as a percentage.

C.4.13 *Vertical axial permanent strain* (ε_p) is the ratio of the vertical permanent deformation to the initial specimen length. Expressed as a percentage.

C.4.14 *Resilient Modulus* (M_r) is defined as the ratio of the applied cyclic stress to the vertical resilient strain ($\sigma_{cyclic}/\varepsilon_a$). Units are in megapascal (MPa).

C.4.15 *Load duration* is the time interval during which the specimen is subjected to a cyclic (deviatoric) stress pulse.

C-3

C.4.16   *Load pulse* is applied as a haversine loading wave form to simulate traffic loading during the testing.

C.4.17   *Cyclic duration* is the time interval between the successive applications of a cyclic stress, 1.0 second in this method.

C.4.18   *Unbound Materials* – These include graded crush stone, natural and processed gravels and gravel soils. No binding or stabilizing agent is used in their preparation.

C.5   SUMMARY OF THE TEST

The test protocol consists of determining the static shear strength of the material in order to establish the stress levels for the resilient and permanent deformation testing.

C.5.1   *Shear strength*: The shear strength test consists of applying a monotonic load at a constant rate of deformation until specimen fails or when the specimen strain reaches the termination strain requirement value.

C.5.2   *Resilient Modulus*: Test consists of applying a repeated axial load of a specified magnitude and duration consisting of a haversine pulse to the same cylindrical specimen. The specimen is subjected to a static confining pressure during the application of repeated axial loading along different predetermined stress paths as a ratio of the static shear strength at the corresponding confining pressure. The resulting vertical resilient strain from the measured vertical displacement is used to calculate the resilient moduli,

C.5.1   Significance and use
The protocol allows for the determination of the stress and environmental dependent characteristics of pavement materials, which can be used as key input parameters in the South African Pavement Design Method (SAPDM). The proposed protocol will make a direct contribution to the revision of SAPDM.

C.5.2   Apparatus used in the proposed method
C.5.2.1 A pressure chamber shall be used for the tri-axial test. The chamber should be large enough to accommodate a cylindrical specimen with a diameter of 150 mm and height of 300 ± 2 mm with internally on-sample mounted deformation measurement device

C.5.2.2 **The Tri-axial pressure chamber:** An acrylic chamber which contains the specimen and the confining air shall be able to withstand required confining pressure. The proposed test method will use a maximum confining pressure of 200 kPa.

C.5.2.3 **Loading device:** The system shall at least comprise of an actuator, loading frame, control panel and a data acquisition device. The loading frame shall be stiff enough to apply a load of 100 kN during the shear test without excessive deformation. It shall be capable of providing varying repeated loads of haversine loading wave form consisting of a load duration of 0.1 second and cyclic duration of 1 second, thus a rest period of 0.9 second. This is applicable for

testing base/subbase materials (according to NCHRP 1-28). For subgrade materials a load pulse having a 0.2 second duration followed by a rest period of 0.8 second duration is applicable. The actuator shall be operated by a servo controlled hydraulic pressure system. A closed-loop electro-hydraulic system is therefore required for both displacement and load controlled testing. A top loading system is recommended in this method. The data acquisition system shall be capable of automatically capturing at least the load, cell pressure, specimen deformation via on-specimen transducers and the actuator movement.

C.5.2.4 **Measuring devices:**

C.5.2.4.1.   The axial load shall be measured using an electronic 100 kN load cell for static tri-axial testing and a 25 kN capacity load cell shall be used during the conditioning and resilient modulus testing. An accuracy of ±5 kN is recommended for the load cell. The load cells shall be checked regularly according to the requirements of the NCHRP 1-28 procedure.

C.5.2.4.2.   Air shall be the fluid used for confining the specimen and the pressure in the cell shall be monitored using a pressure transducer with an accuracy of at least 0.5 kPa.

C.5.2.4.3.   In the proposed method the adopted deformation measurement device for resilient modulus consists of three Linear Variable Differential Transducers (LVDTs) placed vertically and diametrically spaced at 120⁰ supported by two plastic collar clips 100 mm apart, attached to the specimen over the middle section of the specimen. Thus vertical deformation devices shall be inside the chamber.

C.5.2.4.4.   The on-specimen displacement transducers shall have a total stroke of at least 4 mm for the resilient modulus testing with an accuracy of within 2 microns.

C.5.2.4.5.   The on-specimen displacement transducers shall have a total stroke of at least 12 mm for the permanent deformation test.

C.5.2.4.6.   The actuator displacement data shall only be used for monotonic tri-axial testing and permanent deformation determination.

C.5.2.4.7.   The system shall be capable of directly displaying measurements/data from transducers connected to the specimen and tri-axial cell during the testing.

C.5.2.4.8.   A minimum of 200 data points per second per channel shall be recorded.

C.5.3   Specimen preparation equipment

C.5.3.1 Compaction equipment: The current prevailing method of compaction for both unbound and cementitious stabilized material shall be by vibratory table according to standard Method A11T in the TMH1.

C.5.3.2 A cylindrical split metal mould with a collar and base plate capable of producing 150 mm diameter and 300 ± 2 mm high specimens. The total height of the mould shall be about 390 mm.

C.5.3.3 Seamless rubber membrane(s) in the form of a tube, open both ends of internal diameter of 150 mm and a length of about 400 mm. Included is the membrane expander.

C.5.3.4 Rubber O-rings for securing the rubber membrane to the specimen cap and base plate.

C.5.3.5 Vernier callipers, micrometer-gauge and graduated steel rule for measuring the length and diameter of the specimen as well as compacted layer thickness in the mould.

C.5.3.6 A balance of at least 10 kg capacity with an accuracy of no more than ± 0.5 g.

C.5.3.7 Plastic bags (temporally storage), sealable containers for sample curing, is the preferred method.

C.6   SPECIMEN PREPARATION

C.6.1   For the untreated material the following steps apply:

C.6.1.1.   Material preparation: A representative sample will have already been prepared as described in SANS 3001-GR2.

C.6.1.2.   Specimen moulding: Maximum Dry Density (MDD) and Optimum Moisture Content (OMC) of the unbound/untreated material shall be determined as described in SANS 3001-GR30.

C.6.1.C.   For field evaluation purpose, laboratory compacted specimens shall be prepared at in-situ moisture content and at the in-situ dry density.

C.6.1.4.   A sufficient amount of the representative sample for the number of specimens to be made for the specific test shall be weighed (approximately 15.0 kg per specimen).

C.6.1.5. The sample materials shall be mixed until they are homogeneous.

C.6.1.6.   The amount of water to be added for the specimen shall be determined using the mass of dry material of the specimen. First determine the water content of dry material of the sample as described in SANS 3001-GR20 in order to calculate the mass of water that is required to bring the material to the required moisture content for the compaction of the specimen.

C.6.2   The total mass of the material to be compacted shall be based on the target density/volumetric density, with diameter of 150 and height of 300 mm. Since material is compacted in five layers, the sample shall be subdivide into five equal portions and placed in plastic bags.

C.6.3   The material shall then be poured in the mould and compacted to the target density. The thickness of each layer shall be checked to ensure that the appropriate target density is achieved. The density of the compacted specimen shall not vary more than ±2% from the target density.

C.6.4   The top of each layer shall be scarified to enable layer interlocking.

C.6.5   Compaction method: The current method recommends the use of the vibratory table procedure as outlined in TMH1 Method A11T. Compaction should be at 25±2ºC

C.6.6   The specimen shall then be removed from the mould by disassembling the split mould and placed on a porous stone.

C.6.7   The height and diameter of the specimen shall then be measured at a 120º offset to the nearest 0.5 mm and record on the sample preparation sheet.

C.6.8   The mass of the wet specimen shall be measured to the nearest gram.

C.6.9   At least two replica specimens that represent the required test conditions (i.e. comparable density and moisture) shall be prepared for testing.

C.6.10   The moisture content of the remaining material used for the specimen compaction should be verified.

C.6.11   Curing:

C.6.11.1.   *Unbound material*: Back-drying or further wetting procedure shall be followed according to the test requirements.

C.6.12   The height and diameter of the specimen shall be measured at a 120º offset and recorded.

C.6.13   Testing of the specimens shall take place within 48 – 72 hours after specimen preparation or completion of the curing whichever applies

C.6.14   Specimen shall then be taken to the tri-axial testing machine.

C.7   SPECIMEN ASSEMBLY IN TRI-AXIAL CELL

C.7.1   The sides of the base disc and top cap shall be lightly greased to ensure an air or water tight seal with the membrane

C.7.2   Specimen shall then be placed centrally on the tri-axial cell base pedestal.

C.7.3   A rubber membrane shall then be carefully placed around the specimen and around the base disc, taking care not to damage the edges of the specimen. Use of a membrane stretcher is recommended for the placement of the membrane

C.7.4   The top part of the membrane shall then be folded back to expose the top of the specimen. The loading cap shall then be placed on the specimen.

C.7.5   Two O-rings shall be placed around the bottom platen and another two in the loading cap groove to seal the membrane.

C.7.6   Tests with on-specimen transducers:

NOTE: The procedure may vary depending on the type of clamping used.

C.7.6.1 Assemble the LVDT device.

C.7.6.2   The LVDT holder shall then be placed over the membrane, ensuring that there is a good contact between the LVDT holder and the membrane.

C.7.6.3 The distance between the collars shall be adjusted using the spacer.

C.7.6.4   The LVDT holder can be attached with an elastic band to ensure good contact at all times.

C.7.6.5   LVDT's, range ±2.0 mm for resilient modulus testing shall be assembled in the LVDT holder.

C.7.6.6   The stroke of the LVDTs shall be checked to ensure they are all in the correct range to provide optimum displacement for the test.

C.7.6.7   The tips of the LVDT probes shall rest in the centre of the pedestals. Ensure that no cables should impede the movement of the LVDTs.

C.7.7 The top cap drain shall be connected to the top cap drainage port in the cell base. A plastic tube is recommended for this. The top-cap drain shall then be connected to the top-cap drainage port in the base of the tri-axial cell. Ensure that the valve on the top-cap drainage port is closed.

C.7.8 Proper positioning of the specimen is critical. Ensure that the specimen is positioned in the middle of the base plate and that the centre of the top cap is aligned with the centre of the specimen.

C.7.9 The loading ram shall be lubricated with silicon oil and the tri-axial chamber lowered over the specimen and onto the cell base, taking care not to make contact with the specimen.

C.7.10 Perfect alignment of the piston of the actuator with the loading piston of the tri-axial chamber shall be ensured. Check that the tip of the loading ram is aligned with the locating dent in the centre of the top cap before tightening the chamber tie rods.

C.7.11 The tie rods of the chamber shall then be fastened.

C.7.12 The open end of the tube connected to the drainage port shall then be placed in a bucket of water with its valve on the bottom-plate plate drainage port open.

C.7.13 The air supply hose shall be connected to the base plate.

C.7.14 Air shall be supplied to the chamber until the cell pressure is stable at 100 kPa.

I. Listen and check for leakage. Presence of significant air bubbles in the water bucket is an indication of air escaping

II. The top and bottom seals between the membrane and the top cap and base plate, shall be checked if there is evidence of leakage.

III. If there is no evidence of leakage, the valve for the air supply on the cell pressure port shall be closed and the cell pressure released.

C.7.15 As a final check ensure that the lead wires of the LVDTs, load cell and the pressure transducer are connected to their respective connectors.

C.7.16 The actuator shall be lowered to make contact with the top of the specimen, but without loading the specimen.

C.7.17 Specimen is ready for testing.

C.8 MONOTONIC TRI-AXIAL TEST FOR THE DETERMINATION OF SHEAR STRENGTH PARAMETERS

C.8.2.1 The cell pressures for a series of monotonic tests shall be from a combination of these: 0 kPa, 12 kPa, 50 kPa, 100 kPa, 150 kPa and 200 kPa. These cell pressures shall be used to produce a set of three Mohr's circles and the resultant failure envelopes. The choice of the most appropriate range of cell pressure for the monotonic test shall be according to the requirement of the test condition for the type of material as given in Tables C.1 and C.2. However the range of the cell pressures should always correlate to the expected actual field stress values.

C.8.2   Prepare four specimens of comparable moisture content and density (within 4 kg/m3). After the specimen is set up in the tri-axial cell according to C.1.9 to C.1.9.17, except for C.1.9.7, the testing system shall be set in displacement control mode at an equivalent strain rate of 1% per minute.

C.8.3   The actuator shall be adjusted until visual contact is made with loading ram. The load cell reading shall be monitored to prevent loading of the specimen during this process.

C.8.4   The first specimen shall be tested without confinement pressure (σ_3 = 0 kPa). The vertical load shall be applied to the test specimen at a constant strain rate of 1% per minute. The load versus displacement shall be recorded during the test with a minimum sampling rate of 10 Hz, as well as the cell pressure, temperature and specimen/test identifier. The loading shall continue to 6% axial strain. Loading may be stopped when the deviator stress has peaked then dropped 20% or the axial strain has reached 5% beyond the strain at which the peak deviator stress occurred, or when the specimen bulges excessively before the end displacement is reached.

C.8.5   Repeat the entire procedure on the other specimens at the three cell pressures of 50 kPa, 100 kPa, 150 kPa, or 200 kPa, according to test requirements as shown in Tables C.1 and C.2.

C.9   REPEATED LOAD TRI-AXIAL TEST FOR THE DETERMINATION OF THE RESILIENT MODULUS

C.9.2.1   This procedure consists of application of a repeated axial deviator stress of a fixed magnitude to a specimen under constant confining pressure application. The initial stage, called the conditioning stage, consists of 1 000 cycle of loading and unloading. This is followed by specified stress regimes. During the resilient modulus test, the loading system applies a seating/contact load with a superimposed deviator load to the specimen. A haversine shaped load pulse is used. The test is carried out as outlined below.

C.9.2   The tri-axial cell shall be pressurised by opening the air supply regulator until the cell pressure is stable at 100 kPa. A preload/contact stress of 20% of the confining pressure or minimum of 5 kPa shall be applied to the specimen to ensure that the piston stays in contact with the top platens all the time.

C.9.3   1 000 conditioning repetitions shall be applied using a haversine shaped load pulse consisting of 0.1-second followed by 0.9-second rest period for base and subbase material and a pulse consisting of 0.2-second followed by 0.8-second rest for subgrade material, according to NCHRP 1-28 as shown in Figure C.1.

C.9.4   The selection of stress levels for the resilient modulus test: The actual cyclic stress shall be according to the type of material being tested as shown in Tables C.1 and C.2. However, it is recommended that the applied stress level cover the range to which the material will be subjected in the field. The cyclic stress shall be specified as a ratio to the average failure

deviator stress (σ_{df}) obtained from a monotonic tri-axial test, performed on replica specimens at a similar confining pressure and prepared in the same way as those for the resilient modulus test, for example ($\sigma_{cyclic} = 0.2\ \sigma_{df}$).

C.9.5   The test shall be terminated if the total accumulated strain is greater than 5 per cent as measured by the actuator LVDT, before the 1 000 cycles have been applied.

C.9.6   A new specimen shall be used for re-testing.

C.9.7   During the conditioning stage, a comparative check of the output from the vertical deformation transducers shall be conducted. Recommendation from NCHRP 1-28 is that the vertical deformation ratio of two measurements should not exceed 1.10, where the displacement ratio is defined as $R = {\gamma_{max}}/{\gamma_{min}}$. γ_{max} is the largest and γ_{min} is the smaller of the two measurements. High displacement ratio is an indication of specimen misalignment. Test should be stopped and the cause identified, before continuing with testing.

C.9.8   After conditioning, the available measuring range of the on-specimen vertical deformation transducers shall be checked to ensure that it is adequate to complete the test. If necessary, reset the position of the on-specimen vertical displacement transducers in the LVDT device.

C.9.9   This will require that the confining pressure be reduced to zero and disassembling the tri-axial cell. It is advisable to ensure that LVDTs are positioned appropriately at the beginning of the test.

C.9.10   For the subsequent loading stages after the conditioning, apply 100 cycles of loading and unloading using a haversine shaped load pulse consisting of 0.1 second followed by 0.9 second rest period for base and subbase material and 0.2 second followed by 0.8 second rest period for subgrade material. The actual confining pressure and deviator stress levels shall be according to the type of material being tested as shown in Tables C.1 and C.2.

C.9.11   Continue the test until all sequences are completed as shown in Tables C.1 or C.2, depending on the type of material. If at any time the total permanent strain of the specimen exceeds 5%, the test should be stopped and the results reported.

C.9.12   The average recovered deformation for each LVDT, for the last five cycles shall be recorded. Data shall be sampled at a minimum rate of 200 Hz.

C.9.1   Quick Shear

NOTE: Test conditions will vary according to the objective of the shear test

C.9.1.1   Determination of Young's Modulus and Poisson's Ratio: Upon completion of the resilient modulus test, the confining pressure shall be reduced to zero and load at a rate of 1% strain (with respect to initial specimen size) per minute shall be applied until specimen fails or when the specimen strain reaches the termination strain requirement value. Both axial and radial strain shall be recorded with the applied load to calculate the static Young's Modulus and Poisson's ratio.

C.9.1.2   Determination of shear strength: Upon completion of the resilient modulus test, the confining pressure shall be reduced to 50 kPa and load at a rate of 1% strain per minute

shall be applied until specimen fails or when the specimen strain reaches the termination strain requirement value.

C.10 SPECIMEN DISASSEMBLY AND POST TESTING

C.10.1   At the completion of a test, the actuator shall be returned to its starting position, still in contact with the loading ram, but without loading the specimen or loaded with a very small load (max. 50 N).

C.10.2   The confining pressure shall then be reduced to zero and the valve on the cell pressure port in the cell base closed. The cell pressure shall completely be released by opening the air release valve.

C.10.3   The actuator shall then be moved to create sufficient space to remove the tri-axial cell from the loading frame.

C.10.4   The tri-axial chamber tie rods shall then be loosened and the cell chamber lifted from the cell base. Taking care not to make contact with the specimen (the edges of the cell chamber may punch a hole in the membrane).

C.10.5   The membrane shall be removed from the specimen and the tested specimen shall be placed in a sealed plastic bag.

C.10.6   Once all specimens have been tested, each specimen shall be removed from the plastic bags and the entire specimen shall then be broken and used for moisture content determination according to SANS 3001-GR20.

Table C.1:   Loading schedule for the resilient modulus on unbound coarse (Type I) granular material.

Loading sequence	Confining pressure (kPa)	Contact stress (kPa)	Cyclic stress (kPa)	Load repetitions
Conditioning	100	10	$0.3 \times \sigma_{df(100)}$	1000
1	200	20	$0.1 \times \sigma_{df(200)}$	100
2	200	20	$0.3 \times \sigma_{df(200)}$	100
3	200	20	$0.5 \times \sigma_{df(200)}$	100
4	200	20	$0.7 \times \sigma_{df(200)}$	100
5	150	15	$0.1 \times \sigma_{df(150)}$	100
6	150	15	$0.3 \times \sigma_{df(150)}$	100
7	150	15	$0.5 \times \sigma_{df(150)}$	100
8	150	15	$0.7 \times \sigma_{df(150)}$	100
9	100	10	$0.1 \times \sigma_{df(100)}$	100
10	100	10	$0.3 \times \sigma_{df(100)}$	100
11	100	10	$0.5 \times \sigma_{df(100)}$	100
12	100	10	$0.7 \times \sigma_{df(100)}$	100
13	50	5	$0.1 \times \sigma_{df(50)}$	100
14	50	5	$0.3 \times \sigma_{df(50)}$	100
15	50	5	$0.5 \times \sigma_{df(50)}$	100
16	50	5	$0.7 \times \sigma_{df(50)}$	100

Loading sequence	Confining pressure (kPa)	Contact stress (kPa)	Cyclic stress (kPa)	Load repetitions
17	25	5	$0.1 \times \sigma_{df(25)}$	100
18	25	5	$0.3 \times \sigma_{df(25)}$	100
19	25	5	$0.5 \times \sigma_{df(25)}$	100
20	25	5	$0.7 \times \sigma_{df(25)}$	100

Table C.2:   Loading schedule for the resilient modulus on unbound fine (Type II) granular material.

Loading sequence	Confining pressure (kPa)	Contact stress (kPa)	Cyclic stress (kPa)	Load repetitions
Conditioning	100	10	$0.3 \times \sigma_{df(100)}$	1000
1	140	14	$0.1 \times \sigma_{df(140)}$	100
2	140	14	$0.3 \times \sigma_{df(140)}$	100
3	140	14	$0.5 \times \sigma_{df(140)}$	100
4	140	14	$0.7 \times \sigma_{df(140)}$	100
5	80	8	$0.1 \times \sigma_{df(80)}$	100
6	80	8	$0.3 \times \sigma_{df(80)}$	100
7	80	8	$0.5 \times \sigma_{df(80)}$	100
8	80	8	$0.7 \times \sigma_{df(80)}$	100
9	50	5	$0.1 \times \sigma_{df(50)}$	100
10	50	5	$0.3 \times \sigma_{df(50)}$	100
11	50	5	$0.5 \times \sigma_{df(50)}$	100
12	50	5	$0.7 \times \sigma_{df(50)}$	100
13	25	5	$0.1 \times \sigma_{df(25)}$	100
14	25	5	$0.3 \times \sigma_{df(25)}$	100
15	25	5	$0.5 \times \sigma_{df(25)}$	100
16	25	5	$0.7 \times \sigma_{df(25)}$	100

C.11 CALCULATIONS

C.11.1 Monotonic tri-axial test

C.11.1.1 Specimen parameters: The moisture content, dry density and degree of saturation of the specimens shall all be calculated.

C.11.1.2 Tri-axial compression: For each specimen, the applied maximum load and the corresponding deformation shall be determined for the calculation of the failure stress and unit strain. Failure stress shall be calculated as follows:

$$\sigma_{af} = \frac{P_{af}}{A} \cdot 10^{-3}$$

Where

P_{af} = the applied failure load (N)

A = the initial end area of the cylindrical specimen (m^2)

C.11.1.3. Major principal stress at failure is the sum of the axial stress at failure and the confining pressure shall be calculated as follows:

$$\sigma_{1f} = \sigma_{af} + \sigma_3$$

C.11.1.4. Shear strength parameters (ϕ and C) shall be calculated as follows:

First determine the relationship between σ_{1f} and σ_3 ,

$$\sigma_{1f} = A\sigma_3 + B$$

Where

$$A = \frac{1+sin\phi}{1-sin\phi} \text{ and } B = \frac{2.cos\phi}{1-sin\phi}$$

C.11.2 Resilient modulus test

C.11.2.1. Specimen parameters: The moisture content, dry density and degree of saturation of the specimens shall all be calculated.

C.11.2.2. For every applied stress level and at every confining pressure level the following shall be determined for each of the cycles (N) sampled:

C.1.13.2.3.   *Resilient axial strain*: First, the minimum deformation reading $LVDT_{min}$ and the maximum deformation reading $LVDT_{max}$ for each of the three on specimen LVDTs j shall be determined to calculate the average axial deformation $\Delta\delta_{a(N)}$ of the specimen per cycle (N).

$$\Delta\delta_{a(N)} = \frac{\Sigma_{i=1}^{j=3} LVDT_{j,max} - LVDT_{j,min}}{3}$$

Resilient axial strain $\varepsilon_{a(N)}$ per load cycle (N) is given by

$$\varepsilon_{a(N)} = \frac{\Delta\delta_{a(N)}}{L_g}$$

Where

L_g = gauge length

Resilient modulus calculation: First the cyclic stress for each cycle (N) shall be determined.

$$\sigma_{cyclic\,(N)} = \sigma_{d\,(N)} = \sigma_{max(N)} - \sigma_{contact(N)}$$

Resilient modulus M_r at the Nth cycle shall be calculated by

$$M_r = \frac{\sigma_{cyclic(N)}}{\varepsilon_{a(N)}}$$

The average of the last five load cycles in a loading sequence shall be reported, thus,

$$M_r = \frac{\Sigma_{i=1}^{i=l} M_{r,j}}{l}$$

Where *l* is the number of full load cycles sampled, equal to 5 in the proposed protocol.

C.12 REFERENCES

Mgangira, M.B. (2011). '*Proposed protocol for resilient modulus and permanent deformation characteristics of unbound and bound materials*', Report no. SANRAL/SAPDM/B-1c/2011-01, CSIR and University of Stellenbosch, Pretoria, RSA.

National Cooperative Highway Research Program (NCHRP), (2004). '*Project 1-28A: Recommended standard method for routine resilient modulus testing of unbound granular base/subbase materials*

and subgrade soils', NCHRP Research Results Digest No 285, Laboratory determination of resilient modulus for flexible pavement. January 2004, U.S.A.

TMH 1 (1985). '*Technical Methods Highways 1 : Standard test methods for road building materials*', Department of Transport, Pretoria, RSA.

APPENDIX D

TABLE OF CONTENT

LIST OF TABLES

LIST OF FIGURES

PAGE

D. SUMMARY OF TEST RESULTS

D.1 ROUTINE TEST RESULTS

This section contains the routine test results for samples 1 to 5.

D.1.1 Sample 1 – Crushed norite from N4 extension base layer

Table D.1:   Routine test results for N4 extension base layer.

SAMPLE DESCRIPTION			
Sample no	11306	11306	11306
Description	G1(01)	G1(13)	G1(23)
Date Tested	17/06/2010	17/06/2010	17/06/2010
SIEVE ANALYSIS (%Pass)			
37.5 mm	100.00	100.00	100.00
26.5 mm	95.10	85.01	92.18
19.0 mm	73.69	67.48	72.72
13.2 mm	55.30	54.82	56.42
9.5 mm	46.90	47.33	45.87
6.7 mm	39.50	40.26	37.08
4.75 mm	34.50	35.92	32.43
2.00 mm	25.41	26.52	23.70
0.850 mm	19.06	19.66	17.71
0.425 mm	14.29	14.53	13.29
0.075 mm	5.30	5.30	5.00
Grading Modulus	2.6	2.5	2.6
CONSTANTS			
Liquid Limit	N/P	N/P	N/P
Plasticity Limit	N/P	N/P	N/P
Plasticity Index	N/P	N/P	N/P
Linear Shrinkage (%)	N/P	N/P	N/P
COMPACTIONS			
MOD: Max Dry Density (kg/m^3)	2465	2427	2446
Optimum Moisture Cont. (%)	5.4	6.5	6.0
VIB: Max Dry Density (kg/m3)	2610.0	-	-
Optimum Moisture Cont. (%)	5.0	-	-
Dry Density achieved (kg/m^3)	2442	2429	2442
Moulding Moisture Cont. (%)	5.5	6.2	5.6
% of Max Dry Density	99.0	100.0	100.0
% Swell	0.00	0.03	0.02
NRB: Dry Density (kg/m^3)	2317	2378	2378
% of Max Dry Density	93.9	98.0	97.2
% Swell	0.02	0.00	0.03
PROCTOR: Dry Density (kg/m^3)	2273	2276	2314
% of Max Dry Density	92.2	93.7	95.0
% Swell	0.01	0.01	0.01

CBR/UCS VALUES			
100 % Mod AASHTO	260	275	262
98 % Mod AASHTO	226	169	192
95 % Mod AASHTO	168	116	150
93 % Mod AASHTO	136	97	-
ADDITIONAL TESTS			
B14 BRD(Kg/m3) +4.75mm	2.910	2.905	2.909
B14 ARD(kg/m3) +4.75mm	2.941	2.940	2.942
B14 Water Abs. % +4.75mm	0.4	0.4	0.4
B15 BRD(Kg/m3) -4.75mm	2.855	2.842	2.838
B15 ARD(kg/m3) -4.75mm	2.964	2.926	2.922
B15 Water Abs. % -4.75mm	1.2	1.0	1.0
DMI Value	N/A	N/A	N/A

Table D.2:   Durability mill grading analysis for N4 extension base layer.

Sample	11306G1/23			
Date	24-Jun-10			
Sample dry mass	3714.5			
Sieve size	Cum mass (g)	Retained mass (g)	% Retained	% Passing
26.5	3448.3	268.8	7.2%	92.8%
19.0	3179.5	866.0	23.3%	69.4%
13.2	2313.5	504.4	13.6%	55.9%
9.5	1809.1	265.1	7.1%	48.7%
6.7	1544.0	215.0	5.8%	42.9%
4.75	1329.0	161.5	4.3%	38.6%
2.00	1167.0	306.4	8.2%	30.3%
0.85	861.1	225.1	6.1%	24.3%
0.425	636.0	202.8	5.5%	18.8%
0.250	433.2	143.2	3.9%	15.0%
0.150	290.0	124.8	3.4%	11.6%
0.075	165.2	144.8	3.9%	7.7%
<0.075	20.4			
Sample	11306G1/23			
Date	24-Jun-10			
Sample dry mass	3718.5			
Sieve size	Cum mass (g)	Retained mass (g)	% Retained	% Passing
26.5	3444.7	428.8	11.5%	88.5%
19.0	3015.9	633.5	17.0%	71.4%
13.2	2382.4	531.1	14.3%	57.1%
9.5	1851.3	272.4	7.3%	49.8%
6.7	1578.9	240.4	6.5%	43.4%
4.8	1338.5	162.5	4.4%	39.0%
2.00	1176.0	317.4	8.5%	30.5%
0.85	858.6	239.5	6.4%	24.0%
0.425	619.1	211.0	5.7%	18.3%
0.250	408.1	124.8	3.4%	15.0%
0.150	283.3	122.4	3.3%	11.7%
0.075	160.9	136.3	3.7%	8.0%
<0.075	24.6			

Sample	11306G1/23			
Date	24-Jun-10			
Sample dry mass	3730.6			
Sieve size	Cum mass (g)	Retained mass (g)	% Retained	% Passing
26.5	3463.8	219.6	5.9%	94.1%
19.0	3244.2	575.9	15.4%	78.7%
13.2	2668.3	532.4	14.3%	64.4%
9.5	2135.9	402.0	10.8%	53.6%
6.7	1733.9	314.1	8.4%	45.2%
4.8	1419.8	189.4	5.1%	40.1%
2.00	1230.4	384.9	10.3%	29.8%
0.85	845.5	251.7	6.7%	23.1%
0.425	593.8	111.8	3.0%	20.1%
0.250	482.0	216.0	5.8%	14.3%
0.150	266.0	114.7	3.1%	11.2%
0.075	151.3	132.0	3.5%	7.7%
<0.075	19.3			

D.1.2 Sample 2 – Weathered chert from N4 extension upper selected layer

Table D.3: Routine test results for N4 extension upper selected layer.

SAMPLE DESCRIPTION			
Sample no	11307	11307	11307
Description	G5(3)	G5(15)	G5(24)
Date Tested	17/06/2010	17/06/2010	17/06/2010
SIEVE ANALYSIS (%Pass)			
75.0 mm		100.00	
53.0mm	100.00	73.44	100.00
37.5 mm	82.67	66.92	90.17
26.5 mm	71.28	64.28	86.77
19.0 mm	69.13	63.36	81.18
13.2 mm	66.11	60.78	78.32
9.5 mm	63.34	57.58	75.39
6.7 mm	59.77	54.35	71.18
4.75 mm	56.04	51.21	66.58
2.00 mm	46.35	42.06	54.24
0.850 mm	40.51	36.83	46.62
0.425 mm	37.10	33.82	41.48
0.075 mm	28.34	25.20	31.32
Grading Modulus	1.9	2.0	1.7
CONSTANTS			
Liquid Limit	31.34	32.70	31.46
Plasticity Limit	19.25	19.77	19.67
Plasticity Index	12.09	12.93	11.79
Linear Shrinkage (%)	5.83	5.83	5.18
G6 PI = 2*GM +10	13.8	14.0	13.5
COMPACTIONS			
MOD: Max Dry Density (kg/m^3)	2073.5	2052	2063
Optimum Moisture Cont. (%)	10.7	10.3	10.5
VIB: Max Dry Density (kg/m3)	2044.0	-	-
Optimum Moisture Cont. (%)	10.2	-	-
Dry Density achieved (kg/m^3)	2044	2057	2059
Moulding Moisture Cont. (%)	11.3	10.2	12.0
% of Max Dry Density	99.0	100.0	100.0
% Swell	0.30	0.40	0.30
NRB: Dry Density (kg/m^3)	1931	1964	1973
% of Max Dry Density	93.0	95.0	95.0
% Swell	0.50	0.40	0.30
PROCTOR: Dry Density (kg/m^3)	1792	1812	1863
% of Max Dry Density	86.0	88.0	90.0
% Swell	0.50	0.40	0.30
CBR/UCS VALUES			
100 % Mod AASHTO	61	55	47
98 % Mod AASHTO	52	44	41
95 % Mod AASHTO	35	32	33
93 % Mod AASHTO	26	23	23

ADDITIONAL TESTS			
B14 BRD(Kg/m3) +4.75mm	2.739	2.740	2.740
B14 ARD(kg/m3) +4.75mm	3.005	3.004	3.026
B14 Water Abs. % +4.75mm	3.2	3.2	3.4
B15 BRD(Kg/m3) -4.75mm	2.158	2.164	2.102
B15 ARD(kg/m3) -4.75mm	2.867	2.832	2.869
B15 Water Abs. % -4.75mm	11.5	10.9	12.7
REPEAT TESTS			
B14 BRD(Kg/m3) +4.75mm	2.703	2.713	2.704
B14 ARD(kg/m3) +4.75mm	2.931	2.936	2.926
B14 Water Abs. % +4.75mm	2.9	2.8	2.8
DMI Value	575.5	243.5	554.6

Table D.4:   Durability mill grading analysis and Atterberg indicators for N4 extension upper selected layer.

Sample	11307G5/3			
Date	24-Jun-10			
Sample dry mass	3566.6			
Sieve size	Cum mass (g)	Retained mass (g)	% Retained	% Passing
37.5	1815.8	473.5	13.3%	86.7%
26.5	1342.3	144.0	4.0%	82.7%
19.0	1198.3	108.6	3.0%	79.6%
13.2	1089.7	107.2	3.0%	76.6%
9.5	982.5	42.2	1.2%	75.5%
6.7	940.3	20.1	0.6%	74.9%
4.8	920.2	11.4	0.3%	74.6%
2.00	908.8	48.4	1.4%	73.2%
0.85	860.4	139.5	3.9%	69.3%
0.425	720.9	179.8	5.0%	64.3%
0.250	541.1	144.5	4.1%	60.2%
0.150	396.6	154.9	4.3%	55.9%
0.075	241.7	218.1	6.1%	49.8%
<0.075	23.6			
Atterberg indicators				
LL	28.6			
PL	19.6			
PI	9.0			
Corrected linear shrinkage	5.2			
Shrinkage measurement	8.0			
Sample	11307G5/3			
Date	24-Jun-10			
Sample dry mass	3532.5			
Sieve size	Cum mass (g)	Retained mass (g)	% Retained	% Passing
37.5	2676.4	264.5	7.5%	92.5%
26.5	2411.9	278.5	7.9%	84.6%
19.0	2133.4	142.9	4.0%	80.6%
13.2	1990.5	98.4	2.8%	77.8%
9.5	1892.1	49.7	1.4%	76.4%
6.7	1842.4	31.0	0.9%	75.5%

Sieve size	Cum mass (g)	Retained mass (g)	% Retained	% Passing
4.8	1811.4	54.7	1.5%	74.0%
2.00	1756.7	830.8	23.5%	50.4%
0.85	925.9	342.1	9.7%	40.8%
0.425	583.8	194.5	5.5%	35.3%
0.250	389.3	91.6	2.6%	32.7%
0.150	297.7	109.1	3.1%	29.6%
0.075	188.6	176.7	5.0%	24.6%
<0.075	11.9			
Atterberg indicators				
LL		29.9		
PL		20.0		
PI		9.9		
Corrected linear shrinkage		5.2		
Shrinkage measurement		8.0		
Sample	11307G5/3			
Date	24-Jun-10			
Sample dry mass	3566.8			
Sieve size	**Cum mass (g)**	**Retained mass (g)**	**% Retained**	**% Passing**
37.5	1900.6	247.3	6.9%	93.1%
26.5	1653.3	267.8	7.5%	85.6%
19.0	1385.5	104.4	2.9%	82.6%
13.2	1281.1	123.6	3.5%	79.2%
9.5	1157.5	109.6	3.1%	76.1%
6.7	1047.9	83.5	2.3%	73.8%
4.8	964.4	71.0	2.0%	71.8%
2.00	893.4	245.3	6.9%	64.9%
0.85	648.1	199.2	5.6%	59.3%
0.425	448.9	89.2	2.5%	56.8%
0.250	359.7	74.9	2.1%	54.7%
0.150	284.8	96.4	2.7%	52.0%
0.075	188.4	165.3	4.6%	47.4%
<0.075	23.1			
Atterberg indicators				
LL		31.7		
PL		20.0		
PI		11.7		
Corrected linear shrinkage		5.8		
Shrinkage measurement		9.0		

D.1.3   Sample 3 – Weathered dolerite from Road S191 base layer

Table D.5:   Routine test results for Road S191 base layer.

SAMPLE DESCRIPTION			
Sample no	11726	11726	11726
Description	G4/G6	G4/G6	G4/G6
Date Tested	05/05/2011	05/05/2012	05/05/2013
SIEVE ANALYSIS (%Pass)			
53.0mm	100.00	100.00	100.00
37.5 mm	90.81	94.29	94.02
26.5 mm	76.2	69.66	87.91
19.0 mm	63.95	56.22	72.97
13.2 mm	51.11	47.93	59.82
9.5 mm	43.94	41.18	49.85
6.7 mm	38.04	35.9	41.87
4.75 mm	34.29	32.39	37.45
2.00 mm	26.09	24.47	27.74
0.850 mm	19.93	18.72	21.25
0.425 mm	17.01	15.96	18.16
0.075 mm	10.91	10.15	11.43
Grading Modulus	2.5	2.5	2.4
CONSTANTS			
Liquid Limit	30.21	30.27	31.2
Plasticity Limit	22.36	22.62	22.37
Plasticity Index	7.86	7.65	8.83
Linear Shrinkage (%)	4.85	5.18	5.18
PI = 2*GM +10	14.9	15.0	14.9
COMPACTIONS			
MOD: Max Dry Density (kg/m^3)	2343.37	2267.71	2343.37
Optimum Moisture Cont. (%)	6.89	7.59	6.89
VIB: Max Dry Density (kg/m3)	2400	2380	2400
Optimum Moisture Cont. (%)	8.1	7.2	8.1
Dry Density achieved (kg/m^3)	2294		2294
Moulding Moisture Cont. (%)	7.1		7.1
% of Max Dry Density	98		98
% Swell	0.08		0.08
NRB: Dry Density (kg/m^3)	2221.7		2221.7
% of Max Dry Density	95		95
% Swell	0.14		0.14
PROCTOR: Dry Density (kg/m^3)	2122.5		2122.5
% of Max Dry Density	91		91
% Swell	0.12		0.12
CBR/UCS VALUES			
100 % Mod AASHTO			
98 % Mod AASHTO	43.3	27.5	
95 % Mod AASHTO	43.8	29.5	
93 % Mod AASHTO	41.6	28.1	

ADDITIONAL TESTS			
B14 BRD(Kg/m3) +4.75mm	2.7693	2.7629	2.7715
B14 ARD(kg/m3) +4.75mm	2.9027	2.907	2.9104
B14 Water Abs. % +4.75mm	1.66	1.79	1.72
B15 BRD(Kg/m3) -4.75mm	2.357	2.312	2.361
B15 ARD(kg/m3) -4.75mm	2.893	2.877	2.887
B15 Water Abs. % -4.75mm	7.8	8.4	7.7
DMI Value	233.97		

Table D.6:   **Durability mill grading analysis and Atterberg indicators for Road S191 base layer.**

Sample	11726(1)	Sample	11726(2)
Date	S191Base	Date	S191Base
Sample dry mass	13/05/2011	Sample dry mass	13/05/2011
Sieve size	% Passing	Sieve size	% Passing
37.5	100.0	37.5	100.0
26.5	85.2	26.5	91.9
19.0	73.6	19.0	77.0
13.2	58.2	13.2	63.3
9.5	49.5	9.5	55.5
6.7	43.9	6.7	51.0
4.8	39.8	4.8	47.5
2.00	29.8	2.00	39.3
0.85	22.3	0.85	33.2
0.425	18.8	0.425	29.9
0.250	16.7	0.250	27.4
0.150	14.9	0.150	24.8
0.075	12.2	0.075	20.4
<0.075		<0.075	
Atterberg indicators		Atterberg indicators	
LL	30.15	LL	30.15
PL	24.00	PL	24.00
PI	6.15	PI	6.15
Corrected lin. shrinkage	3.24	Corrected lin. shrinkage	3.24
Sample	11726(3)	Sample	11726(4)
Date	S191Base	Date	S191Base
Sample dry mass	13/05/2011	Sample dry mass	13/05/2011
Sieve size	% Passing	Sieve size	% Passing
37.5	100.0	37.5	100.0
26.5	92.1	26.5	93.0
19.0	77.3	19.0	78.6
13.2	65.8	13.2	65.3
9.5	59.1	9.5	56.4
6.7	52.1	6.7	49.5
4.8	47.5	4.8	45.3
2.00	36.1	2.00	35.9
0.85	27.5	0.85	29.8
0.425	23.2	0.425	27.0
0.250	20.5	0.250	25.0

D-8

Sieve size	% Passing	Sieve size	% Passing
0.150	18.3	0.150	23.0
0.075	15.0	0.075	19.3
<0.075		<0.075	
Atterberg indicators		**Atterberg indicators**	
LL	32.44	LL	31.95
PL	25.02	PL	24.13
PI	7.42	PI	7.82
Corrected lin. shrinkage	3.88	Corrected lin. shrinkage	3.88

D.1.4 Sample 4 – Weathered shale from Road P10-2 base layer

Table D.7: Routine test results for Road P10-2 base layer.

SAMPLE DESCRIPTION			
Sample no	11721	11721	11721
Description	G8	G8	G8
Date Tested	16/05/2011	16/05/2011	16/05/2011
SIEVE ANALYSIS (%Pass)			
53.0mm	100.00	100.00	100.00
37.5 mm	95.73	97.15	97.32
26.5 mm	89.36	93.81	91.87
19.0 mm	82.3	85.9	86.37
13.2 mm	74.19	77.12	78.77
9.5 mm	68.72	69.83	72.59
6.7 mm	62.91	64.04	66.22
4.75 mm	57.6	58.87	60.83
2.00 mm	44.96	46.68	47.67
0.850 mm	35.74	37.48	38.13
0.425 mm	31.11	32.97	33.38
0.075 mm	23.66	25.94	25.8
Grading Modulus	2.0	1.9	1.9
CONSTANTS			
Liquid Limit	24.8	29.2	25.6
Plasticity Limit	19.0	19.4	17.9
Plasticity Index	5.8	9.7	7.7
Linear Shrinkage (%)	5.2	5.2	5.2
PI = 2*GM +10	14.0	13.9	13.9
COMPACTIONS			
MOD: Max Dry Density (kg/m^3)	2133		
Optimum Moisture Cont. (%)	8.3		
VIB: Max Dry Density (kg/m3)	2130		
Optimum Moisture Cont. (%)	9.5		
Dry Density achieved (kg/m^3)	2090		
Moulding Moisture Cont. (%)	8.1		
% of Max Dry Density	98		
% Swell	1.8		
NRB: Dry Density (kg/m^3)	1959		
% of Max Dry Density	92		
% Swell	1.7		
PROCTOR: Dry Density (kg/m^3)	1841		
% of Max Dry Density	86		
% Swell	1.8		
CBR/UCS VALUES			
100 % Mod AASHTO	17.0		
98 % Mod AASHTO	15.3		
95 % Mod AASHTO	12.5		
93 % Mod AASHTO	11.0		

ADDITIONAL TESTS			
B14 BRD(Kg/m3) +4.75mm	2.316	2.314	2.343
B14 ARD(kg/m3) +4.75mm	2.738	2.737	2.741
B14 Water Abs. % +4.75mm	6.6	6.7	6.2
B15 BRD(Kg/m3) -4.75mm	2.223	2.216	2.232
B15 ARD(kg/m3) -4.75mm	2.734	2.739	2.748
B15 Water Abs. % -4.75mm	8.4	8.6	8.4
DMI Value	570.63		

Table D.8: **Durability mill grading analysis and Atterberg indicators for Road P10-2 base layer.**

Sample	11721(A)	Sample	11721(B)
Date	P 10-2	**Date**	P 10-2
Sample dry mass	20/05/2011	**Sample dry mass**	20/05/2011
Sieve size	**% Passing**	**Sieve size**	**% Passing**
37.5	100.0	37.5	100.0
26.5	93.3	26.5	98.9
19.0	87.1	19.0	93.9
13.2	78.9	13.2	86.8
9.5	71.6	9.5	83.3
6.7	62.7	6.7	81.1
4.8	56.4	4.8	79.2
2.00	42.5	2.00	70.8
0.85	33.0	0.85	60.3
0.425	28.3	0.425	53.4
0.250	25.6	0.250	49.5
0.150	23.4	0.150	46.2
0.075	20.4	0.075	41.3
<0.075		<0.075	
Atterberg indicators		**Atterberg indicators**	
LL	29.23	LL	25.36
PL	18.54	PL	19.24
PI	10.69	PI	6.12
Corrected lin. shrinkage	7.44	Corrected lin. shrinkage	5.83
Sample	11721(C)	**Sample**	11721(D)
Date	P 10-2	**Date**	P 10-2
Sample dry mass	20/05/2011	**Sample dry mass**	20/05/2011
Sieve size	**% Passing**	**Sieve size**	**% Passing**
37.5	100.0	37.5	100.0
26.5	94.4	26.5	95.7
19.0	88.7	19.0	88.7
13.2	81.5	13.2	79.2
9.5	76.6	9.5	72.4
6.7	70.8	6.7	66.6
4.8	65.7	4.8	61.0
2.00	51.4	2.00	49.5
0.85	40.1	0.85	42.7
0.425	34.1	0.425	39.0
0.250	30.1	0.250	37.8

Sieve size	% Passing	Sieve size	% Passing
0.150	27.0	0.150	36.2
0.075	23.0	0.075	33.4
<0.075		<0.075	
Atterberg indicators		**Atterberg indicators**	
LL	25.08	LL	29.70
PL	18.82	PL	19.80
PI	6.26	PI	9.91
Corrected lin. shrinkage	6.47	Corrected lin. shrinkage	7.12

D.1.5   Sample 5 – Weathered calcrete from Road D804 base layer

Table D.9:   **Routine test results for Road D804 base layer.**

SAMPLE DESCRIPTION			
Sample no	11728	11728	11728
Description	G7/G8	G7/G8	G7/G8
Date Tested	16/05/2011	16/05/2011	16/05/2011
SIEVE ANALYSIS (%Pass)			
53.0mm	100.00	100.00	
37.5 mm	96.28	94.03	100.00
26.5 mm	90.07	92.5	93.03
19.0 mm	86.48	85.67	84.63
13.2 mm	81.4	80.08	79.77
9.5 mm	76.14	74.4	74.13
6.7 mm	71.3	69.03	69.93
4.75 mm	67.2	65.1	65.83
2.00 mm	56.63	53.89	55.17
0.850 mm	49.74	46.53	47.82
0.425 mm	46.43	42.73	44.08
0.075 mm	33.34	26.67	27.71
Grading Modulus	1.6	1.8	1.7
CONSTANTS			
Liquid Limit	28.8	26.8	28.6
Plasticity Limit	18.1	18.7	18.5
Plasticity Index	10.6	8.2	10.1
Linear Shrinkage (%)	6.5	6.5	6.8
PI = 2*GM +10	13.3	13.5	13.5
COMPACTIONS			
MOD: Max Dry Density (kg/m^3)	2037		
Optimum Moisture Cont. (%)	9.4		
VIB: Max Dry Density (kg/m3)	2018		
Optimum Moisture Cont. (%)	10.6		
Dry Density achieved (kg/m^3)	2039		
Moulding Moisture Cont. (%)	9.7		
% of Max Dry Density	100		
% Swell	0.28		
NRB: Dry Density (kg/m^3)	1956		
% of Max Dry Density	96		
% Swell	0.48		
PROCTOR: Dry Density (kg/m^3)	1841		
% of Max Dry Density	90.3		
% Swell	0.47		
CBR/UCS VALUES			
100 % Mod AASHTO	55		
98 % Mod AASHTO	44		
95 % Mod AASHTO	31		
93 % Mod AASHTO	22		

ADDITIONAL TESTS			
B14 BRD(Kg/m3) +4.75mm	2.388	2.352	2.324
B14 ARD(kg/m3) +4.75mm	2.687	2.695	2.691
B14 Water Abs. % +4.75mm	4.7	5.4	5.9
B15 BRD(Kg/m3) -4.75mm	2.2	2.141	2.171
B15 ARD(kg/m3) -4.75mm	2.687	2.713	2.719
B15 Water Abs. % -4.75mm	8.2	9.8	9.3
DMI Value	575.64		

Table D.10:   Durability mill grading analysis and Atterberg indicators for Road D804 base layer.

Sample	11728(A)	Sample	11728(B)
Date	Slurry	**Date**	Slurry
Sample dry mass	20/05/2011	**Sample dry mass**	20/05/2011
Sieve size	**% Passing**	**Sieve size**	**% Passing**
37.5	100.0	37.5	100.0
26.5	97.2	26.5	97.3
19.0	93.6	19.0	91.9
13.2	88.2	13.2	88.5
9.5	83.9	9.5	86.7
6.7	78.2	6.7	85.6
4.8	73.1	4.8	84.5
2.00	59.8	2.00	78.7
0.85	51.2	0.85	69.5
0.425	47.0	0.425	64.0
0.250	43.7	0.250	59.0
0.150	39.8	0.150	54.3
0.075	27.4	0.075	41.9
<0.075		<0.075	
Atterberg indicators		**Atterberg indicators**	
LL	28.25	LL	27.25
PL	19.26	PL	18.57
PI	9.00	PI	8.68
Corrected lin. shrinkage	6.47	Corrected lin. shrinkage	5.83
Sample	11728(C)	**Sample**	11728(D)
Date	Slurry	**Date**	Slurry
Sample dry mass	20/05/2011	**Sample dry mass**	20/05/2011
Sieve size	**% Passing**	**Sieve size**	**% Passing**
37.5	100.0	37.5	100.0
26.5	99.3	26.5	98.75
19.0	96.6	19.0	95.68
13.2	92.4	13.2	90.38
9.5	89.0	9.5	85.46
6.7	85.5	6.7	81.26
4.8	82.0	4.8	76.75
2.00	67.5	2.00	65.1
0.85	57.2	0.85	57.97
0.425	52.2	0.425	54.36
0.250	48.2	0.250	51.65

Sieve size	% Passing	Sieve size	% Passing
0.150	43.0	0.150	48.35
0.075	28.6	0.075	37.39
<0.075		<0.075	
Atterberg indicators		**Atterberg indicators**	
LL	27.62	LL	26.38
PL	18.66	PL	18.11
PI	8.95	PI	8.27
Corrected lin. shrinkage	5.83	Corrected lin. shrinkage	5.83

D.2 STATIC TRI-AXIAL TEST RESULTS

This section contains a summary of the static tri-axial test data and the calibrated failure model parameters with associated graphs for samples 1 to 5.

D.2.1 Sample 1 – Crushed norite from N4 extension base layer

Table D.12 contains the static tri-axial test data. The results are considered acceptable. The calibrated failure model parameters are listed in Table D.11. Figure D.1 illustrates the predicted failure strength as opposed to the observed failure strength. Figure D.2 gives an indication of the suction pressure that could be present at zero confinement and the modelled suction curve.

Table D.11: **Calibrated suction and failure model parameters for N4 extension base layer.**

Suction parameters		Failure parameters	
φ	7.50	a	4.786
ω	5.05	b	0.139
ρ	1.51E+03	c	0.735
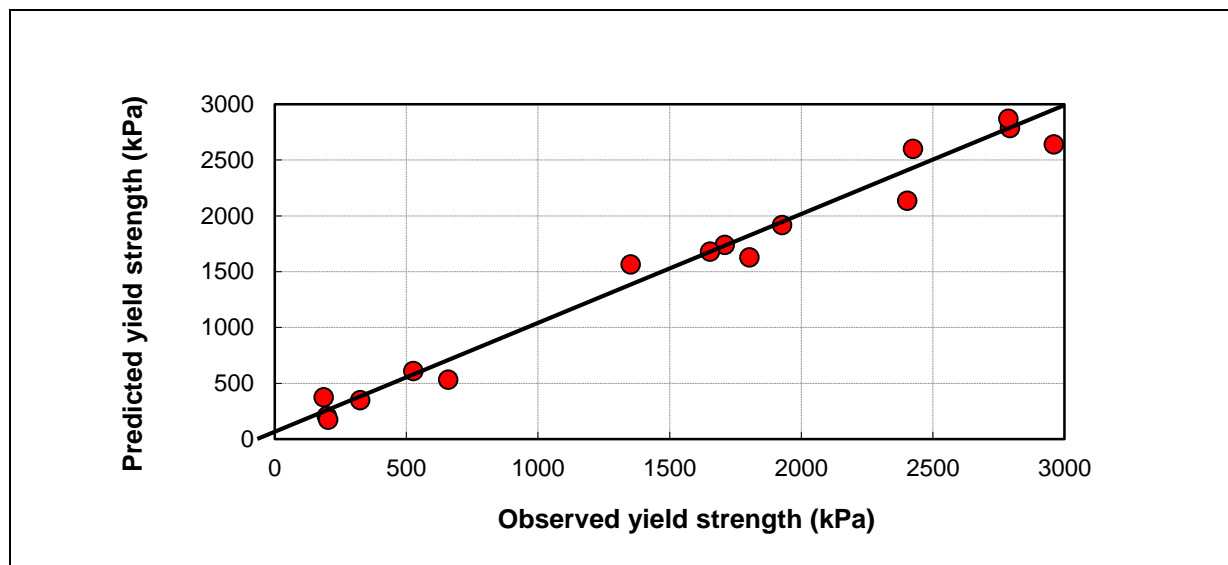
Figure D.1: **Failure stress plot for N4 extension base layer.**

Figure D.2: **Suction model and measured stress at zero confinement pressure for N4 extension base layer.**

Table D.12: Static tri-axial test data for N4 extension base layer.

Sample #	Dry density (kg/m³)	Density (VD) (%)	Moisture Content (MC) (%)	Saturation (%)	Confining stress (σ₃) (kPa)	Static test results						Actual MC (%)	Actual Dry density (kg/ m³)
						Failure load kN	Failure stress (kPa)	Principle stress σ₁ (kPa)	p (kPa)	q (kPa)	Cohesion and friction angle		
11306G1_01	2480	84.1	1.0	15.6	0.5	11.9	658.5	659.0	329.8	329.2		0.7	2473
11306G1_02	100.6			15.6	100.5	29.2	1609.5	1709.9	905.2	804.7	98.3	0.5	2449
11306G1_03				15.6	198.8	47.1	2594.4	2793.2	1496.0	1297.2	56.1	0.6	2459
11306G1_04	2480	84.1	3.2	49.9	0.5	3.4	185.7	186.1	93.3	92.8		2.4	2453
11306G1_05	100.6			49.9	100.9	28.2	1553.1	1654.0	877.5	776.6	27.1	2.7	2468
11306G1_06				49.9	200.1	50.1	2759.8	2959.8	1579.9	1379.9	60.0	2.4	2453
11306G1_07	2480	84.1	4.6	71.7	1.0	3.6	197.3	198.2	99.6	98.6		4.0	2509
11306G1_08	100.6			71.7	100.4	22.7	1251.9	1352.3	726.3	626.0	29.7	4.0	2473
11306G1_09				71.7	198.9	40.4	2225.3	2424.2	1311.6	1112.6	56.8	4.0	2491
11306G1_10	2550	86.5	0.8	15.1	0.5	9.5	526.2	526.7	263.6	263.1		0.5	2528
11306G1_11	103.4			15.1	100.8	41.8	2302.1	2403.0	1251.9	1151.1	86.4	0.7	2537
11306G1_12				15.1	200.3	49.1	2707.0	2907.3	1553.8	1353.5	59.1	0.6	2536
11306G1_13	2550	86.5	2.6	49.0	0.5	5.9	324.2	324.7	162.6	162.1		2.8	2512
11306G1_14	103.4			49.0	100.9	33.1	1826.6	1927.6	1014.2	913.3	49.4	2.3	2536
11306G1_15				49.0	198.6	52.9	2914.4	3113.0	1655.8	1457.2	60.2	2.7	2534
11306G1_16	2550	86.5	4.2	79.2	1.1	3.7	202.6	203.7	102.4	101.3		4.2	2563
11306G1_17	103.4			79.2	100.8	30.9	1702.4	1803.2	952.0	851.2	38.2	4.5	2519
11306G1_18				79.2	203.7	46.9	2582.8	2786.5	1495.1	1291.4	59.0	4.4	2566

D.2.2 Sample 2 – Weathered chert from N4 extension upper selected layer

Table D.12 contains the static tri-axial test data. The results are considered acceptable. The calibrated failure model parameters are listed in Table D.11. Figure D.1 illustrates the predicted failure strength as opposed to the observed failure strength. Figure D.2 gives an indication of the suction pressure that could be present at zero confinement and the modelled suction curve.

Table D.13:   Calibrated suction and failure model parameters for N4 extension upper selected layer.

Suction parameters		Failure parameters	
φ	10.45	a	0.000
ω	0.005	b	3.190
ρ	7.33E+04	c	1.391

Figure D.3:   Failure stress plot for N4 extension upper selected layer.

D-19
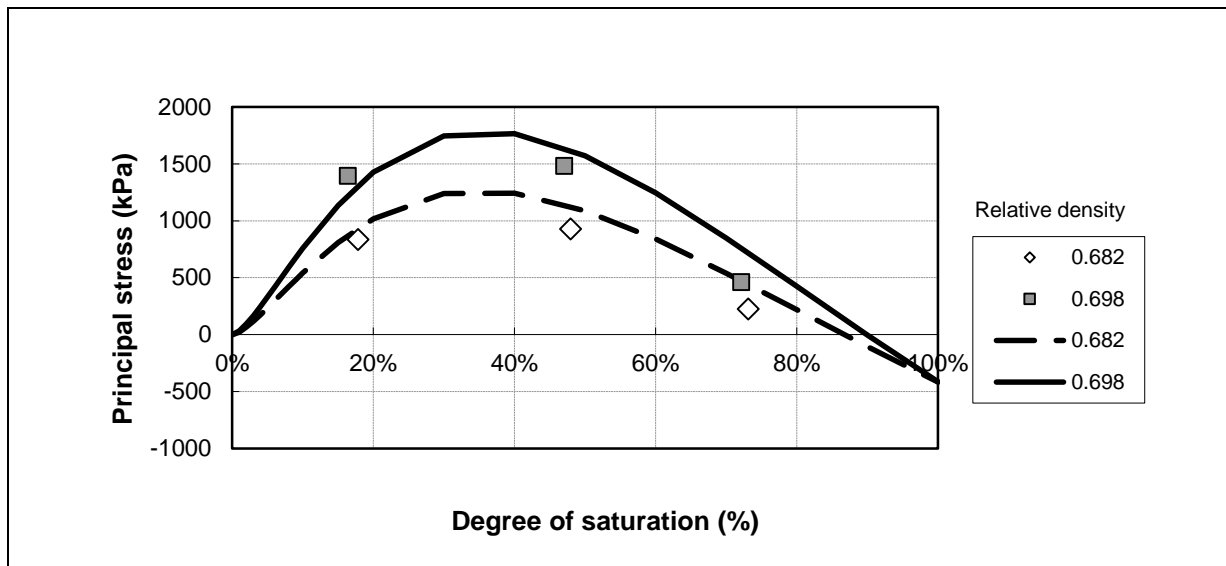
Figure D.4:   **Suction model and measured stress at zero confinement pressure for N4 extension upper selected layer.**

Table D.14:   Static tri-axial test data for N4 extension upper selected layer.

Sample #	Dry density (kg/m³)	Density (VD) (%)	Moisture Content (MC) (%)	Saturation (%)	Confining stress (σ_3) (kPa)	Static test results						Actual MC (%)	Actual Dry density (kg/ m³)
						Failure load kN	Failure stress (kPa)	Principle stress σ_1 (kPa)	p (kPa)	q (kPa)	Cohesion and friction angle		
11307G5_01	2070	71.5%	2.5	18.2%	0	25.3	1395.0	1395.0	697.5	697.5		2.4	2038
11307G5_02	100.0				100	39.1	2156.9	2257.1	1178.7	1078.4	232.8	2.5	2033
11307G5_03					201	53.9	2971.2	3171.8	1686.2	1485.6	52.9	2.6	2032
11307G5_04	2070	71.5%	7.0	50.8%	-1	26.9	1483.9	1483.2	741.3	741.9		7.0	2020
11307G5_05	100.0				100	40.9	2251.3	2351.5	1225.8	1125.7	322.3	7.0	2020
11307G5_06					200	40.5	2234.5	2434.7	1317.4	1117.2	44.3	7.0	2021
11307G5_07	2070	71.5%	11.0	79.9%	-1	8.4	462.4	461.9	230.7	231.2		11.1	2004
11307G5_08	100.0				100	14.6	805.3	905.7	503.1	402.7	129.5	11.1	2003
11307G5_09					200	17.5	961.7	1162.0	681.1	480.8	34.1	11.1	2018
11307G5_10	2007	69.3%	2.8	18.3%	0	15.2	836.7	836.4	418.0	418.3		2.8	1979
11307G5_11	97.0				101	32.7	1804.1	1904.6	1002.6	902.0	161.3	2.9	1985
11307G5_12					200	38.7	2133.6	2333.8	1267.0	1066.8	50.7	3.0	1993
11307G5_13	2007	69.3%	7.8	51.0%	0	16.9	929.6	929.2	464.4	464.8		7.7	1979
11307G5_14	97.0				100	27.2	1499.9	1600.4	850.4	749.9	178.3	7.9	1967
11307G5_15					200	37.9	2088.4	2288.7	1244.5	1044.2	48.0	7.9	1966
11307G5_16	2007	69.3%	11.9	77.8%	0	4.1	225.3	224.8	112.2	112.6		11.8	1974
11307G5_17	97.0				100	8.8	487.4	587.7	344.1	243.7	63.6	11.6	1963
11307G5_18					200	12.7	700.3	900.4	550.3	350.1	32.9	11.5	1959

D-21

D.2.3 Sample 3 – Weathered dolerite from Road S191 base layer

Table D.12 contains the static tri-axial test data. The results are considered acceptable. The calibrated failure model parameters are listed in Table D.11. Figure D.1 illustrates the predicted failure strength as opposed to the observed failure strength. Figure D.2 gives an indication of the suction pressure that could be present at zero confinement and the modelled suction curve.

Table D.15:   Calibrated suction and failure model parameters for Road S191 base layer.

Suction parameters		Failure parameters	
φ	0.00	a	7.273
ω	7.084	b	1.660
ρ	2.42E+03	c	0.458
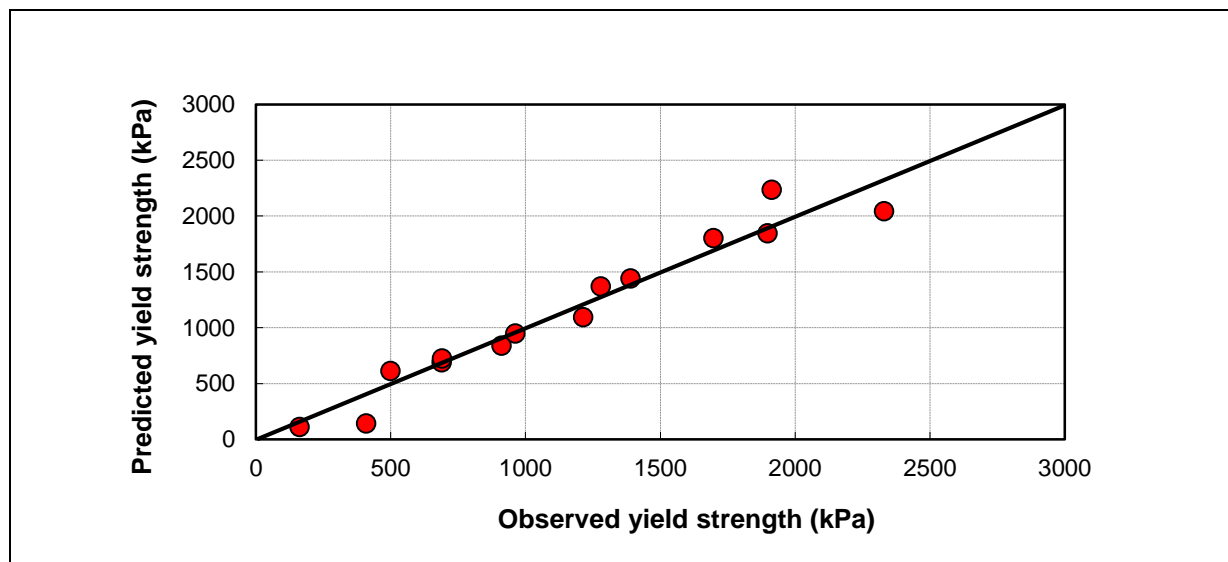
Figure D.5:   Failure stress plot for Road S191 base layer.
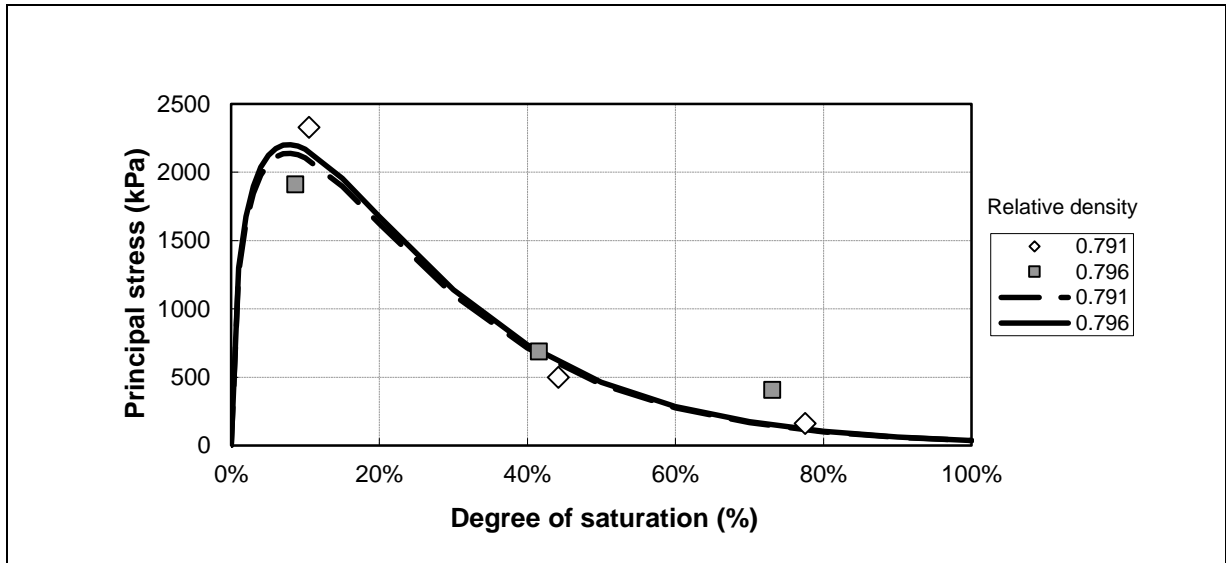
Figure D.6: **Suction model and measured stress at zero confinement pressure for Road S191 base layer.**

Table D.16:   Static tri-axial test data for Road S191 base layer.

Sample #	Dry density (kg/m³)	Density (VD) (%)	Moisture Content (MC) (%)	Saturation (%)	Confining stress (σ_3) (kPa)	Static test results						Actual MC (%)	Actual Dry density (kg/ m³)
						Failure load kN	Failure stress (kPa)	Principle stress σ_1 (kPa)	p (kPa)	q (kPa)	Cohesion and friction angle		
11726G6_01	2356	81.0%	0.70	8.7%	0	33.8	1912	1912	955.5	956		0.8	2319
11726G6_02	99.0				101	55.0	3110	3211	1656	1555	282.0	0.7	2319
11726G6_03					200	72.3	4089	4288	2244	2044	57.7	0.8	2316
11726G6_04	2356	81.0%	3.60	44.6%	0	12.2	688	688	343.6	344.1		3.7	2314
11726G6_05	99.0				100	24.5	1389	1489	794.4	694.3	135.0	3.7	2309
11726G6_06					200	33.6	1897	2097	1148	948.7	48.8	3.9	2309
11726G6_07	2356	81.0%	6.50	80.6%	0	7.3	409	408	203.9	204.3		6.6	2305
11726G6_08	99.0				101	16.1	910	1012	556.3	455.2	97.0	6.3	2315
11726G6_09					200	21.5	1213	1413	806.7	606.5	42.1	6.5	2309
11726G6_10	2332	80.2%	0.80	9.4%	-1	41.2	2329	2328	1164	1165		1.0	2294
11726G6_11	98.0				100	58.2	3292	3392	1746	1646	452.1	0.9	2313
11726G6_12					200	55.4	3136	3336	1768	1568	47.8	0.9	2310
11726G6_13	2332	80.2%	4.00	47.1%	-1	8.8	498	498	248.6	249.2		3.9	2315
11726G6_14	98.0				101	22.6	1278	1379	739.5	639	102.7	3.9	2305
11726G6_15					200	30.0	1696	1896	1048	848	48.9	4.0	2306
11726G6_16	2332	80.2%	7.20	84.8%	0	2.9	161	160	79.96	80.44		7.1	2297
11726G6_17	98.0				100	12.2	690	790	445.3	344.8	43.4	7.0	2290
11726G6_18					200	17.0	961	1161	680.8	480.7	42.1	7.3	2276

D.2.4 Sample 4 – Weathered shale from Road P10-2 base layer

Table D.12 contains the static tri-axial test data. The results are considered acceptable. The calibrated failure model parameters are listed in Table D.11. Figure D.1 illustrates the predicted failure strength as opposed to the observed failure strength. Figure D.2 gives an indication of the suction pressure that could be present at zero confinement and the modelled suction curve.

Table D.17: Calibrated suction and failure model parameters for Road P10-2 base layer.

Suction parameters		Failure parameters	
φ	29.98	a	6.294
ω	3.284	b	1.627
ρ	2.71E+06	c	0.613
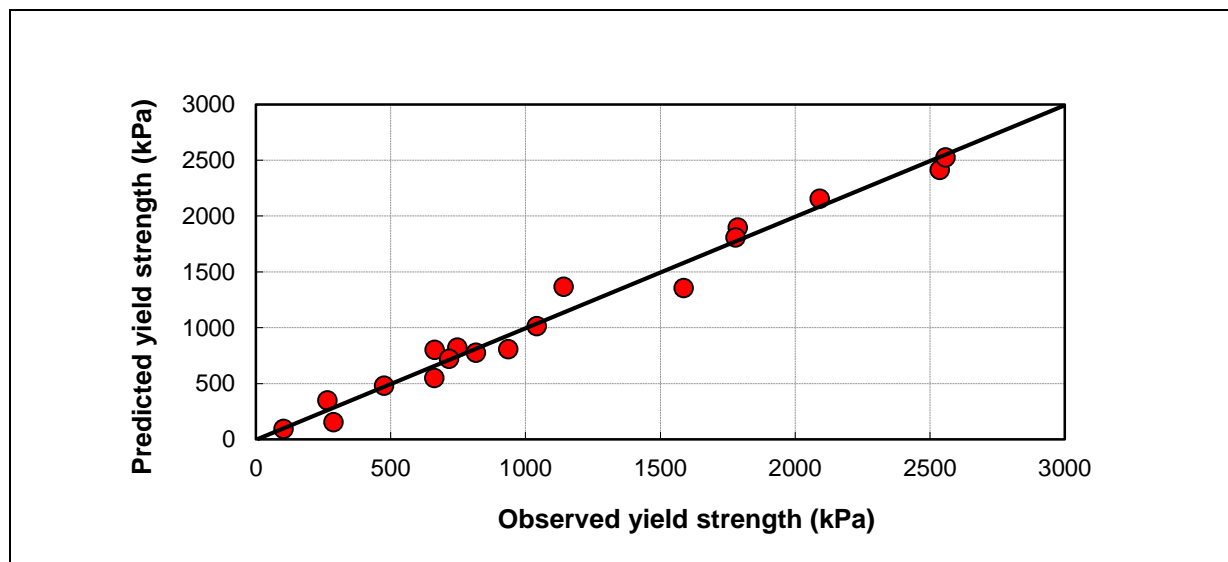
Figure D.7: Failure stress plot for Road P10-2 base layer.
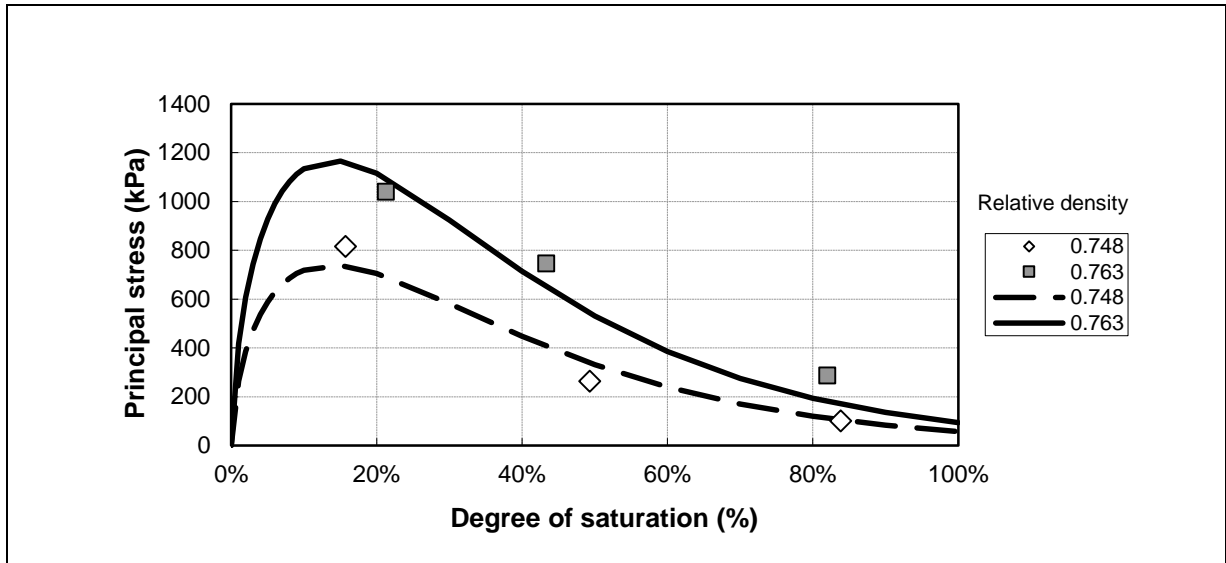
Figure D.8: **Suction model and measured stress at zero confinement pressure for Road P10-2 base layer.**

Table D.18: Static tri-axial test data for Road P10-2 base layer.

| Sample # | Dry density (kg/m³) | Density (VD) (%) | Moisture Content (MC) (%) | Saturation (%) | Confining stress (σ_3) (kPa) | Static test results | | | | | | Actual MC (%) | Actual Dry density (kg/ m³) |
						Failure load kN	Failure stress (kPa)	Principle stress σ_1 (kPa)	p (kPa)	q (kPa)	Cohesion and friction angle		
11721G8_01	2130	77.6%	2.10	20.0%	-1	18.9	1042	1040.933	520.1	520.8		2.4	2089
11721G8_02	100.0				100	30.6	1687	1786.847	943.5	843.4	191.8	2.3	2090
11721G8_03					201	42.4	2335	2535.857	1368	1168	49.7	2.5	2079
11721G8_04	2130	77.6%	6.00	57.1%	0	13.6	747	746.5695	373.1	373.5		4.7	2117
11721G8_05	100.0				100	27.0	1486	1586.412	843.4	743	151.6	4.9	2113
11721G8_06					200	34.3	1891	2091.237	1146	945.6	48.1	4.2	2129
11721G8_07	2130	77.6%	9.70	92.2%	0	5.2	288	287.2874	143.4	143.8		9.5	2082
11721G8_08	100.0				101	10.2	560	660.7517	380.7	280.1	83.9	9.6	2075
11721G8_09					200	13.3	735	934.8121	567.4	367.4	32.0	9.6	2073
11721G8_10	2088	76.0%	2.20	19.1%	-1	14.8	816	815.5432	407.4	408.1		1.9	2060
11721G8_11	98.0				100	30.5	1678	1778.808	939.6	839.2	143.5	1.8	2064
11721G8_12					200	42.8	2358	2557.941	1379	1179	52.6	1.8	2064
11721G8_13	2088	76.0%	6.60	57.4%	0	4.8	265	264.2886	131.9	132.4		6.0	2058
11721G8_14	98.0				100	10.2	562	662.1478	381.2	280.9	59.9	7.0	2046
11721G8_15					200	17.1	941	1141.352	670.7	470.6	38.9	6.1	2066
11721G8_16	2088	76.0%	10.60	92.2%	0	1.8	102	101.3973	50.45	50.94		10.4	2047
11721G8_17	98.0				100	6.8	374	474.5426	287.4	187.1	34.3	10.5	2039
11721G8_18					200	9.4	516	715.48	457.6	257.9	30.8	10.4	2046

D.2.5   Sample 5 – Weathered calcrete from Road D804 base layer

Table D.12 contains the static tri-axial test data. The results are considered acceptable. The calibrated failure model parameters are listed in Table D.11. Figure D.1 illustrates the predicted failure strength as opposed to the observed failure strength. Figure D.2 gives an indication of the suction pressure that could be present at zero confinement and the modelled suction curve.

Table D.19:   Calibrated suction and failure model parameters for Road D804 base layer.

| Suction parameters		Failure parameters	
φ	0.00	a	7.270
ω	7.084	b	1.659
ρ	2.43E+03	c	0.458
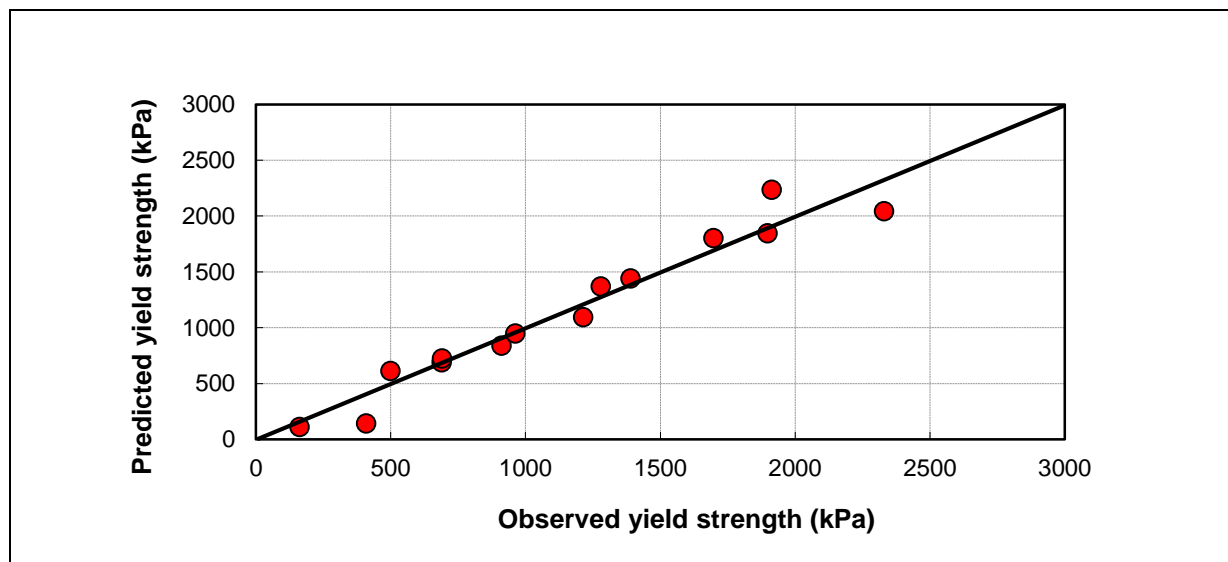
Figure D.9:   Failure stress plot for Road D804 base layer.
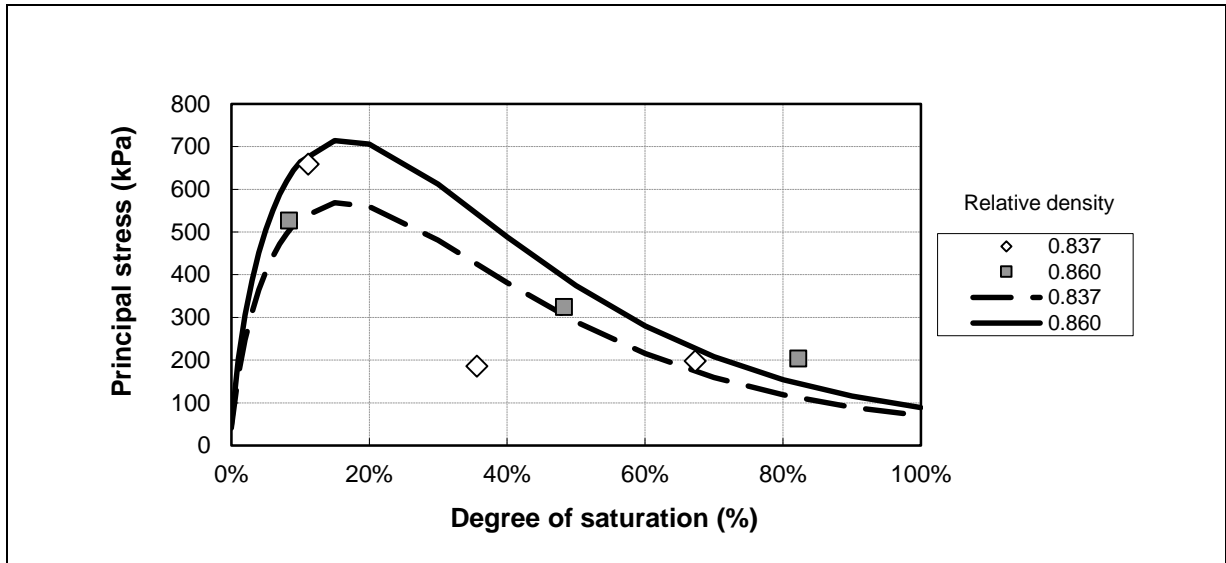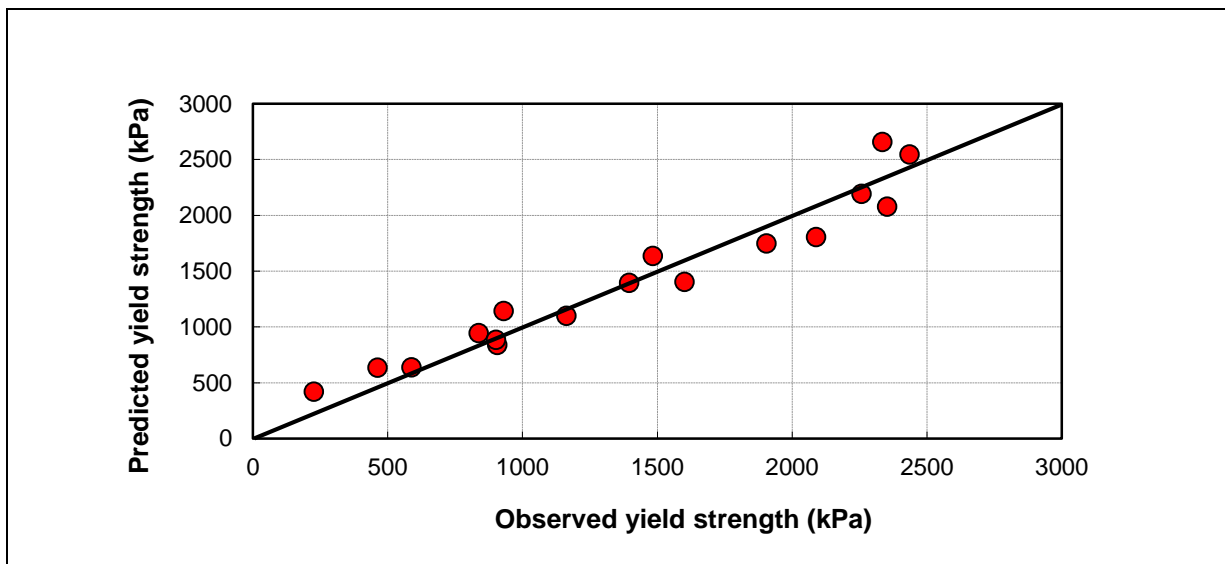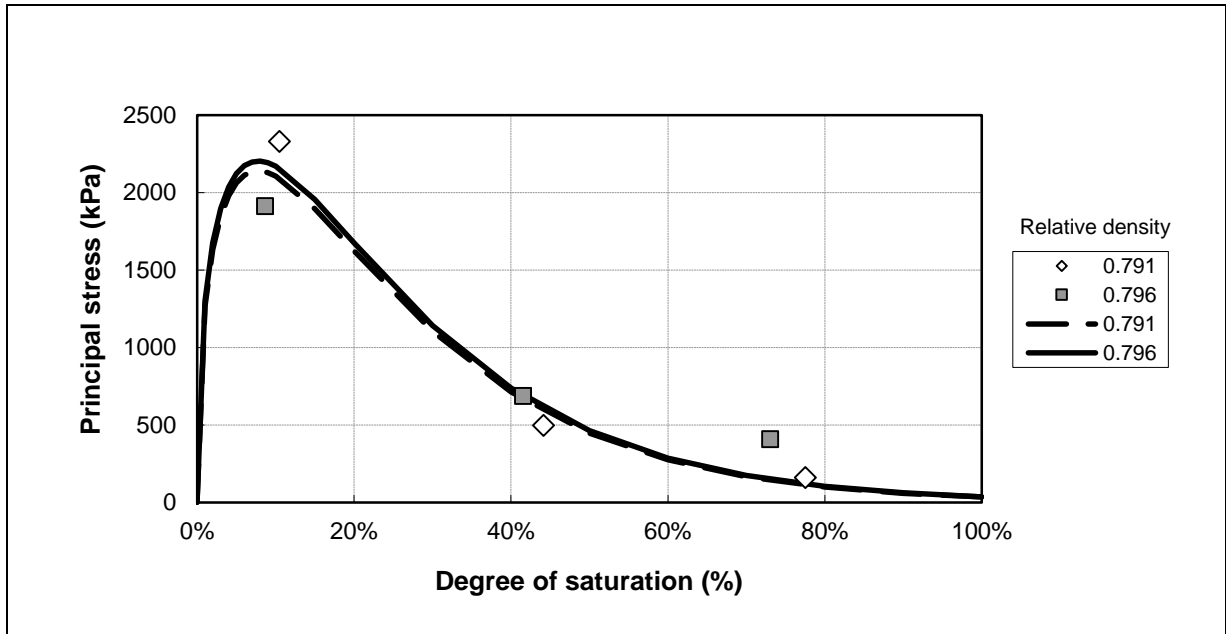
Figure D.10: Suction model and measured stress at zero confinement pressure for Road D804 base layer.

Table D.20:   Static tri-axial test data for Road D804 base layer.

Sample #	Dry density (kg/m³)	Density (VD) (%)	Moisture Content (MC) (%)	Saturation (%)	Confining stress (σ₃) (kPa)	Static test results						Actual MC (%)	Actual Dry density (kg/ m³)
						Failure load kN	Failure stress (kPa)	Principle stress σ₁ (kPa)	p (kPa)	q (kPa)	Cohesion and friction angle		
11728G7_01	2018	74.4%	1.00	7.9%	0	29.5	1663	1663	832	832		3.6	1984.0
11728G7_02	100.0				100	42.1	2379	2479	1290	1189	309.0	3.5	1984.0
11728G7_03					200	52.1	2945	3145	1672	1472	49.7	3.7	1977.0
11728G7_04	2018	74.4%	6.00	47.3%	0	15.2	856	856	428	428		5.5	1993.0
11728G7_05	100.0				101	23.3	1319	1420	760	660	202.7	5.7	1994.0
11728G7_06					200	28.2	1593	1793	997	796	40.6	5.9	1981.0
11728G7_07	2018	74.4%	11.00	86.7%	0	3.7	207	207	104	104		10.5	1997.0
11728G7_08	100.0				100	9.9	559	659	380	279	55.3	10.4	2002.0
11728G7_09					201	14.4	811	1012	606	406	37.0	10.6	1989.0
11728G7_10	1978	72.9%	1.10	8.0%	0	17.5	990	990	495	495		2.5	1956.0
11728G7_11	98.0				100	32.1	1811	1911	1006	906	181.2	2.3	1952.0
11728G7_12					200	42.1	2378	2577	1389	1189	51.1	2.3	1951.0
11728G7_13	1978	72.9%	11.90	86.9%	0	0.8	47	47	24	24		12.5	1936.0
11728G7_15	98.0				100	5.0	282	383	242	141	21.4	12.3	1949.0
11728G7_14					200	6.2	347	548	374	174	26.0	12.2	1951.0
11728G7_16	1978	72.9%	6.50	47.4%	0	6.4	358	358	179	179		6.9	1947.0
11728G7_17	98.0				100	15.7	882	982	541	441	81.5	6.8	1950.0
11728G7_18					200	22.1	1247	1447	824	624	43.7	6.3	1957.0

D.3   RESILIENT MODULUS TRI-AXIAL TEST LOADING SCHEDULES

This section contains the loading schedules used for resilient tri-axial tests for samples 1 to 5. The test results from each test cannot be included here due to the quantity of data points generated during processing.

D.3.1 Sample 1 – Crushed norite from N4 extension base layer

Table D.21: Resilient modulus tri-axial loading schedule for N4 extension base layer (VD = 0.841).

Seq	Confining Stress kPa	Contact Stress		% Sat	20%	50%	80%	20%	50%	80%		Predicted failure strength		
		kPa	kN	% of Failure	Cyclic Stress									
					kPa			kN			Nrep	20%	50%	80%
0	100	10.0	0.181	30%	560	494	452	10.168	8.964	8.197	1000	1868	1647	1506
1	200	20.0	0.363	10%	289	265	248	5.248	4.814	4.507	100	2892	2653	2484
2	200	20.0	0.363	30%	868	796	745	15.745	14.442	13.521	100	2892	2653	2484
3	200	20.0	0.363	50%	1446	1326	1242	26.241	24.070	22.536	100	2892	2653	2484
18	200	20.0	0.363	70%	2025	1857	1739	36.738	33.698	31.550	100	2892	2653	2484
5	150	15.0	0.272	10%	240	217	202	4.355	3.939	3.659	100	2400	2171	2016
6	150	15.0	0.272	30%	720	651	605	13.064	11.818	10.977	100	2400	2171	2016
7	150	15.0	0.272	50%	1200	1085	1008	21.773	19.697	18.295	100	2400	2171	2016
19	150	15.0	0.272	70%	1680	1520	1411	30.482	27.575	25.612	100	2400	2171	2016
8	100	10.0	0.181	10%	187	165	151	3.389	2.988	2.732	100	1868	1647	1506
9	100	10.0	0.181	30%	560	494	452	10.168	8.964	8.197	100	1868	1647	1506
10	100	10.0	0.181	50%	934	823	753	16.946	14.939	13.661	100	1868	1647	1506
20	100	10.0	0.181	70%	1307	1153	1054	23.725	20.915	19.125	100	1868	1647	1506
11	50	5.0	0.091	10%	127	105	92	2.312	1.909	1.671	100	1274	1052	921
12	50	5.0	0.091	30%	382	316	276	6.937	5.728	5.013	100	1274	1052	921
13	50	5.0	0.091	50%	637	526	460	11.561	9.547	8.356	100	1274	1052	921
21	50	5.0	0.091	70%	892	737	645	16.186	13.366	11.698	100	1274	1052	921
15	25	2.5	0.045	10%	94	71	57	1.703	1.281	1.040	100	938	706	573
16	25	2.5	0.045	30%	282	212	172	5.109	3.844	3.119	100	938	706	573
17	25	2.5	0.045	50%	469	353	286	8.515	6.407	5.198	100	938	706	573
22	25	2.5	0.045	70%	657	494	401	11.921	8.969	7.278	100	938	706	573

Table D.22: **Resilient modulus tri-axial loading schedule for N4 extension base layer (VD = 0.865).**

Seq	Confining Stress kPa	Contact Stress kPa	Contact Stress kN	% Sat / % of Failure	20%	50%	80%	20%	50%	80%	Nrep	Predicted failure strength 20%	Predicted failure strength 50%	Predicted failure strength 80%
					Cyclic Stress kPa			Cyclic Stress kN						
0	100	10.0	0.181	30%	653	566	510	11.848	10.278	9.263	1000	2177	1888	1702
1	200	20.0	0.363	10%	331	301	280	6.013	5.462	5.075	100	3314	3010	2797
2	200	20.0	0.363	30%	994	903	839	18.039	16.386	15.224	100	3314	3010	2797
3	200	20.0	0.363	50%	1657	1505	1398	30.064	27.311	25.373	100	3314	3010	2797
18	200	20.0	0.363	70%	2320	2107	1958	42.090	38.235	35.523	100	3314	3010	2797
5	150	15.0	0.272	10%	277	247	227	5.019	4.486	4.125	100	2766	2472	2273
6	150	15.0	0.272	30%	830	742	682	15.058	13.458	12.374	100	2766	2472	2273
7	150	15.0	0.272	50%	1383	1236	1137	25.097	22.430	20.624	100	2766	2472	2273
19	150	15.0	0.272	70%	1936	1731	1591	35.135	31.401	28.874	100	2766	2472	2273
8	100	10.0	0.181	10%	218	189	170	3.949	3.426	3.088	100	2177	1888	1702
9	100	10.0	0.181	30%	653	566	510	11.848	10.278	9.263	100	2177	1888	1702
10	100	10.0	0.181	50%	1088	944	851	19.747	17.130	15.439	100	2177	1888	1702
20	100	10.0	0.181	70%	1524	1322	1191	27.646	23.981	21.614	100	2177	1888	1702
11	50	5.0	0.091	10%	152	123	105	2.763	2.229	1.902	100	1523	1229	1048
12	50	5.0	0.091	30%	457	369	314	8.289	6.688	5.706	100	1523	1229	1048
13	50	5.0	0.091	50%	761	614	524	13.815	11.147	9.511	100	1523	1229	1048
21	50	5.0	0.091	70%	1066	860	734	19.341	15.606	13.315	100	1523	1229	1048
15	25	2.5	0.045	10%	116	85	66	2.099	1.538	1.199	100	1156	848	661
16	25	2.5	0.045	30%	347	254	198	6.296	4.615	3.598	100	1156	848	661
17	25	2.5	0.045	50%	578	424	330	10.493	7.692	5.996	100	1156	848	661
22	25	2.5	0.045	70%	810	593	463	14.690	10.769	8.394	100	1156	848	661

D.3.2 Sample 2 – Weathered chert from N4 extension upper selected layer

Table D.23: Resilient modulus tri-axial loading schedule for N4 extension upper selected layer (VD = 0.715).

Seq	Confining Stress kPa	Contact Stress kPa	Contact Stress kN	% Sat % of Failure	18% Cyclic Stress kPa	18% Cyclic Stress kN	Nrep	Predicted failure strength 18%	% Sat % of Failure	51% Cyclic Stress kPa	51% Cyclic Stress kN	Nrep	Predicted failure strength 51%
0	100	10.0	0.181	30%	682	12.369	1000	2272	30%	627	11.379	1000	2090
1	200	20.0	0.363	10%	316	5.731	100	3158	10%	265	4.813	100	2652
2	200	20.0	0.363	30%	947	17.192	100	3158	30%	796	14.439	100	2652
3	200	20.0	0.363	50%	1579	28.653	100	3158	50%	1326	24.065	100	2652
18	200	20.0	0.363	70%	2211	40.114	100	3158	70%	1857	33.691	100	2652
5	150	15.0	0.272	10%	272	4.927	100	2715	10%	237	4.303	100	2371
6	150	15.0	0.272	30%	815	14.780	100	2715	30%	711	12.909	100	2371
7	150	15.0	0.272	50%	1358	24.634	100	2715	50%	1186	21.515	100	2371
19	150	15.0	0.272	70%	1901	34.488	100	2715	70%	1660	30.121	100	2371
8	100	10.0	0.181	10%	227	4.123	100	2272	10%	209	3.793	100	2090
9	100	10.0	0.181	30%	682	12.369	100	2272	30%	627	11.379	100	2090
10	100	10.0	0.181	50%	1136	20.615	100	2272	50%	1045	18.966	100	2090
20	100	10.0	0.181	70%	1590	28.861	100	2272	70%	1463	26.552	100	2090
11	50	5.0	0.091	10%	183	3.319	100	1829	10%	181	3.283	100	1809
12	50	5.0	0.091	30%	549	9.957	100	1829	30%	543	9.850	100	1809
13	50	5.0	0.091	50%	915	16.596	100	1829	50%	905	16.416	100	1809
21	50	5.0	0.091	70%	1280	23.234	100	1829	70%	1267	22.983	100	1809
15	25	2.5	0.045	10%	161	2.917	100	1608	10%	167	3.028	100	1669
16	25	2.5	0.045	30%	482	8.752	100	1608	30%	501	9.085	100	1669
17	25	2.5	0.045	50%	804	14.586	100	1608	50%	834	15.141	100	1669
22	25	2.5	0.045	70%	1125	20.420	100	1608	70%	1168	21.198	100	1669

Table D.24: Resilient modulus tri-axial loading schedule for N4 extension upper selected layer (VD = 0.715 and VD = 0.693).

Seq	Confining Stress kPa	Contact Stress kPa	Contact Stress kN	% Sat % of Failure	80% Cyclic Stress kPa	80% Cyclic Stress kN	Nrep	Predicted failure strength 80%	% Sat % of Failure	18% Cyclic Stress kPa	18% Cyclic Stress kN	Nrep	Predicted failure strength 18%
0	100	10.0	0.181	30%	253	4.589	1000	843	30%	743	13.482	1000	2477
1	200	20.0	0.363	10%	120	2.174	100	1198	10%	248	4.494	100	2477
2	200	20.0	0.363	30%	359	6.522	100	1198	30%	743	13.482	100	2477
3	200	20.0	0.363	50%	599	10.869	100	1198	50%	1238	22.470	100	2477
18	200	20.0	0.363	70%	839	15.217	100	1198	70%	1734	31.457	100	2477
5	150	15.0	0.272	10%	102	1.852	100	1020	10%	208	3.781	100	2084
6	150	15.0	0.272	30%	306	5.555	100	1020	30%	625	11.342	100	2084
7	150	15.0	0.272	50%	510	9.259	100	1020	50%	1042	18.904	100	2084
19	150	15.0	0.272	70%	714	12.962	100	1020	70%	1458	26.465	100	2084
8	100	10.0	0.181	10%	84	1.530	100	843	10%	169	3.068	100	1690
9	100	10.0	0.181	30%	253	4.589	100	843	30%	507	9.203	100	1690
10	100	10.0	0.181	50%	421	7.648	100	843	50%	845	15.338	100	1690
20	100	10.0	0.181	70%	590	10.707	100	843	70%	1183	21.473	100	1690
11	50	5.0	0.091	10%	67	1.208	100	665	10%	130	2.354	100	1297
12	50	5.0	0.091	30%	200	3.623	100	665	30%	389	7.063	100	1297
13	50	5.0	0.091	50%	333	6.038	100	665	50%	649	11.772	100	1297
21	50	5.0	0.091	70%	466	8.453	100	665	70%	908	16.480	100	1297
15	25	2.5	0.045	10%	58	1.046	100	577	10%	110	1.998	100	1101
16	25	2.5	0.045	30%	173	3.139	100	577	30%	330	5.993	100	1101
17	25	2.5	0.045	50%	288	5.232	100	577	50%	550	9.988	100	1101
22	25	2.5	0.045	70%	404	7.325	100	577	70%	771	13.984	100	1101

Table D.25:   Resilient modulus tri-axial loading schedule for N4 extension upper selected layer (VD = 0.693).

Seq	Confining Stress kPa	Contact Stress		% Sat	51%	51%		Predicted failure strength	% Sat	80%	80%		Predicted failure strength
		kPa	kN	% of Failure	Cyclic Stress				% of Failure	Cyclic Stress			
					kPa	kN	Nrep	51%		kPa	kN	Nrep	80%
0	100	10.0	0.181	30%	482	8.738	1000	1605	30%	171	3.108	1000	571
1	200	20.0	0.363	10%	228	4.142	100	2283	10%	91	1.648	100	908
2	200	20.0	0.363	30%	685	12.426	100	2283	30%	272	4.944	100	908
3	200	20.0	0.363	50%	1141	20.709	100	2283	50%	454	8.240	100	908
18	200	20.0	0.363	70%	1598	28.993	100	2283	70%	636	11.536	100	908
5	150	15.0	0.272	10%	194	3.527	100	1944	10%	74	1.342	100	740
6	150	15.0	0.272	30%	583	10.582	100	1944	30%	222	4.026	100	740
7	150	15.0	0.272	50%	972	17.636	100	1944	50%	370	6.710	100	740
19	150	15.0	0.272	70%	1361	24.691	100	1944	70%	518	9.394	100	740
8	100	10.0	0.181	10%	161	2.913	100	1605	10%	57	1.036	100	571
9	100	10.0	0.181	30%	482	8.738	100	1605	30%	171	3.108	100	571
10	100	10.0	0.181	50%	803	14.564	100	1605	50%	285	5.180	100	571
20	100	10.0	0.181	70%	1124	20.389	100	1605	70%	400	7.252	100	571
11	50	5.0	0.091	10%	127	2.298	100	1267	10%	40	0.730	100	402
12	50	5.0	0.091	30%	380	6.895	100	1267	30%	121	2.190	100	402
13	50	5.0	0.091	50%	633	11.491	100	1267	50%	201	3.650	100	402
21	50	5.0	0.091	70%	887	16.087	100	1267	70%	282	5.110	100	402
15	25	2.5	0.045	10%	110	1.991	100	1097	10%	32	0.577	100	318
16	25	2.5	0.045	30%	329	5.973	100	1097	30%	95	1.731	100	318
17	25	2.5	0.045	50%	549	9.955	100	1097	50%	159	2.885	100	318
22	25	2.5	0.045	70%	768	13.936	100	1097	70%	223	4.039	100	318

D.3.3 Sample 3 – Weathered dolerite from Road S191 base layer

Table D.26: Resilient modulus tri-axial loading schedule for Road S191 base layer (VD = 0.796).

Seq	Confining Stress kPa	Contact Stress kPa	Contact Stress kN	% Sat / % of Failure	20%	50%	80%	20%	50%	80%	Nrep	20%	50%	80%
					Cyclic Stress kPa			Cyclic Stress kN				Predicted failure strength		
0	100	10.0	0.181	30%	735	369	214	13.343	6.697	3.875	1000	2451	1230	712
1	200	20.0	0.363	10%	301	165	98	5.470	2.986	1.774	100	3014	1646	977
2	200	20.0	0.363	30%	904	494	293	16.410	8.958	5.321	100	3014	1646	977
3	200	20.0	0.363	50%	1507	823	489	27.350	14.930	8.869	100	3014	1646	977
18	200	20.0	0.363	70%	2110	1152	684	38.290	20.902	12.416	100	3014	1646	977
5	150	15.0	0.272	10%	275	146	86	4.989	2.641	1.555	100	2749	1455	857
6	150	15.0	0.272	30%	825	437	257	14.967	7.922	4.665	100	2749	1455	857
7	150	15.0	0.272	50%	1375	728	428	24.945	13.204	7.775	100	2749	1455	857
19	150	15.0	0.272	70%	1925	1019	600	34.924	18.486	10.885	100	2749	1455	857
8	100	10.0	0.181	10%	245	123	71	4.448	2.232	1.292	100	2451	1230	712
9	100	10.0	0.181	30%	735	369	214	13.343	6.697	3.875	100	2451	1230	712
10	100	10.0	0.181	50%	1226	615	356	22.239	11.161	6.458	100	2451	1230	712
20	100	10.0	0.181	70%	1716	861	498	31.135	15.626	9.041	100	2451	1230	712
11	50	5.0	0.091	10%	210	94	52	3.818	1.709	0.940	100	2104	942	518
12	50	5.0	0.091	30%	631	282	155	11.453	5.126	2.821	100	2104	942	518
13	50	5.0	0.091	50%	1052	471	259	19.089	8.543	4.702	100	2104	942	518
21	50	5.0	0.091	70%	1473	659	363	26.724	11.960	6.583	100	2104	942	518
15	25	2.5	0.045	10%	190	75	38	3.453	1.357	0.685	100	1903	748	377
16	25	2.5	0.045	30%	571	224	113	10.359	4.072	2.055	100	1903	748	377
17	25	2.5	0.045	50%	951	374	189	17.265	6.787	3.424	100	1903	748	377
22	25	2.5	0.045	70%	1332	524	264	24.171	9.502	4.794	100	1903	748	377

Table D.27: Resilient modulus tri-axial loading schedule for Road S191 base layer (VD = 0.791).

Seq	Confining Stress kPa	Contact Stress kPa	Contact Stress kN	% Sat / % of Failure	20% kPa	50% kPa	80% kPa	20% kN	50% kN	80% kN	Nrep	Predicted failure strength 20%	Predicted failure strength 50%	Predicted failure strength 80%
0	100	10.0	0.181	30%	685	407	255	12.422	7.383	4.635	1000	2282	1356	851
1	200	20.0	0.363	10%	298	188	124	5.405	3.417	2.243	100	2978	1883	1236
2	200	20.0	0.363	30%	894	565	371	16.214	10.250	6.730	100	2978	1883	1236
3	200	20.0	0.363	50%	1489	941	618	27.023	17.083	11.217	100	2978	1883	1236
18	200	20.0	0.363	70%	2085	1318	865	37.833	23.916	15.704	100	2978	1883	1236
5	150	15.0	0.272	10%	265	164	106	4.804	2.968	1.919	100	2647	1636	1057
6	150	15.0	0.272	30%	794	491	317	14.412	8.904	5.756	100	2647	1636	1057
7	150	15.0	0.272	50%	1324	818	529	24.020	14.840	9.593	100	2647	1636	1057
19	150	15.0	0.272	70%	1853	1145	740	33.627	20.776	13.431	100	2647	1636	1057
8	100	10.0	0.181	10%	228	136	85	4.141	2.461	1.545	100	2282	1356	851
9	100	10.0	0.181	30%	685	407	255	12.422	7.383	4.635	100	2282	1356	851
10	100	10.0	0.181	50%	1141	678	426	20.704	12.306	7.725	100	2282	1356	851
20	100	10.0	0.181	70%	1597	949	596	28.985	17.228	10.815	100	2282	1356	851
11	50	5.0	0.091	10%	187	102	60	3.386	1.859	1.084	100	1866	1025	597
12	50	5.0	0.091	30%	560	307	179	10.159	5.578	3.251	100	1866	1025	597
13	50	5.0	0.091	50%	933	512	299	16.932	9.296	5.419	100	1866	1025	597
21	50	5.0	0.091	70%	1306	717	418	23.705	13.014	7.586	100	1866	1025	597
15	25	2.5	0.045	10%	163	82	43	2.959	1.496	0.785	100	1630	824	433
16	25	2.5	0.045	30%	489	247	130	8.876	4.487	2.355	100	1630	824	433
17	25	2.5	0.045	50%	815	412	216	14.793	7.478	3.925	100	1630	824	433
22	25	2.5	0.045	70%	1141	577	303	20.710	10.470	5.496	100	1630	824	433

D.3.4 Sample 4 – Weathered shale from Road P10-2 base layer

Table D.28: Resilient modulus tri-axial loading schedule for Road P10-2 base layer (VD = 0.776).

Seq	Confining Stress kPa	Contact Stress kPa	Contact Stress kN	% Sat / % of Failure	20%	50%	80%	20%	50%	80%	Nrep	20%	50%	80%
					Cyclic Stress kPa			Cyclic Stress kN				Predicted failure strength		
0	100	10.0	0.181	30%	736	401	208	13.356	7.274	3.783	1000	2453	1336	695
1	200	20.0	0.363	10%	313	177	99	5.677	3.219	1.792	100	3128	1774	988
2	200	20.0	0.363	30%	939	532	296	17.030	9.657	5.376	100	3128	1774	988
3	200	20.0	0.363	50%	1564	887	494	28.384	16.095	8.960	100	3128	1774	988
18	200	20.0	0.363	70%	2190	1242	691	39.737	22.533	12.544	100	3128	1774	988
5	150	15.0	0.272	10%	280	156	85	5.087	2.839	1.540	100	2803	1564	849
6	150	15.0	0.272	30%	841	469	255	15.260	8.516	4.621	100	2803	1564	849
7	150	15.0	0.272	50%	1402	782	424	25.434	14.193	7.702	100	2803	1564	849
19	150	15.0	0.272	70%	1962	1095	594	35.607	19.871	10.783	100	2803	1564	849
8	100	10.0	0.181	10%	245	134	69	4.452	2.425	1.261	100	2453	1336	695
9	100	10.0	0.181	30%	736	401	208	13.356	7.274	3.783	100	2453	1336	695
10	100	10.0	0.181	50%	1227	668	347	22.259	12.124	6.305	100	2453	1336	695
20	100	10.0	0.181	70%	1717	935	486	31.163	16.973	8.826	100	2453	1336	695
11	50	5.0	0.091	10%	207	108	52	3.757	1.963	0.937	100	2070	1082	517
12	50	5.0	0.091	30%	621	325	155	11.270	5.890	2.812	100	2070	1082	517
13	50	5.0	0.091	50%	1035	541	258	18.783	9.817	4.687	100	2070	1082	517
21	50	5.0	0.091	70%	1449	757	362	26.297	13.744	6.562	100	2070	1082	517
15	25	2.5	0.045	10%	186	94	41	3.379	1.707	0.748	100	1862	941	412
16	25	2.5	0.045	30%	559	282	124	10.136	5.122	2.245	100	1862	941	412
17	25	2.5	0.045	50%	931	470	206	16.893	8.536	3.741	100	1862	941	412
22	25	2.5	0.045	70%	1303	659	289	23.651	11.951	5.238	100	1862	941	412

Table D.29: Resilient modulus tri-axial loading schedule for Road P10-2 base layer (VD = 0.745).

Seq	Confining Stress kPa	Contact Stress kPa	Contact Stress kN	% Sat % of Failure	20% Cyclic Stress kPa	50% kPa	80% kPa	20% kN	50% kN	80% kN	Nrep	Predicted failure strength 20%	50%	80%
0	100	10.0	0.181	30%	461	268	155	8.373	4.860	2.808	1000	1538	893	516
1	200	20.0	0.363	10%	218	130	77	3.960	2.356	1.402	100	2182	1298	772
2	200	20.0	0.363	30%	655	389	232	11.879	7.067	4.205	100	2182	1298	772
3	200	20.0	0.363	50%	1091	649	386	19.799	11.778	7.009	100	2182	1298	772
18	200	20.0	0.363	70%	1528	909	541	27.718	16.489	9.812	100	2182	1298	772
5	150	15.0	0.272	10%	188	111	65	3.407	2.009	1.183	100	1877	1107	652
6	150	15.0	0.272	30%	563	332	196	10.220	6.026	3.550	100	1877	1107	652
7	150	15.0	0.272	50%	939	554	326	17.034	10.044	5.917	100	1877	1107	652
19	150	15.0	0.272	70%	1314	775	456	23.847	14.062	8.283	100	1877	1107	652
8	100	10.0	0.181	10%	154	89	52	2.791	1.620	0.936	100	1538	893	516
9	100	10.0	0.181	30%	461	268	155	8.373	4.860	2.808	100	1538	893	516
10	100	10.0	0.181	50%	769	446	258	13.954	8.099	4.680	100	1538	893	516
20	100	10.0	0.181	70%	1077	625	361	19.536	11.339	6.553	100	1538	893	516
11	50	5.0	0.091	10%	114	64	35	2.075	1.161	0.638	100	1144	640	352
12	50	5.0	0.091	30%	343	192	106	6.226	3.484	1.915	100	1144	640	352
13	50	5.0	0.091	50%	572	320	176	10.376	5.807	3.192	100	1144	640	352
21	50	5.0	0.091	70%	801	448	246	14.527	8.130	4.469	100	1144	640	352
15	25	2.5	0.045	10%	91	49	25	1.654	0.885	0.452	100	911	488	249
16	25	2.5	0.045	30%	273	146	75	4.962	2.655	1.356	100	911	488	249
17	25	2.5	0.045	50%	456	244	125	8.270	4.425	2.259	100	911	488	249
22	25	2.5	0.045	70%	638	341	174	11.578	6.194	3.163	100	911	488	249

D.3.5 Sample 5 – Weathered calcrete from Road D804 base layer

Table D.30: Resilient modulus tri-axial loading schedule for Road D804 base layer (VD = 0.744).

Seq	Confining Stress kPa	Contact Stress kPa	Contact Stress kN	% Sat / % of Failure	20%	50%	80%	20%	50%	80%	Nrep	Predicted failure strength 20%	50%	80%
					Cyclic Stress kPa			kN						
0	100	10.0	0.181	30%	1100	457	176	19.957	8.290	3.188	1000	3666	1523	586
1	200	20.0	0.363	10%	449	208	96	8.152	3.770	1.740	100	4493	2078	959
2	200	20.0	0.363	30%	1348	623	288	24.456	11.310	5.219	100	4493	2078	959
3	200	20.0	0.363	50%	2246	1039	479	40.761	18.849	8.698	100	4493	2078	959
18	200	20.0	0.363	70%	3145	1454	671	57.065	26.389	12.177	100	4493	2078	959
5	150	15.0	0.272	10%	408	180	77	7.403	3.268	1.402	100	4080	1801	773
6	150	15.0	0.272	30%	1224	540	232	22.210	9.803	4.207	100	4080	1801	773
7	150	15.0	0.272	50%	2040	900	386	37.017	16.339	7.012	100	4080	1801	773
19	150	15.0	0.272	70%	2856	1261	541	51.824	22.875	9.817	100	4080	1801	773
8	100	10.0	0.181	10%	367	152	59	6.652	2.763	1.063	100	3666	1523	586
9	100	10.0	0.181	30%	1100	457	176	19.957	8.290	3.188	100	3666	1523	586
10	100	10.0	0.181	50%	1833	761	293	33.261	13.817	5.314	100	3666	1523	586
20	100	10.0	0.181	70%	2566	1066	410	46.566	19.344	7.439	100	3666	1523	586
11	50	5.0	0.091	10%	325	124	40	5.898	2.256	0.720	100	3251	1243	397
12	50	5.0	0.091	30%	975	373	119	17.695	6.769	2.159	100	3251	1243	397
13	50	5.0	0.091	50%	1625	622	198	29.492	11.281	3.598	100	3251	1243	397
21	50	5.0	0.091	70%	2275	870	278	41.289	15.794	5.038	100	3251	1243	397
15	25	2.5	0.045	10%	304	110	30	5.521	2.001	0.546	100	3042	1103	301
16	25	2.5	0.045	30%	913	331	90	16.562	6.004	1.639	100	3042	1103	301
17	25	2.5	0.045	50%	1521	552	151	27.603	10.007	2.732	100	3042	1103	301
22	25	2.5	0.045	70%	2130	772	211	38.644	14.010	3.825	100	3042	1103	301

Table D.31: Resilient modulus tri-axial loading schedule for Road D804 base layer (VD = 0.714).

Seq	Confining Stress kPa	Contact Stress kPa	Contact Stress kN	% Sat % of Failure	20%	50%	80%	20%	50%	80%	Nrep	Predicted failure strength 20%	Predicted failure strength 50%	Predicted failure strength 80%
					Cyclic Stress kPa			kN						
0	100	10.0	0.181	30%	500	241	122	9.071	4.367	2.208	1000	1666	802	406
1	200	20.0	0.363	10%	243	131	74	4.401	2.376	1.350	100	2425	1309	744
2	200	20.0	0.363	30%	728	393	223	13.203	7.127	4.050	100	2425	1309	744
3	200	20.0	0.363	50%	1213	655	372	22.005	11.878	6.749	100	2425	1309	744
18	200	20.0	0.363	70%	1698	916	521	30.807	16.630	9.449	100	2425	1309	744
5	150	15.0	0.272	10%	205	106	58	3.714	1.917	1.044	100	2047	1057	576
6	150	15.0	0.272	30%	614	317	173	11.143	5.752	3.133	100	2047	1057	576
7	150	15.0	0.272	50%	1023	528	288	18.571	9.587	5.222	100	2047	1057	576
19	150	15.0	0.272	70%	1433	740	403	26.000	13.422	7.310	100	2047	1057	576
8	100	10.0	0.181	10%	167	80	41	3.024	1.456	0.736	100	1666	802	406
9	100	10.0	0.181	30%	500	241	122	9.071	4.367	2.208	100	1666	802	406
10	100	10.0	0.181	50%	833	401	203	15.118	7.278	3.679	100	1666	802	406
20	100	10.0	0.181	70%	1166	562	284	21.165	10.189	5.151	100	1666	802	406
11	50	5.0	0.091	10%	128	55	23	2.328	0.989	0.423	100	1283	545	233
12	50	5.0	0.091	30%	385	164	70	6.983	2.967	1.269	100	1283	545	233
13	50	5.0	0.091	50%	641	273	117	11.639	4.946	2.116	100	1283	545	233
21	50	5.0	0.091	70%	898	382	163	16.295	6.924	2.962	100	1283	545	233
15	25	2.5	0.045	10%	109	42	15	1.978	0.754	0.264	100	1090	415	146
16	25	2.5	0.045	30%	327	125	44	5.933	2.261	0.793	100	1090	415	146
17	25	2.5	0.045	50%	545	208	73	9.888	3.768	1.321	100	1090	415	146
22	25	2.5	0.045	70%	763	291	102	13.844	5.275	1.849	100	1090	415	146

APPENDIX E

TABLE OF CONTENT

E. NEGATIVE CORRELATION COEFFICIENT

E.1 BACKGROUND

Regression analysis were utilised in calibration of the cord modulus model where the correlation coefficient (R^2), amongst other indicators, were used as indicator of the accuracy of the analysis.

R^2 gives an indication of the linearity of the relationship between Y and X (Van As, 2003), i.e. how well a regression line fits the data. For linear regression, R^2 is simply the square of the sample correlation coefficient between the outcomes and their predicted values, or in the case of simple linear regression, between the outcome and the values being used for prediction. In such cases, the values vary from 0 to 1, with 1 indicating a line fitting the data perfectly. In this thesis R^2 will be calculated using the following equation in the processing of the measured data in MS Excel spreadsheets.

$$R^2 = 1 - \frac{SS_{err}}{SS_{tot}} = 1 - \frac{\Sigma((y_i - f_i)^2)}{\Sigma((y_i - \bar{y})^2)} = 1 - \frac{\Sigma(M_{obs} - M_{pred})^2}{\Sigma((M_{obs} - Ave_{obs})^2)} \qquad \text{(E.1)}$$

Where

SS_{err} = residual sum of squares;

SS_{tot} = total sum of squares;

y_i = observed values of the data set;

f_i = associated modelled values;

$\bar{y}$ = mean of the observed data (Draper and Smith, 1998; Everitt, 2002).

However, R^2 does not indicate whether:

- the independent variables are a true cause of the changes in the dependent variable;
- omitted-variable bias exists;
- the correct regression was used;
- the most appropriate set of independent variables has been chosen;
- there is co-linearity present in the data; or
- the model might be improved by using transformed versions of the existing set of independent variables (Draper and Smith, 1998; Everitt, 2002).

E.2 NEGATIVE R^2 VALUES

The following section contains explanations from various sources on how negative values for R^2 may occur.

When MS Excel is used to calculate R^2 values, often erroneous negative R^2 values are calculated. However, as indicated in Section E.1 correlation coefficient values calculated by MS Excel was not used in this thesis. '*An R-squared value that is inserted on a chart with a linear trend line is always incorrect in the case where the **Set Intercept = 0** box is selected. (Cases with non-linear trend lines or values other than zero for setting the intercept, or both, have not been investigated.)*', (htpp://support.microsoft.com/kb/829249).

Negative values of R^2 may occur when fitting non-linear trends to data. In these instances, the mean of the data provides a fit to the data that is superior to that of the trend under this goodness of fit analysis (Cameron and Windmeijer, 1997).

As indicated by Equation E.1, R^2 is defined as:

$$R^2 = 1 - \frac{SS_{err}}{SS_{tot}}$$
(E.2)

'*Appearances can be deceptive. R^2 is not really the square of anything. If SS_{err} is larger than SS_{tot}, R^2 will be negative (see equation above). While it is surprising to see something called "squared" have a negative value, it is not impossible (since R^2 is not actually the square of R).*

How can this happen? SS_{err} is the sum of the squares of the vertical distances of the points from a curve (or line). SS_{tot} is the sum of the squares of the vertical distances of the points from a horizontal line drawn at the mean Y value. SS_{err} will exceed SS_{tot} when the line or curve fits the data even worse than does a horizontal line.

R^2 will be negative when the line or curve does an awful job of fitting the data. This can happen when you fit a poorly chosen model (perhaps by mistake, or perhaps because the model was fit to a different data set), or .when you apply constraints to the model that don't make any sense (perhaps you entered a positive number when you intended to enter a negative number), or for example, if you constrain the Hill slope of a dose-response curve to be greater than 1.0, but the curve actually goes downhill (so the Hill slope should be negative), you might end up with a negative R^2 value and nonsense values for the parameters.' (GraphPad - FAQ 711 - How can R^2 be negative?)

E.3 REFERENCES

Cameron, A.C., Windmeijer, F.A.G. (1997). '*An R-squared measure of goodness of fit for some common non-linear regression models*', Journal of Econometrics, Volume 77, Issue 2, April 1997, pp. 329-342.

Draper, N.R. and Smith, H. (1998). '*Applied regression analysis*', 3rd Edition, Wiley-Interscience, New York, U.S.A.

Everitt, B.S. (2002). '*Cambridge dictionary of statistics*', 2nd Edition, Cambridge University Press, U.K.

GraphPad - FAQ 711 - How can R^2 be negative? web home page assessed on 18 April 2013.

htpp://support.microsoft.com/kb/829249 web home page assessed on 18 April 2013.

Van As, S.C. (2003). '*Applied statistics for Civil Engineers*', B.Eng (Honours) course material, University of Pretoria, Pretoria, RSA.

APPENDIX F

TABLE OF CONTENT

F. SUB-VARIABLE VALUES VERSUS SATURATION

F.1   SUB-VARIABLE VALUES VERSUS SATURATION

This section contains the graphs depicting the calibrated sub-variables ('α_1', 'β_1', 'α_2', 'α_3' and 'β_3') opposed to the saturation for each individual test result for samples 1 to 5.

N4 Extension base layer

N4 Extension upper selected layer

Road P10-2 base layer

Road S191 base layer

Road D804 base layer

N4 Extension base layer

N4 Extension upper selected layer

Road P10-2 base layer

Road S191 base layer

Road D804 base layer

N4 Extension base layer

N4 Extension upper selected layer

Road P10-2 base layer

Road S191 base layer

Road D804 base layer

N4 Extension base layer

N4 Extension upper selected layer

Road P10-2 base layer

Road S191 base layer

Road D804 base layer

N4 Extension base layer

N4 Extension upper selected layer

Road P10-2 base layer

Road S191 base layer

Road D804 base layer

APPENDIX G

TABLE OF CONTENT

LIST OF TABLES

G. MODEL CALIBRATION RESULTS

G.1   MODEL CALIBRATION PER SAMPLE

This section contains the model calibration plots and statistical data for samples 1 to 5.

G.1.1 Sample 1 – Crushed norite from N4 extension base layer
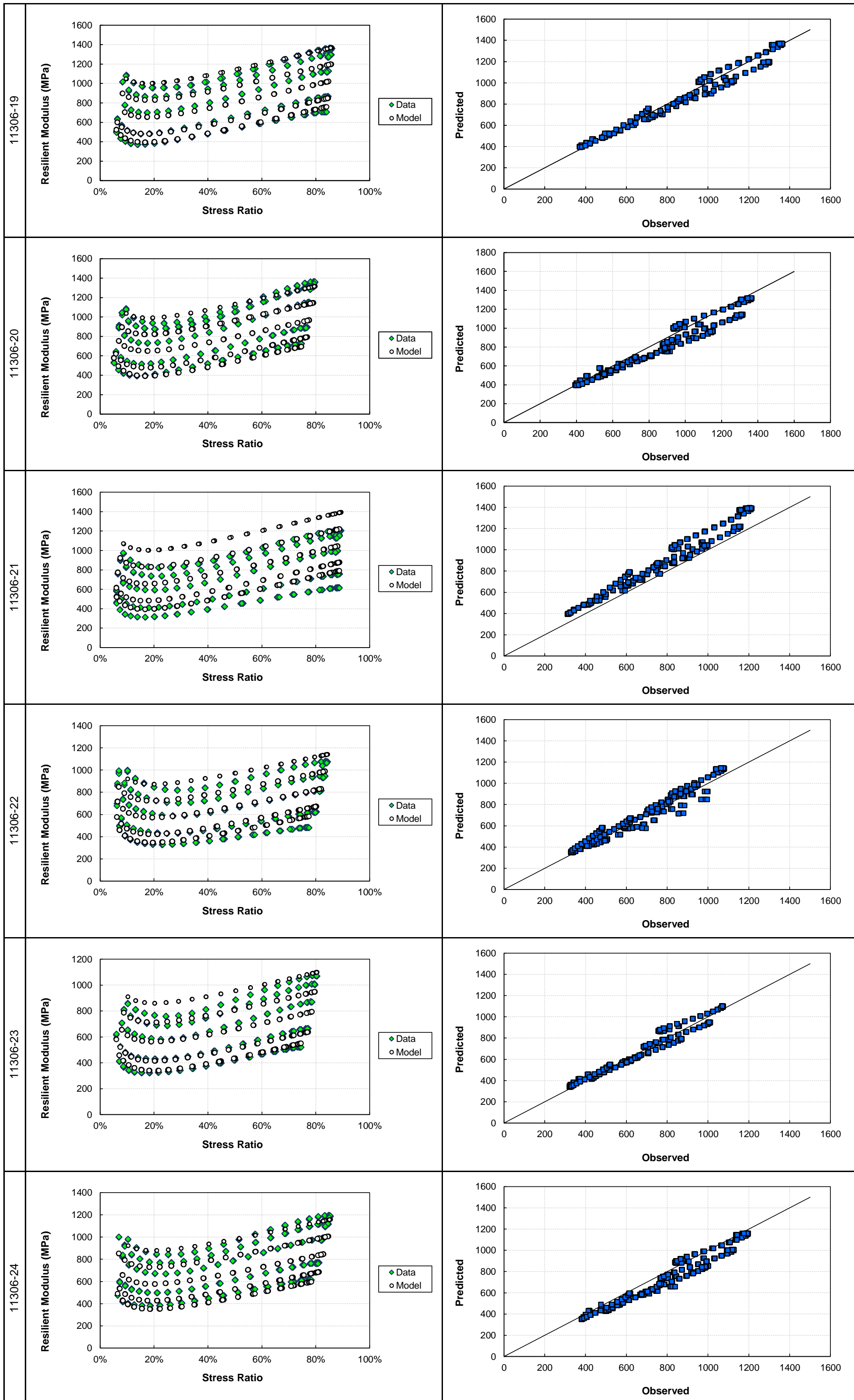
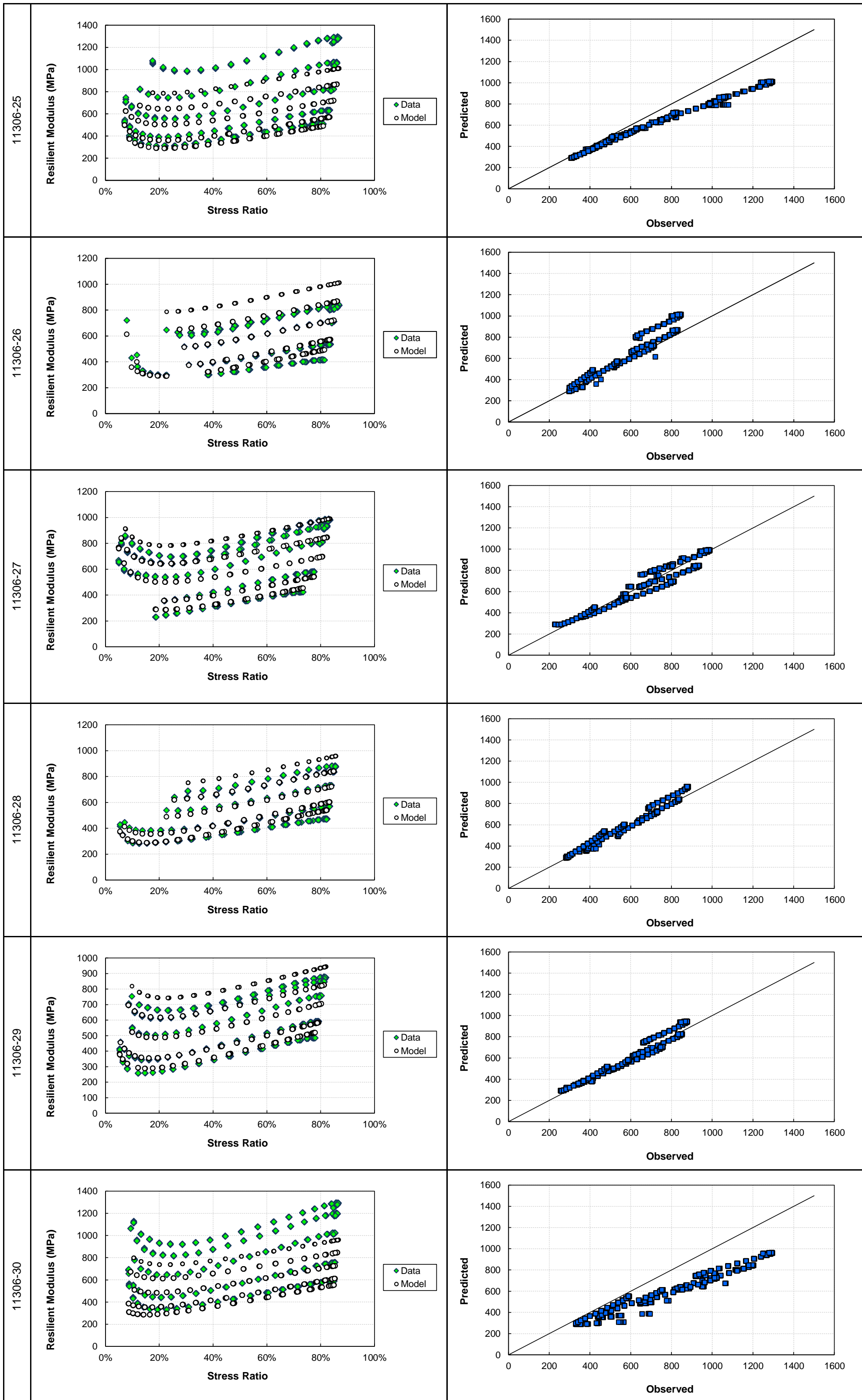**Table G.1:** **Model variables and statistical results for N4 extension base layer.**

Sample #	Volumetric Density (VD) (kg/m^3)	Saturation (S) (%)	a		b	c		R^2	SEE (MPa)	Average Error (%)
			α_1	β_1	α_2	α_3	β_3			
11306-19	0.82	0.14	78.53	3.41	680.97	19.06	0.013	0.96	55.0	5.6%
11306-20	0.83	0.16	78.26	3.36	677.47	19.16	0.011	0.95	63.9	5.7%
11306-21	0.82	0.14	78.57	3.41	681.54	19.05	0.013	0.59	161.8	20.8%
11306-22	0.82	0.43	60.02	3.00	543.11	20.57	0.002	0.94	53.4	7.0%
11306-23	0.83	0.45	55.33	2.98	526.30	20.72	0.002	0.96	45.4	5.3%
11306-24	0.82	0.41	61.99	3.01	551.42	20.50	0.002	0.89	76.6	8.5%
11306-25	0.82	0.66	16.97	2.84	461.81	21.79	0.001	0.68	159.8	17.4%
11306-26	0.82	0.65	17.50	2.84	462.26	21.77	0.001	0.83	71.3	7.4%
11306-27	0.82	0.67	14.78	2.83	459.95	21.88	0.001	0.88	70.9	8.3%
11306-28	0.80	0.13	87.24	2.24	464.83	9.41	0.068	0.25	157.4	20.0%
11306-29	0.81	0.13	86.96	2.25	463.71	9.55	0.068	0.26	150.7	19.2%
11306-30	0.80	0.12								
11306-31	0.79	0.42	51.11	2.69	386.10	20.44	0.049	0.81	80.5	11.2%
11306-32	0.80	0.42	50.72	2.69	385.55	20.53	0.048	0.74	125.2	14.6%
11306-33	0.80	0.46	44.29	2.73	376.69	22.13	0.046	0.82	97.0	13.0%
11306-34	0.80	0.69	16.53	2.89	340.15	30.84	0.035	0.88	85.3	10.0%
11306-35	0.79	0.62	24.18	2.84	350.64	27.84	0.038	0.95	51.2	9.6%
11306-36	0.79	0.63	22.96	2.85	349.02	28.26	0.038	0.90	53.9	8.7%

G.1.2   Sample 2 – Weathered chert from N4 extension upper selected layer

Table G.2: **Model variables and statistical results for N4 extension upper selected layer.**

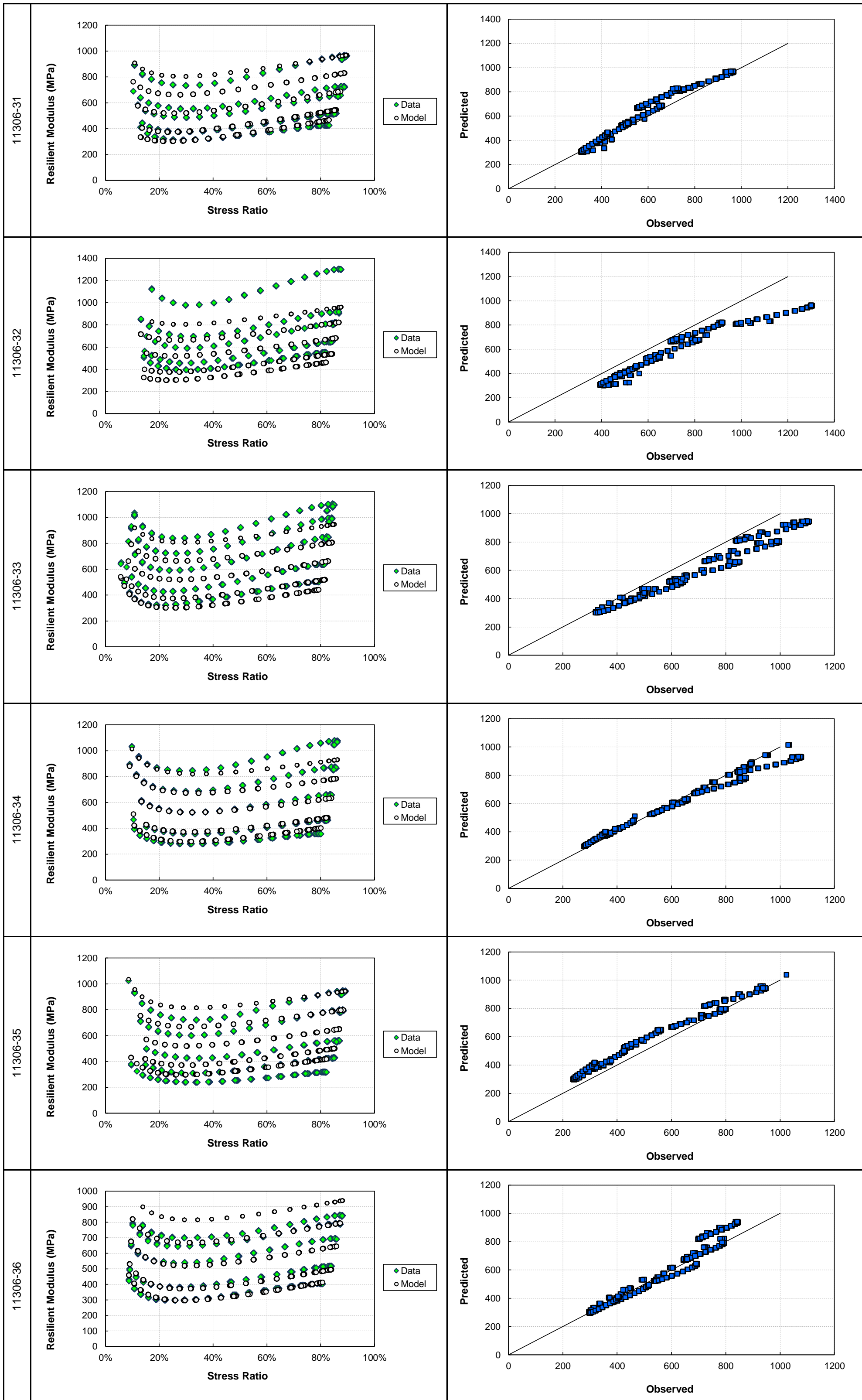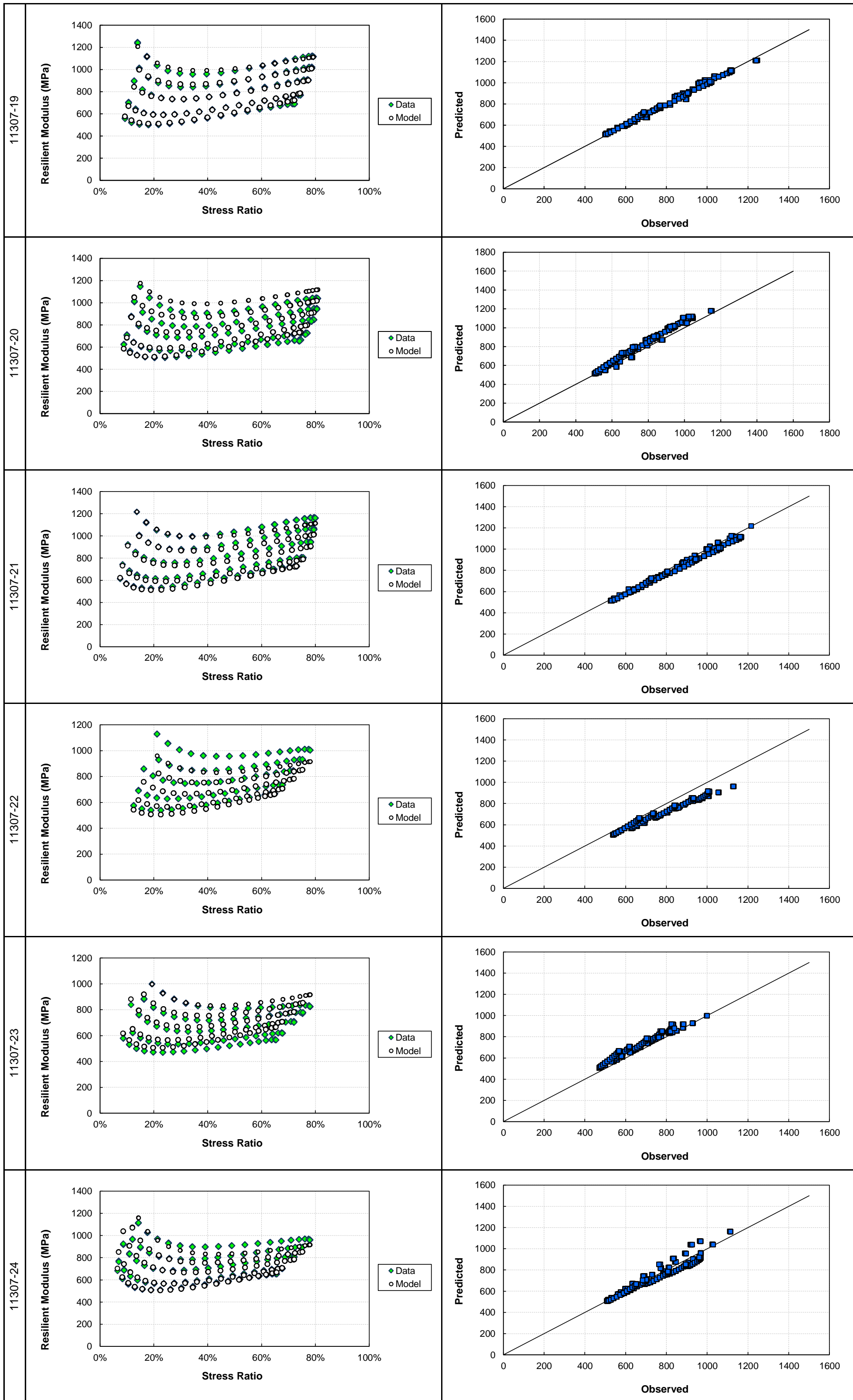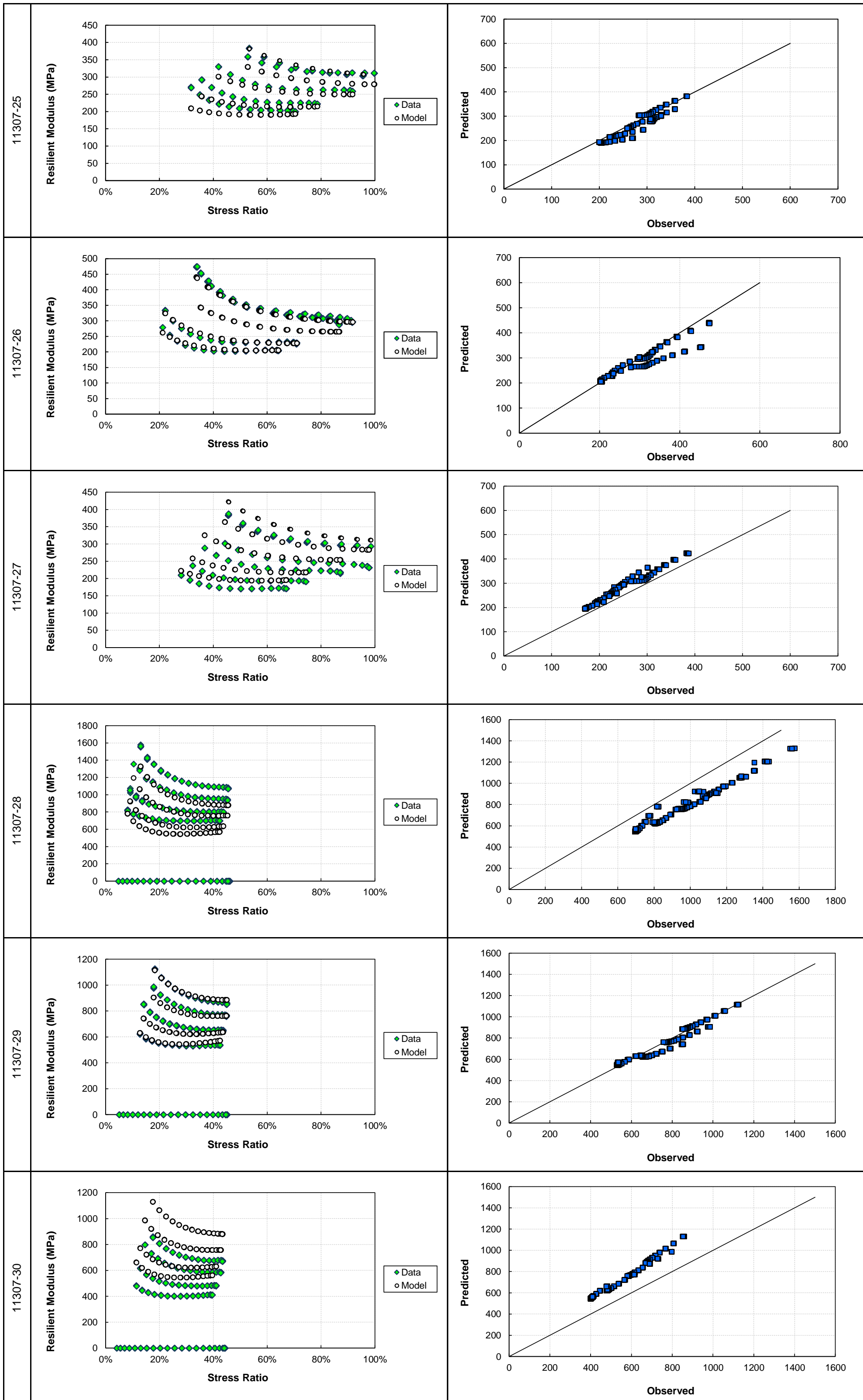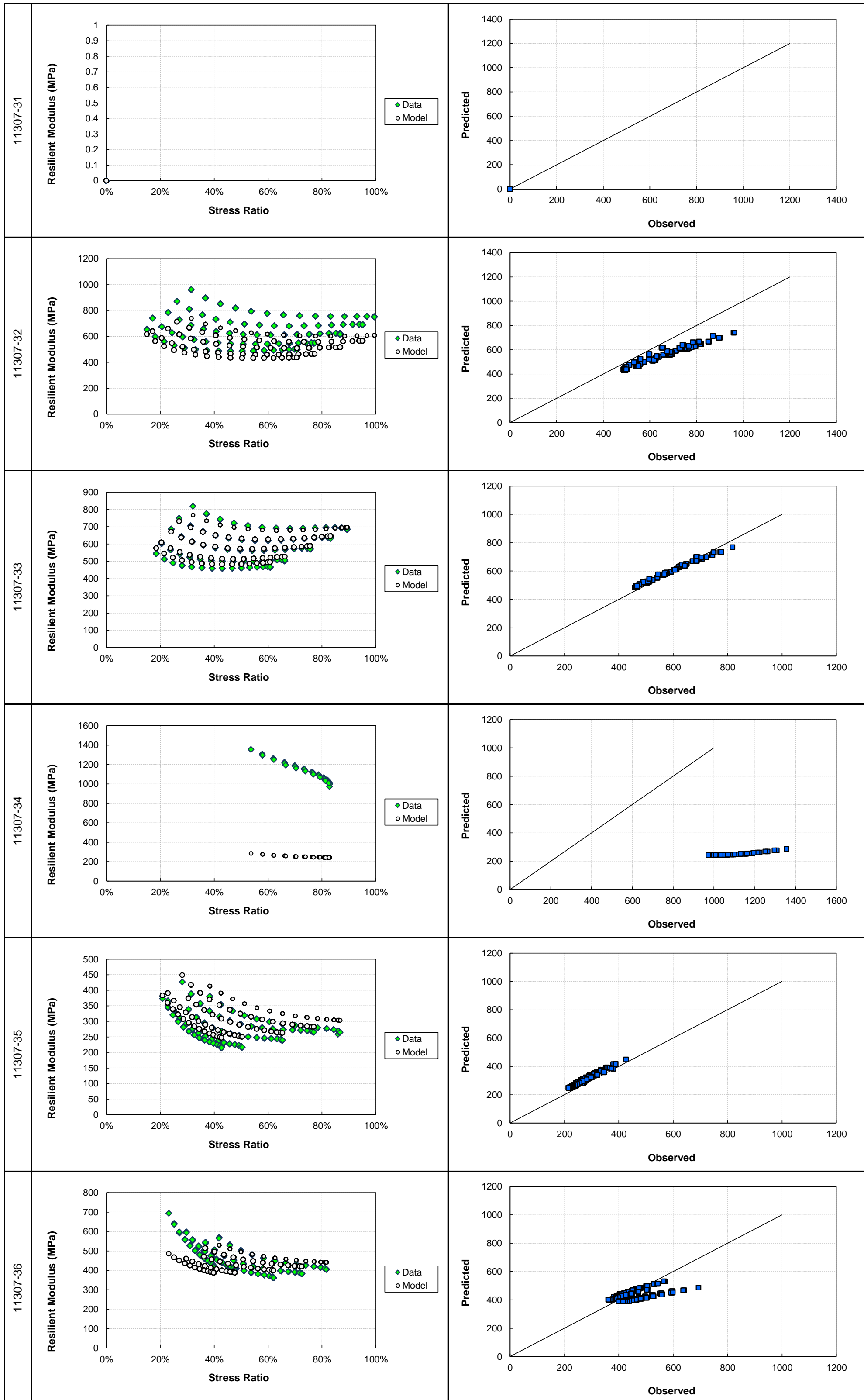| Sample #	Volumetric Density (VD) (kg/m³)	Saturation (S) (%)	a		b	c		R²	SEE (MPa)	Average Error (%)
			α_1	β_1	α_2	α_3	β_3			
11307-19	0.70	0.18	253.03	1.63	551.21	13.44	0.32	0.99	16.9	1.7%
11307-20	0.70	0.18	253.03	1.63	551.21	13.44	0.32	0.86	58.7	6.8%
11307-21	0.70	0.18	253.03	1.63	551.21	13.44	0.32	0.96	35.0	3.5%
11307-22	0.70	0.46	253.02	0.50	551.03	14.91	0.45	0.70	80.5	8.7%
11307-23	0.70	0.46	253.02	0.51	551.06	14.89	0.44	0.80	54.1	7.6%
11307-24	0.70	0.46	253.02	0.51	551.07	14.89	0.44	0.92	39.8	3.8%
11307-25	0.69	0.74	78.24	-0.06	100.46	16.36	0.62	0.79	21.1	6.5%
11307-26	0.69	0.73	92.25	-0.05	101.38	16.31	0.61	0.81	30.0	5.8%
11307-27	0.69	0.74	81.94	-0.06	100.68	16.34	0.62	0.53	34.8	14.1%
11307-28	0.68	0.16	233.21	1.11	510.08	24.42	0.59	0.10	257.7	19.6%
11307-29	0.69	0.16	233.21	1.14	510.08	24.00	0.59	0.75	136.1	6.2%
11307-30	0.69	0.16	233.21	1.11	510.08	24.42	0.59	-0.62	254.2	33.4%
11307-31	0.68	0.49								
11307-32	0.68	0.48	233.21	0.48	166.98	43.42	0.34	-0.08	110.9	15.6%
11307-33	0.69	0.47	233.21	0.49	269.15	43.14	0.35	0.96	17.2	2.6%
11307-34	0.68	0.73								
11307-35	0.68	0.70	57.54	0.26	85.27	56.80	0.24	0.40	31.5	11.2%
11307-36	0.68	0.69	190.89	0.27	85.27	56.27	0.24	0.25	53.5	8.5%

G.1.2 Sample 2 – Weathered chert from N4 extension upper selected layer

Table G.2:   Model variables and statistical results for N4 extension upper selected layer.

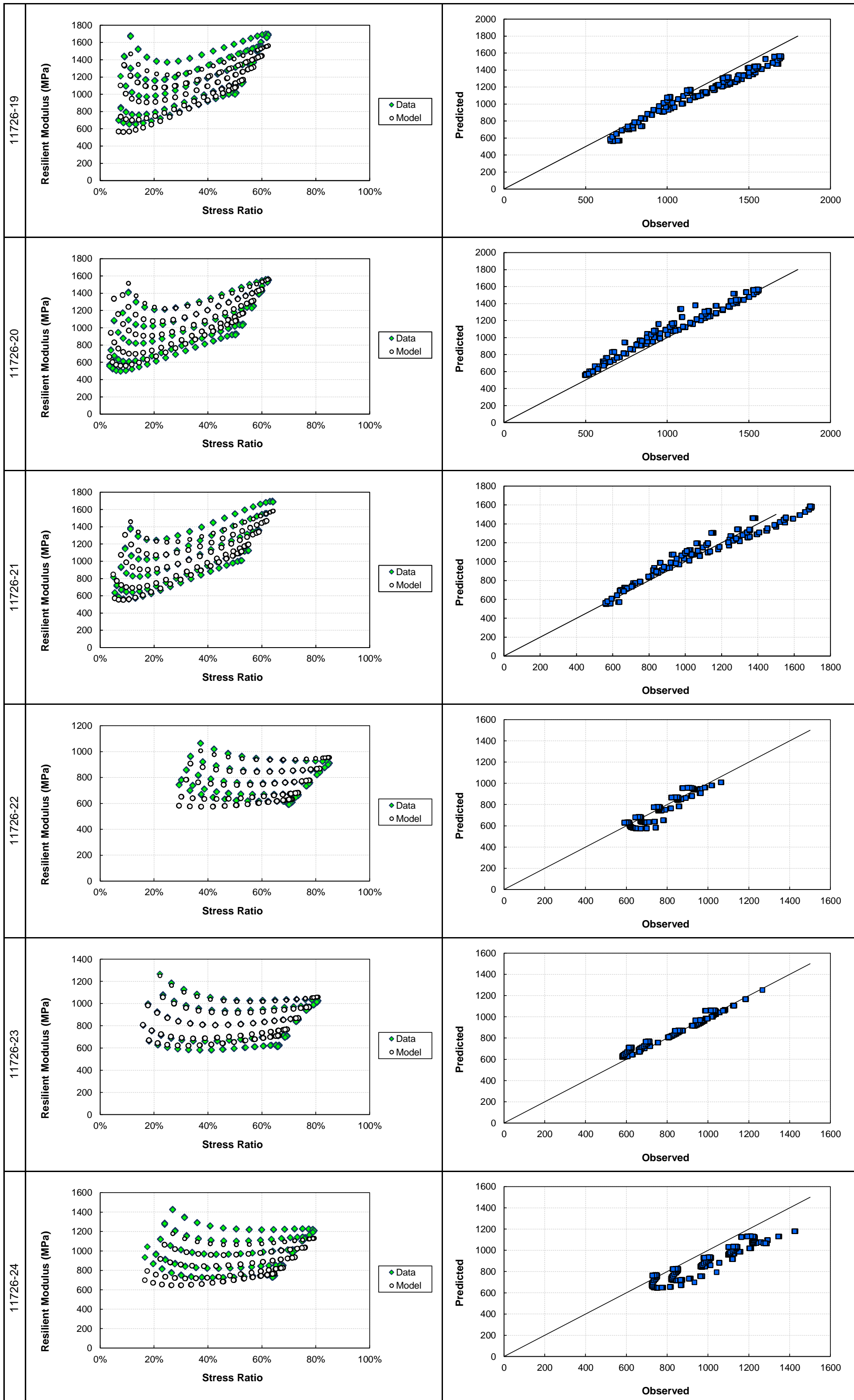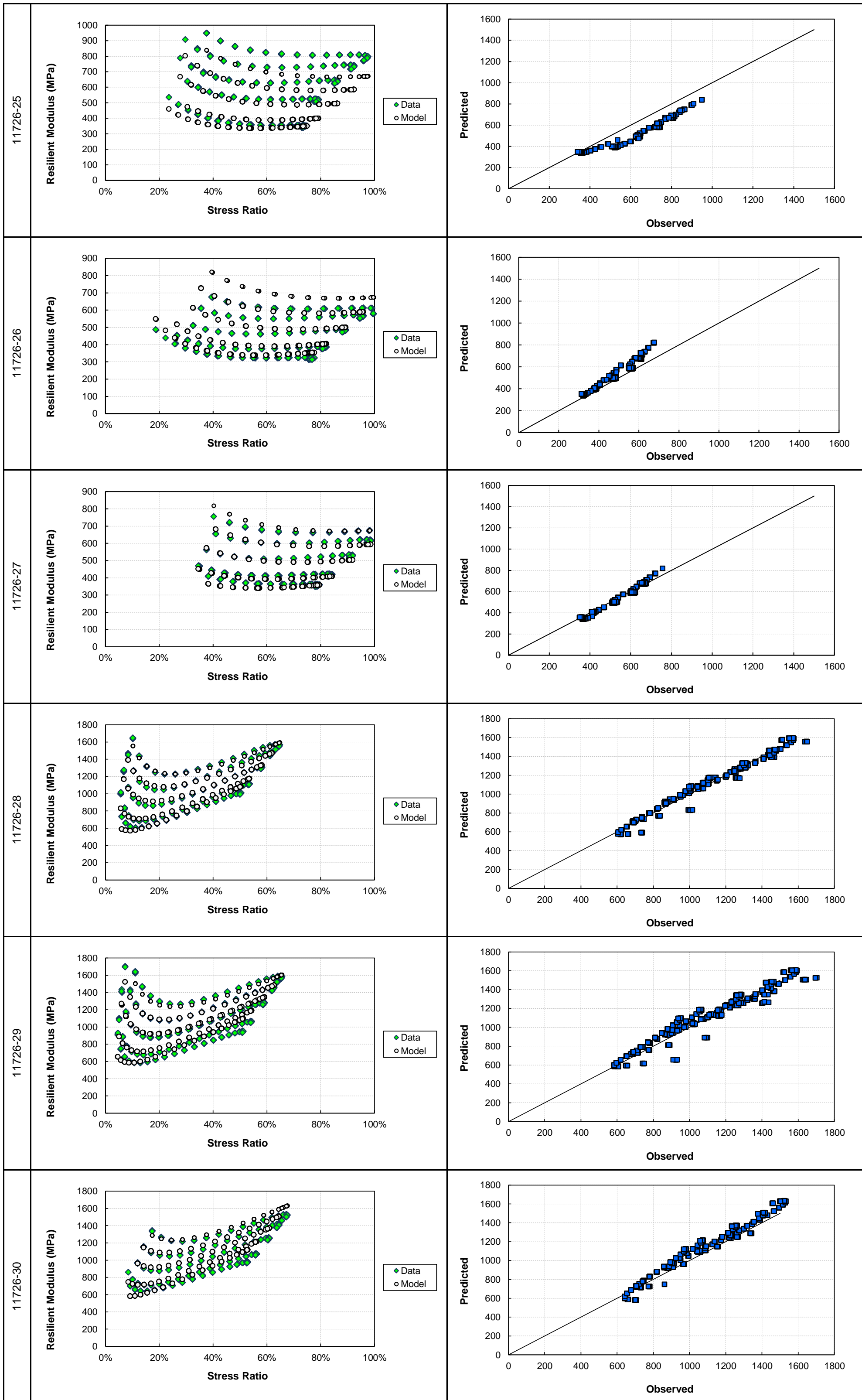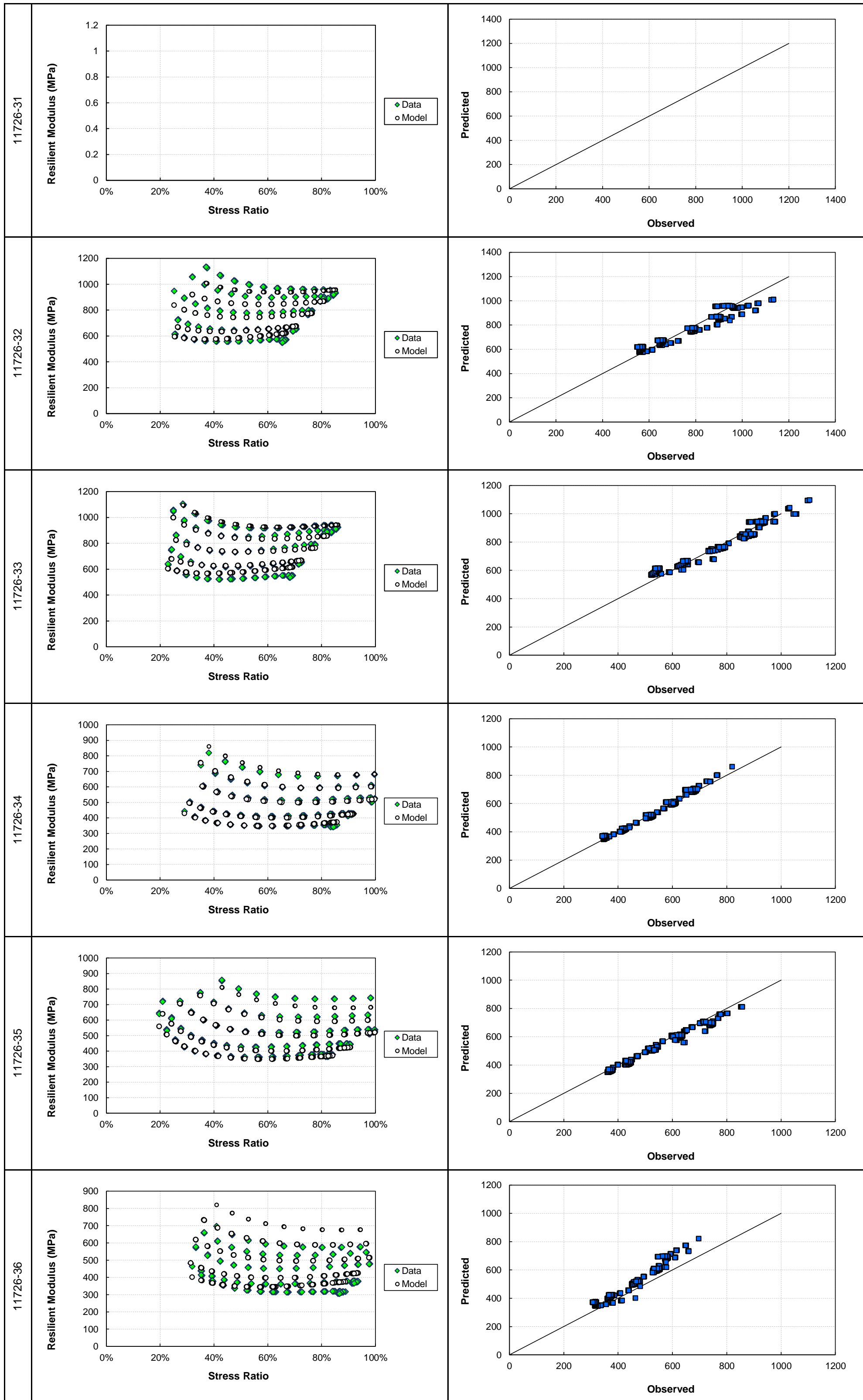| Sample #	Volumetric Density (VD) (kg/m³)	Saturation (S) (%)	a		b	c		R²	SEE (MPa)	Average Error (%)
			α_1	β_1	α_2	α_3	β_3			
11307-19	0.70	0.18	253.03	1.63	551.21	13.44	0.32	0.99	16.9	1.7%
11307-20	0.70	0.18	253.03	1.63	551.21	13.44	0.32	0.86	58.7	6.8%
11307-21	0.70	0.18	253.03	1.63	551.21	13.44	0.32	0.96	35.0	3.5%
11307-22	0.70	0.46	253.02	0.50	551.03	14.91	0.45	0.70	80.5	8.7%
11307-23	0.70	0.46	253.02	0.51	551.06	14.89	0.44	0.80	54.1	7.6%
11307-24	0.70	0.46	253.02	0.51	551.07	14.89	0.44	0.92	39.8	3.8%
11307-25	0.69	0.74	78.24	-0.06	100.46	16.36	0.62	0.79	21.1	6.5%
11307-26	0.69	0.73	92.25	-0.05	101.38	16.31	0.61	0.81	30.0	5.8%
11307-27	0.69	0.74	81.94	-0.06	100.68	16.34	0.62	0.53	34.8	14.1%
11307-28	0.68	0.16	233.21	1.11	510.08	24.42	0.59	0.10	257.7	19.6%
11307-29	0.69	0.16	233.21	1.14	510.08	24.00	0.59	0.75	136.1	6.2%
11307-30	0.69	0.16	233.21	1.11	510.08	24.42	0.59	-0.62	254.2	33.4%
11307-31	0.68	0.49								
11307-32	0.68	0.48	233.21	0.48	166.98	43.42	0.34	-0.08	110.9	15.6%
11307-33	0.69	0.47	233.21	0.49	269.15	43.14	0.35	0.96	17.2	2.6%
11307-34	0.68	0.73								
11307-35	0.68	0.70	57.54	0.26	85.27	56.80	0.24	0.40	31.5	11.2%
11307-36	0.68	0.69	190.89	0.27	85.27	56.27	0.24	0.25	53.5	8.5%

G.1.3 Sample 3 – Weathered dolerite from Road S191 base layer

G-6

Table G.3: **Model variables and statistical results for Road S191 base layer.**

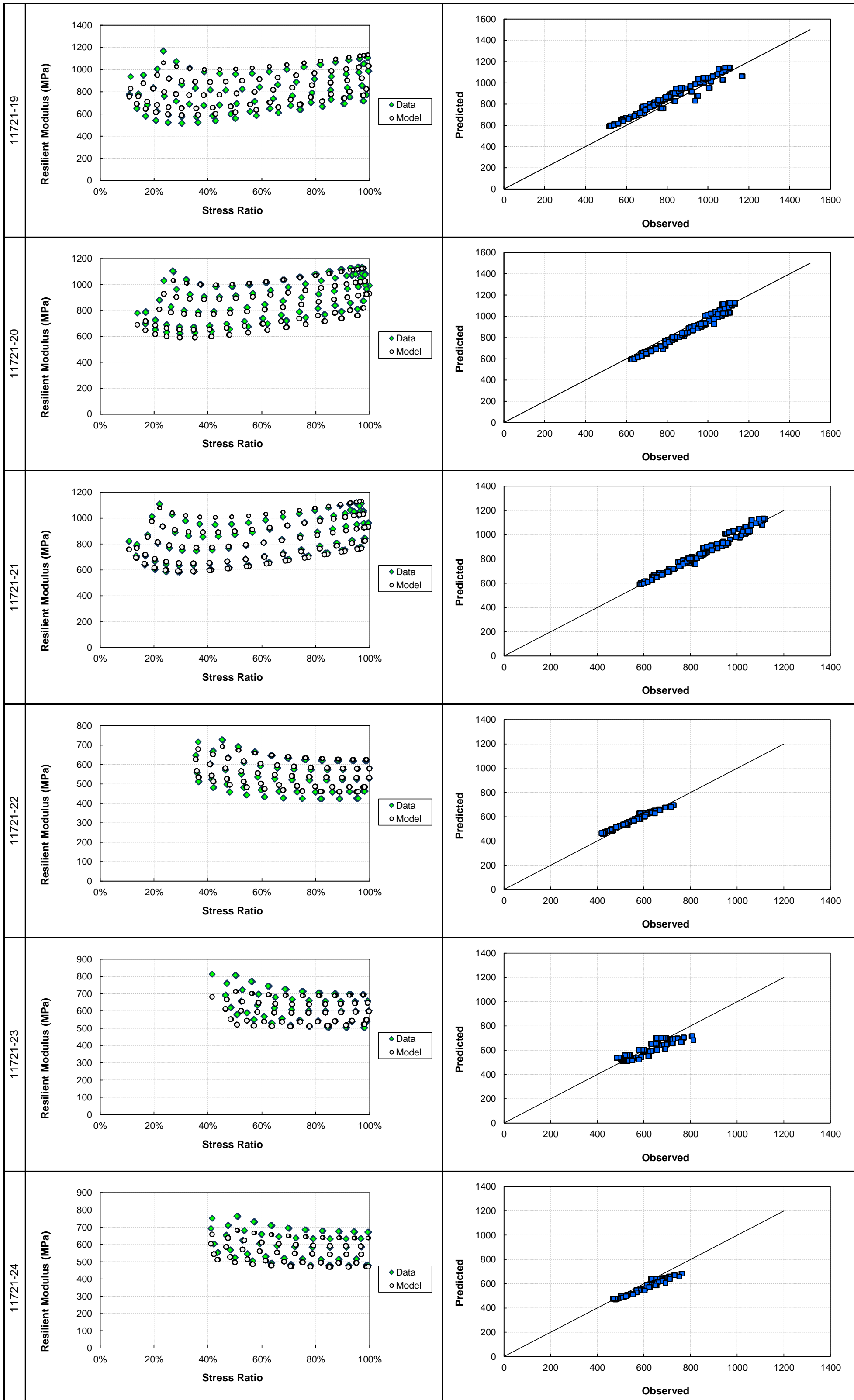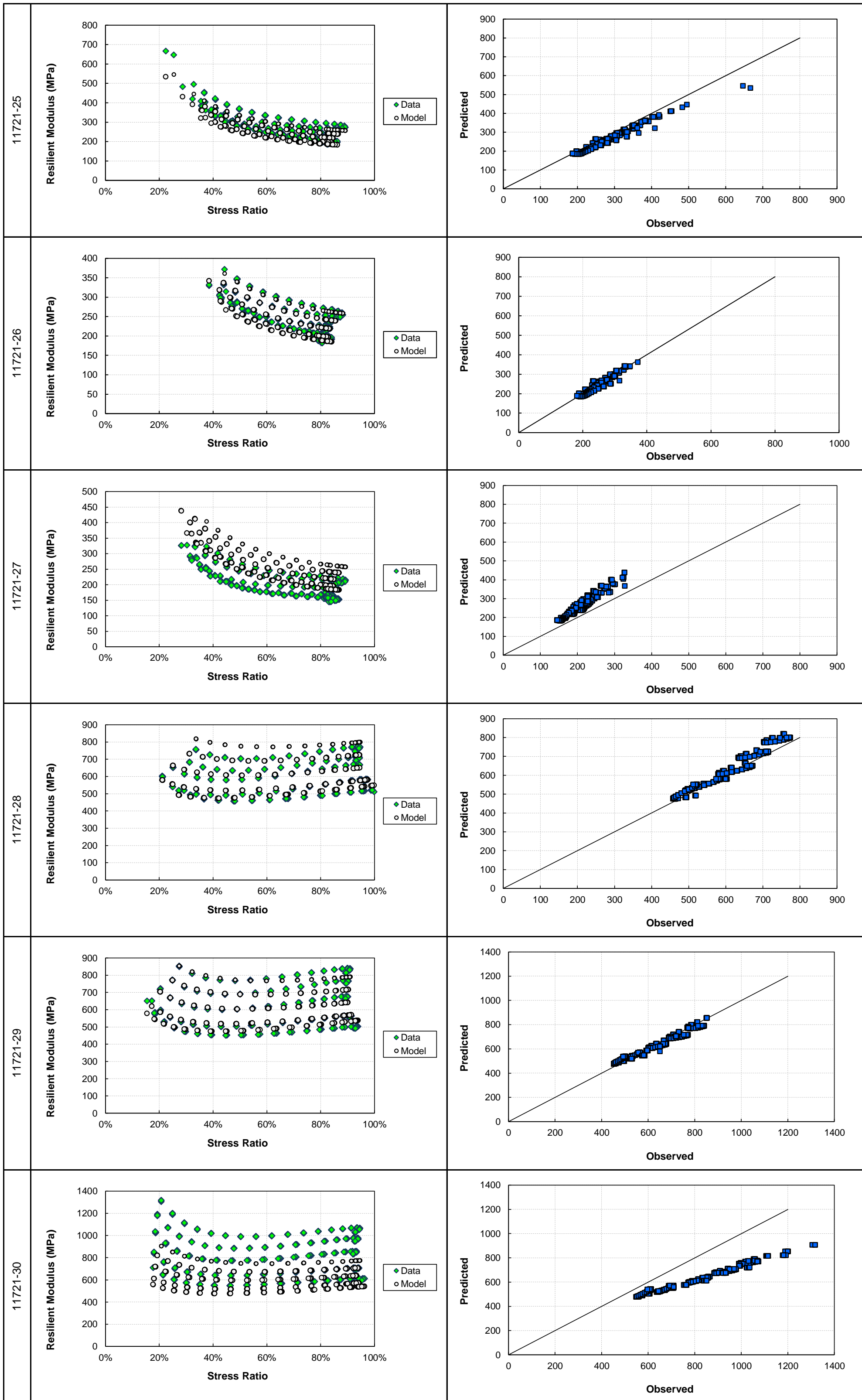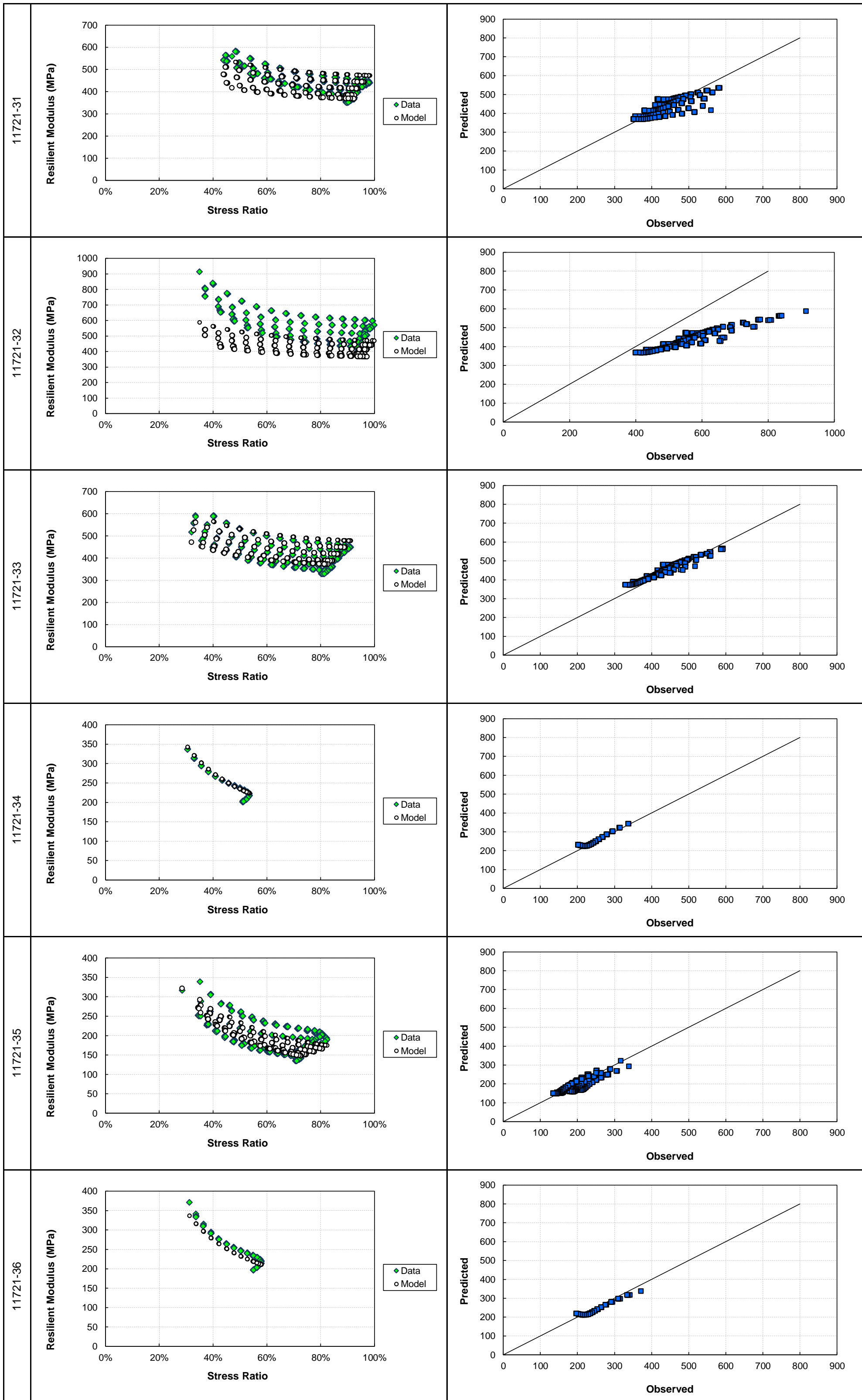| Sample #	Volumetric Density (VD) (kg/m³)	Saturation (S) (%)	a		b	c			R²	SEE (MPa)	Average Error (%)
			α_1	β_1	α_2	α_3	β_3				
11726-19	0.80	0.09	281.69	1.00	1495.54	-0.77	0.466	0.89	99.2	7.0%
11726-20	0.80	0.09	281.69	1.01	1495.54	-1.12	0.465	0.92	85.6	7.8%
11726-21	0.80	0.09	281.69	1.01	1495.54	-1.63	0.464	0.94	76.2	5.8%
11726-22	0.80	0.43	272.12	0.96	369.01	37.85	0.567	0.87	43.8	4.1%
11726-23	0.80	0.41	279.42	0.96	501.60	35.82	0.561	0.95	36.5	3.8%
11726-24	0.80	0.40	280.50	0.96	596.04	34.92	0.558	0.58	120.3	10.1%
11726-25	0.80	0.71	0.00	0.95	278.91	70.59	0.670	0.46	121.6	17.0%
11726-26	0.80	0.72	0.00	0.95	278.91	71.66	0.673	0.77	51.5	8.3%
11726-27	0.80	0.73	0.00	0.95	278.91	72.54	0.676	0.97	21.3	3.6%
11726-28	0.79	0.10	281.69	1.00	1495.54	0.07	0.468	0.98	41.8	3.1%
11726-29	0.79	0.11	281.69	1.00	1495.54	1.03	0.470	0.95	67.6	5.2%
11726-30	0.79	0.11	281.69	1.00	1495.54	0.89	0.470	0.91	77.4	6.2%
11726-31	0.79	0.42								
11726-32	0.79	0.43	272.39	0.96	370.78	37.81	0.567	0.91	46.7	4.6%
11726-33	0.79	0.43	269.61	0.96	355.84	38.18	0.568	0.96	32.3	3.6%
11726-34	0.79	0.77	0.00	0.95	278.91	76.99	0.692	0.99	14.5	2.1%
11726-35	0.79	0.77	0.00	0.95	278.91	77.13	0.692	0.96	27.7	3.8%
11726-36	0.79	0.75	0.00	0.95	278.91	75.00	0.685	0.55	67.9	12.5%

© University of Pretoria

G.1.4   Sample 4 – Weathered shale from Road P10-2 base layer

Table G.4: **Model variables and statistical results for Road P10-2 base layer.**

Sample #	Volumetric Density (VD) (kg/m³)	Saturation (S) (%)	a		b	c			R²	SEE (MPa)	Average Error (%)
			α_1	β_1	α_2	α_3	β_3				
11721-19	0.76	0.20	282.30	1.89E+00	404.78	37.46	0.17	0.86	61.6	7.6%
11721-20	0.76	0.20	282.30	1.88E+00	404.78	37.66	0.17	0.91	44.0	4.5%
11721-21	0.76	0.20	282.30	1.92E+00	404.78	36.93	0.17	0.98	23.4	2.1%
11721-22	0.76	0.54	282.27	8.34E-01	83.70	70.45	0.12	0.91	22.8	3.9%
11721-23	0.76	0.52	282.28	8.65E-01	147.97	68.95	0.12	0.82	33.8	4.0%
11721-24	0.76	0.53	282.27	8.43E-01	94.28	70.03	0.12	0.77	36.5	5.2%
11721-25	0.76	0.84	0.15	3.46E-01	64.70	100.51	0.08	0.83	24.6	7.7%
11721-26	0.76	0.84	0.15	3.45E-01	64.70	100.57	0.08	0.91	11.3	3.5%
11721-27	0.76	0.84								
11721-28	0.73	0.19	256.27	1.25E+00	221.88	33.55	0.23	0.88	32.6	4.3%
11721-29	0.73	0.20	256.27	1.23E+00	221.88	33.98	0.23	0.95	27.4	3.5%
11721-30	0.73	0.22	256.27	1.14E+00	221.87	36.07	0.21	-0.366	207.8	22.2%
11721-31	0.74	0.51	256.27	5.33E-01	35.16	59.52	0.08	0.60	33.5	5.2%
11721-32	0.73	0.52	256.27	5.23E-01	35.16	60.08	0.08	-0.96	132.6	21.0%
11721-33	0.74	0.50	256.27	5.44E-01	35.17	58.87	0.08	0.86	21.2	4.6%
11721-34	0.74	0.81								
11721-35	0.74	0.82								
11721-36	0.73	0.83								

G.1.5   Sample 5 – Weathered calcrete from Road D804 base layer

Table G.5: **Model variables and statistical results for Road D804 base layer.**

Sample #	Volumetric Density (VD) (kg/m³)	Saturation (S) (%)	a		b	c		R²	SEE (MPa)	Average Error (%)
			α_1	β_1	α_2	α_3	β_3			
11728-19	0.73	0.21								
11728-20	0.73	0.20	409.45	1.03	526.94	35.26	0.25	0.52	85.3	9.7%
11728-21	0.73	0.21	409.45	1.01	525.94	36.33	0.24	0.57	93.5	8.0%
11728-22	0.73	0.43	409.33	0.75	68.72	56.76	0.17	0.74	33.3	3.8%
11728-23	0.73	0.43	409.32	0.75	68.61	56.87	0.17	0.94	20.6	2.0%
11728-24	0.73	0.43	409.28	0.75	68.21	57.33	0.17	0.93	23.4	2.3%
11728-25	0.72	0.77	0.05	0.53	66.73	89.39	0.10	0.89	17.5	5.3%
11728-26	0.73	0.80	0.01	0.52	66.73	92.79	0.10	0.96	12.9	3.4%
11728-27	0.73	0.79	0.01	0.52	66.73	91.82	0.10	0.93	15.4	5.5%
11728-28	0.70	0.21	347.07	1.08	199.23	58.88	0.16	0.86	37.0	3.9%
11728-29	0.70	0.20	347.07	1.10	199.24	57.73	0.18	0.78	61.0	6.1%
11728-30	0.70	0.20	347.07	1.10	199.24	57.79	0.17	0.77	57.3	7.8%
11728-31	0.70	0.40	328.33	0.72	76.66	83.51	0.04	0.33	59.8	6.7%
11728-32	0.70	0.41	317.82	0.70	60.20	84.77	0.04	0.68	41.7	4.5%
11728-33	0.70	0.41	313.01	0.70	55.34	85.22	0.04	0.17	46.6	7.1%
11728-34	0.71	0.79								
11728-35	0.71	0.77	6.83	0.34	21.25	132.76	0.00	0.65	40.2	12.7%
11728-36	0.71	0.78	6.83	0.33	21.25	134.21	0.00	0.69	25.9	10.3%